Towards Improving The Accuracy of Implicit Solvent Models and Understanding Electrostatic Catalysis in Complex Solvent Environments

Longkun Xu

March 6, 2022

Australian National University

A thesis submitted for the degree of Doctor of Philosophy of
The Australian National University

Declaration

This thesis presents my own original work and, to the best of my knowledge, contains no material written or published by any other person, except where due reference has been made. This work has not been previously submitted for any other degree or diploma at any university or institution.

Longkun Xu

March 6, 2022

List of Abbreviations

MD	molecular dynamics
COSMO-RS	conductor like screening model for real solvents
ADF	Amsterdam density functional
LAMMPS	large-scale atomic/molecular massively parallel simulator
SMD	solvation model based on density
PCM	polarizable continuum model
HF	Hartree-Fock
DFT	density functional theory
OLED	organic light emitting diodes
EEF	external electric field
CFG	charged functional group
STM-BJ	scanning tunnelling microscopy break-junction
ESF	electrostatic scaling factor
OCP	open-circuit potential
DLPNO-CCSD	domain based pair natural orbital coupled cluster
SCF	self-consistent field
SCRF	self-consistent reaction field
SEI	solid electrolyte interphase
AIMD	*ab initio* molecular dynamics
DFTB	density functional based tight binding
GFN-XTB	semi-empirical extended tight-binding
FMO	fragment molecular orbital
EFP	effective fragment potential
SMFA	systematic molecular fragmentation by annihilation
GEBF	eneralized energy-based fragmentation
QM	quantum mechanics
MM	molecular mechanics
S-QM/MM	sequential quantum mechanics/molecular mechanics
ML	machine learning
DPMD	deep potential molecular dynamics
GPU	graphic processing unit
vdW	van der Waals
SES	solvent excluded surface
SAS	solvent accessible surface
ASC	apparent surface charge
ILs	ionic liquids
RTILS	room-temperature ionic liquids
ICILs	liquid-crystalline ionic liquids
RDF	radial distribution function
SHE	standard hydrogen electrode

Acknowledgements

First and foremost, I'd like to thank my supervisor Prof. Michelle Coote. I sincerely appreciate all the support from her in the past 3 years as well as the opportunity and scholarship from her that enable me to study abroad and experience all the beautiful things in Australia (especially the stunning sunset in Canberra!).

I'd also like to thank all the members in the Coote group for creating a wonderful working environment, especially the helpful discussions about MD simulations and other topics with Dr. Li-Juan Yu and Mitchell Blyth. Also, I thank Dr. Li-Juan Yu and Dr. Rhys Murphy for helping proofreading this thesis. In the early stage of my PhD, Dr. Benjamin Noble and Fergus Rogers shared their valuable experience about electrostatic catalysis, COSMO-RS in ADF and the usage of group scripts. Catherine Simpson kindly shared the script used to scan the directions of external electric fields. The preliminary works and draft by former members of the group (Dr. Ganna Gryn'ova and Dr. Junming Ho) on solvation modelling should also be acknowledged here.

I'd also like to thank other people for their help. I need to thank Prof. Ekaterina I. Izgorodina and her students (especially Peter Halat, Michael Robinson and Dr. Luke Wylie) at Monash University for helpful discussions about ionic liquids. Prof. Christopher J. Cramer kindly answered my questions about the atomic radii in SMD model via emails. Prof. H. Bernhard Schlegel and his student Sebastien Hebert kindly explained the data in their publication. Dr. Axel Kohlmeyer answered several of my questions in the LAMMPS mail list. Dr. Zhenxing Wang kindly answered my questions about the constant potential method that he implemented in LAMMPS. Hugo Macdermott-Opeskin provided a useful discussion about MD simulation. I thank Dr. Tian Lu for the discussions about the use of Multiwfn program, the calculations of atomic polarizability and other aspects of computational chemistry. I benefited a lot from reading his blogs in the past years. Prof. Agilio A. H. Padua and his student Kateryna Goloviznina kindly answered my questions about the use of their CL&Pol force field. I also need to thank the support team of COSMOlogic (mainly Dr. Frank Eckert), Gaussian (mainly Dr. Doug Fox) and NCI (mainly Dr. Rika Kobayashi) for their help.

During the past 3 years, my research projects has encountered several challenges and I benefited a lot from reading the online discussions and resources including the mail list of LAMMPS, ORCA forum, CCL, ResearchGate, computational chemistry blogs, Github open-source codes and scripts, and other platforms I forget to mention here.

Last but not least, the long-term support from my parents means a lot to me. They don't quite understand my research but always support all my decisions along the way. I thank the love and happiness from my girlfriend Dr. Xiaohan Gong, which are very important, especially during a PhD study through the COVID-19 pandemic.

Abstract

This thesis develops improved protocols for studying solvation free energies, chemical properties and reactions in solution and uses them to explore the possibility of harnessing complex non-standard solvent environments to catalyse chemical reactions. The thesis covers different but related topics:

Topic 1 is improving the accuracy of implicit solvent models. Implicit solvent models are simple cost-effective strategies for modelling solvent as a polarizable continuum. However, the accuracy of this approach can be quite variable. Herein, we examine approaches to improving their accuracy through cavity scaling, the choice of theoretical level and the inclusion of explicit solvent molecules. For SMD, we show that the best performance is achieved when cavity scaling is not employed, while for PCM we present a series of ESF values that are radii, solvent and ion type dependent. For both families of method, we also highlight the importance of choosing an appropriate level of theory, and identify when explicit solvent molecules are required.

Topic 2 is electrostatic catalysis in complex solvent environments. The first approach is using ordered solvent and ionic liquids. Recent nanoscale experiments have shown that electric fields are capable of catalysing and controlling chemical reactions, but experimental platforms for scaling these effects remain elusive. Herein, two different approaches to addressing this challenge are explored. The first is using the internal electric field of ordered solvents and ionic liquids. A multi-scale modelling approach was developed using a polarizable force field based molecular dynamic simulation, post-HF, DFT, semi-empirical quantum chemical calculations and wave function analysis techniques. We showed that after exposure to an external electric field, ensembles of solvent or ionic liquid molecules become ordered and this ordering can generate an internal electric field, which persists even after the external potential is removed. Experimental collaborators subsequently detected this field as an open-circuit potential that is strong and long-lived. Computationally we showed that this field is enough to lower reaction barriers by as much as 20 kcal/mol, and we also developed a predictive model to choose ionic liquids that optimize this field.

In the second approach, we harnessed the electric fields of the gas-water interface. Experimental collaborators showed that in the presence of static, inert gas bubbles, the oxidation potential of HO anion was dramatically lowered (by more than 0.5 V), much more than any subtle concentration effects predicted by the Nernst equation. Further experiments showed that a high unbalanced concentration of HO^- ions (as much as 5 M) accumulate at the interface. Our multi-scale modelling calculations showed that this reduction in potential was due to the mutual repulsion of the HO anions and as little as 1 M unbalanced excess was enough to explain the experimental results. The work raises opportunities in reducing the cost of electrochemical processes, and points to electrostatic effects contributing to the well-known catalytic effects of "on water" reactions.

Works in this thesis are useful in the future studies of solution-phase pK_a, redox potentials, electrostatic catalysis, interfaces, and ionic liquids based electrochemical devices.

Contents

Chapter 1

Introduction

1.1 Overview

One feature of the Earth compared with other planets is the presence of water. It is recognized that water is critical for plate tectonics on Earth and possibly shapes the surface of Mars.[1] Water, as the molecule of life, influences the development of life.[2] Among all the 125 important unsolved questions proposed in 2005,[3] one question was about the structure of water, which seems simple but is actually complicated.[4]

Besides water, other solvents including organic solvents,[5] ionic liquids,[6] solvent mixtures,[7] deep eutectic solvents[8] and electrolyte solutions,[9] are widely investigated in chemistry. This forms a very important branch of science: solvent effects.

Generally, it is widely recognized that solvent effects can influence many aspects of chemical reactions. Chemical reactivity,[10] reaction rate,[11] mechanisms[12] and selectivity[13] can be dramatically different in gas-phase and solution-phase. Solvent molecules are important for designing organic synthesis,[14] they can work as both reaction media and the catalysts themselves.[15]

For photochemistry, as early as 1956, Masao and co-workers reported solvent effects on the fluorescence spectra and the dipole moments of excitepd molecules.[16] The concept of *solvatochromism* has been frequently discussed[17]. In addition to the absorption wavelength of electronic spectra, spectral shape[18] and vibrational spectroscopy[19] can also be heavily influenced by solvent effects. Further, solvent alters the excited-state dynamics of molecules and can directly inform the design of solar cell dyes[20], OLED[21] and photocatalysts.[22]

Electrochemical properties such as redox potential can also be dramatically affected by solvent effects.[23] The solid-liquid interface[24] and the associated structures and properties of liquids under electric fields[25] determine the performance of electrochemical devices (e.g., batteries[26] and supercapacitors[27]) and electrocatalysts[28]. Additionally, the concept of electrosynthesis offers a new approach for efficient synthesis, and can also be influenced by solvent effects.[29]

Considering the importance of solvent effects on different aspects of chemistry, it is meaningful to develop methods for comprehensively understanding of them. It was proposed by Hey and co-workers that scientific research has four paradigms including empirical evidence, scientific theory, computational science and data science.[30] It was pointed out by Dirac in 1929 that "*The underlying physical laws necessary for the mathematical*

theory of a large part of physics and the whole of chemistry are thus completely known, and the difficulty is only that the exact application of these laws leads to equations much too complicated to be solvable. It therefore becomes desirable that approximate practical methods of applying quantum mechanics should be developed, which can lead to an explanation of the main features of complex atomic systems without too much computation".[31] computational chemistry methods (e.g., DFT) was established on the basis of scientific theories (e.g., quantum mechanics, classical mechanics and electrodynamics) and computational science (e.g., high-performance computing). Besides, the development of classical MD force fields and computational solvation science is also based on both scientific theory and largely empirical parameterization, which includes empirical evidence (for obtaining experimental values of target properties) and data science (for efficient optimization of parameter set). Practical quantum chemistry uses various approximate methods, usually based on DFT or ab initio molecular orbital theory, to solve the Schrödinger equation. However, even using modern high-performance computing, the computational cost of such calculations remains high to the extent that only relatively small systems comprising at most a few 100 atoms in a vacuum can be studied. For larger systems, be they an ensemble of small molecules or a single larger molecule such as a protein or polymer, quantum mechanics is typically abandoned in favour of highly parameterised classical mechanics methods, with a concurrent loss of accuracy and generalizability. This raises a particular challenge when attempting to use quantum-chemical methods to accurately predict the behaviour of chemical reactions in solution, though one that is increasingly be met with success.[32–37]. Generally, we can classify all solvation modelling methods into implicit solvent modelling and explicit solvent modelling, which depends on whether the molecular details of solvent molecules are included in calculations. Both implicit and explicit solvent modelling can be used with computational methods at difference scales, e.g., quantum chemistry methods or force field methods. Each method can be employed for both static calculations and time-dependent dynamic simulations. A more detailed introduction about these methods and associated applications in different fields is presented in Chapter 2 and Chapter 3.

Another key concept in this thesis is *electrostatic catalysis*, which means to engineer electrostatic interactions in chemical systems to realize efficient catalysis. It has been shown that electrostatic catalysis can be applied to chemical reactions regardless of whether a redox process is involved.[38–42] Different forms of electric fields can be employed to dramatically influence the free energy landscape of reactions by changing the interactions between electric field and transition states, reactants and products. It has been shown that electrostatic catalysis can be achieved by using enzymes,[43] ionic aggregates,[44] oriented metal ions,[45] EEF,[42] tribo-electrification[46] and CFG[47, 48]. Although the STM-BJ approach successfully implemented electrostatic catalysis at molecular level,[42] the prospect of electrostatic catalysis needs access to scalable platforms.[49]

Theoretical and computational tools have also been used to investigate electrostatic catalysis. The pioneering work of Shaik and co-workers[38] has demonstrated the effects of external electric fields on the *endo/exo* selectivity of Diels–Alder reactions. In recent years, pH-switchable local electric fields have been examined. Further details on designed local electric fields can be found in Ref[50]. Local electric fields can be obtained by incorporating charged sites on substrates or catalysts.[47, 48, 51, 52] The choice of charged sites can be determined by comparing the resulting electric field and the reaction axis.

Most computational works in this regard use accurate quantum chemical methods with and without implicit solvent models, which generally provides highly accurate modelling of electrostatic catalysis.

One bottleneck of electrostatic catalysis is the solvent attenuation problem (see Figure 1.1), i.e., the electrostatic interactions are highly reduced in polar solvents compared with that in the gas phase.[47] It was also shown that the solvent polarity can affect the bond dissociation Gibbs free energy.[40] The recent work of Shaik and co-workers reported the solvent attenuation at molecular level as well as the relationship between solvent attenuation and solvent ordering.[53]
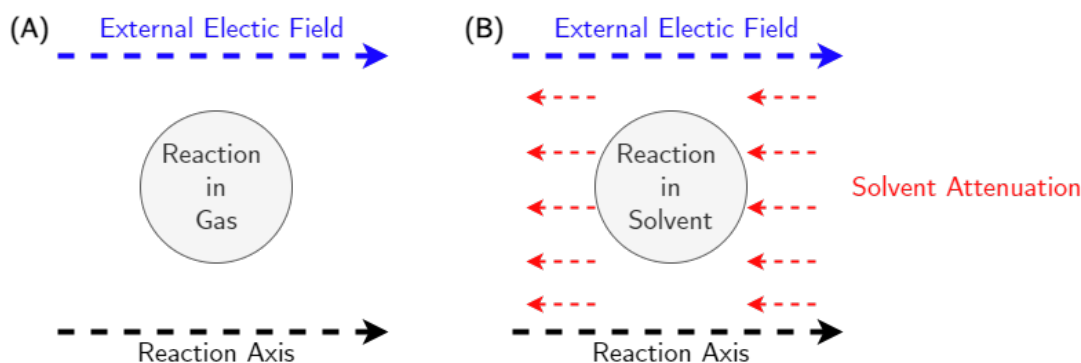

Figure 1.1: The scheme of solvent attenuation problem and the comparison of the effects of external electric field in gas (A) and solvent (B).

This thesis focuses on the roles of solvent environments in electrostatic catalysis. Indeed, it is well established that the solvent and enzyme environments themselves can work as both the reaction media and catalyst.[43, 54] An example is the Marcus theory which highlights the roles of solvent reorganization in outer-sphere electron transfer reactions.[54] Besides the bulk solution phase, interfaces between different phases (e.g., air-water, solid-liquid and water-oil interfaces) usually provide unique features due to the unbalanced local charges and hydrogen-bonding interactions.[55–57] For example, under some circumstances, the orientation of the solvent molecules can be manipulated[58] at the electrochemical double-layer structure at the interfaces between charged electrodes and electrolyte.[59] To understand electrostatic catalysis in these complex solvent environments, quantum chemical methods and implicit solvent models are usually not good enough, thus we need both MD simulation and explicit solvent simulation techniques at different scales for configuration sampling and energy calculations. Actually, employing MD simulation techniques to simulate chemical systems under external electric field is widely studied in the community by using constant potential method[60] or uniform electric fields.[61] Techniques beyond the limits of classical force fields, e.g., ReaxFF, which allows bond dissociation in MD simulations, is also actively developed to capture reaction details in the simulation.[62]

More details about electrostatic catalysis, ordered solvent and air-water interfaces are presented in Chapter 2, Chapter 4 and Chapter 5.

Based on the above concepts, the aims of this thesis are:

(1) Review different computational methods for solvation modelling and associated applications.

(2) Compare and analyse different methods to improve the accuracy of implicit solvent models using pK_a predictions as a case study.

(3) Study electrostatic catalysis in an ordered solvent environment (with experimental collaborators) and develop computational methods to analyse structures and properties of ordered solvents and ionic liquids under external electric fields.

(4) Investigate the electrostatic catalysis resulting from the accumulated OH^- ions at the air-water interface (with experimental collaborators).

1.2 Outline of Thesis

This thesis is organized as the following:

Chapter 2 presents an extensive review (*Publication 1*) about solvation modelling techniques and their applications in studying pK_a, redox potential, photochemical properties, reaction mechanisms and catalysis. In detail, the concepts of different solvation modelling techniques and important factors associated with these methods are reviewed. We highlight some solvation databases, recommended parameters and the comparisons between different methods. A selection of important applications in last five years are introduced. Finally the outlook for future work is given.

Chapter 3 includes our efforts to improve the accuracy of implicit solvent models including SMD (*Publication 2*) and PCM (*Publication 3*). Details and important factors of implicit solvent models are introduced. Different strategies for improving the accuracy of SMD solvation energies are compared and tested with aqueous pK_a calculations of a wide range of solute types. Using the extensive MNSOL-v2012 data base, we present a set of optimized ESF for PCM-UAHF and PCM-UAKS calculations of solvation free energies in various solvents. The optimized ESF values are also tested via pK_a predictions in water and acetonitrile. Additionally, we present the mixed theoretical level for SMD and mixed-ESF for PCM calculations, which can dramatically improve the accuracy.

Chapter 4 includes our work studying ordered solvents and ionic liquids, and associated electrostatic catalysis. Details about electrostatic catalysis, the roles of solvent environment and ordered solvents and ionic liquids are reviewed. In *Publication 4* employing classical MD simulations with the Drude oscillator-based polarizable force field, quantum chemical calculations, and ONIOM (DFT:semi-empirical) multi-scale energy calculations, we investigate the feasibility of using ordered solvent and ionic liquids for electrostatic catalysis. In *Publication 5* collaborating with experimental chemists, different experimental and computational techniques to characterize the ordering degree of different ionic liquids under external electric field are introduced. The calculated values agree well with the observed OCP. A relationship between calculated ion dipole projections and experimental OCP is proposed for future studies of ordered ionic liquids in electrochemical systems.

Chapter 5 introduces details about the air-water interface and its unique features. We present our work (*Publication 6*) where we use semi-empirical MD simulations and ONIOM(CCSD(T)/CBS:DHDFT) methods to study the effects of the concentration of OH anions at the gas-liquid interface of bubble system on the oxidation potential of OH anion itself.

Chapter 6 provides the summary of this thesis and outlook for future works.

1.3 List of Publications

This thesis is presented as a series of manuscripts and published articles. In each publication I am either the first author or the first computational author.

Publication 1. <u>**Longkun Xu**</u> and Michelle L. Coote. "Recent Advances in Solvation Modelling Applications: Chemical Properties, Reaction Mechanisms and Catalysis" *Annu. Rep. Comput. Chem.* (**First author, Submitted, Invited review**)

Publication 2. <u>**Longkun Xu**</u> and Michelle L. Coote. "Methods To Improve the Calculations of Solvation Model Density Solvation Free Energies and Associated Aqueous pK_a Values: Comparison between Choosing an Optimal Theoretical Level, Solute Cavity Scaling, and Using Explicit Solvent Molecules" *J. Phys. Chem. A.* **2019** 123 (34), 7430-7438. (**First author, Published**)

Publication 3. <u>**Longkun Xu**</u> and Michelle L. Coote. "Improving the Accuracy of PCM-UAHF and PCM-UAKS Calculations Using Optimized Electrostatic Scaling Factors" *J. Chem. Theory Comput.* **2019** 15 (12), 6958-6967. (**First author, Published**)

Publication 4. <u>**Longkun Xu**</u>, Ekaterina I. Izgorodina and Michelle L. Coote. "Ordered Solvents and Ionic Liquids Can be Harnessed for Electrostatic Catalysis" *J. Am. Chem. Soc.* **2020** 142 (29), 12826–12833. (**First author, Published**)

Publication 5. Mattia Belotti, Xin Lyu, <u>**Longkun Xu**</u>, Peter Halat, Nadim Darwish, Debbie S. Silvester, Ching Goh, Ekaterina I. Izgorodina, Michelle L. Coote and Simone Ciampi "Experimental Evidence of Long-Lived Electric Fields of Ionic Liquid Bilayers" *J. Am. Chem. Soc.* **2021** 143 (42), 17431–17440. (**First computational author, Published**)

Publication 6. Yan B. Vogel, Cameron W. Evans, Mattia Belotti, <u>**Longkun Xu**</u>, Isabella C. Russell, Li-Juan Yu, Alfred K. K. Fung, Nicholas S. Hill, Nadim Darwish, Vinicius R. Gonçales, Michelle L. Coote, K. Swaminathan Iyer, Simone Ciampi. "The Corona of A Surface Bubble Promotes Electrochemical Reactions" *Nat. Commun.* **2020** 11(1): 1-8. (**First computational author, Published**)

Bibliography

[1] A. R Sarafian, S. G Nielsen, H. R Marschall, F. M McCubbin, and B. D Monteleone, "Early accretion of water in the inner solar system from a carbonaceous chondrite–like source", *Science* **346**(6209), pp. 623–626 (2014).

[2] F Franks, *Water: a matrix of life* volume 21, Royal Society of Chemistry (2000).

[3] D Kennedy and C Norman, "What don't we know", *Science* **309**(5731), pp. 75 (2005).

[4] L. G. M Pettersson, R. H Henchman, and A Nilsson, "Water–The most anomalous liquid", *Chemical Reviews* **116**(13), pp. 7459–7462 (2016).

[5] D. R Lide, *Handbook of organic solvents*, CRC press (1994).

[6] R. D Rogers and K. R Seddon, "Ionic liquids–solvents of the future?", *Science* **302**(5646), pp. 792–793 (2003).

[7] Y Marcus, *Solvent mixtures: properties and selective solvation*, CRC Press (2002).

[8] B. B Hansen, S Spittle, B Chen, D Poe, Y Zhang, J. M Klein, A Horton, L Adhikari, T Zelovich, and B. W Doherty, "Deep eutectic solvents: A review of fundamentals and applications", *Chemical Reviews* **121**(3), pp. 1232–1285 (2020).

[9] R. A Robinson and R. H Stokes, *Electrolyte solutions*, Courier Corporation (2002).

[10] C Reichardt, "Solvent effects on chemical reactivity", *Pure and Applied Chemistry* **54**(10), pp. 1867–1884 (1982).

[11] A Wangler, R Canales, C Held, T Luong, R Winter, D Zaitsau, S Verevkin, and G Sadowski, "Co-solvent effects on reaction rate and reaction equilibrium of an enzymatic peptide hydrolysis", *Physical Chemistry Chemical Physics* **20**(16), pp. 11317–11326 (2018).

[12] G Litwinienko and K Ingold, "Solvent effects on the rates and mechanisms of reaction of phenols with free radicals", *Accounts of Chemical Research* **40**(3), pp. 222–230 (2007).

[13] S Mukherjee and M. A Vannice, "Solvent effects in liquid-phase reactions: I. Activity and selectivity during citral hydrogenation on Pt/SiO_2 and evaluation of mass transfer effects", *Journal of Catalysis* **243**(1), pp. 108–130 (2006).

[14] M.-O Simon and C.-J Li, "Green chemistry oriented organic synthesis in water", *Chemical Society Reviews* **41**(4), pp. 1415–1427 (2012).

[15] C Zhao, X Ma, X Wu, D. L Thomsen, V. M Bierbaum, and J Xie, "Single solvent molecules induce dual nucleophiles in gas-phase ion–molecule nucleophilic substitution reactions", *The Journal of Physical Chemistry Letters* **12**, pp. 7134–7139 (2021).

[16] N Mataga, Y Kaifu, and M Koizumi, "Solvent effects upon fluorescence spectra and the dipolemoments of excited molecules", *Bulletin of the Chemical Society of Japan* **29**(4), pp. 465–470 (1956).

[17] A Marini, A Muñoz-Losa, A Biancardi, and B Mennucci, "What is solvatochromism?", *The Journal of Physical Chemistry B* **114**(51), pp. 17128–17135 (2010).

[18] T. J Zuehlsdorff and C. M Isborn, "Combining the ensemble and Franck-Condon approaches for calculating spectral shapes of molecules in solution", *The Journal of Chemical Physics* **148**(2), pp. 024110 (2018).

[19] A Buckingham, "Solvent effects in vibrational spectroscopy", In A. D Buckingham, editor, *Optical, Electric and Magnetic Properties of Molecules* , pp. 223–230. Elsevier (1997).

[20] A. M El-Zohry and B Zietz, "Concentration and solvent effects on the excited state dynamics of the solar cell dye d149: the special role of protons", *The Journal of Physical Chemistry C* **117**(13), pp. 6544–6553 (2013).

[21] D Chercka, S.-J Yoo, M Baumgarten, J.-J Kim, and K Müllen, "Pyrene based materials for exceptionally deep blue OLEDs", *Journal of Materials Chemistry C* **2**(43), pp. 9083–9086 (2014).

[22] R Kuriki, O Ishitani, and K Maeda, "Unique solvent effects on visible-light CO_2 reduction over ruthenium (II)-complex/carbon nitride hybrid photocatalysts", *ACS Applied Materials & Interfaces* **8**(9), pp. 6011–6018 (2016).

[23] H Svith, H Jensen, J Almstedt, P Andersson, T Lundbäck, K Daasbjerg, and M Jonsson, "On the nature of solvent effects on redox properties", *The Journal of Physical Chemistry A* **108**(21), pp. 4805–4811 (2004).

[24] D. P Woodruff, *The solid-liquid interface*, CUP Archive (1973).

[25] Y Zhao, K Dong, X Liu, S Zhang, J Zhu, and J Wang, "Structure of ionic liquids under external electric field: a molecular dynamics simulation", *Molecular Simulation* **38**(3), pp. 172–178 (2012).

[26] Y.-K Han, J Jung, S Yu, and H Lee, "Understanding the characteristics of high-voltage additives in Li-ion batteries: Solvent effects", *Journal of Power Sources* **187**(2), pp. 581–585 (2009).

[27] W Yang, Z Gao, J Ma, J Wang, B Wang, and L Liu, "Effects of solvent on the morphology of nanostructured Co_3O_4 and its application for high-performance supercapacitors", *Electrochimica Acta* **112**, pp. 378–385 (2013).

[28] A Rendón-Calle, S Builes, and F Calle-Vallejo, "Substantial improvement of electrocatalytic predictions by systematic assessment of solvent effects on adsorption energies", *Applied Catalysis B: Environmental* **276**, pp. 119147 (2020).

[29] S Ming, Z Feng, D Mo, Z Wang, K Lin, B Lu, and J Xu, "Solvent effects on electrosynthesis, morphological and electrochromic properties of a nitrogen analog of PEDOT", *Physical Chemistry Chemical Physics* **18**(7), pp. 5129–5138 (2016).

[30] A. J Hey, S Tansley, and K. M Tolle, *The fourth paradigm: data-intensive scientific discovery* volume 1, Microsoft Research Redmond, WA (2009).

[31] P. A. M Dirac, "Quantum mechanics of many-electron systems", *Proceedings of the Royal Society of London. Series A, Containing Papers of a Mathematical and Physical Character* **123**(792), pp. 714–733 (1929).

[32] C Daniel, "Photochemistry and photophysics of transition metal complexes: Quantum chemistry", *Coordination Chemistry Reviews* **282**, pp. 19–32 (2015).

[33] R. K Venkatraman and A. J Orr-Ewing, "Photochemistry of benzophenone in solution: A tale of two different solvent environments", *Journal of the American Chemical Society* **141**(38), pp. 15222–15229 (2019).

[34] H Su, C Lian, J Liu, and H Liu, "Machine learning models for solvent effects on electric double layer capacitance", *Chemical Engineering Science* **202**, pp. 186–193 (2019).

[35] D Domınguez-Ariza, C Hartnig, C Sousa, and F Illas, "Combining molecular dynamics and ab initio quantum-chemistry to describe electron transfer reactions in electrochemical environments", *The Journal of Chemical Physics* **121**(2), pp. 1066–1073 (2004).

[36] M Izadyar, M Gholizadeh, M Khavani, and M. R Housaindokht, "Quantum chemistry aspects of the solvent effects on 3, 4-dimethyl-2, 5-dihydrothiophen-1, 1-dioxide pyrolysis reaction", *The Journal of Physical Chemistry A* **117**(12), pp. 2427–2433 (2013).

[37] S. H Mushrif, S Caratzoulas, and D. G Vlachos, "Understanding solvent effects in the selective conversion of fructose to 5-hydroxymethyl-furfural: A molecular dynamics investigation", *Physical Chemistry Chemical Physics* **14**(8), pp. 2637–2644 (2012).

[38] R Meir, H Chen, W Lai, and S Shaik, "Oriented electric fields accelerate Diels–Alder reactions and control the endo/exo selectivity", *ChemPhysChem* **11**(1), pp. 301–310 (2010).

[39] G Gryn'ova, D. L Marshall, S. J Blanksby, and M. L Coote, "Switching radical stability by pH-induced orbital conversion", *Nature Chemistry* **5**(6), pp. 474–481 (2013).

[40] G Gryn'ova and M. L Coote, "Origin and scope of long-range stabilizing interactions and associated SOMO–HOMO conversion in distonic radical anions", *Journal of the American Chemical Society* **135**(41), pp. 15392–15403 (2013).

[41] S Shaik, S. P De Visser, and D Kumar, "External electric field will control the selectivity of enzymatic-like bond activations", *Journal of the American Chemical Society* **126**(37), pp. 11746–11749 (2004).

[42] A. C Aragonès, N. L Haworth, N Darwish, S Ciampi, N. J Bloomfield, G. G Wallace, I Diez-Perez, and M. L Coote, "Electrostatic catalysis of a Diels–Alder reaction", *Nature* **531**(7592), pp. 88–91 (2016).

[43] A Warshel, P. K Sharma, M Kato, Y Xiang, H Liu, and M. H Olsson, "Electrostatic basis for enzyme catalysis", *Chemical Reviews* **106**(8), pp. 3210–3235 (2006).

[44] Y Pocker and R. F Buchholz, "Electrostatic catalysis of ionic aggregates. I. Ionization and dissociation of trityl chloride and hydrogen chloride in lithium perchlorate-diethyl ether solutions", *Journal of the American Chemical Society* **92**(7), pp. 2075–2084 (1970).

[45] S Winstein, S Smith, and D Darwish, "Large salt effects in non-polar solvents", *Journal of the American Chemical Society* **81**(20), pp. 5511–5512 (1959).

[46] H Baytekin, A Patashinski, M Branicki, B Baytekin, S Soh, and B. A Grzybowski, "The mosaic of surface charge in contact electrification", *Science* **333**(6040), pp. 308–312 (2011).

[47] H. M Aitken and M. L Coote, "Can electrostatic catalysis of Diels–Alder reactions be harnessed with pH-switchable charged functional groups?", *Physical Chemistry Chemical Physics* **20**(16), pp. 10671–10676 (2018).

[48] M. T Blyth and M. L Coote, "A pH-switchable electrostatic catalyst for the Diels–Alder reaction: Progress toward synthetically viable electrostatic catalysis", *The Journal of Organic Chemistry* **84**(3), pp. 1517–1522 (2019).

[49] S Ciampi, I Diez-Perez, M. L Coote, and N Darwish, "Experimentally harnessing electric fields in chemical transformations", In S Shaik and T Stuyver, editors, *Effects of Electric Fields on Structure and Reactivity* , pp. 71–118. Royal Society of Chemistry Publishing (2021).

[50] M. T Blyth and M. L Coote, "Recent advances in designed local electric fields", In S Shaik and T Stuyver, editors, *Effects of Electric Fields on Structure and Reactivity* , pp. 119–146. Royal Society of Chemistry Publishing (2021).

[51] L.-J Yu and M. L Coote, "Electrostatic switching between SN_1 and SN_2 pathways", *The Journal of Physical Chemistry A* **123**(2), pp. 582–589 (2018).

[52] N. S Hill and M. L Coote, "Internal oriented electric fields as a strategy for selectively modifying photochemical reactivity", *Journal of the American Chemical Society* **140**(50), pp. 17800–17804 (2018).

[53] K Dutta Dubey, T Stuyver, S Kalita, and S Shaik, "Solvent organization and rate regulation of a Menshutkin reaction by oriented external electric fields are revealed by combined MD and QM/MM calculations", *Journal of the American Chemical Society* **142**(22), pp. 9955–9965 (2020).

[54] R. A Marcus, "On the theory of oxidation-reduction reactions involving electron transfer. I.", *The Journal of Chemical Physics* **24**(5), pp. 966–978 (1956).

[55] M Chaplin, "Theory vs experiment: what is the surface charge of water", *Water* **1**(1), pp. 1–28 (2009).

[56] Y Jung and R Marcus, "On the theory of organic catalysis "on water"", *Journal of the American Chemical Society* **129**(17), pp. 5492–5502 (2007).

[57] P Norcott and C McErlean, "Synthesis of carbazoloquinone natural products 'on-water'", *Organic & Biomolecular Chemistry* **13**(24), pp. 6866–6878 (2015).

[58] P Sharma and T Bhatti, "A review on electrochemical double-layer capacitors", *Energy Conversion and Management* **51**(12), pp. 2901–2912 (2010).

[59] E Spohr, "Computer simulation of the structure of the electrochemical double layer", *Journal of Electroanalytical Chemistry* **450**(2), pp. 327–334 (1998).

[60] Z Wang, Y Yang, D. L Olmsted, M Asta, and B. B Laird, "Evaluation of the constant potential method in simulating electric double-layer capacitors", *The Journal of Chemical Physics* **141**(18), pp. 184102 (2014).

[61] N. J English, "Molecular dynamics in the presence of external electric fields", In S Shaik and T Stuyver, editors, *Effects of Electric Fields on Structure and Reactivity* , pp. 263–316. Royal Society of Chemistry Publishing (2021).

[62] F Miao and X Cheng, "Effect of electric field on polarization and decomposition of RDX molecular crystals: a ReaxFF molecular dynamics study", *Journal of Molecular Modeling* **26**(1), pp. 1–7 (2020).

Chapter 2

Review of Computational Methods for Solvation Modelling

2.1 Introduction

As introduced in Chapter 1, solvent effects are important in many aspects of chemistry including photochemistry, electrochemistry, reaction mechanisms and catalysis. Methods at different size and time scales are proposed for solvation modelling. In this Chapter, we provide a detailed introduction about the following methods and their applications, which is the basis for the contents for the remaining chapters of this thesis.

(1) Implicit solvent models with quantum chemical methods. This method is the standard and most widely used method in the community of electronic structure calculations. Popular methods include the well-known SMD,[1] various PCM,[2] COSMO[3] and its derivatives C-PCM[4, 5] and COSMO-RS[6]. These implicit solvent models are often used with DFT or HF calculations, although the combination of implicit solvent models with other quantum chemical methods (e.g., semi-empirical methods[7], fragmentation methods[8] and DLPNO-CCSD methods[9]) have appeared recently. With these methods, the solute-solvent many body interactions can be simplified as the two-body interactions between the solute and polarizable continuum medium with mean field approximation. The solvent effect is introduced as a perturbation term to the gas-phase Hamiltonian of the solute and is solved through the standard SCF framework, which is usually called the SCRF method.[10] Thus, the molecular details of solvent molecules are sacrificed so that computational costs can be largely saved. As a consequence, it is possible to model the structure and energy of solvated solute accurately by adding minor computational costs compared with the gas-phase solute modelling. The intrinsic drawback of these methods is that they do not perform well for systems with strong solute-solvent explicit interactions.[11] Two examples are electrolytes and deep eutectic solvents. Explicit interactions between Li^+ and electrolyte solvent and associated solvation structures determines SEI formation and battery performance.[12] The tunable nature of deep eutectic solvents is also closely related with explicit interactions, especially the hydrogen-bond interactions.[13] Additionally, although some variants of SMD and COSMO, e.g., SMD-GIL [14] and COSMO-RS[3] attempt to solve some problems, it is still hard to use implicit solvent models to simulate complex environments, e.g, ionic liquids,[15] solvent mixtures,[16] solvent environments with high concentration,[17] solvent environments at

non-standard temperature and pressure[18]. More details about these methods are presented in Section 2.2 and Chapter 3.

(2) Solvent simulation with force field methods. With force field methods, the interactions between particles and the associated potential energy in the system are described using parameter sets. The parameters can be optimized by fitting experimental quantities or be directly calculated via quantum chemical calculations. As computational costs of force field methods are much smaller than that of quantum chemical methods, it is a typical strategy for modelling large scale systems and simulating the dynamics of systems, e.g., proteins.[19] These methods are influenced by many factors including force field parameters and sampling methods. Force field methods mainly include classical force fields (e.g., AMBER,[20] CHARMM[21] and OPLS-AA[22]), polarizable force fields (e.g., AMOEBA[23] and Drude oscillator based CHARMM[24]), reactive force fields (e.g., ReaxFF[25]) and coarse-grained force fields (e.g., Martini[26]). Another important factor is the sampling methods, for example, end-point sampling (e.g., MM/GBSA[27]) and various alchemical and enhanced sampling based free energy methods (e.g., free energy perturbation,[28] thermodynamic integration,[29] metadynamics[30] and umbrella sampling[31]). Although force field methods are much cheaper than quantum chemical methods, one of their drawbacks compared with quantum chemical methods is the poor transferability to different chemical systems, which makes re-development of force fields usually challenging. The poor transferability of force field methods is probably one reason to explain why machine-learning potential methods (e.g., ANI[32]) get popular. Besides, although more advanced forms of force fields (e.g., polarizable force field and reactive force field) have been developed, using force field methods for complex chemical reactions, such as reactions in which different electronic states and conical intersection are involved, remains a challenge. Another intrinsic drawback is that force field methods do not perform well for chemical systems in which quantum effects (e.g., quantum tunnelling[33] and quantum nuclear effects[34]) are important. Thus, explicit solvent simulation is not always superior to implicit solvent models, as outlined in a recent joint study from Nau, Grimme, Gilson and co-workers on the hydrophobe challenge,[35] as well as a recent work from Ho and co-workers.[36] Among all force field methods, the polarizable force field is particularly essential for studying the electrostatic catalysis in this thesis. More details about this are presented in Section 2.2 and Chapter 4.

(3) Explicit solvent simulations with quantum chemistry methods. This method combines the advantages of (1) and (2) and it is becoming increasingly popular. One example is AIMD simulation.[37] Because such methods are computationally intensive compared to classical MD, the use of this method remains limited by the system size and simulation time. Thus, many approximations are introduced on the basis of AIMD. First, the *ab initio* methods can be replaced with cheaper electronic structure methods including semi-empirical PM7, DFTB and GFN-XTB methods (e.g., see respectively Ref.[38] for PM7-MD, Ref.[39] for DFTB-MD and Ref.[40] for GFN-XTB-MD). In addition to, FMO-MD represents another method to reduce computational costs.[41] Other approximations include the EFP method[42], SMFA method[43] and GEBF method[44]. More detailed explanations of above concepts can be found in corresponding references and also in section 2.2 and chapter 5.

(4) Multi-scale methods. Multi-scale philosophy provides a good balance between computational accuracy and costs. One example is using QM/MM-MD methods[45, 46]

to replace AIMD methods mentioned above. Another multi-scale protocol is to run MD simulations with a relatively cheaper method while calculating the energies with a more accurate and expensive method using a set of configurations taken from the MD simulation. For example, the use of the so-called quantum chemical cluster method is widely used in modelling enzymatic reactions.[47] Similarly, S-QM/MM method was proposed by Canuto and co-workers[48]. Additionally, multi-scale methods can be used in different parts of one computational protocol, for example, we can run MD simulations with QM/MM methods while calculating energies using QM/QM' methods. However, further development of multi-scale methods is needed as current methods still have issues. For example, Cui and co-workers listed a few issues with QM/MM methods for biomolecular modelling.[49] It was concluded that more efficient and accurate choices of QM region size, potential function and free energy calculation methods are important. Moreover, current treatment of long-range interactions and polarization effects also can be improved. Among all multi-scale methods, ONIOM is the most widely used, more details are presented in Section 2.2, Chapter 4 and Chapter 5.

(5) Other aspects. Besides equilibrium solvation, non-equilibrium solvation is important in the study of superfast processes, such as electronic excited state and electron-transfer reactions in solution.[50–53] Nuclear quantum effect is another aspect which has gained increasing attention recently.[54] Quantum dynamic simulation techniques have been applied to study various chemical properties.[55, 56] Recently, ML and cheminformatics techniques have been applied to many aspects of solvation modelling.[57–61] Particularly, the recent development of DPMD techniques pushed the limits of AIMD up to 100 million atoms.[62] Solvation modelling methods (both implicit and explicit) have been implemented using GPU.[63, 64]

Above is a brief introduction to different computational methods for solvation modelling. These solvation modelling techniques have been applied to various chemical properties and reactions, including those particularly relevant to this thesis (e.g., pK_a values, redox potentials, electrostatic catalysis). As this thesis mainly focuses on solvation modelling and electrostatic catalysis, explaining all the above methods in details is beyond the scope. More specific introductions to these methods can be found in corresponding references. However, for methods which are important to this thesis, e.g., polarizable force field and implicit solvent models, their theories will be elaborated in following chapters.

It is worthwhile to note that although we mainly focus on a few properties (pK_a, redox potential, photochemistry properties) in measuring the accuracy of solvation modelling, there are many other critical properties that benefit from accurate solvation modelling. For example, partition coefficient between different solvents is closely related with the accuracy of solvation free energy and hydrophobic/hydrophilic properties of chemical compounds.[65] We also need to mention that the focus of this chapter is to discuss the accuracy of solvation modelling and solvent effects on these chemical properties. However, we do not analyse the details of these applications. For example, solvatochromic shift is one active research topic for both computational and experimental chemistry,[66, 67] while we investigate how the accuracy of solvation free energies influence calculated vertical excitation energies, we will not introduce details of other aspects of photochemistry, e.g., nonadiabatic photochemistry, which itself is a large field and beyonds the scope of a PhD thesis. As a contrast, we introduce theories of pK_a with more details than other properties because it is directly related with the contents in Chapter 3.

2.2 Publication 1

Recent Advances in Solvation Modelling Applications: Chemical Properties, Reaction Mechanisms and Catalysis

Longkun Xu, Michelle L. Coote
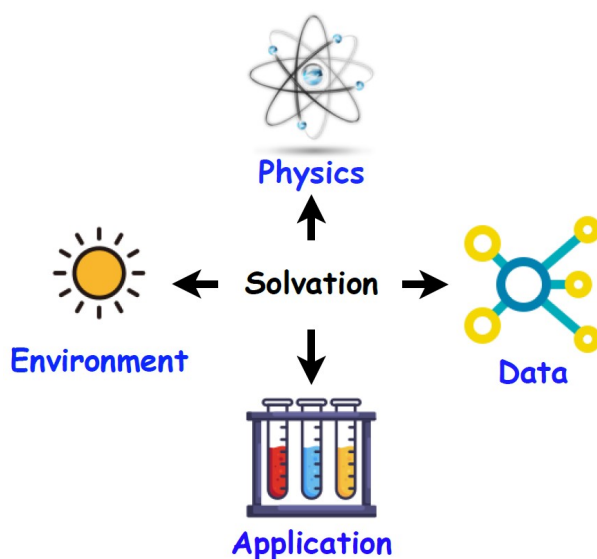
This publication is a manuscript submitted for peer review for the invited review of *Annual Reports in Computational Chemistry*. I reviewed the literature and wrote the draft manuscripts. Prof. Michelle Coote assisted with the direction of the review and corrected my drafts. The document for the statement of contributions is placed in the Appendix.

Recent Advances in Solvation Modelling Applications: Chemical Properties, Reaction Mechanisms and Catalysis

Longkun Xu and Michelle L. Coote*

Research School of Chemistry, Australian National University, Canberra, Australian Capital Territory 2601, Australia

E-mail: michelle.coote@anu.edu.au

Abstract: In this work we review recent studies in the field of computational solvation. Methods at different scales from ab initio to force field calculations with both implicit solvent and explicit solvent modelling are covered. Developments in data science and computer hardware are also highlighted, as are solvation databases, recommended parameters and benchmarking results. Recent applications employing different solvation modelling techniques are showcases, and remaining challenges are discussed.

1

1. Introduction

While practical accurate quantum chemical methodologies for predicting chemical behaviour in a vacuum are now routine, at least for the types of species typically found in molecular synthetic chemistry, most practical chemistry actually occurs in solution. Unfortunately, computational techniques for modelling reactions in solution are comparatively less well developed and typically remain the largest source of error in such calculations.[1-3] Indeed, our understanding of solvent effects at the microscopic level remains relatively limited. Even the structure of water is not well understood,[4] let alone more complex solvents such as ionic liquids (ILs),[5] deep eutectic solvents (DES)[6] and electrolyte solutions.[7]

Broadly speaking, there are two conceptually different approaches to modelling reactions in solution. The first is to focus on predicting the Gibbs free energy of solvation of various species, which can then be combined with accurate gas-phase calculations to predict behaviour in solution. The second is to focus on predicting the chemical behaviour in solution directly. In either case, there are many different computational techniques for modelling solvent, differing in their accuracy, complexity and computational cost, and ranging from simple continuum model approximations,[8-11] to large-scale simulations of ensembles of explicit solvent molecules[12-15] to macroscopic methods such as computational fluid dynamics techniques.[16] Solvent is modelled using a wide range of computational methods including quantum dynamics (e.g., ring polymer and path integral molecular dynamics ~~molecular dynamics~~),[17] ab initio [18] and density functional theory (DFT) quantum mechanical (QM) methods,[19] tight-binding[20] and semi-empirical QM methods,[21-22] multi-scale methods with different embedding schemes,[23] fragmentation methods,[24] force field methods (classical force field, polarizable force field and reactive force field),[25-29] and Coarse-Grained (CG) methods.[30-31] With the development of data science, cheminformatics and machine learning (ML) methods are also becoming important.[32] Solvent modelling using graphics processing units (GPUs)[33] are also emerging. Almost all of these approaches can be used with both implicit and explicit solvent simulations, and nearly all methods can be combined with static calculations and dynamic simulations, which generates a wide choice of methodology.

Owing to their importance, computational solvation methods have been extensively reviewed. In the case of implicit solvent models, we draw attention to the classic reviews by Tomasi and co-workers,[8] Cramer and Truhlar,[9] Klamt,[10] Orozco and Luque,[34] Mitchell and co-workers,[35] as well as an excellent recent update by Herbert.[36] For the explicit solvent simulations, we highlight the reviews of Jorgensen,[12] Mobley and co-workers,[13] Levy and Gallicchio,[14] Onufriev and Izadi.[15] These reviews extensively cover the theory and history of solvation modelling, and our aim is not to duplicate these. In the present work we instead focus primarily on the recent application of different computational methods to studying solvent effects on chemical reactions, with a particular emphasis on the important factors to consider when choosing computational methods for solvation modelling, and how these interplay with one another (see Figure 1). In what follows we first define the Gibbs free energy of solvation and discuss the sources and limitations of the solvation Gibbs free energies used for training and benchmarking solvation models. We then provide a brief overview of the different types of solvation models, with a focus on their assumptions, advantages, limitations and best practice recommendations, before finally highlighting some recent applications of solvation models in computational chemistry.
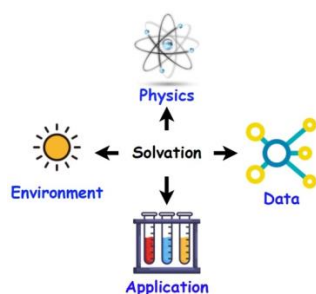
2

Figure 1. The main factors for solvation modelling
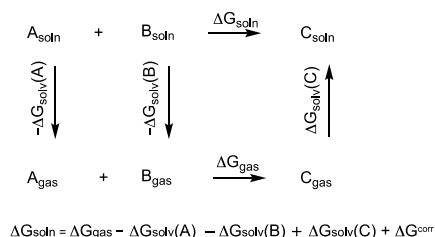
2 Solvation Gibbs Free Energy

The solvation Gibbs free energy represents the change in Gibbs free energy when a solute is transferred between the gas phase and solution phase at a specified temperature and pressure (equation 1). [37]

$$\Delta G_{solv} = G_{soln} - G_{gas} \qquad (1)$$

Solvation energies are often the focus of computational solvation modelling as they provide a means of converting gas-phase computational predictions, which can usually be made very accurately through the combination of electronic structure methods and ideal gas partition functions, to solution-phase predictions (Scheme 1). In applying such thermocycles one needs to pay close attention to the standard states at which the gas-phase Gibbs free reaction energy (ΔG_{gas}) and the various Gibbs free energies of solvation (ΔG_{solv}) are obtained. For example, ΔG_{gas} is typically calculated using ideal gas partition functions at a specified temperature (T) and pressure (P), whereas ΔG_{solv} is typically calculated for a standard state of 1 M. Before combining the two types of quantity in a thermodynamic cycle they need to be converted to the same standard state. Assuming, ideal gas behaviour, conversion of ΔG_{gas} at some specified T and P to a standard state of 1M is achieved by adding a correction term:

$$\Delta G^{corr} = \Delta nRT \ln \frac{RT}{P} \qquad (2)$$

where: Δn is the change in the number of molecules on either side of the equation and R is the universal gas constant. [38]

$$\Delta G_{soln} = \Delta G_{gas} - \Delta G_{solv}(A) - \Delta G_{solv}(B) + \Delta G_{solv}(C) + \Delta G^{corr}$$

Scheme 1. Thermocycle for converting gas-phase to solution-phase Gibbs free energies

3

Experimentally Gibbs free energies of solvation are determined by measuring the equilibrium constant for partition of a solute between the two phases in question, though in practice this can be difficult for species with low vapor pressures, and becomes impossible for species that are not stable in isolation (e.g., ions and unstable reactive intermediates). In those cases, so-called experimental solvation energies are obtained by comparison of experimental gas and solution-phase reaction energies, such as a comparison of gas-phase and solution-phase acidities. This yields an experimental value for the overall solvation energy contribution to a chemical reaction, which is then converted into a value for an individual species using experimental or computational values of the individual solvation energies of all of the other species in reaction to decouple their contributions.[39] Large databases such as the Minnesota Solvation Database (MNSOL)[39] have been compiled in this way and are used to both parameterize and to benchmark computational solvation models. Other useful databases include the recently updated FreeSolv database developed by Mobley and co-workers,[13] and the CombiSolv-QM and CombiSolv-Exp data bases, which are the basis of Vermeire and Green's proposed transfer-learning predictions.[40] Table 1 lists the main databases currently available. In addition to these, the CompSol databank of Privat and co-workers includes over 35,000 solvation chemical potentials, entropy and enthalpy data for 1969 pure species and 14102 binary mixtures, Acree and co-workers have presented a data base of partition coefficients for more than 2800 different solute-solvent combinations, and Driver and Hunter[41] have published a database of solvent similarity indices.

Table 1. An overview of popular data base of solvation free energies

Name	No. of Solutes	No. of Solvents	No. of Solvation Free Energies	Notes	Reference
MNSol-v2012	790	92	3037	The data base used for SMD development	Ref.[39]
FreeSolv (version 0.5)	643	1 (water)	643	Both experimental and computational data	Ref.[13]
CombiSolv-QM	11029	284	1 million	Calculated using COSMO-RS	Ref.[40]
CombiSolv-Exp	1368	291	10145	Compiled from publicly available databases.[13, 39, 42-43]	Ref.[40]

3 Brief Overview of Solvation Models and their Performance for Solvation Energies

In this section, we provide a brief overview of the types of solvation models available with a focus on their assumptions, advantages, limitations and best practice recommendations. Where available, benchmarking information on their accuracy for solvation energy predictions is also cited. For more detailed information on the models, the reader is referred to the original references and / or recent reviews which are cited as relevant.

3.1 Continuum Models
Theoretical Background. The simplest and most cost-effective approach to modelling solvation energies is using continuum models, in which one treats the solvent as an "implicit" continuous medium instead of an ensemble of individual "explicit" solvent molecules by constructing an effective Hamiltonian for the solute in the presence of a polarized dielectric.[8-11, 34, 36] In this way,

4

the complicated many-body interactions between solute and solvent molecules can be simplified as two-body interactions between solute and the polarizable medium. There are a number of methods used to model the electrostatic interactions between solute and solvent, the most popular of which is the apparent surface charge (ASC) scheme, in which the solute is embedded in a cavity with a charge density at its surface.[44] Because the polarization of the solute by the solvent is the same as the polarization of the solvent by the solute, then, given the solute charge density, the surface charge can be determined self-consistently by solution of Poisson's equation. There are a variety continuum models that vary in the way in which the surface charges are defined, the approximations used to solve the resulting macroscopic Poisson equation, and the nature of any additional so-called non-electrostatic terms that are also often included in the total solvation energy. Important examples include the original PCM model[45] model[45-46] and its integral equation formalism IEF-PCM[47], the original conductor-like screening model COSMO[48] and its closely related variant C-PCM,[49] and the Minnesota solvent models (SMx, e.g. x=6[50], 8[51], D[52]). COSMO-RS[34-37] is considered a semi-implicit solvent model in that it uses an initial COSMO calculation to generate a set of screening charges that are then used to calculate the chemical potential or the solution free energy of the solute via a statistical mechanical procedure involving the interacting screening charges of the solute and solvent molecule. For detailed descriptions of these and related continuum solvent methods we refer the reader to the original references or recent reviews.[8-11, 34, 36]

Level of Theory. When using continuum models to calculate solvation energies, a number of factors can affect the final result, as have been highlighted by several authors.[38, 53-64] In understanding these influences, it is important to note that, while the models themselves are based on physical principles, they are ultimately semi-empirical in nature, containing parameters such as radii, that are ultimately tuned by fitting solvation Gibbs free energy predictions to corresponding experimental data. Thus, their accuracy is usually maximized when applied to systems that are similar to their original training sets and used at the same level of theory for which they were originally parameterized. As an example, Table 2 collects the recommended theoretical levels as used when parameterizing the original SMD model.[52] For this model and others, improving the level theory beyond the parameterization level does not always lead to improved performance as the parameters may implicitly already be correcting the underlying errors in the electronic structure method.[38, 65-66] At the same, benchmarking reveals that improvements are sometimes needed, especially if explicit solvent molecules are included and/or systems differ substantially from the original parameterization training sets.[65, 67] Thus, while the default recommendation is to apply continuum methods at their parameterization level, benchmarking is advisable, particularly if explicit solvent is involved.

Table 2. Recommended theoretical levels for SMD solvation free energies

Solute/Solvent Combinations	Recommended Theoretical Levels	Note
All neutral solute/solvent combinations	M052X/6-31G(d)	More details can be found in Table 7 and Table 8 in Ref.[52]
Cations in acetonitrile	M052X/6-31+G(d,p)	More details can be found in Table 10 in Ref.[52]
Anions in acetonitrile	B3LYP/6-31G(d)	
Cations in DMSO	M052X/6-31+G(d,p) [a]	
Anions in DMSO	M052X/6-31+G(d,p)	
Cations in methanol	M052X/MIDI!6D	

5

Anions in methanol	M052X/6-31G(d)	
Cations in water	M052X/6-31+G(d,p) [a]	
Anions in water	HF/6-31G(d) [a]	

[a] SM8 performs better than SMD

Approximations for Large-Scale Systems. Although standard implicit solvent models should be used with the DFT or HF methods for which they are parameterized, there are implementations of implicit solvent models with lower-level methods for studying larger systems. For example, the COSMO solvent model was implemented in MOPAC to allow COSMO-PM6 and COSMO-PM7 calculations.[68] Jensen and co-workers implemented SMD with semi-empirical methods and tested the performance using the MNSOL data base, concluding that the errors obtained were unsurprisingly larger than that when using DFT but could be improved by re-optimizing the radii.[69] Implicit solvent models have also been used with QM-based fragmentation methods. For example, Okiyama and co-workers developed the FMO-PBSA method which combines the fragment molecular orbital (FMO) method with an implicit solvent model based on the Poisson Boltzmann surface area (PBSA).[70-71] Fedorov and co-workers developed a solvent screening model for the molecular electrostatic potential based on FMO method, which was applied to study proteins.[72] Collins and Ho employed the systematic molecular fragmentation by annihilation (SMFA) method to calculate the solute-solvent interactions for a system consisting of one solute in 160 water molecules, the authors found with their fragmentation method, the computational costs can be decreased by 14 times compared with the full QM brute force calculation.[73] Another strategy for large-scale QM simulations is the linear-scaling DFT method, using the Order-N Electronic Total Energy Package (ONETEP).[74] Recently it was shown by Skylaris and co-workers that linear-scaling DFT can be used with continuum solvent simulation to simulate electrolyte solutions, which is useful for electrochemical studies.[75] For complex large-scale systems, for example solid-liquid interface, methods have also been developed to efficiently model both the solid slab and continuum solvent.[76] All of the above three families of methods provide options for employing implicit solvent models on large systems.

Cavity-Scaling. While some solvent models, such as SMD,[52] have been parameterized using solvation data for a wide range of solvents, others were originally parameterized to solvation data for a more limited range (e.g., PCM-UAHF was parameterized against aqueous solvation energies only[77]). The electrostatic scaling factor (ESF)[8] was introduced to improve the accuracy of continuum models by scaling their radii for different solvents and different ion-types (i.e., treating cations, anions and neutral separately). ESF values are typically determined by fitting predicted solvation energies, or other solvent dependent properties such as pK_a values or redox potentials, to experimental data.[56, 58-60, 78-102] In doing this, one needs to be careful that the ESF is not correcting for other errors in the calculation. For instance, if fitting to redox potentials or pK_a values, one needs to ensure that the correction is correcting only for errors in the solvation energies, and not for errors arising from the use of an inadequate level of theory to model the bond breaking processes in the chemical reaction. Nonetheless, when done carefully, it is clear that ESF can improve accuracy for some solvent models, though reassuringly they are less important for models such as SMD[52] that are parameterized on a broad range of solvents.[65] In Table 3 we collect a series of recommended ESF values.

6

Table 3. Summary of recommended ESF values

Solute Type	Solvent Type	Quantity	Solvent Model	ESF	Note
Neutral molecules	Acetonitrile	Solvation free energy	IEFPCM/HF/6-31G(d) using UAHF radii	1.2	The results are taken from Ref. [66]. This same reference[66] also provides corresponding ESF values for: IEFPCM-UAKS/PBE1PBE/6-31G(d) CPCM-UAHF/HF/6-31G(d) CPCM-UAKS/PBE1PBE/6-31G(d).
	Aniline			1.1	
	Benzene			1.1	
	carbon tetrachloride			1.0	
	Chlorobenzene			1.1	
	Chloroform			1.1	
	Cyclohexane			1.1	
	Dichloroethane			1.2	
	Diethyl ether			1.1	
	Dimethyl sulfoxide			1.3	
	Ethanol			1.4	
	Heptane			1.1	
	Methylene chloride			1.2	
	Nitromethane			1.3	
	Octanol			1.1	
	Tetrahydrofuran			1.2	
	Toluene			1.1	
	water			1.2	
Neutral molecules	Carbon tetrachloride	Transfer free energy		2.1	
	Benzene			1.6	
	Chlorobenzene			1.4	
	Chloroform			1.5	
	Cyclohexane			1.2	
	Dichloroethane			1.2	
	Diethyl ether			1.5	
	Heptane			1.2	
	Octanol			2.1	
CHNO cations	Acetonitrile	Solvation free energy		1.1	
Other cations				1.1	
CHNO anions				1.5	
Other anions				1.4	
CHNO cations	Dimethyl Sulfoxide			1.1	
CHNO anions				1.5	
Other anions				1.5	
CHNO cations	Water			1.2	
Other cations					
CHNO anions					

7

Other anions					
Organic univalent anions	Dimethylformamide	Solvation free energy	IEFPCM/HF/6-31+G(d,p) with GAMESS radii	1.39	Taken from Ref.[59]
	Acetonitrile			1.36	
Anions	Dimethyl Sulfoxide	Solvation free energy	IEFPCM/HF/6-31+G(d,p) with GAMESS radii	1.35	Taken from Ref.[56]
Both neutral and anionic compounds	Dimethyl Sulfoxide	Solvation free energy	PCM/HF/6-31+G(d,p) with Bondi radii	1.35	Taken from Ref.[57]
Organic acids	Acetonitrile	pK_a	PCM/B3LYP/6-31+G(d,p) with Bondi radii	1.2	Taken from Ref.[58]
Nitroxides	Acetonitrile	Redox potential	PCM/B3LYP/6-31G(d) with UAKS radii	1.45	Taken from Ref.[60]
Amino acid side-chain analogues	Water	Solvation free energy	IEFPCM with different theoretical levels using UAKS radii	1.2	Taken from Ref.[61]

Thermocycles versus Direct Calculation. Another complication with continuum models is the treatment of any structural changes that occur upon solvation. By construction, continuum models calculate the Gibbs free energy of solvation as the difference in the electronic energies in the presence and absence of the solvent field, plus any non-electrostatic terms. These are then parameterized to experimental Gibbs free energies of solvation. The implicit assumption is that any differences between the solution-phase and gas-phase thermal and entropic contributions either cancel, or are built into the non-electrostatic terms when present in the model, or are otherwise implicitly built into the electronic energy in the solution phase through its parameterization.[38] Either way, this is likely to be reasonable for small rigid molecules whose structure does not significantly change upon solvation, but is expected to be problematic for larger, more flexible molecules, particularly those (such as amino acids) whose solution-phase structure is not stable in the gas phase and vice versa.[62, 103] Because solvation energies are calculated from the difference of solution- and gas-phase electronic energies, allowing the geometry to change between gas and solution is possible in principle, but in practice errors tend to be significant if large structural changes occur upon solvation.[53, 62]

As a result, when geometries change substantially upon solvation other approaches are often used. These include by-passing solvation energies altogether and calculating Gibbs free energies in solution directly from the energies, geometries and frequencies calculated in the presence of the solvent field using ideal gas-phase partition functions. This is known as the direct method, and can be very effective for modelling reactions in solution.[53] When using this approach, one must remember that the ideal gas partition functions are typically defined for a standard state of some temperature (T) and pressure (P), whereas solution-phase Gibbs free energies are defined for a standard state of 1M, and so the change of state correction term (equation 2 above) needs to be included even though the partition functions use solution-phase geometries and frequencies.[38]

Another approach is to attempt to minimize the structural changes between the gas- and solution-phases by stabilizing the solution-phase structure in the gas-phase using explicit solvent molecules, and by basing all calculations within the thermodynamic cycle on the solution-phase conformer of this solute-solvent complex. This approach, known as a cluster-continuum model, has the added advantage of incorporating explicit solute-solvent interactions, and helps to improve the accuracy

8

of thermocycle approaches to solution-phase Gibbs free reaction barriers and energies.[104] However, by incorporating explicit solvent molecules in the gas- and solution-phase calculations, the Gibbs free energy changes are no longer strictly Gibbs free energies of solvation, comparable to experimental data. Moreover, as noted below, because continuum models are parameterized in the absence of explicit solvent molecules, introducing them in conjunction with a solvent field introduces possibility of "double counting" and uncertainty over when, where and how many explicit solvent molecules are needed for a given problem.[99, 105-110]

Temperature and Pressure Effects. Most continuum models are parameterized against experimental solvation Gibbs free energies at room temperature and pressure, and their predictions should strictly be limited to those conditions. However, some models have been developed to take account of temperature and/or pressure, albeit with some limitations in scope or functionality. A more specific review about the quantum chemical modelling of pressure effects was recently presented by Stauch.[111] Among the available methods, Levesque and co-workers developed a method to include the pressure effects simply by computing an optimized ~~V~~van der Walls volume of the solute and removing the ~~undue~~ free energy to create such volume in the fluid. The accuracy of obtained hydration free energies of a benchmark of small neutral drug-like molecules was shown to reach the accuracy of more time-consuming molecular simulations.[112] Cammi[113-114] introduced a modified version of PCM, called XP-PCM, in which effects of high pressure are introduced reducing the cavity size, increasing the step potential at the boundary between the solute and the solvent, and by increasing the density and dielectric permittivity of the solvent. COSMO-RS[34-37] is often regarded as one of the most successful implicit solvation models for both pressure-dependent and temperature-dependent solvation properties.[115] In this model, temperature and pressure is incorporated through a statistical mechanical procedure involving the interacting screening charges of the solute and that of the solvent molecule. Liu and Eisenberg presented a Poisson-Fermi-based method to model ionic solvation at variable temperature.[116] Models such as SM8T[117] introduce temperature dependence to continuum models by parameterizing to temperature dependent training data for systems, and accounting for the known temperature dependence of parameters such as the solvent dielectric constant. Models such as these can be very accurate,[118] but their applicability is limited to the types of solute-solvent systems for which temperature-dependent experimental data is available for model training.

Benchmarking. With a large number of available implicit solvent models and tuneable parameters, it is natural to conduct comparisons between different solvation models. Table 4 summarizes ~~the~~ some recent comparisons of QM based implicit solvent calculations, while benchmarking of MD based implicit solvent models, we recommended the work of Knight and Brooks,[119] and the work of Van der Spoel and co-workers.[120] It needs to be noted explicitly that the performance of different implicit solvent models is heavily dependent on the computational details, the parameters used and the solute/solvent combinations tested. Thus, it is not meaningful to conclude which implicit solvent model is the best without a specific context. Nevertheless, some general insights can be obtained from these comparisons. The comparison in Ref.[121] suggests SMD performs much better than generalized Born (GB) and Poisson–Boltzmann (PB) models, due to SMD's inclusion of the non-electrostatic contribution to solvation free energy. The comparison in Ref.[66] suggests SMD performs better than CPCM-UAHF and COSMO-RS. However, for the solvation free energy of ions, the accuracy of all three models is not satisfactory, which is one direction for future development of implicit solvent models. In contrast, the comparison in Ref.[122] suggests the newly developed uESE model is more accurate than SMD, especially for ions.

Table 4. Benchmarking Information for different implicit solvation models.

Test Set	Solvation Model	Accuracy	Note
228 combinations of neutral organic solvents and solutes	PB	Correlation R=0.51 ± 0.05	We only present the best performer respectively for GB and SMD family. Results were taken from Table 1 of Ref.[121]
	GB-OBC-II	Correlation R=0.25 ± 0.06	
	SMD/M062X/6-31+G(d,p)	Correlation R=0.77 ± 0.03	
82 combinations of organic molecules (both neutral species and ions) in two solvents (water and acetonitrile)	CPCM-UAHF	Mean absolute error = 1.32 kcal/mol for neutral species and 6.33 kcal/mol for ions	Results are taken from Ref.[66]
	SMD	Mean absolute error = 0.82 kcal/mol for neutral species and 5.31 kcal/mol for ions	
	COSMO-RS	Mean absolute error = 0.79 kcal/mol for neutral species and 8.36 kcal/mol for ions	
2892 combinations of solutes in 92 solvents	SMD	Mean absolute error=1.33 kcal/mol	The mean absolute error is calculated using the data in Ref.[122] where more specific results of each solute and solvent type are presented.
	uESE	Mean absolute error=1.16 kcal/mol	
55 solutes in 1-octanol and water	SMD	Mean absolute error=2.70 kJ/mol in 1-octanol and 1.90 kJ/mol in water	Results are taken from Table 1 in Ref.[123]
	SM8	Mean absolute error=2.24 kJ/mol in 1-octanol and 2.08 kJ/mol in water	
	SM12-MK	Mean absolute error=5.46 kJ/mol in 1-octanol and 5.91 kJ/mol in water	
	SM12-CM5	Mean absolute error=1.84 kJ/mol in 1-octanol and 2.25 kJ/mol in water	
	COSMO-RS	Mean absolute error=1.97 kJ/mol in 1-octanol and 1.92 kJ/mol in water	

3.2. Explicit Solvent Models

The alternative to approximating the solvent as a continuum, is to model a solute in a large ensemble of explicit solvent molecules. Similar to implicit solvent calculations, explicit solvent

simulations can be treated as part of a thermodynamic cycle, or can be used to study reactions in solution directly. Although most works use direct method, recent examples of the thermodynamic cycle method can be seen in Ref. [124-125], in which the authors calculated the gas-phase reaction energies using accurate quantum chemical methods while the solvation free energies were calculated with free energy perturbation (FEP) methods. Either way, in order to deal with the size and complexity of such a system, various approximations are required, both with respect to the level of theory used for the ensemble and the conformational sampling process. Clearly it is not feasible to directly study the long-time dynamics of chemical reactions in ensembles of 100s of solvent molecules at high levels of theory (e.g., complete basis set coupled cluster theory), while also ensuring the complete conformational space of the solute/solvent ensemble is sampled. Simplifications need to be made, the most important being the choice of method, the sampling approach and the system size.[126] In this section, we outline the three main conceptual approaches to explicit solvent modelling (~~molecular dynamics~~MD, quantum chemistry, and multi-scale approaches), and then discuss the various sampling methods used.

~~Molecular Dynamics~~Molecular Dynamics. ~~Molecular dynamics~~MD ~~(MD)~~ using classical force fields are the most commonly used to study explicit solvent. The force field describes both bonded and non-bonded interactions between particles and associated potential energy with parameter sets, which are optimized by fitting to experimental data or directly calculated via quantum chemical calculations. Their functional forms can be different in different force fields. For water, the most important solvent, several force fields were developed specifically, for example TIP3P,[127] TIP4P,[128] SPC/E[129] and their derivatives. Recent comparisons of these water force fields can be found in Ref.[130] While for more general organic compounds, ~~p~~Popular force fields include AMBER,[131] CHARMM[132] and OPLS-AA.[133] One drawback of these classical force fields is that the fixed-charge scheme cannot properly describe the polarization effects within the system. To solve this problem, several polarizable force fields[134-135] have been proposed, including the fluctuating point charge method,[136] induced dipole method (e.g., the AMOEBA force field)[27], the Drude oscillator method[137] and the recently developed GFN-FF.[138] A massively parallel polarizable force field was recently implemented in the Tinker-HP program.[139] Variants of these polarizable force fields have been developed for special cases, such as ionic liquids (CL&Pol[140-141] and OPLS-2009IL[142], for a review see Ref.[143]), biomolecular systems,[144] and for use with implicit solvent models.[145] Classical or polarizable MD can be further simplified by introducing the coarse-grained approximation, in which a subgroups of atoms are simulated as single interaction site. The most popular method in this regard is the series of Martini force fields.[146-147] At the other extreme, to model chemical reactions where bond breaking and forming occurs, reactive force fields such as ReaxFF[29] have been developed. Another approach is using the machine learning techniques to develop force field (e.g., ANI-1[148]) or directly generate the potentials and forces (e.g., deep-potential ~~molecular dynamics~~MD (DPMD)[149]).

The choice of force field can significantly influence the accuracy of calculated solvation free energies. The recent works of Hunenberger and co-workers compared the performance of 9 force fields from the GROMOS, CHARMM, OPLS, AMBER, and OpenFF families using the experimental cross-solvation free energies. After a comprehensive benchmark, the authors found GROMOS-2016H66 and OPLS-AA force field afforded the best accuracy with the root-mean-square errors (RMSEs) as low as 2.9 kJ/mol (see Figure 2).[150-151] Procacci and co-workers compared different force field types for the solvation free energy and octanol/water partition coefficients of drug-like organic molecules, it was found that the GAFF2/SPCE combination gave the best results.[152] Again, we caution that the conclusion of computational method benchmarking is dependent on the computational details, especially for force-field based calculations, in which the variables are many.
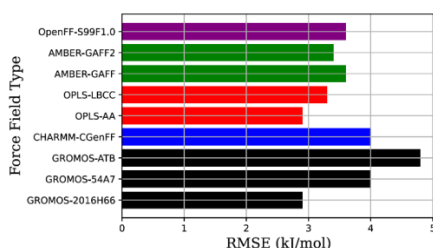
Figure 2. Calculated ~~root mean square error (~~RMSE~~)~~ for solvation free energies obtained with different force fields, original results and more details can be found from Table 2 in Ref.[150]

All of the parameters of a force field can influence the accuracy of explicit solvation models; here we highlight a few critically important ones. Atomic charge is a common parameter in all force fields, and a focus for including polarization effects. For example, Kelly and Smith developed the alchemically polarized charges (APolQ) method which includes the polarization effects via tuning the partial charges and the tests gave satisfactory accuracy.[153] The choice of partial charge should be based on both the force field type and the studied property. For example, for the OPLS-AA force field, three schemes (i.e., 1.2*CM5, 1.14*CM1A and 1.14*CM1A-LBCC) for calculating partial charges are frequently used. In the work of Jorgensen and co-workers,[154] the performance these charge schemes were compared (see Table 5). After the localized bond charge corrections (LBCC) were introduced, the performance of 1.14*CM1A-LBCC was the best for the predicting hydration free energies, but the worst for heats of vaporization and densities, for which 1.2*CM5 was recommended instead (see Table 5). This is just one example to show the role of partial charge in force field-based calculations. Some partial charge schemes are widely used due to their good balance and excellent performance for key chemical properties. For instance, the Merz-Kollman[155] and RESP[156] charges are widely used due to their advantages for the electrostatic potential.

Table 5. The mean absolute deviations using different partial charge schemes with the OPLS-AA force field.[a]

	Hydration Free Energies kcal· mol^{-1}	Heat of Vaporization kcal· mol^{-1}	Densities g·cm^{-3}
1.14*CM1A	1.26	1.40	23.79
1.14*CM1A-LBCC	0.61	1.40	24.41
1.2*CM5	1.21	1.20	21.50

[a] Original results and more details can be found in Ref.[154]

Another key parameter in force fields is the atomic polarizability, which is important for polarizable force fields. It is well-known that polarization effects are crucial for improving the accuracy of solvation free energies.[157] For instance, York and co-workers compared a set of QM/MM protocols to calculate the hydration free energies with and without the Drude oscillator model, with the authors finding that the use of polarizable force field and the choice of QM methods are both important.[158] N~~gooskov~~ and co-workers employed both the Drude polarizable force field and non-polarizable CHARMM force field to analyze the protein hydration, finding that the polarizable force field can produce more accurate hydration free energies and protein-water interactions.[159] An

extensive list of the atomic polarizabilities for different atom types of organic molecules can be found in Table 1 of Ref. [160]. For atomic polarizability values of ionic liquids, we recommend the results in Table 2 and Table 3 of Schröder and co-workers.[161] Table 6 collects the atomic polarizability values of key atom types from Ref. [160-161]. Like other parameters in force fields, the atomic polarizability of atom types not included in Table 6 can be calculated with accurate quantum chemical methods or machine learning techniques. Example protocols can respectively be found in the work of Schröder and co-workers,[161] and the work of Schröder, MacKerell and co-workers.[162]

Table 6. Recommended atomic polarizability values taken from Ref.[160-161]

Atom Type	Atomic Polarizability Å^3	Atom Type of Ionic Liquids	Atomic Polarizability of Ionic Liquids
C in alkane (CH3- or -CH2- or -CH<), carbonyl (aldehyde, amide, acid)	1.334	H	0.323
H in alkane (CH3- or -CH2- or -CH<), hydroxyl (water, alcohol), acid (HO), amine, amide nitrogen, sulfhydryl	0.496	B	0.578
O in hydroxyl (water, alcohol) and carbonyl (aldehyde, amide, acid)	0.496	C	1.016 for sp^3, 1.122 for cation sp^2, 1.432 for anion sp^2, 1.587 for SP
C in aromatic carbon	1.750	N	1.208 for cation, 1.698 for anion
H in aromatic (HC)	0.696	O	1.144
N in amine nitrogen (ammonia, amine) and amide nitrogen	1.073	F	0.625
S in sulfur	2.800	P	1.237

Quantum-Chemical Methods. Solute-solvent ensembles can be directly described using quantum chemical methods, e.g., the well-known Born–Oppenheimer MD,[163] ab initio MD (AIMD)[164] and Car–Parrinello MD methods[165]. The most frequently used method in this regard is DFT, which is computationally intensive for long-time dynamics of large systems. This cost can be reduced by making approximations, such as using semi-empirical methods (e.g., GFN2-XTB-MD[22]), fragmentation methods (e.g., FMO-MD[166]) or multi-scale methods (e.g., QM/MM-MD)[23]. One advantage of these methods is that the comparison between their accuracy is straightforward and less dependent on the choice of parameters compared with force field methods. Nonetheless, as these methods are typically more expensive, their description of the interactions may improve but this comes with a computational cost that leads to other compromises, such as system size and simulation length. For instance, although ~~in principle~~ AIMD methods can explain underlying physics for both static and dynamic properties of molecules (e.g., water[167-168]) because they are based on accurate QM methods, ~~are more accurate than force field methods~~, some studies have shown that a classical MD simulation with properly designed force field parameters can outperform QM methods, especially it was found that classical MD simulation with a long time scale is better than a shorter AIMD simulation.[169] In AIMD and its variants, the description of the interactions in the systems can be further improved by including the nuclear quantum effects,[170] with popular

13

methods including path integral ~~molecular dynamics~~MD (PIMD)[171] and ring polymer ~~molecular dynamics~~MD (RPMD).[172]

Multi-scale modelling. Multi-scale methods strike a good balance between computational costs and accuracy, and are widely used in explicit solvent calculations of solvation free energies. However, the choice of multi-scale scheme can affect the results. The most famous method is the ONIOM scheme of Morokuma, which can further be separated into three classes (i.e., mechanical embedding, electrostatic embedding and polarized embedding) according to which method is used to model the mutual polarization between two or more layers.[173-174] QM/MM can be carried out with classical force fields and polarizable force fields, with an introduction to the latter provided by Lipparini, Mennucci, Piquemal and co-workers.[175] Besides QM/MM, another multi-scale embedding method is QM/QM' methods which combine high level QM calculations with a low level QM' embedding, for example, wavefunction calculations in DFT environment (WF-in-DFT). There are many types of QM/QM' embedding schemes including the simple ONIOM QM/QM' scheme (where mutual polarization is conducted at QM' level), projection-based QM/QM' embedding,[176] and many other examples.[177-178] For a recent reviews of quantum mechanical embedding methods, we recommend the work of Schatz, Ratner and co-workers,[179] while an excellent review of QM/MM methods can be found in Ref. [180].

Sampling methods. The accuracy of explicit solvent modelling also depends heavily on the sampling methods used. One approach is end-point sampling, which as the name suggests samples only the end point of a simulation.[181-182] Popular end-point methods include the molecular mechanics ~~Poisson-Boltzmann~~PB surface area (MM/PBSA) and the molecular mechanics ~~generalized Born~~GB surface area (MM/GBSA), which are widely used for the calculations of solvation free energies and associated host-guest binding affinities and drug design.[182-184] However, in some cases, the accuracy of end-point sampling is poor, and more sophisticated approaches are necessary. One such family of methods are alchemical free energy calculations, which gradually mutate a subset of atoms of a system from the initial state to the final state, through a series of intermediate steps. Popular methods in this family include ~~free energy perturbation (~~FEP~~)~~,[185-186] and thermodynamic integration (TI)[187], and these two methods have been widely used for the calculations of solvation free energies. The other philosophy is to apply a bias potential based on collective variables, which makes it easier to reach the rare events at high energies. These so-called enhanced sampling methods are widely used to study reactions in solution. Popular methods in this family include metadynamics[188] and adaptive biasing force (ABF) method.[189] Although alchemical and enhanced sampling methods are often thought to be more accurate than end-point sampling methods, their computational costs are high, they can be subject to convergence issues and are generally more complex to use, although the development of tools like PLUMED[190] are helping to change this. For more detailed information on enhanced sampling methods and alchemical methods, the reader is referred to several extensive reviews in the literature.[191-195]

Alchemical methods and enhanced sampling methods have been widely used for the calculations of solvation free energies. To name just a few recent examples, Idrissi and co-workers employed metadynamics simulations to calculate the solvation free energy of a model cellobiose molecule in different solvent environments including water, ionic liquids, solvent mixture_s_ and supercritical CO_2.[196] Khuttan and co-workers developed a method which allows the solvation free energy to be calculated via a single concerted alchemical coupling step instead of the commonly used sequence of two distinct coupling steps for Lennard-Jones and electrostatic interactions.[197] Kelly and Smith developed a method which calculates the alchemical free energy via fixed-charge scheme in which the polarization effects are corrected via updating partial charges according to QM/MM calculations.[198] Procacci developed non-equilibrium alchemical methods for computing free

energies of solvation,[199] which was further applied to study the ligands of the SARS-CoV-2 main protease.[200] Recently Korshunova and Carloni employed the alchemical transformations within the Hamiltonian adaptive resolution scheme to study ligand binding affinities and hydration free energies.[201] Hernandez and co-workers developed the adaptive steered ~~molecular dynamics~~MD (ASMD) which reduces the number of trajectories that must be sampled by discarding those trajectories that have deviated far from the equilibrium path in stages.[202] Prasetyo and Hofer employed QM/MM-MD based TI method to calculate the hydration free energy of carbon dioxide in aqueous solution.[203]

The accuracy of end-point sampling methods, alchemical and enhanced sampling methods have been often compared. A good summary for MMPBSA and MMGBSA methods is provided in Table 1 of Ref. [181]. The conclusions therein provide more details about how the choice of parameters (e.g., simulation length, dielectric constant and radii set, etc.) affect the accuracy of end-point methods. The MMPBSA.py script developed by Roitberg and co-workers is one frequently used tool for efficient calculations of end-state free energies.[204] The accuracy of alchemical methods can be influenced by many parameters, and we refer the reader to the recent tutorial review of Mey, Chodera, Mobley, Shirts and co-workers.[205] Of particular note, a large number of windows should be used to reach a good accuracy of alchemical methods.[206] Effects of the choice of software packages on the reproducibility of alchemical calculations have been reported by Loeffler and co-workers.[207] The recent review of Aitchison, Luo and co-workers highlights the important factors for end-point methods and alchemical methods on solvation modelling, binding free energies and associated drug discovery.[208] Sun and co-workers highlighted the importance of both sampling methods and force field types, comparing the performance of end-point methods (MM/PBSA and MM/GBSA) and alchemical methods (TI and MBAR) with both the AMBER14SB and AMBER19SB force fields.[209] Their main results are collected in Figure 3, which highlights the advantages of alchemical methods and the effects of force field types.
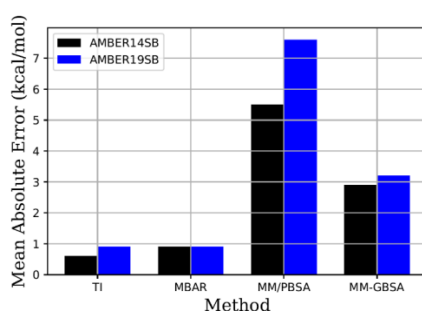

Figure 3. Mean absolute error (MAE, unit in kcal/mol) of free energy differences. Original data and more details can be found in Ref.[209]

3.4 Comparison between Implicit and Explicit Solvent Simulations

Implicit solvent models and explicit solvent simulations each have their own advantages and drawbacks. There are some studies comparing the performance of the two approaches for the calculation of solvation free energies. Inevitably, each conclusion is usually different and depends on many factors including computational details and the systems under study. For example, Wang,

van der Spoel and co-workers[121] found that the implicit solvent models are relatively poor compared with the explicit solvent simulation. While it is often believed that the accuracy of explicit solvent simulations is more accurate and can be used as benchmarking data for the development of implicit solvent models,[120, 210] sometimes implicit solvent models can give excellent results. For example, Ho and co-workers[125] compared different implicit solvent models and explicit solvent simulation (FEP~~free energy perturbation~~), using the Menschutkin reaction as the test system. The authors found the explicit solvent simulation gives a much larger error compared with implicit solvent models due to the Lennard-Jones parameters, a finding also reported in the work of Mobley and co-workers.[211] The error could be addressed via the end-state MM to QM correction. The good performance of implicit solvent models in the prediction of octanol–water partition coefficients was also observed by Kundi and Ho.[123] Lee, Lim and Kim compared implicit and explicit solvent simulation of hydration free energy of non-polar solutes and provide insights into the further development of implicit solvent models.[212] Steinmann and co-workers compared implicit and explicit solvation models for solvation free energies at the water/Ru(0001) interface.[213] Both implicit solvent models and MM-FEP calculations gave good results, but it was concluded that MM-FEP would be more easily generalized to other solvents. Additionally, polarizing the subsystem before running MM-FEP calculations was shown to offer benefits. Gilson, Grimme, Nau and co-workers compared implicit and explicit solvent simulation using the HYDROPHOBE Challenge, i.e., host–guest binding of hydrocarbons to cucurbiturils.[214] It was found that QM methods can perform very well for predicting the absolute binding free energies, especially for small molecules in water. More recent works comparing implicit and explicit solvent simulation can be found in Ref. [215-217].

3.3. Machine Learning

Data science has been proposed as the fourth paradigm for scientific discovery,[218] and is growing in importance in chemistry aided by the curation extensive data sets of chemical properties such as *MoleculeNet*.[219] A range of different ~~machine learning (~~ML~~)~~ and deep learning techniques have been employed for solvation modelling. For example, Green and co-workers established an extensive data base of solvation free energies based on COSMO-RS calculations and employed transfer learning and directed-message passing neural network to improve out-of-sample predictions of solvation free energies.[40] Similarly, based on the calculational results of implicit solvent models and feed-forward neural networks, Alibakhshi and Hartke developed a method which can significantly increase the prediction accuracy of solvation free energies.[220] Based on gas-phase MD simulation and MM-PBSA calculations, Rauer and Bereau employed ML to predict hydration free energy of a large subset of the chemical space of small organic (CHNO) molecules, finding that the atomic-decomposition ansatz can offer significantly added transfer-ability.[221]

ML techniques have also been employed with QM/MM methods to predict the solvation free energies, for example, in the work of Yang and co-workers,[222] by using the gradient boosting algorithms, the authors address the challenges of insufficient sampling and updating ML models on-the-fly. Michel and co-workers employed FEP alchemical free energy calculations with ML methods to calculate the hydration free energies, and the results suggest that this method outperforms both pure ML predictions and pure FEP calculations. Riniker, Hansen and co-workers employed both MD simulation and different fingerprint/ML model combinations to predict the self-solvation free energies. The information taken from MD simulation includes intramolecular and intermolecular potential energy and its LJ and electrostatic components, radius of gyration and solvent-accessible surface area.[223] Llinas and co-workers combined ML with a 3D-RISM model to predict solvation free energy in multiple solvents, the authors concluded their method offers the possibility to predict solvation free energy of any solute in any solvent with root mean squared errors less than 1 kcal/mol.[224] ML techniques have also been applied to generate force field parameters (e.g., partial charge[225]) by training the model using high-quality QM results, and neural

16

networks have been used to aid the design of collective variables in enhanced sampling simulations.[226-227]

Without input from any calculations, Lim and Jung proposed the MLSolvA model in which a neural network was used to predict pairwise atomic interactions.[228] Similarly, Priyakumar and co-workers employed graph neural network methods to predict solvation free energies.[229] The features used in this work, which could guide for future related works, are collected in Table 7. With experimental descriptors of solvent and QM descriptors of solute, Adjiman and co-workers employed the quantitative structure property relationships (QSPRs) method to predict the solvation free energy of 295 solutes in 210 solvents with totally 1777 data points, the obtained accuracy of multivariate linear regression (MLR) methods yields a coefficient of determination (R^2) of 0.88 and a ~~root mean squared error (~~RMSE~~)~~ of 0.59 kcal/mol for the training set.[230]

Table 7. Atom (node) and bond (edge) features used for the graph neural network in Ref.[229]

Node Features	Description	Edge Features	Description
Atom type	H, C, N, O, F…	Bond type	Single, double, triple, aromatic
Implicit valence	Binary	Bond is in conjugation	Binary
Radical electrons	Binary	Bond is in ring	Binary
Chirality	R, S or none	Bond stereochemistry	E, Z
Number of hydrogens	Number		
Hybridization	sp, sp^2, sp^3, sp^3d		
Acidic	Binary		
Basic	Binary		
Aromatic	Binary		
Donor	Binary		
Acceptor	Binary		

3.4 Computer Hardware
Besides data science, the development of computer hardware is another engine for the innovation in computational chemistry. One example is the development of ~~graphics processing units (~~GPU~~)~~. One of the most famous contributions in this field is the TeraChem program[231] of Martinez and co-workers, which includes a GPU implementation of a polarizable continuum model.[232] Chen and co-workers implemented the ~~generalized Born~~GB with molecular volume and solvent accessible surface area (GBMV2/SA) implicit solvent model within the CHARMM/OpenMM module. The authors found the GPU acceleration offers 60 to 70-fold speedup on a single NVIDIA TITAN X (Pascal) graphics card for MD simulations of both folded and unstructured proteins of various sizes.[233] Huang and Simmerling compared the speed of GBSA solvation calculation on CPUs versus GPUs using the Amber program and they found an obvious speedup when GPU is used.[234] More specific reports of using GPU with the AMBER program can be seen in the work of Walker, York and co-workers.[235] Qi and Luo tested the robustness and efficiency of Poisson–Boltzmann modelling on GPU.[236]

3.5 Ongoing Challenges and Developments

Although implicit and explicit solvent simulation techniques have achieved great success, some challenges still remain, and these are the focus of ongoing method development. The first, is the relatively low accuracy of non-electrostatic solvation components, especially for implicit solvent models (see, for example, Table 4 above). Recent steps to address this problem include the implicit solvation using the superposition approximation (IS-SPA), which was recently been applied to study peptides by McCullagh and co-workers.[237] Pettitt and co-workers developed a method in which the nonpolar solvation free energy is calculated by TI method using proximal distribution functions (pDF)-reconstructed solute–solvent interaction energy, which produced satisfied accuracy.[238] Wenzel and co-workers employed a non-polar term with atom type dependent surface tension coefficients which is combined with an accurate ~~generalized Born~~GB term, the method gives satisfactory accuracy when compared with TIP3P water model.

The second challenge is that errors in solvation free energy calculations of ionic solutes (including the proton[239]) are usually much larger than that of neutral species, as can be seen in a recent extensive assessment conducted by Yin and co-workers.[240] Moreover, as explained in Section 2, the experimental Gibbs free energies of solvation for ions cannot be measured directly, and hence there is a lack of accurate training data for developing and benchmarking computational models. The structure of solvated ions (e.g., Li^+), which is particularly relevant for the design of batteries,[241] is a challenge for solvation models. The cluster model is often used for improving the accuracy of solvation free energies of ions, as recently demonstrated by Leonhard and co-workers.[242] Bardhan and co-workers introduced a nonlinear function of the local electric field and the microscopic interface potential (static potential) to the dielectric continuum model, which can be used to predict the solvation thermodynamics (free energy, entropy, heat capacities) and transfer free energy of ions in both solvent and water-cosolvent mixtures.[243] Duignan, Mundy and co-workers studied the solvation free energy of single ions using different protocols, the authors found that the Ewald summation in MD simulation needs to be corrected, the authors observed a good linear relationship between the single ion solvation free energy and charging free energies for cations while a small non-linearity for small anions.[244] In his review, Budkov summarized the contribution of developing statistical field theory of salt solutions of zwitterionic and multi-polar molecules.[245] Rempe and co-workers studied the solution free energies of metal ions employing quasi-chemical theory (QCT).[246] Slavicek and co-workers calculated the solvation free energy of ions using a modified ensemble cluster-continuum approach where the solvation free energy is estimated using the vertical quantities of a charged-neutralized system, and an ensemble of structures from MD simulation was used.[247] Masella and co-workers used the cluster pair approximation to calculate ion hydration free energies and water surface potential in water nano drops, with polarizable force fields based on an induced point dipole approach.[248] Hofer and Hunenberger successfully employed QM/MM-MD to study the solvation free energy of proton, sodium and potassium ions, where both ions and their first solvation shell are included in QM.[249] As shown in Table 4, the recently developed uESE solvation model performs particularly well for the solvation of ions.[250] Keith and co-workers employed static cluster calculations, ~~ and~~ sketch maps and a nonlinear dimensionality reduction algorithm~~the ML method~~ to predict the solvation free energies of ions, and the obtained results for different ions having charges 2^+, 1^+, 1^-, and 2^- agree well with the experimental reference.[251]

The third challenge is the solvation free energy calculations in complex solvent environments including the solvent mixtures, electrolyte solution, ionic liquids ~~(IL)~~, deep eutectic solvents ~~(DES)~~ and various interfaces (e.g., water-air, oil-water, etc).[252] For modelling solvent mixtures with QM based implicit solvent models, one method is to change the parameters of implicit solvent models (e.g., SMD) according to the fraction of solvent mixtures. For example, Hu and Luo presented a set

18

of parameters for DMSO-methanol binary solvent mixtures.[253] COSMO-RS is another well-known model for modelling the solvation properties in solvent mixtures.[10] Stein, Herbert and Head-Gordon introduced a linear approximation for weak electrostatic potentials, finite size of the mobile electrolyte ions, and a Stern-layer correction to the Poisson–Boltzmann model for implicit solvation of electrolyte solutions.[254] Luo and co-workers compared the performance of continuum solvation modelling with explicit solvent modelling and experimental reference, using the molality-dependent chemical potentials for sodium chloride (NaCl) electrolyte as the test. The authors found that the nonlinear PB method performs better than linear PB model, and inclusion of non-electrostatic components is essential.[255] Abdel-Azeim developed the force field for electrolyte solution within the framework of OPLS-AA.[256] Steinmann and co-workers developed the SolvHybrid method which performs QM/MM calculations of solvation free energy at the metal/water interface.[257] Force field methods have been developed and used to study the solvation of ions at interfaces, with the results comparing favourably to experimental surface tensions and other quantities.[258-259] ML techniques have also been applied to model hydrated properties and complex solvent environments. For example, Laidi and co-workers used neural networks and support vector machines to calculate the activity coefficient at infinite dilution of water in ionic liquids.[260] Donadio and co-workers showed how to use classical MD, AIMD, TDDFT and machine learning methods to study the absorption spectra of two phenolic molecules at the air-ice interface.[261]

4. Applications

Herein we provide a collection~~snapshot~~ of recent applications of solvation modelling, with a particular focus on applications for which the solvent modelling is a key and demanding component of the calculation.

4.1 pK_a

The pK_a of an acid is defined by equation (3), where K_a is the equilibrium constant for its deprotonation reaction:

$$\mathrm{p}K_a = -\log_{10}(K_a) \qquad (3)$$

The protonation state of a species is related to other aspects of its chemistry including ~~They can be used to determine the protonation state of the species, which is further related to other aspects of its chemistry including~~ its solubility, chemical reactivity, photochemistry, conformation, binding free energies, and biological activity ~~and so forth~~.[262-270] pK_a values are strongly affected by the solvent environment, and are normally determined experimentally by potentiometric or photometric titrations. However, these can be difficult or impossible to measure for reactive intermediates, for very strong acids, and for species in low polarity solvents or in complex environments such as at interfaces or within the active site of an enzyme. Computational predictions of the pK_a, particularly in these difficult cases, are thus critically important. Additionally ~~At the same time~~, ~~involving as they do charged species,~~ computation of pK_a values represents a difficult test of solvation models as charged species are involved.~~,~~ ~~H~~and h~~ence~~ pK_a values are frequently used to benchmark computational solvation models. Computational predictions of pK_a values have been extensively reviewed elsewhere,[105, 271-274] here we highlight some of ongoing issues ~~for field, as they relate to solvation energy calculations~~. As our focus in on solvation modelling, the use of machine learning and cheminformatics tools to predict pK_a values directly is beyond the scope of this work, which is also true for other applications hereafter.

Implicit Solvation. When using implicit solvation to calculate the pK_a values, one of the first decisions that needs to be made is whether to study the solution-phase reaction directly or using

19

a thermocycle (Figure 4). As explained in Section 3, both approaches offer advantages and disadvantages. The direct method has to assume that ideal gas partition functions are valid in solution, and one has to compromise between choosing a level of theory appropriate for modelling the bond breaking processes versus the parameterization level of the solvent model. In contrast, the thermocycle method avoids these problems, but has problems closing the thermocycle when the gas- and solution-phase structures are significantly different to one another. Ho investigated the relative performance of the direct and thermocycle approach for a test set of pK_a values and redox potentials, showing that the direct method indeed offered advantages for species such as amino acids, where the gas and solution phase species exist as different tautomers, but otherwise the approaches offered similar accuracy.[275] A similar conclusion was drawn by Haworth et al.[62] in benchmarking study of pK_a values of conformationally flexible amines, though this study also highlighted the need for isodesmic schemes and inclusion of explicit solvent molecules in order to achieve accurate results. These latter factors are now discussed in turn.

(a) Absolute pKa

$$HA_{soln} \xrightarrow{\Delta G_{soln}} H^+_{soln} + A^-_{soln}$$

(b) Proton Exchange

$$HA_{soln} + Ref^-_{soln} \xrightarrow{\Delta G_{soln}} HRef_{soln} + A^-_{soln}$$

$$HA_{gas} \xrightarrow{\Delta G_{gas}} H^+_{gas} + A^-_{gas}$$

$$HA_{gas} + Ref^-_{soln} \xrightarrow{\Delta G_{gas}} HRef_{gas} + A^-_{gas}$$

$$pK_a = \frac{\Delta G_{soln}}{RTln(10)}$$

$$pK_a = \frac{\Delta G_{soln}}{RTln(10)} + pK_a(HRef)$$
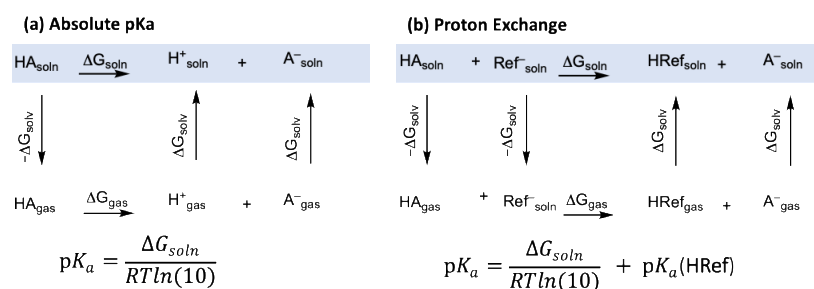
Figure 4. Thermodynamic cycles for (a) absolute or (b) relative pK_a calculations. In each case, the solution phase reaction (shaded blue) can be calculated directly (direct method) or via the thermocycle shown (thermocycle method).

Isodesmic schemes (Figure 4b) have been introduced to address some of larger sources of error when calculating pK_a values, particularly when using continuum models and/or low levels of theory. The basic idea is that rather than calculate the absolute acidity of a compound, one calculates the relative acidity via a proton exchange reaction with a reference acid, which has with an accurately known pK_a value in the same solvent. Provided the reference acid is structurally similar to the "analyte" one can expect systematic error cancellation, from both the bond breaking calculations and the solvation energies. Indeed, this systematic error cancellation can sometimes allow lower-cost semi-empirical methods to be used with reasonable accuracy.[276] Moreover, this approach avoids the need to calculate the proton, whose solvation energy can be a large source of error.[277] This is seen in Figure 5, which is based on data taken from an excellent recent review by Malloum and co-workers.[278] The principle disadvantage of the isodesmic method is that it requires an accurately known pK_a value for a reference acid in the same solvent. This becomes problematic for the prediction of pK_a values in low polarity solvents and other environments such as enzyme active sites that are difficult to study experimentally, which are precisely the types of conditions for which theory is often needed in the first place. Nonetheless, in such cases reference values can be obtained through more accurate calculations and/or using empirical schemes for the conversion of pK_a values between different solvents.[279]
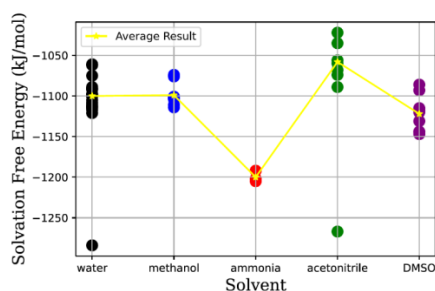
20

Figure 5. The reported solvation free energies of proton in different solvents. The average result in five solvents is respectively -1100, -1099, -1200, -1058 and -1122 kJ/mol.

The inclusion of one or more explicit solvent molecules in a so-called cluster-continuum or micro-solvation method is often considered to be necessary to improve the accuracy of pK_a calculations. However, there continue to be mixed results regarding when they are needed, and how they should be used. The original implicit-explicit[107] and cluster-continuum[280] schemes, shown in Figure 6, were designed for aqueous solution. The former mimics the absolute pK_a approach in Figure 4a, but with one or more explicit water molecules solvating the conjugate base (A⁻). This can be generalized to other solvents by replacing water with the relevant explicit solvent. The cluster continuum scheme in Figure 6b can be loosely thought of as the proton exchange analogue of the implicit-explicit model, albeit using water as both the reference acid as well as the explicit solvent. While this is less easily generalized to other solvents, there is a more general proton exchange version, suitable for any solvent and any reference acid, given by Figure 6c.[105] Unsurprisingly, the cluster continuum proton exchange method generally gives better results than using either the implicit-explicit method or the proton exchange method in isolation.[62, 105]

21
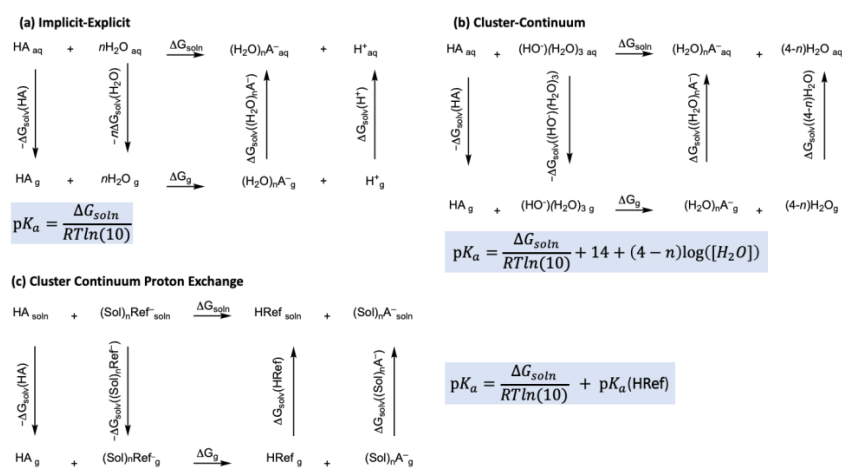
Figure 6. The original (a) implicit-explicit[107] and (b) cluster-continuum[280] schemes for prediction of aqueous pKa values, and (c) the proton-exchange version of them, generalized to any solvent (Sol) and reference acid HRef.[105] All three schemes can used as thermocycles as shown, or can be implemented with direct calculation of the solution phase only.

More generally, studies have shown that explicit solvent molecules can significantly improve the accuracy of pKa predictions but not always. For instance, it was reported by Pliego and co-workers that using a cluster-continuum model can improve pK_a predictions by around 6 pK_a unit for some cases.[109] In a similar vein, Ho and Coote[105] showed that inclusion of 1 and sometimes 2 explicit solvent molecules improved performance of all continuum models ~~tested~~ for a test set of 55 aqueous pK_a values of neutral acids, spanning carbon acids, inorganic acids, carboxylic acids, phenols and alcohols. However, when additional solvent molecules were included that the error tended to increase, presumably due to double counting of solvent effects from the implicit and explicit solvent.[105] Studies generally recommend the inclusion of one explicit solvent molecule for pK_a calculations involving anions, particularly in aqueous solution. [107, 281-282] For instance, Thapa and Schlegel found that including one explicit water reduced the error in aqueous pK_a values of substituted alcohols, phenols and hydroperoxides by approximately 3 pK_a units.[283] In a related study they found that the improvement resulting from explicit solvent molecules in pK_a values involving neutrals and cations was modest while that in pK_a values involving neutrals and anions was quite significant,[284] a conclusion also echoed by Xu and Coote for nucleobases.[65] Indeed studies have shown that the errors ~~in the~~ in the pK_a values of the amines and anilines increased after adding one solvent molecule to both the neutral and cationic species.[285] However, reactions involving multiply charged positive species, such as polyprotic amines,[62] do tend to benefit from explicit solvation.

~~Molecular Dynamics.~~Molecular Dynamics. Force field-based methods are used to study pK_a values of large systems, including proteins, and/or smaller molecules in large ensembles of explicit solvent.[274] As protonation / deprotonation are bond-breaking processes, special techniques are needed to predict pK_a values using molecular mechanics. Warshel was one of the first to tackle this problem by reformulating the problem of pK_a prediction as the problem of predicting the change in solvation energy associated with moving the charge from water to the protein.[286] In this way one can use microscopic free energy calculations to determine the pK_a values of protein residues. When there are multiple ionizable residues, one can essentially use brute force to evaluate the free energies of various possible protonation states, but this quickly becomes unmanageable for complex systems. Constant-pH ~~molecular dynamics~~MD (CpHMD) was developed to allow for the variation of the protonation states without a priori enumeration of the relevant states.[287-288] Broadly speaking, there are two different approaches, according to whether the protonation states are represented by discreet coordinates using Monte-Carlo sampling,[289-290] or as an additional continuous titration degree of freedom decoupled from the conformational dynamics.[291] The original formulations used implicit solvent; however, explicit solvent formulations have since been developed.[292] Numerous other improvements to both approaches have been developed,[287-288] such as improving the description of long-range electrostatics,[293] improving the physical description of the proton transfer process with empirical valence bond theory,[294] improving conformational sampling using pH-based replica exchange,[292, 295] and the development of GPU implementations.[296] Various wrapper programs such as PypKa[297] have also been introduced to improve their ease of use.

In benchmarking studies, CpHMD~~constant pH molecular dynamics~~ provides a convenient and potentially accurate method for studying large and conformationally complex systems, and is

22

particularly useful for determining proton states of polyprotic acids and bases like proteins.[298] Unsurprisingly, the choice of force field has a significant effect on the accuracy of pK_a predictions, with the chosen force field needing to be capable of modelling the solute, the solvent and their interactions. The choice of force field is to some extent system specific; however, as with other solvation processes,[157] it has been generally noted that polarizable force fields out-perform~~ed~~ fixed charge force fields for pK_a caluclations.[299-300] Moreover, because proton transfer is a bond breaking process, AIMD methods are often invoked, particularly for difficult systems such as transition-metal complexes,[301] or water autoionization.[302] Indeed, in this latter case, the incorporation of nuclear quantum effects via ~~ab initio path integral molecular dynamics~~ PIMD is also necessary. For example Thomsen and Shiga showed that neglect of tunnelling effects can lead to errors of up to 4.5 ± 0.9 pK_a units in the case of liquid water.[303] For larger systems, the cost of AIMD can be reduced using semi-empirical methods such as DFTB,[304] and its accuracy can in turn be improved with data augmented approaches.[305]

4.2 Photochemistry

Photochemical processes are central to a wide range of chemical, biological and engineering applications including photocatalysis, photoligation, photovoltaics, photosynthesis, phytochrome proteins, and photodynamic therapy.[306] They can be more complex to model than ground state reactions, both with respect to the electronic structures of solute itself and environment response to the electronic excitation of solute. Photochemical methods and their applications have been reviewed elsewhere (see for example Refs [307] and [308]); in this section, we focus on the specific problem of modelling solvent effects on these processes. Solvent effects on a wide range ~~types~~ of spectra (from electronic to vibrational spectra) were recently reviewed by Chergui.[309] The solvent can influence photochemistry in a variety of ways, from helping to stabilize polar excited states,[310] to altering energy levels through hydrogen bonding with lone pairs,[311-312] to displacing ligands and coordinating with photocatalysts,[313-314] participating in and catalysing photochemical reactions,[315-319] and even in some cases promoting intersystem crossing via the heavy atom effect.[320] The solvent environment can influence Raman optical activity (ROA), IR, and vibrational circular dichroism (VCD) spectra of (R)and (S)-pantolactone.[321] , linear and non-linear response properties in aqueous solution,[322] two-photon absorption cross sections, and the well-known vibrational Stark effects.[323]

Non-equilibrium Solvation. Compared with the ground-state, the treatment of solvent effects in vertical photochemical processes is complicated by non-equilibrium solvation and solvent reorganization energy. These result from the different time scales for the response of electrons and nuclei to the change of the electronic distribution of solute: the electronic distribution of solvent responds to th~~is~~e change immediately (fast polarization) while the nuclei response is relatively slow (slow polarization). This is illustrated in Figure 7 where state 2 and state 4 are non-equilibrium states, and 1→2 and 3→4 correspond respectively to vertical excitation and emission process. Solvent reorganization energy is defined as the energy change that results from slow polarization (i.e., from state 2 to state 3 in Figure 7), while the non-equilibrium solvation energy is the solvation energy of the non-equilibrium species (states 2 and 4 in Figure 7). The non-equilibrium solvation free energy and solvent reorganisation energy were originally defined within the general framework of Marcus theory of electron transfer[324]; for reviews relating specifically to photochemistry we refer the reader to the work of Marenich and co-workers[325] and Herbert and co-workers.[326]
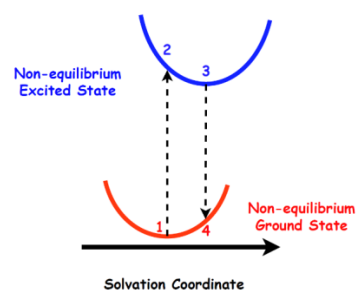
Figure 7. A simple scheme for non-equilibrium excited state and ground state

Two main schemes have been proposed to calculate the non-equilibrium solvation free energy: linear-response and state-specific. The former calculates excited-state energies based on the transition density between ground and excited states, the latter is based on the excited-state electron density and thus provides a more complete (and accurate) account of the polarization between solute and solvent in excited states.[327-328] Yin and co-workers used the state-specific polarizable force field based two-points method to calculate the total reorganization energy of vertical charge transfer (CT) -reactions in oligoacene crystals.[329] Li and co-workers calculated the solvation free energy of non-equilibrium states using an auxiliary equilibrium state, the associated reorganization energy and vertical excitation energies obtained with the new non-equilibrium solvation model agree well with the experimental results.[330-334] Non-equilibrium solvation effects have been shown to be important for accurately modelling vertical ionization energies,[335] the dynamics of photo-dissociation in liquids,[336] and intramolecular electron transfer, where it has been shown that reorganization of the first solvation shell is coupled with the back electron transfer.[337] The important role of solvent reorganization of ionic liquids in electronic spectra and photodissociation has also been highlighted.[338]

Implicit Solvent. Photochemical properties in solution are most often studied by combining time-dependent quantum chemical methods with implicit solvent models. The thermodynamic cycle method is rarely used for photochemical properties such as vertical excitation energies. Although most works focus on the influence of method choice for excited-state electronic structure calculations, the choice of implicit solvent models and their parameters can also influence the calculated electronic spectra. For example, Mu, Wang and co-workers found that the parameters of SMD are in good correlation with electronic excitation index.[339] The size of solute cavity can dramatically affect the obtained excitation energies, for example, Provorse Long and Isborn found the universal force field (UFF) radii need to be scaled by a factor of 1.5 to give reasonable excitation energies for linear response PCM approach with explicit solvent molecules, while for the state-specific one, an even larger PCM cavity is expected.[99] It is also well-known that the spectral shift in solution can be correlated with solvent properties (e.g., $E_T(30)$ and others) through the Lippert-Mataga equation and multiple linear regression analysis.[340]

Explicit Solvent. Like other chemical processes, explicit solute-solvent interactions are often important in photochemical processes, and explicit solvent molecules need to be included in the excited state calculations. For example, the work of Caricato suggests that a micro-solvation correction can further improve the accuracy of EOM-CCSD-PCM results by capturing the missing hydrogen-bond interactions in PCM,[341] while micro-solvation is crucial to providing an accurate

description of excited-state intramolecular proton transfer,[342] solvent dipolarity and polarizability in solvatochromic sensors,[343] and even Raman spectroscopy.[344] A standard way to simulate the electronic spectra in explicit solvent environments is to perform static TDDFT calculations on snapshots from explicit solvent MD simulations. For example, Petrone, Rega and co-workers performed both force-field and ~~AIMD~~ab initio MD simulation for chromophores in water and methanol. Several configurations were taken from the trajectories and subjected to TD-DFT calculations in order to simulate the absorption spectra.[345] Erhart, Moth-Poulsen and co-workers employed MD simulation and TD-DFT calculations to study the solvent effects on the photochemical properties and reactions of norbornadiene-quadricyclane systems, and the authors found that the choice of solvent can influence both the energy storage and quantum yield.[346] The method used to generate the solvent-solute clusters is also important. For instance, Nogueira, Gonzalez and co-workers compared classical MM-MD, QM/MM-MD sampling, Wigner quantum sampling and a hybrid protocol, concluding that a QM description of the chromophore during the MD simulation is needed.[347] Sampling is also important. For instance, Mirón and Lebrero employed different QM/MM Linear Response TD-DFT schemes to study the excited state properties of indole in complex environments, concluding that the use of different starting structures for MD simulation is more important than the length of a single MD trajectory.[348] A more specific review about modelling excited states in explicit solvent was recently provided by Zuehlsdorff and Isborn,[349] while a review of QM/MM methods for photochemistry can be found in the work of Boulanger and Harvey.[350]

When modelling photochemistry in explicit solvent environments, polarization effects are particularly important to reach fully consistent mutual polarization between solvent and excited-state solute. For example, Lipparini, Mennucci, Li and co-workers combined the real-time TDDFT with the polarizable mixed quantum mechanical and molecular mechanical (QM/MMPol) method.[351] Nogueira, Gonzalez and co-workers compared the solvent effects in the calculation of excited states with different methods including QM/PCM and QM/MM with different embedding techniques. The authors concluded QM/PCM performs the best while polarized embedding is necessary for QM/MM.[347] Technically, QM/QM' methods can produce better treatment of the mutual polarization between QM (solute) and QM' (solvent) region. For example, Bennie, Curchod, Manby and Glowacki employed projector-based EOM-CCSD/DFT embedding to study the excitation energy of acrolein solvated in water, concluding that the EOM-CCSD/DFT method can reproduce the accuracy of full EOM-CCSD calculation, an error of less than 0.01 eV for excitation energies.[352] Goodpaster and co-workers performed TD-DFT-in-DFT and EOM-CCSD-in-DFT excited state calculations using projection-based quantum embedding methodologies.[353] Caricato and co-workers developed the QM/QM' method to simulate UV/Vis absorption spectra including the polarization effects with embedded charges.[354] Crespo-Otero and co-workers proposed the ONIOM(QM/QM') method based on the Ewald method, which was successfully applied to study photochemistry in molecular crystals.[355]

4.3 Redox Potentials
Redox reactions are those that involve actual or formal electron transfer from one reagent to another, resulting in oxidation of the electron donor and reduction of the electron acceptor. Redox processes are crucial in many chemical and biochemical processes, as well as photoelectric devices and energy storage.[356-357] The reduction potential $E°(O|R)$ is a direct measure of the thermodynamic feasibility of an oxidation–reduction half-reaction, and is given by equation (4)

$$E°(O|R) = -\frac{\Delta G}{nF} - E°_{REF} \qquad (4)$$

25

where ΔG is the Gibbs free energy change of half reaction (5), n is the number of electrons transferred in that half reaction and E°_{REF} is the potential of the reference electrode under the same conditions.

$$O_{soln} + n \, e^-_{gas} \rightarrow R_{soln} \qquad\qquad (5)$$

Like pK_a values, redox reactions typically involve at least one charged species and are thus heavily influenced by solvent effects. These in turn are further complicated by the presence of electrolyte in standard electrochemical experiments. There is also the added complication of how to treat the electron, and how to choose an appropriate and accurate value for the reference electrode (which in turn should treat the electron in an identical manner so it cancels from the cell potential). One also needs to be careful when comparing computed redox potentials, which correspond to conditional formal potentials, to experimental half-wave potentials from cyclic voltammetry, particularly for irreversible electrochemical processes. More methodological detail can found in the general reviews of Coote, Cramer, Truhlar and co-workers,[358-359] while Johansson and co-workers have reviewed the modelling and simulations of different types of electrolyte solution in the sodium-ion battery,[360] Schwarz and Sundararaman have reviewed first-principle methods for electrochemical interfaces,[361] and Borodin and co-workers have reviewed the modelling of redox potentials in electrolytes and solid-liquid interface structures.[362]

Implicit Solvent. For the calculations of redox potentials in water and commonly used organic solvents, the most widely used method is still QM calculations combined with implicit solvent simulation, using either thermodynamic cycle method or direct method. While the choice of quantum-chemical method is important ~~also critical~~ (and beyond the scope of this review), the choice of implicit solvation models is also critical. Depending on the particular solute-solvent combination, different continuum models give superior performance, presumably due to their similarity or otherwise with the original training data for the solvent model. For example, Guerard and Arey compared the performance of SM8, SMD, C-PCM, IEF-PCM and COSMO-RS for the oxidation potential of a wide range of organic compounds in both water and acetonitrile (see Figure 8A). Their results suggest that SMD is the best choice overall among all tested solvation models. However, in a different study Marenich et al.[359] found that CPCM-UAKS was superior for a test set of nitroxide radicals, SMD was superior for a test set of anilines, and COSMO-RS was superior for a test set of phenols, and gave superior overall performance for the systems studied (see Figure 8B). Clearly benchmarking is necessary, and method choice should be on a case-by-case basis. What is worth noting from both of these studies, which are typical of the field as a whole, is that average accuracy achievable by the best implicit solvation methods is usually in the range of 0.1-0.2 V, though this can usually be improved to within "chemical accuracy" (ca. 0.05V) using isodesmic approaches if experimental data is available for a structurally similar reference species (see for example Refs. [363-365] in which this is done for the oxidation of various stable free radicals). Because geometries tend to change less on oxidation or reduction compared with protonation/deprotonation, comparative studies in which the same level of theory is used with thermocycles versus the direct method find negligible difference in accuracy for redox potentials.[63]
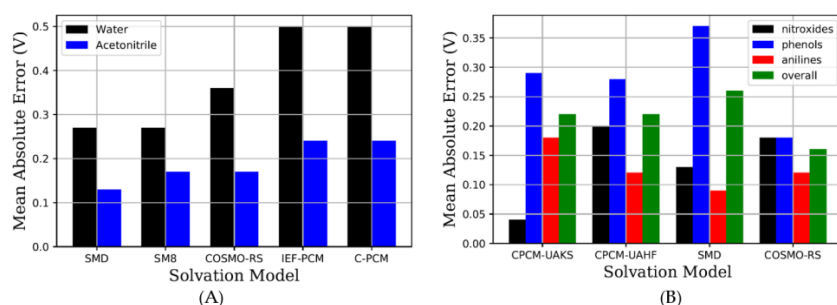
26

Figure 8. (A) Mean absolute error for oxidation potentials (V) of a test set of 22 organic compounds in water and 19 in acetonitrile (including phenols, methoxybenzenes, anilines, indoles, aliphatic amines and organosulfur compounds), as calculated with different solvation models in water and acetonitrile. Original data and more details can be found in Table 4 of Ref.[366]; (B) Mean absolute error the containing aqueous reduction potentials (V) of 30 phenols and aqueous oxidation potentials (V) of 15 anilines and 7 nitroxide radicals, calculated by combining high-level G3MP2-CC(+) gas phase calculations with a range of different solvation models. Original data and more details can be found in Ref. [359].

Explicit Solvent. When not using isodesmic methods, explicit solute-solvent interactions are usually important for accurate prediction of redox potentials, especially for bare ions. For instance, Fernades and co-workers studied the Fe^{3+}/Fe^{2+} reduction potential as a function of the number of of explicit water molecules.[367] What was interesting in this case is that the inclusion of explicit solvent molecules not only improves the overall accuracy, but also reduces the error in the electronic structure method, presumably by stabilizing the ion (Figure 9). Explicit solvent molecules are crucial when modelling redox reactions in complex environments like solid electrolytes[368-372] or when modelling complex species like polyoxometalates.[373] Moreover, numerous studies have shown that electrolytes and/or ionic liquids can form ion pairs with oxidised or reduced species, dramatically shifting their redox potentials.[374-380] In such cases, studying the relevant ion pair in a continuum model generally gives good results. It should also be noted that the solvent and/or electrolyte can sometimes participate in or compete with electrochemical reactions (e.g. solvents such as acetonitrile, DMSO and THF can act as a nucleophile in S_N2 reactions of oxidised alkoxyamines[381]) and clearly in those cases needs to be included explicitly.

Depending on the size of the system and the complexity of the solvent environment, the two principle approaches to modelling explicit solvation in redox potentials is either through a cluster-continuum approach or using multi-scale methods. In the first approach a small number of explicit solvent or electrolyte molecules are included in the quantum-chemical calculation that is performed in an implicit solvent environment (for examples see Refs [374, 379]). For the second method, QM/MM or QM/MM-MD methods are often used, analogous to those introduced in Section 3.2.[362] In the latter case, the obtained accuracy is affected by many factors including the simulation time, the number of snapshots, the size of QM region and polarization effects, which have been shown to be particularly crucial.[382] A recent discussion of multi-scale methods for redox potentials can be found in the work of Sterling and Bjornsson.[383] In their study, the authors employed GFN-XTB/MM-MD to conduct sampling for the end states of a redox process, and then a multi-layer scheme was designed to calculate the

27

energies so as to include both the quantum nature of solute and the polarization effects from the solvent environment. A similar protocol was also used by Wang and Voorhis.[384] Because of the low computational costs and the excellent versatility of GFN-XTB methods, MD simulations using straight GFN-XTB without MM or running GFN-XTB energy calculations for redox potential calculations can also be found in recent years.[385-386] The advantage of the GFN2-XTB method against other semi-empirical methods for redox potential calculations was highlighted in the recent benchmarking study of Hansen, Grimme and others.[387]
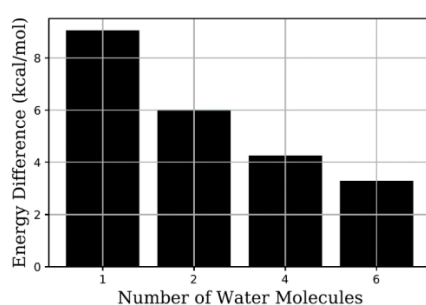
Figure 9. The difference of CCSD(T)/CBS and MP2/CBS results of $\Delta E^{Fe3+/Fe2+}$ using different numbers of water molecules. Original data and more details can be found in Table 5 of Ref.[367]

4.5 Other Chemical Reactions

The nature of the solvent affects the kinetics and thermodynamics of most chemical reactions.[388-389] To list just a few examples, solvent effects are critical in catalytic processes for biomass upgrading,[390-391] reactions involving ion-pair intermediates,[392-393] in hydrolysis reactions,[394] in governing the competition between nucleophilic substitution and elimination processes,[395-396] and cycloadditions.[397-399] Depending on the systems, a range of different methods are used to model solvation effects.

Implicit Solvent. As bond-breaking processes, most chemical reactions are studied with QM methods at high levels of theory, and the most cost-effective method for including the solvent environment in such calculations is with continuum models. Numerous benchmarking studies have been performed. To quote just one example, Pliego and co-workers[400] studied a series of S_N2 and S_NAr reactions, showing that the accuracy of the free energy barriers depended on both the DFT functional and solvation model, with the best combination giving results to within 2 kcal mol^{-1} of experiment (Figure 10). In general, if the reactions involve only neutral species and explicit solute-solvent interactions such as hydrogen bonding are not significant, implicit solvent models perform well, with the best choice of method being system-dependent.
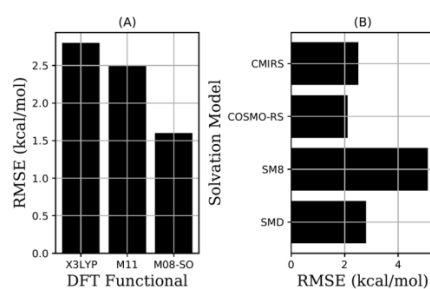
28

Figure 10. RMSE of the free energy barriers of 9 S_N2 and S_NAr reactions obtained with different DFT functional (A) and implicit solvation models (B). Original data and more details can be found in Table 1 and Table 2 from Ref. [400].

Micro-solvation. Inclusion of explicit solvent molecules is often necessary for accurate study of reaction mechanisms and catalysis. They are obviously essential if the solvent is itself a reagent or catalyst (as is the case for acetone and water in the proline-catalysed aldol reaction[401-402]), but inclusion of additional solvent molecules is also critical when hydrogen bonding and other explicit interactions are important in stabilizing reagents, transition states and/or intermediates. For example, the inclusion of two additional explicit water molecules (in addition to the HO^-/H_2O reagent itself), together with SMD implicit solvation, was necessary to reproduce experimental half-lives for the base-catalysed hydrolysis of benzamidine.[394] In this system, the additional waters form a hydrogen-bonded network are added with the reagent. The importance of including additional explicit solvent molecules is true more generally for water-mediated reactions.[403-404] The importance of explicit solvation has also been recently highlighted for many other cases, including the ring-opening reactions of donor-acceptor cyclopropanes,[405] hydrosilylation of α-hydroxy aziridines,[406] proton transfer reactions,[407-409] for the methanol mediated Morita-Baylis-Hillman reaction,[410] the zwitterionization of glycine in water,[411] and when reactions are carried out in chiral media.[412] The number and location of these molecules becomes an important variable. In their study of the methanol mediated Morita-Baylis-Hillman reaction, Sure and co-workers authors proposed a protocol to judge whether and where to include explicit solvent molecules based on the computed screening charge density.[410] In their study of the zwitterionization of glycine, Marx and co-workers conducted AIMD simulations to optimize solute-solvent clusters, compared results obtained with different numbers of water molecules to find convergence.[411] In their study of benzamidine hydrolysis, Coote, White and co-workers rationally designed hydrogen bonded networks and then subjected them to systematic conformational searching in order to find the most stable structures, with the resulting reaction rates then evaluated against experiment.[394]

Explicit Solvent. For some reactions, micro-solvation is not sufficient, and fully explicit treatment of the solvent environment is necessary. For example, Bulo and co-workers studied nucleophilic addition to carbonyls and found that micro-solvation cannot fully reproduce the activation barrier obtained with conventional QM/MM simulation.[413] Fully explicit solvent treatments are particularly important for complex solvents, such as ionic liquids,[414-415] mixed-solvent environments[416] and deep eutectic solvents,[417] as well heterogenous systems,[418-420] and reactions at various types of interfaces.[421-426] They are also important if the solvent has been macroscopically ordered through, for example, exposure to electric fields or fluid mechanics, as this ordering generates internal electric fields that can catalyse reactions.[427] When modelling chemical reactions

29

in fully explicit environments, some of form of ~~molecular dynamics~~MD needs to be performed. At the same time, the chemical reaction itself needs to be treated with a sufficient electronic structure method to capture the bond breaking processes involved. As a result, the methods typically used include AIMD, often performed with lower-cost methods such as DFTB, or multiscale QM/MM methods, though for some applications, reactive force fields have also been developed. As with other solvation applications, the importance of using polarizable force fields is frequently highlighted (see, for example, Ref. [428]). The importance of solvation dynamics and non-equilibrium solvation is also frequently highlighted (see for example Refs. [393, 395-396, 429-430]).

5. Conclusions

As most practical chemistry occurs in solution, modelling and understanding solvents effects is a crucial part of modern computational chemistry. A wide range of both implicit and explicit solvent methods have been employed to study solvation, from ab initio to force field methods, including both static calculations and dynamic simulations. Machine learning either as a means to parameterising computational methods, or as an end itself, is also increasingly making an impact. For modelling chemical reactions in standard solutions under standard conditions, implicit solvent models continue to provide the simplest and most cost-effective method for treating the solvent without sacrificing the accuracy of the underlying electronic structure calculations. Moreover, as outlined in Section 3.5, ongoing improvements to the treatment of the non-electrostatic solvation components of solvation, to the treatment of ions, and to the treatment of temperature and pressure effects are further expanding the scope and accuracy of these models. Where explicit solute-solvent interactions are important, micro-solvation techniques, in which a small number of explicit solvents are used in conjunction with a continuum solvent model, have been extremely effective. These add to the cost of calculations, and deciding how many explicit solvent molecules to include and where to place them is not always straightforward. However, as outlined throughout this review, various strategies have been developed for addressing this problem, ranging from chemical intuition to the use of brute-force ~~ab initio molecular dynamics~~AIMD, and when used carefully micro-solvation methods usually provide the gold standard for modelling most solution-phase chemical processes.

~~Molecular dynamics~~MD simulations of large ensembles of solvent molecules are necessary for many applications, but particularly heterogeneous media, reactions at interfaces, reactions in complex solvents like ionic liquids or deep eutectic solvents, or reactions under non-equilibrium conditions where, for example, external forces (such as electric fields) are used to impose a macroscopic structure on the solvent environment. They are also important when non-equilibrium solvation contributes to chemical reactivity and selectivity. For such simulations, the key ongoing challenges revolve around accuracy of the force-field parameters and the sampling method, with enhanced sampling being critical. When classical ~~molecular dynamics~~MD is used, multi-scale QM/MM methods are needed so that the bond breaking processes are treated an appropriate QM level of theory, while the MM region is treated with an appropriate polarisable force field. Such calculations can be both difficult to set up and expensive to run, and alternative approaches based on reactive force fields or ~~ab initio molecular dynamics~~AIMD are desirable. In the latter case, the largest challenge is still the limitations of time length and system size due to the high computational costs. The recent success of employing deep potential in AIMD offers a way forward. The further development of accurate QM/QM' embedding schemes, and better methods for describing the mutual polarization between solute and solvent, remains important, especially for non-equilibrium states and excited states. Equally important will be the development of tools to automatize the

parameter generation, modelling, sampling and analysis of complex systems in a robust "black box" manner. Developments such as these will not only promote the better understanding of fundamental chemistry, but improve our ability to predict behaviour in real-world applications, such as energy storage or in-silico drug design.

Acknowledgement

References

1.   Mata, R. A.; Suhm, M. A., Benchmarking quantum chemical methods: Are we heading in the right direction? *Angew. Chem. Int. Ed.* **2017,** *56* (37), 11011-11018.

2.   Maldonado, A. M.; Hagiwara, S.; Choi, T. H.; Eckert, F.; Schwarz, K.; Sundararaman, R.; Otani, M.; Keith, J. A., Quantifying Uncertainties in Solvation Procedures for Modeling Aqueous Phase Reaction Mechanisms. *J. Phys. Chem. A* **2021,** *125* (1), 154-164.

3.   Harvey, J. N.; Himo, F.; Maseras, F.; Perrin, L., Scope and challenge of computational methods for studying mechanism and reactivity in homogeneous catalysis. *ACS Catal.* **2019,** *9* (8), 6803-6813.

4.   Kennedy, D.; Norman, C., What don't we know. *Science* **2005,** *309* (5731), 75.

5.   Rogers, R. D.; Seddon, K. R., Ionic liquids--solvents of the future? *Science* **2003,** *302* (5646), 792-793.

6.   Smith, E. L.; Abbott, A. P.; Ryder, K. S., Deep eutectic solvents (DESs) and their applications. *Chemical reviews* **2014,** *114* (21), 11060-11082.

7.   Aurbach, D.; Talyosef, Y.; Markovsky, B.; Markevich, E.; Zinigrad, E.; Asraf, L.; Gnanaraj, J. S.; Kim, H.-J., Design of electrolyte solutions for Li and Li-ion batteries: a review. *Electrochimica Acta* **2004,** *50* (2-3), 247-254.

8.   Tomasi, J.; Mennucci, B.; Cammi, R., Quantum mechanical continuum solvation models. *Chem. Rev.* **2005,** *105* (8), 2999-3094.

9.   Cramer, C. J.; Truhlar, D. G., Implicit solvation models: equilibria, structure, spectra, and dynamics. *Chem. Rev.* **1999,** *99* (8), 2161-2200.

10.   Klamt, A., The COSMO and COSMO-RS solvation models. *Wiley Interdisc. Rev. Comput. Mol. Sci.* **2011,** *1* (5), 699-709.

11.   Mennucci, B., Continuum Solvation Models: What Else Can We Learn from Them? *J. Phys. Chem. Lett.* **2010,** *1* (10), 1666-1674.

12.   Jorgensen, W. L., Free energy calculations: a breakthrough for modeling organic chemistry in solution. *Acc. Chem. Res.* **1989,** *22* (5), 184-189.

13.   Duarte Ramos Matos, G.; Kyu, D. Y.; Loeffler, H. H.; Chodera, J. D.; Shirts, M. R.; Mobley, D. L., Approaches for calculating solvation free energies and enthalpies demonstrated with an update of the FreeSolv database. *J. Chem. Eng. Data* **2017,** *62* (5), 1559-1569.

14.   Levy, R. M.; Gallicchio, E., Computer simulations with explicit solvent: recent progress in the thermodynamic decomposition of free energies and in modeling electrostatic effects. *Annu. Rev. Phys. Chem.* **1998,** *49* (1), 531-567.

15.   Onufriev, A. V.; Izadi, S., Water models for biomolecular simulations. *Wiley Interdisc. Rev. Comput. Mol. Sci.* **2018,** *8* (2), e1347.

16.   Anderson, J. D.; Wendt, J., *Computational fluid dynamics*. Springer: 1995; Vol. 206.

17.   Craig, I. R.; Manolopoulos, D. E., Quantum statistics and classical mechanics: Real time correlation functions from ring polymer molecular dynamics. *J. Chem. Phys* **2004,** *121* (8), 3368-3373.

18.   Hehre, W. J., Ab initio molecular orbital theory. *Accounts of Chemical Research* **1976,** *9* (11), 399-406.

19.   Kohn, W.; Becke, A. D.; Parr, R. G., Density Functional theory of Electronic Structure. *J. Phys. Chem.* **1996,** *100*, 12974–12980.

20.   Andersen, O. K.; Jepsen, O., Explicit, first-principles tight-binding theory. *Physical Review Letters* **1984,** *53* (27), 2571.

21.   Stewart, J. J., Optimization of parameters for semiempirical methods II. Applications. *Journal of computational chemistry* **1989,** *10* (2), 221-264.

22.   Bannwarth, C.; Ehlert, S.; Grimme, S., GFN2-xTB—An accurate and broadly parametrized self-consistent tight-binding quantum chemical method with multipole electrostatics and density-dependent dispersion contributions. *J. Chem. Theory Comput.* **2019,** *15* (3), 1652-1671.

23.   Karplus, M., Development of multiscale models for complex chemical systems: from H+ H2 to biomolecules (Nobel lecture). *Angew. Chem. Int. Ed.* **2014,** *53* (38), 9992-10005.

24.   Gordon, M. S.; Fedorov, D. G.; Pruitt, S. R.; Slipchenko, L. V., Fragmentation methods: A route to accurate calculations on large systems. *Chem. Rev.* **2012,** *112* (1), 632-672.

25.   Lemkul, J. A.; Huang, J.; Roux, B.; MacKerell Jr, A. D., An empirical polarizable force field based on the classical drude oscillator model: development history and recent applications. *Chem. Rev* **2016,** *116* (9), 4983-5013.

26.   Warshel, A.; Kato, M.; Pisliakov, A. V., Polarizable force fields: history, test cases, and prospects. *J. Chem. Theory Comput.* **2007,** *3* (6), 2034-2045.

27.   Ponder, J. W.; Wu, C.; Ren, P.; Pande, V. S.; Chodera, J. D.; Schnieders, M. J.; Haque, I.; Mobley, D. L.; Lambrecht, D. S.; DiStasio Jr, R. A., Current status of the AMOEBA polarizable force field. *J. Phys. Chem. B* **2010,** *114* (8), 2549-2564.

28.   Senftle, T. P.; Hong, S.; Islam, M. M.; Kylasa, S. B.; Zheng, Y.; Shin, Y. K.; Junkermeier, C.; Engel-Herbert, R.; Janik, M. J.; Aktulga, H. M., The ReaxFF reactive force-field: development, applications and future directions. *Npj Comput. Mater.* **2016,** *2* (1), 1-14.

29.   Van Duin, A. C.; Dasgupta, S.; Lorant, F.; Goddard, W. A., ReaxFF: a reactive force field for hydrocarbons. *J. Phys. Chem. A* **2001,** *105* (41), 9396-9409.

30.   Izvekov, S.; Voth, G. A., A multiscale coarse-graining method for biomolecular systems. *J. Phys. Chem. B* **2005,** *109* (7), 2469-2473.

31.   Marrink, S. J.; Risselada, H. J.; Yefimov, S.; Tieleman, D. P.; De Vries, A. H., The MARTINI force field: coarse grained model for biomolecular simulations. *J. Phys. Chem. B* **2007,** *111* (27), 7812-7824.

32.   Mater, A. C.; Coote, M. L., Deep Learning in Chemistry. *J. Chem Inf. Model.* **2019,** *59* (6), 2545-2559.

33.   Friedrichs, M. S.; Eastman, P.; Vaidyanathan, V.; Houston, M.; Legrand, S.; Beberg, A. L.; Ensign, D. L.; Bruns, C. M.; Pande, V. S., Accelerating molecular dynamic simulation on graphics processing units. *J. Comput. Chem.* **2009,** *30* (6), 864-872.

34.   Orozco, M.; Luque, F. J., Theoretical Methods for the Description of the solvent effect in biomolecular systems. *Chem. Rev.* **2000,** *100*, 4187–4225.

35.   Skyner, R.; McDonagh, J.; Groom, C.; Van Mourik, T.; Mitchell, J., A review of methods for the calculation of solution free energies and the modelling of systems in solution. *Phys. Chem. Chem. Phys* **2015,** *17* (9), 6174-6191.

36.   Herbert, J. M., Dielectric continuum methods for quantum chemistry. *Wiley Interdiscip. Rev. Comput. Mol. Sci.* **2021,** *11* (4), e1519.

32

37.   Minkin, V. I., Glossary of terms used in theoretical organic chemistry. *Pure and Applied Chemistry* **1999,** *71* (10), 1919-1981.

38.   Ho, J.; Klamt, A.; Coote, L. M., Comment on the Correct Use of Continuum Solvent Models. *J. Phys. Chem. A* **2010,** *114* (51), 13442-13444.

39.   Marenich, A. V.; Kelly, C. P.; Thompson, J. D.; Hawkins, G. D.; Chambers, C. C.; Giesen, D. J.; Winget, P.; Cramer, C. J.; Truhlar, D. G., Minnesota Solvation Database (MNSOL) version 2012. **2020**.

40.   Vermeire, F. H.; Green, W. H., Transfer learning for solvation free energies: From quantum chemistry to experiments. *Chem. Eng. J.* **2021,** *418*, 129307.

41.   Driver, M. D.; Hunter, C. A., Solvent similarity index. *Phys. Chem. Chem. Phys.* **2020,** *22* (21), 11967-11975.

42.   Moine, E.; Privat, R.; Sirjean, B.; Jaubert, J.-N., Estimation of solvation quantities from experimental thermodynamic data: Development of the comprehensive compSol databank for pure and mixed solutes. *J. Phys. Chem. Ref. Data* **2017,** *46* (3), 033102.

43.   Grubbs, L. M.; Saifullah, M.; Nohelli, E.; Ye, S.; Achi, S. S.; Acree Jr, W. E.; Abraham, M. H., Mathematical correlations for describing solute transfer into functionalized alkane solvents containing hydroxyl, ether, ester or ketone solvents. *Fluid. Phase. Equilib.* **2010,** *298* (1), 48-53.

44.   Scalmani, G.; Frisch, M., Continuous surface charge polarizable continuum models of solvation. I. General formalism. *J. Chem. Phys.* **2010,** *132* (11), 114110.

45.   Miertuš, S.; Scrocco, E.; Tomasi, J., Electrostatic interaction of a solute with a continuum. A direct utilizaion of *ab initio* molecular potentials for the prevision of solvent effects. *J. Chem. Phys* **1981,** *55* (1), 117-129.

46.   Miertuš, S.; Scrocco, E.; Tomasi, J., Electrostatic interaction of a solute with a continuum. A direct utilizaion of AB initio molecular potentials for the prevision of solvent effects. *Chem. Phys.* **1981,** *55* (1), 117-129.

47.   Cancès, E.; Mennucci, B.; Tomasi, J., A new integral equation formalism for the polarizable continuum model: Theoretical background and applications to isotropic and anisotropic dielectrics. *J. Chem. Phys.* **1997,** *107* (8), 3032-3041.

48.   Klamt, A.; Schüürmann, G., COSMO: a new approach to dielectric screening in solvents with explicit expressions for the screening energy and its gradient. *J. Chem. Soc. Perkin Trans. 2* **1993,** (5), 799-805.

49.   Barone, V.; Cossi, M., Quantum Calculation of Molecular Energies and Energy Gradients in Solution by a Conductor Solvent Model. *J. Phys. Chem. A* **1998,** *102* (11), 1995-2001.

50.   Kelly, C. P.; Cramer, C. J.; Truhlar, D. G., SM6: A density functional theory continuum solvation model for calculating aqueous solvation free energies of neutrals, ions, and solute-water clusters. *J. Chem. Theory Comput.* **2005,** *1* (6), 1133-1152.

51.   Marenich, A. V.; Olson, R. M.; Kelly, C. P.; Cramer, C. J.; Truhlar, D. G., SM8. *J. Chem. Theor. Comput.* **2007,** *3*, 2011-2033.

52.   Marenich, A. V.; Cramer, C. J.; Truhlar, D. G., Universal Solvation Model Based on Solute Electron Density and on a Continuum Model of the Solvent Defined by the Bulk Dielectric Constant and Atomic Surface Tensions. *J. Phys. Chem. B* **2009,** *113* (18), 6378-6396.

53.   Ribeiro, R. F.; Marenich, A. V.; Cramer, C. J.; Truhlar, D. G., Use of solution-phase vibrational frequencies in continuum models for the free energy of solvation. *J. Phys. Chem. B* **2011,** *115* (49), 14556-14562.

54.   Lian, P.; Johnston, R. C.; Parks, J. M.; Smith, J. C., Quantum chemical calculation of pK_as of environmentally relevant functional groups: Carboxylic acids, amines, and thiols in aqueous solution. *J. Phys. Chem. A* **2018,** *122* (17), 4366-4374.

55.   Psciuk, B. T.; Lord, R. L.; Munk, B. H.; Schlegel, H. B., Theoretical determination of one-electron oxidation potentials for nucleic acid bases. *J. Chem. Theory Comput.* **2012,** *8* (12), 5107-5123.

56.   Pliego Jr, J. R.; Riveros, J. M., Parametrization of the PCM model for calculating solvation free energy of anions in dimethyl sulfoxide solutions. *Chem. Phys. Lett.* **2002,** *355* (5-6), 543-546.

57.   Fu, Y.; Liu, L.; Li, R.-Q.; Liu, R.; Guo, Q.-X., First-principle predictions of absolute pK_a of organic acids in dimethyl sulfoxide solution. *J. Am. Chem. Soc.* **2004,** *126* (3), 814-822.

58.   Fu, Y.; Liu, L.; Yu, H.-Z.; Wang, Y.-M.; Guo, Q.-X., Quantum-Chemical Predictions of Absolute Standard Redox Potentials of Diverse Organic Molecules and Free Radicals in Acetonitrile. *J. Am. Chem. Soc.* **2005,** *127* (19), 7227-7234.

59.   Böes, E. S.; Livotto, P. R.; Stassen, H., Solvation of monovalent anions in acetonitrile and N, N-dimethylformamide: Parameterization of the IEF-PCM model. *J. Chem. Phys* **2006,** *331* (1), 142-158.

60.   Gryn'ova, G.; Barakat, J. M.; Blinco, J. P.; Bottle, S. E.; Coote, M. L., Computational Design of Cyclic Nitroxides as Efficient Redox Mediators for Dye-Sensitized Solar Cells. *Chem. Eng. J.* **2012,** *18* (24), 7582-7593.

61.   Wen, M.; Jiang, J.; Wang, Z.-X.; Wu, C., How accurate are the popular PCM/GB continuum solvation models for calculating the solvation energies of amino acid side-chain analogs? *Theor. Chem. Acc.* **2014,** *133* (5), 1-11.

62.   Haworth, N. L.; Wang, Q.; Coote, M. L., Modeling Flexible Molecules in Solution: A pK_a Case Study. *J. Phys. Chem. A* **2017,** *121* (27), 5217-5225.

63.   Ho, J., Are thermodynamic cycles necessary for continuum solvent calculation of pK_as and reduction potentials? *Phys. Chem. Chem. Phys* **2015,** *17* (4), 2859-2868.

64.   Klamt, A.; Mennucci, B.; Tomasi, J.; Barone, V.; Curutchet, C.; Orozco, M.; Luque, F. J., On the performance of continuum solvation methods. A comment on "Universal approaches to solvation modeling". *Acc. Chem. Res.* **2009,** *42* (4), 489-492.

65.   Xu, L.; Coote, M. L., Methods to improve the calculations of solvation model density solvation free energies and associated aqueous pK_a values: Comparison between choosing an optimal theoretical level, solute cavity scaling, and using explicit solvent molecules. *J. Phys. Chem. A* **2019,** *123* (34), 7430-7438.

66.   Xu, L.; Coote, M. L., Improving the accuracy of PCM-UAHF and PCM-UAKS calculations using optimized electrostatic scaling factors. *J. Chem. Theory Comput.* **2019,** *15* (12), 6958-6967.

67.   Li, W.; Song, G.; Zhang, J.; Song, J.; Wang, H.; Shi, Y.; Ding, G., Estimation of octanol-water partition coefficients of PCBs based on the solvation free energy. *Comput. Theor. Chem.* **2021,** *1202*, 113324.

68.   Kriz, K.; Rezac, J., Reparametrization of the COSMO solvent model for semiempirical methods PM6 and PM7. *J. Chem. Inf. Model.* **2019,** *59* (1), 229-235.

69.   Kromann, J. C.; Steinmann, C.; Jensen, J. H., Improving solvation energy predictions using the SMD solvation method and semiempirical electronic structure methods. *J. Chem. Phys.* **2018,** *149* (10), 104102.

70.   Okiyama, Y.; Nakano, T.; Watanabe, C.; Fukuzawa, K.; Mochizuki, Y.; Tanaka, S., Fragment molecular orbital calculations with implicit solvent based on the Poisson--Boltzmann equation: implementation and DNA study. *J. Phys. Chem. B* **2018,** *122* (16), 4457-4471.

71.   Okiyama, Y.; Watanabe, C.; Fukuzawa, K.; Mochizuki, Y.; Nakano, T.; Tanaka, S., Fragment molecular orbital calculations with implicit solvent based on the Poisson--Boltzmann equation: II. Protein and its ligand-binding system studies. *J. Phys. Chem. B* **2018,** *123* (5), 957-973.

72.   Fedorov, D. G.; Brekhov, A.; Mironov, V.; Alexeev, Y., Molecular electrostatic potential and electron density of large systems in solution computed with the fragment molecular orbital method. *J. Phys. Chem. A* **2019,** *123* (29), 6281-6290.

34

73.   Collins, M. A.; Ho, J., Accelerating the Calculation of Solute--Solvent Interaction Energies through Systematic Molecular Fragmentation. *J. Phys. Chem. A* **2019,** *123* (39), 8476-8484.

74.   Skylaris, C.-K.; Haynes, P. D.; Mostofi, A. A.; Payne, M. C., Introducing ONETEP: Linear-scaling density functional simulations on parallel computers. *J. Chem. Phys.* **2005,** *122* (8), 084119.

75.   Dziedzic, J.; Bhandari, A.; Anton, L.; Peng, C.; Womack, J. C.; Famili, M.; Kramer, D.; Skylaris, C.-K., Practical Approach to Large-Scale Electronic Structure Calculations in Electrolyte Solutions via Continuum-Embedded Linear-Scaling Density Functional Theory. *J. Phys. Chem. C* **2020,** *124* (14), 7860-7872.

76.   Mathew, K.; Kolluru, V. C.; Mula, S.; Steinmann, S. N.; Hennig, R. G., Implicit self-consistent electrolyte model in plane-wave density-functional theory. *J. Chem. Phys* **2019,** *151* (23), 234101.

77.   Barone, V.; Cossi, M.; Tomasi, J., A new definition of cavities for the computation of solvation free energies by the polarizable continuum model. *J. Chem. Phys.* **1997,** *107* (8), 3210-3221.

78.   Shen, K.; Fu, Y.; Li, J.-N.; Liu, L.; Guo, Q.-X., What are the pK_a values of C–H bonds in aromatic heterocyclic compounds in DMSO? *Tetrahedron* **2007,** *63*, 1568-1576.

79.   Barone, V.; Carnimeo, I.; Scalmani, G., Computational Spectroscopy of Large Systems in Solution: The DFTB/PCM and TD-DFTB/PCM Approach. *J. Chem. Theory Comput.* **2013,** *9*, 2052-2071.

80.   Preat, J.; Loos, P.-F.; Assfeld, X.; Jacquemin, D.; Perpe`te, E. A., DFT and TD-DFT Investigation of IR and UV Spectra of Solvated Molecules: Comparison of Two SCRF Continuum Models. *Int. J. Quantum Chem.* **2007,** *107*, 574-585.

81.   Lee, T. B.; McKee, M. L., Dependence of pK_a on solute cavity for diprotic and triprotic acids. *Phys. Chem. Chem. Phys.* **2011,** *13*, 10258-10269.

82.   Khalili, F.; Henni, A.; East, A. L. L., Entropy contributions in pK_a computation: Application to alkanolamines and piperazines. *J. Mol. Struct* **2009,** *916*, 1-9.

83.   Close, D. M.; Wardman, P., Calculations of the Energetics of Oxidation of Aqueous Nucleosides and the Effects of Prototropic Equilibria. *J. Phys. Chem. A* **2016,** *120*, 4043-4048.

84.   Close, D. M.; Wardman, P., Calculation of Standard Reduction Potentials of Amino Acid Radicals and the Effects of Water and Incorporation into Peptides. *J. Phys. Chem. A* **2018,** *122*, 439-445.

85.   Cammi, R.; Verdolino, V.; Mennucci, B.; Tomasi, J., Towards the elaboration of a QM method to describe molecular solutes under the effect of a very high pressure. *Chem. Phys.* **2008,** *344*, 135-141.

86.   Amovilli, C.; Floris, F. M., Solubility of water in liquid hydrocarbons: a bridge between the polarizable continuum model and the mobile order theory. *Phys. Chem. Chem. Phys.* **2002,** *5*, 363-368.

87.   Brinck, T.; Larsen, A. G.; Madsen, K. M.; Daasbjerg, K., Solvation of Carbanions in Organic Solvents: A Test of the Polarizable Continuum Model. *J. Phys. Chem. B* **2000,** *104*, 9887-9893.

88.   Hebert, S. P.; Schlegel, H. B., Computational Study of the pH-Dependent Competition between Carbonate and Thymine Addition to the Guanine Radical. *Chem. Res. Toxicol.* **2019,** *32* (1), 195-210.

89.   F.J.Luque; M.J.Negre; Orozco, M., An AMI-SCRF Approach to the Study of Changes in Molecular Properties Induced by Solvent. *J. Phys. Chem.* **1993,** *97*, 4386-4391.

90.   Modesto, O.; F.J.Luque, Optimization of the cavity size for *ab initio* MST-SCRF calculations of monovalent ions *Chem. Phys.* **1994,** *182*, 237-248.

91.   Luque, F. J.; Bachs, M.; Alemán, C.; Orozco, M., Extension of MST/SCRF method to organic solvents: *Ab initio* and semiempirical parametrization for neutral solutes in CCl$_4$. *J.Comput.Chem* **1996,** *17*, 806-820.

92.   Curutchet, C.; Orozco, M.; Luque, F. J., Solvation in octanol: parametrization of the continuum MST model. *J.Comput.Chem* **2001,** *22* (11), 1180-1193.

93.   Curutchet, C.; Bidon-Chanal, A.; Soteras, I.; Orozco, M.; Luque, F. J., MST Continuum Study of the Hydration Free Energies of Monovalent Ionic Species. *J. Phys. Chem. B* **2005,** *109* (8), 3565-3574.

94.   Soteras, I.; Forti, F.; Orozco, M.; Luque, F. J., Performance of the IEF-MST Solvation Continuum Model in a Blind Test Prediction of Hydration Free Energies. *J. Phys. Chem. B* **2009,** *113* (27), 9330-9334.

95.   Fu, Y.; Liu, L.; Li, R.-Q.; Liu, R.; Guo, Q.-X., First-Principle Predictions of Absolute pK_a's of Organic Acids in Dimethyl Sulfoxide Solution. *J. Am. Chem. Soc.* **2004,** *126* (3), 814-822.

96.   Kim, H.; Park, J.; Lee, Y. S., A protocol to evaluate one electron redox potential for iron complexes. *J.Comput.Chem* **2013,** *34* (26), 2233-2241.

97.   Verdolino, V.; Cammi, R.; Munk, B. H.; Schlegel, H. B., Calculation of pK_a Values of Nucleobases and the Guanine Oxidation Products Guanidinohydantoin and Spiroiminodihydantoin using Density Functional Theory and a Polarizable Continuum Model. *J. Phys. Chem. B* **2008,** *112* (51), 16860-16873.

98.   Psciuk, B. T.; Schlegel, H. B., Computational Prediction of One-Electron Reduction Potentials and Acid Dissociation Constants for Guanine Oxidation Intermediates and Products. *J. Phys. Chem. B* **2013,** *117* (32), 9518-9531.

99.   Provorse Long, M. R.; Isborn, C. M., Combining explicit quantum solvent with a polarizable continuum model. *J. Phys. Chem. B* **2017,** *121* (43), 10105-10117.

100.   Yang, X.; Lei, H.; Gao, P.; Thomas, D. G.; Mobley, D. L.; Baker, N. A., Atomic radius and charge parameter uncertainty in biomolecular solvation energy calculations. *J. Chem. Theory Comput.* **2018,** *14* (2), 759-767.

101.   Mirzaei, S.; Ivanov, M. V.; Timerghazin, Q. K., Improving Performance of the SMD Solvation Model: Bondi Radii Improve Predicted Aqueous Solvation Free Energies of Ions and p K a Values of Thiols. *J. Phys. Chem. A* **2019,** *123* (44), 9498-9504.

102.   Engelage, E.; Schulz, N.; Heinen, F.; Huber, S. M.; Truhlar, D. G.; Cramer, C. J., Refined SMD Parameters for Bromine and Iodine Accurately Model Halogen-Bonding Interactions in Solution. *Chem. Eng. J.* **2018,** *24* (60), 15983-15987.

103.   Sastre, S.; Casasnovas, R.; Munoz, F.; Frau, J., Isodesmic reaction for accurate theoretical pK_a calculations of amino acids and peptides. *Phys. Chem. Chem. Phys* **2016,** *18* (16), 11202-11212.

104.   Pliego Jr, J. R., Basic hydrolysis of formamide in aqueous solution: a reliable theoretical calculation of the activation free energy using the cluster-continuum model. *Chem. Phys.* **2004,** *306* (1-3), 273-280.

105.   Ho, J.; Coote, M. L., A universal approach for continuum solvent pK_a calculations: are we there yet? *Theor. Chem. Acc.* **2010,** *125* (1), 3-21.

106.   Pliego, J. R.; Riveros, J. e., M., The cluster- continuum model for the calculation of the solvation free energy of ionic species. *J. Phys. Chem. A* **2001,** *105* (30), 7241-7247.

107.   Kelly, C. P.; Cramer, C. J.; Truhlar, D. G., Adding Explicit Solvent Molecules to Continuum Solvent Calculations for the Calculation of Aqueous Acid Dissociation Constants. *J. Phys. Chem. A* **2006,** *110*, 2493-2499.

108.   Bryantsev, V. S.; Diallo, M. S.; Goddard Iii, W. A., Calculation of solvation free energies of charged solutes using mixed cluster/continuum models. *J. Phys. Chem. B* **2008,** *112* (32), 9709-9719.

109.   Pliego Jr, J. R.; Riveros, J. M., Hybrid discrete-continuum solvation methods. *Wiley Interdiscip. Rev. Comput. Mol. Sci.* **2020,** *10* (2), e1440.

110.   Wu, W.; Kieffer, J., New hybrid method for the calculation of the solvation free energy of small molecules in aqueous solutions. *J. Chem. Theory Comput.* **2018,** *15* (1), 371-381.

111.   Stauch, T., Quantum chemical modeling of molecules under pressure. *Int. J. Quantum Chem.* **2021,** *121* (3), e26208.
112.   Robert, A.; Luukkonen, S.; Levesque, M., Pressure correction for solvation theories. *J. Chem. Phys.* **2020,** *152* (19), 191103.
113.   Cammi, R., A new extension of the polarizable continuum model: Toward a quantum chemical description of chemical reactions at extreme high pressure. *Journal of Computational Chemistry* **2015,** *36* (30), 2246-2259.
114.   Cammi, R., Quantum chemistry at the high pressures: The eXtreme pressure polarizable continuum model (XP-PCM). In *Frontiers of Quantum Chemistry*, Springer: 2018; pp 273-287.
115.   Hellweg, A.; Eckert, F., Brick by brick computation of the gibbs free energy of reaction in solution using quantum chemistry and COSMO-RS. *AIChE J.* **2017,** *63* (9), 3944-3954.
116.   Liu, J.-L.; Eisenberg, B., Poisson-Fermi modeling of ion activities in aqueous single and mixed electrolyte solutions at variable temperature. *J. Chem. Phys.* **2018,** *148* (5), 054501.
117.   Chamberlin, A. C.; Levitt, D. G.; Cramer, C. J.; Truhlar, D. G., Modeling Free Energies of Solvation in Olive Oil. *Mol. Pharmaceutics* **2008,** *5* (6), 1064-1079.
118.   Gupta, M.; Svendsen, H. F., Modeling temperature dependent and absolute carbamate stability constants of amines for CO2 capture. *Int. J. Greenh. Gas Control.* **2020,** *98*, 103061.
119.   Knight, J. L.; Brooks III, C. L., Surveying implicit solvent models for estimating small molecule absolute hydration free energies. *J. Comput. Chem.* **2011,** *32* (13), 2909-2923.
120.   Zhang, H.; Tan, T.; Van der Spoel, D., Generalized born and explicit solvent models for free energy calculations in organic solvents: Cyclodextrin dimerization. *J. Chem. Theory Comput.* **2015,** *11* (11), 5103-5113.
121.   Zhang, J.; Zhang, H.; Wu, T.; Wang, Q.; van der Spoel, D., Comparison of implicit and explicit solvent models for the calculation of solvation free energy in organic solvents. *J. Chem. Theory Comput.* **2017,** *13* (3), 1034-1043.
122.   Vyboishchikov, S. F.; Voityuk, A. A., Fast non-iterative calculation of solvation energies for water and non-aqueous solvents. *J. Comput. Chem.* **2021,** *42* (17), 1184-1194.
123.   Kundi, V.; Ho, J., Predicting Octanol-Water Partition Coefficients: Are Quantum Mechanical Implicit Solvent Models Better than Empirical Fragment-Based Methods? *J. Phys. Chem. B* **2019,** *123* (31), 6810-6822.
124.   Liu, Z.; Patel, C.; Harvey, J. N.; Sunoj, R. B., Mechanism and reactivity in the Morita–Baylis–Hillman reaction: the challenge of accurate computations. *Phys. Chem. Chem. Phys* **2017,** *19* (45), 30647-30657.
125.   Chen, J.; Shao, Y.; Ho, J., Are explicit solvent models more accurate than implicit solvent models? A case study on the Menschutkin reaction. *J. Phys. Chem. A* **2019,** *123* (26), 5580-5589.
126.   Vennelakanti, V.; Nazemi, A.; Mehmood, R.; Steeves, A. H.; Kulik, H. J., Harder, better, faster, stronger: large-scale QM and QM/MM for predictive modeling in enzymes and proteins. *Curr. Opin. Struct. Biol.* **2022,** *72*, 9-17.
127.   Jorgensen, W. L.; Chandrasekhar, J.; Madura, J. D.; Impey, R. W.; Klein, M. L., Comparison of simple potential functions for simulating liquid water. *J. Chem. Phys* **1983,** *79* (2), 926-935.
128.   Abascal, J. L.; Vega, C., A general purpose model for the condensed phases of water: TIP4P/2005. *J. Chem. Phys* **2005,** *123* (23), 234505.
129.   Berendsen, H.; Grigera, J.; Straatsma, T., The missing term in effective pair potentials. *J. Phys. Chem.* **1987,** *91* (24), 6269-6271.
130.   Espinosa, J. R.; Wand, C. R.; Vega, C.; Sanz, E.; Frenkel, D., Calculation of the water-octanol partition coefficient of cholesterol for SPC, TIP3P, and TIP4P water. *J. Chem. Phys* **2018,** *149* (22), 224501.

131.   Cornell, W. D.; Cieplak, P.; Bayly, C. I.; Gould, I. R.; Merz, K. M.; Ferguson, D. M.; Spellmeyer, D. C.; Fox, T.; Caldwell, J. W.; Kollman, P. A., A second generation force field for the simulation of proteins, nucleic acids, and organic molecules. *J. Am. Chem. Soc.* **1995,** *117* (19), 5179-5197.

132.   MacKerell Jr, A. D.; Bashford, D.; Bellott, M.; Dunbrack Jr, R. L.; Evanseck, J. D.; Field, M. J.; Fischer, S.; Gao, J.; Guo, H.; Ha, S., All-atom empirical potential for molecular modeling and dynamics studies of proteins. *J. Phys. Chem. B* **1998,** *102* (18), 3586-3616.

133.   Jorgensen, W. L.; Maxwell, D. S.; Tirado-Rives, J., Development and testing of the OPLS all-atom force field on conformational energetics and properties of organic liquids. *J. Am. Chem. Soc.* **1996,** *118* (45), 11225-11236.

134.   Lin, F.-Y.; MacKerell, A. D., Force fields for small molecules. In *Biomolecular Simulations*, Springer: 2019; pp 21-54.

135.   Jing, Z.; Liu, C.; Cheng, S. Y.; Qi, R.; Walker, B. D.; Piquemal, J.-P.; Ren, P., Polarizable force fields for biomolecular simulations: Recent advances and applications. *Annu. Rev. Biophys.* **2019,** *48*, 371-394.

136.   Patel, S.; Brooks III, C. L., Fluctuating charge force fields: recent developments and applications from small molecules to macromolecular biological systems. *Mol. Simul.* **2006,** *32* (3-4), 231-249.

137.   Lamoureux, G.; MacKerell Jr, A. D.; Roux, B., A simple polarizable model of water based on classical Drude oscillators. *J. Chem. Phys.* **2003,** *119* (10), 5185-5197.

138.   Spicher, S.; Grimme, S., Robust atomistic modeling of materials, organometallic, and biochemical systems. *Angew. Chem. Int.* **2020,** *132* (36), 15795-15803.

139.   Lagardère, L.; Jolly, L.-H.; Lipparini, F.; Aviat, F.; Stamm, B.; Jing, Z. F.; Harger, M.; Torabifard, H.; Cisneros, G. A.; Schnieders, M. J.; Gresh, N.; Maday, Y.; Ren, P. Y.; Ponder, J. W.; Piquemal, J.-P., Tinker-HP: a massively parallel molecular dynamics package for multiscale simulations of large complex systems with advanced point dipole polarizable force fields. *Chem. Sci.* **2018,** *9* (4), 956-972.

140.   Goloviznina, K.; Canongia Lopes, J. N.; Costa Gomes, M.; Pádua, A. A. H., Transferable, polarizable force field for ionic liquids. *J. Chem. Theory Comput.* **2019,** *15* (11), 5858-5871.

141.   Goloviznina, K.; Gong, Z.; Costa Gomes, M. F.; Pádua, A. A. H., Extension of the CL&Pol Polarizable Force Field to Electrolytes, Protic Ionic Liquids, and Deep Eutectic Solvents. *J. Chem. Theory Comput.* **2021,** *17* (3), 1606-1617.

142.   Doherty, B.; Zhong, X.; Gathiaka, S.; Li, B.; Acevedo, O., Revisiting OPLS force field parameters for ionic liquid simulations. *J. Chem. Theory Comput.* **2017,** *13* (12), 6131-6145.

143.   Bedrov, D.; Piquemal, J.-P.; Borodin, O.; MacKerell Jr, A. D.; Roux, B.; Schröder, C., Molecular dynamics simulations of ionic liquids and electrolytes using polarizable force fields. *Chem. Rev.* **2019,** *119* (13), 7940-7995.

144.   Chu, H.; Cao, L.; Peng, X.; Li, G., Polarizable force field development for lipids and their efficient applications in membrane proteins. *Wiley Interdiscip. Rev. Comput. Mol. Sci.* **2017,** *7* (5), e1312.

145.   Aleksandrov, A.; Lin, F.-Y.; Roux, B.; MacKerell Jr, A. D., Combining the polarizable Drude force field with a continuum electrostatic Poisson--Boltzmann implicit solvation model. *J. Comput. Chem.* **2018,** *39* (22), 1707-1719.

146.   Souza, P. C. T.; Alessandri, R.; Barnoud, J.; Thallmair, S.; Faustino, I.; Grünewald, F.; Patmanidis, I.; Abdizadeh, H.; Bruininks, B. M. H.; Wassenaar, T. A.; Kroon, P. C.; Melcr, J.; Nieto, V.; Corradi, V.; Khan, H. M.; Domański, J.; Javanainen, M.; Martinez-Seara, H.; Reuter, N.; Best, R. B.; Vattulainen, I.; Monticelli, L.; Periole, X.; Tieleman, D. P.; Vries, A. H. d.; Marrink, S. J.,

Martini 3: a general purpose force field for coarse-grained molecular dynamics. *Nat. Methods* **2021**, 1-7.

147.   Marrink, S. J.; De Vries, A. H.; Mark, A. E., Coarse grained model for semiquantitative lipid simulations. *J. Phys. Chem. B* **2004,** *108* (2), 750-760.

148.   Smith, J. S.; Isayev, O.; Roitberg, A. E., ANI-1: an extensible neural network potential with DFT accuracy at force field computational cost. *Chem. Sci.* **2017,** *8* (4), 3192-3203.

149.   Zhang, L.; Han, J.; Wang, H.; Car, R.; Weinan, E., Deep potential molecular dynamics: a scalable model with the accuracy of quantum mechanics. *Phys. Rev. Lett.* **2018,** *120* (14), 143001.

150.   Kashefolgheta, S.; Wang, S.; Acree Jr, W. E.; Hunenberger, P., Evaluation of nine condensed-phase force fields of the GROMOS, CHARMM, OPLS, AMBER, and OpenFF families against experimental cross-solvation free energies. *Phys. Chem. Chem. Phys* **2021,** *23*, 13055-13074.

151.   Kashefolgheta, S.; Oliveira, M. P.; Rieder, S. R.; Horta, B. A.; Acree Jr, W. E.; Hünenberger, P. H., Evaluating Classical Force Fields against Experimental Cross-Solvation Free Energies. *J. Chem. Theory Comput.* **2020,** *16* (12), 7556-7580.

152.   Vassetti, D.; Pagliai, M.; Procacci, P., Assessment of GAFF2 and OPLS-AA general force fields in combination with the water models TIP3P, SPCE, and OPC3 for the solvation free energy of druglike organic molecules. *J. Chem. Theory Comput.* **2019,** *15* (3), 1983-1995.

153.   Kelly, B. D.; Smith, W. R., A Simple Method for Including Polarization Effects in Solvation Free Energy Calculations When Using Fixed-Charge Force Fields: Alchemically Polarized Charges. *ACS Omega* **2020,** *5* (28), 17170-17181.

154.   Dodda, L. S.; Vilseck, J. Z.; Tirado-Rives, J.; Jorgensen, W. L., 1.14* CM1A-LBCC: localized bond-charge corrected CM1A charges for condensed-phase simulations. *J. Phys. Chem. B* **2017,** *121* (15), 3864-3870.

155.   Besler, B. H.; Merz Jr, K. M.; Kollman, P. A., Atomic charges derived from semiempirical methods. *J. Comput. Chem.* **1990,** *11* (4), 431-439.

156.   Bayly, C. I.; Cieplak, P.; Cornell, W.; Kollman, P. A., A well-behaved electrostatic potential based method using charge restraints for deriving atomic charges: the RESP model. *J. Phys. Chem.* **1993,** *97* (40), 10269-10280.

157.   Milne, A. W.; Jorge, M., Polarization corrections and the hydration free energy of water. *J. Chem. Theory Comput.* **2018,** *15* (2), 1065-1078.

158.   Konig, G.; Pickard, F. C.; Huang, J.; Thiel, W.; MacKerell, A. D.; Brooks, B. R.; York, D. M., A comparison of QM/MM simulations with and without the Drude oscillator model based on hydration free energies of simple solutes. *Molecules* **2018,** *23* (10), 2695.

159.   Ngo, V. A.; Fanning, J. K.; Noskov, S. Y., Comparative analysis of protein hydration from MD simulations with additive and polarizable force fields. *Adv. Theory Simul.* **2019,** *2* (2), 1800106.

160.   Ren, P.; Wu, C.; Ponder, J. W., Polarizable atomic multipole-based molecular mechanics for organic molecules. *J. Chem. Theory Comput.* **2011,** *7* (10), 3143-3161.

161.   Heid, E.; Szabadi, A.; Schröder, C., Quantum mechanical determination of atomic polarizabilities of ionic liquids. *Phys. Chem. Chem. Phys* **2018,** *20* (16), 10992-10996.

162.   Heid, E.; Fleck, M.; Chatterjee, P.; Schröder, C.; MacKerell Jr, A. D., Toward prediction of electrostatic parameters for force fields that explicitly treat electronic polarization. *J. Chem. Theory Comput.* **2019,** *15* (4), 2460-2469.

163.   Barnett, R. N.; Landman, U., Born-Oppenheimer molecular-dynamics simulations of finite systems: Structure and dynamics of $(H_2O)_2$. *Phys. Rev. B* **1993,** *48* (4), 2081.

164.   Iftimie, R.; Minary, P.; Tuckerman, M. E., *Ab initio* molecular dynamics: Concepts, recent developments, and future trends. *PNAS* **2005,** *102* (19), 6654-6659.

165.   Iannuzzi, M.; Laio, A.; Parrinello, M., Efficient exploration of reactive potential energy surfaces using Car-Parrinello molecular dynamics. *Phys. Rev. Lett.* **2003,** *90* (23), 238302.

166.   Komeiji, Y.; Nakano, T.; Fukuzawa, K.; Ueno, Y.; Inadomi, Y.; Nemoto, T.; Uebayasi, M.; Fedorov, D. G.; Kitaura, K., Fragment molecular orbital method: application to molecular dynamics simulation,'*ab initio* FMO-MD'. *Chem. Phys. Lett.* **2003,** *372* (3-4), 342-347.

167.   Wang, J.; Román-Pérez, G.; Soler, J. M.; Artacho, E.; Fernández-Serra, M.-V., Density, structure, and dynamics of water: The effect of van der Waals interactions. *J. Chem. Phys* **2011,** *134* (2), 024516.

168.   Crespo, Y.; Hassanali, A., Characterizing the local solvation environment of OH⁻ in water clusters with AIMD. *J. Chem. Phys* **2016,** *144* (7), 074304.

169.   Crabb, E.; France-Lanord, A.; Leverick, G.; Stephens, R.; Shao-Horn, Y.; Grossman, J. C., Importance of Equilibration Method and Sampling for *Ab Initio* Molecular Dynamics Simulations of Solvent–Lithium-Salt Systems in Lithium-Oxygen Batteries. *J. Chem. Theory Comput.* **2020,** *16* (12), 7255-7266.

170.   Markland, T. E.; Ceriotti, M., Nuclear quantum effects enter the mainstream. *Nat. Rev. Chem.* **2018,** *2* (3), 1-14.

171.   Marx, D.; Parrinello, M., *Ab initio* path integral molecular dynamics: Basic ideas. *J. Chem. Phys.* **1996,** *104* (11), 4077-4082.

172.   Habershon, S.; Manolopoulos, D. E.; Markland, T. E.; Miller III, T. F., Ring-polymer molecular dynamics: Quantum effects in chemical dynamics from classical trajectories in an extended phase space. *Annu. Rev. Phys. Chem.* **2013,** *64*, 387-413.

173.   Chung, L. W.; Sameera, W. M. C.; Ramozzi, R.; Page, A. J.; Hatanaka, M.; Petrova, G. P.; Harris, T. V.; Li, X.; Ke, Z.; Liu, F.; Li, H.-B.; Ding, L.; Morokuma, K., The ONIOM Method and Its Applications. *Chem. Rev.* **2015,** *115* (12), 5678-5796.

174.   Vreven, T.; Byun, K. S.; Komáromi, I.; Dapprich, S.; Montgomery Jr, J. A.; Morokuma, K.; Frisch, M. J., Combining quantum mechanics methods with molecular mechanics methods in ONIOM. *J. Chem. Theory Comput.* **2006,** *2* (3), 815-826.

175.   Loco, D.; Lagardère, L.; Caprasecca, S.; Lipparini, F.; Mennucci, B.; Piquemal, J.-P., Hybrid QM/MM molecular dynamics with AMOEBA polarizable embedding. *J. Chem. Theory Comput.* **2017,** *13* (9), 4025-4033.

176.   Lee, S. J. R.; Welborn, M.; Manby, F. R.; Miller III, T. F., Projection-based wavefunction-in-DFT embedding. *Acc. Chem. Res.* **2019,** *52* (5), 1359-1368.

177.   Govind, N.; Wang, Y. A.; Da Silva, A. J. R.; Carter, E. A., Accurate *ab initio* energetics of extended systems via explicit correlation embedded in a density functional environment. *Chem. Phys. Lett.* **1998,** *295* (1-2), 129-134.

178.   Libisch, F.; Huang, C.; Carter, E. A., Embedded correlated wavefunction schemes: Theory and applications. *Acc. Chem. Res.* **2014,** *47* (9), 2768-2775.

179.   Jones, L. O.; Mosquera, M. A.; Schatz, G. C.; Ratner, M. A., Embedding methods for quantum chemistry: applications from materials to life sciences. *J. Am. Chem. Soc.* **2020,** *142* (7), 3281-3295.

180.   Ainsley, J.; Lodola, A.; Mulholland, A. J.; Christov, C. Z.; Karabencheva-Christova, T. G., Combined quantum mechanics and molecular mechanics studies of enzymatic reaction mechanisms. *Adv. Protein. Chem. Struct. Biol.* **2018,** *113*, 1-32.

181.   Wang, E.; Sun, H.; Wang, J.; Wang, Z.; Liu, H.; Zhang, J. Z. H.; Hou, T., End-point binding free energy calculation with MM/PBSA and MM/GBSA: strategies and applications in drug design. *Chem. Rev.* **2019,** *119* (16), 9478-9508.

182.   Fogolari, F.; Corazza, A.; Esposito, G., Free energy, enthalpy and entropy from implicit solvent end-point simulations. *Front. Mol. Biosci.* **2018,** *5*, 11.

183.   Huai, Z.; Yang, H.; Li, X.; Sun, Z., SAMPL7 TrimerTrip host--guest binding affinities from extensive alchemical and end-point free energy calculations. *J. Comput. Aided Mol. Des.* **2021,** *35* (1), 117-129.

184.   Mishra, S. K.; Koča, J., Assessing the Performance of MM/PBSA, MM/GBSA, and QM--MM/GBSA Approaches on Protein/Carbohydrate Complexes: Effect of Implicit Solvent Models, QM Methods, and Entropic Contributions. *J. Phys. Chem. B* **2018,** *122* (34), 8113-8121.

185.   Shivakumar, D.; Williams, J.; Wu, Y.; Damm, W.; Shelley, J.; Sherman, W., Prediction of absolute solvation free energies using molecular dynamics free energy perturbation and the OPLS force field. *J. Chem. Theory Comput.* **2010,** *6* (5), 1509-1519.

186.   Cabeza de Vaca, I.; Zarzuela, R.; Tirado-Rives, J.; Jorgensen, W. L., Robust free energy perturbation protocols for creating molecules in solution. *J. Chem. Theory Comput.* **2019,** *15* (7), 3941-3948.

187.   Straatsma, T. P.; Berendsen, H. J. C., Free energy of ionic hydration: Analysis of a thermodynamic integration technique to evaluate free energy differences by molecular dynamics simulations. *J. Chem. Phys.* **1988,** *89* (9), 5876-5886.

188.   Barducci, A.; Bonomi, M.; Parrinello, M., Metadynamics. *Wiley Interdiscip. Rev. Comput. Mol. Sci.* **2011,** *1* (5), 826-843.

189.   Darve, E.; Rodríguez-Gómez, D.; Pohorille, A., Adaptive biasing force method for scalar and vector free energy calculations. *J. Chem. Phys* **2008,** *128* (14), 144120.

190.   Tribello, G. A.; Bonomi, M.; Branduardi, D.; Camilloni, C.; Bussi, G., PLUMED 2: New feathers for an old bird. *Comput. Phys. Commun.* **2014,** *185* (2), 604-613.

191.   Yang, Y. I.; Shao, Q.; Zhang, J.; Yang, L.; Gao, Y. Q., Enhanced sampling in molecular dynamics. *J. Chem. Phys* **2019,** *151* (7), 070902.

192.   Shirts, M. R.; Mobley, D. L., An introduction to best practices in free energy calculations. In *Biomolecular Simulations*, Springer: 2013; pp 271-311.

193.   Chodera, J. D.; Mobley, D. L.; Shirts, M. R.; Dixon, R. W.; Branson, K.; Pande, V. S., Alchemical free energy methods for drug discovery: progress and challenges. *Curr. Opin. Struct. Biol.* **2011,** *21* (2), 150-160.

194.   Shirts, M. R.; Mobley, D. L.; Chodera, J. D., Alchemical free energy calculations: ready for prime time? *Annu. Rep. Comput. Chem* **2007,** *3*, 41-59.

195.   Ganesan, A.; Coote, M. L.; Barakat, K., Molecular 'time-machines' to unravel key biological events for drug design. *WIREs Comput. Mol. Sci.* **2017,** *7* (4), e1306.

196.   Vyalov, I.; Vaksler, Y.; Koverga, V.; Miannay, F. A.; Kiselev, M.; Idrissi, A., Solvation free energy of solvation of biomass model cellobiose molecule: A molecular dynamics analysis. *J. Mol. Liq.* **2017,** *245*, 97-102.

197.   Khuttan, S.; Azimi, S.; Wu, J. Z.; Gallicchio, E., Alchemical transformations for concerted hydration free energy estimation with explicit solvation. *J. Chem. Phys.* **2021,** *154* (5), 054103.

198.   Kelly, B. D.; Smith, W. R., Alchemical hydration free-energy calculations using molecular dynamics with explicit polarization and induced polarity decoupling: an On--the--Fly polarization approach. *J. Chem. Theory Comput.* **2020,** *16* (2), 1146-1161.

199.   Procacci, P., Accuracy, precision, and efficiency of nonequilibrium alchemical methods for computing free energies of solvation. I. Bidirectional approaches. *J. Chem. Phys.* **2019,** *151* (14), 144113.

200.   Macchiagodena, M.; Pagliai, M.; Karrenbrock, M.; Guarnieri, G.; Iannone, F.; Procacci, P., Virtual Double-System Single-Box: A Nonequilibrium Alchemical Technique for Absolute Binding Free Energy Calculations: Application to Ligands of the SARS-CoV-2 Main Protease. *J. Chem. Theory Comput.* **2020,** *16* (11), 7160-7172.

201.	Korshunova, K.; Carloni, P., Ligand Affinities within the Open-Boundary Molecular Mechanics/Coarse-Grained Framework (I): Alchemical Transformations within the Hamiltonian Adaptive Resolution Scheme. *J. Phys. Chem. B* **2021,** *125* (3), 789-797.
202.	Zhuang, Y.; Bureau, H. R.; Quirk, S.; Hernandez, R., Adaptive steered molecular dynamics of biomolecules. *Mol.Simul.* **2020**, 1-12.
203.	Prasetyo, N.; Hofer, T. S., Structure, Dynamics, and Hydration Free Energy of Carbon Dioxide in Aqueous Solution: A Quantum Mechanical/Molecular Mechanics Molecular Dynamics Thermodynamic Integration (QM/MM MD TI) Simulation Study. *J. Chem. Theory Comput.* **2018,** *14* (12), 6472-6483.
204.	Miller III, B. R.; McGee Jr, T. D.; Swails, J. M.; Homeyer, N.; Gohlke, H.; Roitberg, A. E., MMPBSA. py: an efficient program for end-state free energy calculations. *J. Chem. Theory Comput.* **2012,** *8* (9), 3314-3321.
205.	Mey, A. S.; Allen, B.; Macdonald, H. E. B.; Chodera, J. D.; Kuhn, M.; Michel, J.; Mobley, D. L.; Naden, L. N.; Prasad, S.; Rizzi, A., Best practices for alchemical free energy calculations [Article v 1.0]. *arXiv preprint arXiv:.03067* **2020**.
206.	Li, Y.; Nam, K., Repulsive soft-core potentials for efficient alchemical free energy calculations. *J. Chem. Theory Comput.* **2020,** *16* (8), 4776-4789.
207.	Loeffler, H. H.; Bosisio, S.; Duarte Ramos Matos, G.; Suh, D.; Roux, B.; Mobley, D. L.; Michel, J., Reproducibility of free energy calculations across different molecular simulation software packages. *J. Chem. Theory Comput.* **2018,** *14* (11), 5567-5582.
208.	King, E.; Aitchison, E.; Luo, R., Recent Developments in Free Energy Calculations for Drug Discovery. *Front. Mol. Biosci. 8:712085*, doi: 10.3389/fmolb.2021.712085.
209.	Huai, Z.; Shen, Z.; Sun, Z., Binding thermodynamics and interaction patterns of inhibitor-major urinary protein-I binding from extensive free-energy calculations: benchmarking AMBER force fields. *J. Chem. Inf. Model* **2020,** *61* (1), 284-297.
210.	Bottaro, S.; Lindorff-Larsen, K.; Best, R. B., Variational optimization of an all-atom implicit solvent force field to match explicit solvent simulation data. *J. Chem. Theory Comput.* **2013,** *9* (12), 5641-5652.
211.	Mobley, D. L.; Bayly, C. I.; Cooper, M. D.; Shirts, M. R.; Dill, K. A., Small molecule hydration free energies in explicit solvent: an extensive test of fixed-charge atomistic simulations. *J. Chem. Theory Comput.* **2009,** *5* (2), 350-358.
212.	Lee, H.; Lim, H.-K.; Kim, H., Hydration thermodynamics of non-polar aromatic hydrocarbons: comparison of implicit and explicit solvation models. *Molecules* **2018,** *23* (11), 2927.
213.	Steinmann, S. N.; Sautet, P.; Michel, C., Solvation free energies for periodic surfaces: comparison of implicit and explicit solvation models. *Phys. Chem. Chem. Phys.* **2016,** *18* (46), 31850-31861.
214.	Assaf, K. I.; Florea, M.; Antony, J.; Henriksen, N. M.; Yin, J.; Hansen, A.; Qu, Z.-w.; Sure, R.; Klapstein, D.; Gilson, M. K.; Grimme, S.; Nau, W. M., Hydrophobe challenge: a joint experimental and computational study on the host--guest binding of hydrocarbons to cucurbiturils, allowing explicit evaluation of guest hydration free-energy contributions. *J. Phys. Chem. B* **2017,** *121* (49), 11144-11162.
215.	Liu, H.; Chen, F.; Sun, H.; Li, D.; Hou, T., Improving the Efficiency of Non-equilibrium Sampling in the Aqueous Environment via Implicit-Solvent Simulations. *J. Chem. Theory Comput.* **2017,** *13* (4), 1827-1836.
216.	Sun, Z.; Wang, X., Thermodynamics of Helix formation in small peptides of varying length in vacuo, implicit solvent and explicit solvent: Comparison between AMBER force fields. *J.Theor. Comput. Chem.* **2019,** *18* (03), 1950015.

42

217.   Kanchi, S.; Gosika, M.; Ayappa, K. G.; Maiti, P. K., Dendrimer interactions with lipid bilayer: Comparison of force field and effect of implicit vs explicit solvation. *J. Chem. Theory Comput.* **2018,** *14* (7), 3825-3839.

218.   Hey, A. J.; Tansley, S.; Tolle, K. M., *The fourth paradigm: data-intensive scientific discovery*. Microsoft research Redmond, WA: 2009; Vol. 1.

219.   Wu, Z.; Ramsundar, B.; Feinberg, E. N.; Gomes, J.; Geniesse, C.; Pappu, A. S.; Leswing, K.; Pande, V., MoleculeNet: a benchmark for molecular machine learning. *Chem. Sci.* **2018,** *9* (2), 513-530.

220.   Alibakhshi, A.; Hartke, B., Improved prediction of solvation free energies by machine-learning polarizable continuum solvation model. *Nat. Commun.* **2021,** *12* (1), 1-7.

221.   Rauer, C.; Bereau, T., Hydration free energies from kernel-based machine learning: Compound-database bias. *J. Chem. Phys.* **2020,** *153* (1), 014101.

222.   Zhang, P.; Shen, L.; Yang, W., Solvation free energy calculations with quantum mechanics/molecular mechanics and machine learning models. *J. Phys. Chem. B* **2018,** *123* (4), 901-908.

223.   Gebhardt, J.; Kiesel, M.; Riniker, S.; Hansen, N., Combining molecular dynamics and machine learning to predict self-solvation free energies and limiting activity coefficients. *J. Chem. Inf. Model.* **2020,** *60* (11), 5319-5330.

224.   Subramanian, V.; Ratkova, E.; Palmer, D.; Engkvist, O.; Fedorov, M.; Llinas, A., Multisolvent Models for Solvation Free Energy Predictions Using 3D-RISM Hydration Thermodynamic Descriptors. *J. Chem. Inf. Model.* **2020,** *60* (6), 2977-2988.

225.   Bleiziffer, P.; Schaller, K.; Riniker, S., Machine learning of partial charges derived from high-quality quantum-mechanical calculations. *J. Chem. Inf. Model* **2018,** *58* (3), 579-590.

226.   Bonati, L.; Rizzi, V.; Parrinello, M., Data-driven collective variables for enhanced sampling. *J. Phys. Chem. Lett* **2020,** *11* (8), 2998-3004.

227.   Bonati, L.; Zhang, Y.-Y.; Parrinello, M., Neural networks-based variationally enhanced sampling. *PNAS* **2019,** *116* (36), 17641-17647.

228.   Lim, H.; Jung, Y., MLSolvA: solvation free energy prediction from pairwise atomistic interactions by machine learning. *J. Cheminformatics* **2021,** *13* (1), 1-10.

229.   Pathak, Y.; Mehta, S.; Priyakumar, U. D., Learning Atomic Interactions through Solvation Free Energy Prediction Using Graph Neural Networks. *J. Chem. Inf. Model* **2021,** *61* (2), 689-698.

230.   Borhani, T. N.; Garcia-Munoz, S.; Luciani, C. V.; Galindo, A.; Adjiman, C. S., Hybrid QSPR models for the prediction of the free energy of solvation of organic solute/solvent pairs. *Phys. Chem. Chem. Phys.* **2019,** *21* (25), 13706-13720.

231.   Seritan, S.; Bannwarth, C.; Fales, B. S.; Hohenstein, E. G.; Kokkila-Schumacher, S. I. L.; Luehr, N.; Snyder Jr, J. W.; Song, C.; Titov, A. V.; Ufimtsev, I. S.; Wang, L.-P.; Martínez, T. J., TeraChem: Accelerating electronic structure and ab initio molecular dynamics with graphical processing units. *J. Chem. Phys.* **2020,** *152* (22), 224110.

232.   Liu, F.; Luehr, N.; Kulik, H. J.; Martinez, T. J., Quantum chemistry for solvated molecules on graphical processing units using polarizable continuum models. *J. Chem. Theory Comput.* **2015,** *11* (7), 3131-3144.

233.   Gong, X.; Chiricotto, M.; Liu, X.; Nordquist, E.; Feig, M.; Brooks III, C. L.; Chen, J., Accelerating the Generalized Born with Molecular Volume and Solvent Accessible Surface Area Implicit Solvent Model Using Graphics Processing Units. *J. Comput. Chem.* **2020,** *41* (8), 830-838.

234.   Huang, H.; Simmerling, C., Fast pairwise approximation of solvent accessible surface area for implicit solvent simulations of proteins on CPUs and GPUs. *J. Chem. Theory Comput.* **2018,** *14* (11), 5797-5814.

235.   Lee, T.-S.; Cerutti, D. S.; Mermelstein, D.; Lin, C.; LeGrand, S.; Giese, T. J.; Roitberg, A.; Case, D. A.; Walker, R. C.; York, D. M., GPU-accelerated molecular dynamics and free energy methods in Amber18: performance enhancements and new features. *J. Chem. Inf. Model.* **2018,** *58* (10), 2043-2050.

236.   Qi, R.; Luo, R., Robustness and Efficiency of Poisson--Boltzmann Modeling on Graphics Processing Units. *J. Chem. Inf. Model.* **2018,** *59* (1), 409-420.

237.   Lake, P. T.; Mattson, M. A.; McCullagh, M., Implicit Solvation Using the Superposition Approximation (IS-SPA): Extension to Peptides in a Polar Solvent. *J. Chem. Theory Comput.* **2021,** *17* (2), 703-713.

238.   Ou, S.-C.; Drake, J. A.; Pettitt, B. M., Nonpolar solvation free energy from proximal distribution functions. *J. Phys. Chem. B* **2017,** *121* (15), 3555-3564.

239.   Zhang, H.; Jiang, Y.; Yan, H.; Yin, C.; Tan, T.; van der Spoel, D., Free-energy calculations of ionic hydration consistent with the experimental hydration free energy of the proton. *J. Phys. Chem. Lett* **2017,** *8* (12), 2705-2712.

240.   Zhang, H.; Jiang, Y.; Yan, H.; Cui, Z.; Yin, C., Comparative assessment of computational methods for free energy calculations of ionic hydration. *J. Chem. Inf. Model* **2017,** *57* (11), 2763-2775.

241.   Callsen, M.; Sodeyama, K.; Futera, Z. k.; Tateyama, Y.; Hamada, I., The solvation structure of lithium ions in an ether based electrolyte solution from first-principles molecular dynamics. *J. Phys. Chem. B* **2017,** *121* (1), 180-188.

242.   Kröger, L. C.; Müller, S.; Smirnova, I.; Leonhard, K., Prediction of Solvation Free Energies of Ionic Solutes in Neutral Solvents. *J. Phys. Chem. A* **2020,** *124* (20), 4171-4181.

243.   Molavi Tabrizi, A.; Goossens, S.; Mehdizadeh Rahimi, A.; Knepley, M.; Bardhan, J. P., Predicting solvation free energies and thermodynamics in polar solvents and mixtures using a solvation-layer interface condition. *J. Chem. Phys.* **2017,** *146* (9), 094103.

244.   Duignan, T. T.; Baer, M. D.; Schenter, G. K.; Mundy, C. J., Electrostatic solvation free energies of charged hard spheres using molecular dynamics with density functional theory interactions. *J. Chem. Phys.* **2017,** *147* (16), 161716.

245.   Budkov, Y. A., Statistical field theory of ion--molecular solutions. *Phys. Chem. Chem. Phys.* **2020,** *22* (26), 14756-14772.

246.   Chaudhari, M. I.; Pratt, L. R.; Rempe, S. B., Utility of chemical computations in predicting solution free energies of metal ions. *Mol. Simul.* **2018,** *44* (2), 110-116.

247.   Tomaník, L.; Muchová, E.; Slavíček, P., Solvation energies of ions with ensemble cluster-continuum approach. *Physical Chemistry Chemical Physics* **2020,** *22* (39), 22357-22368.

248.   Houriez, C.; Real, F.; Vallet, V.; Mautner, M.; Masella, M., Ion hydration free energies and water surface potential in water nano drops: The cluster pair approximation and the proton hydration Gibbs free energy in solution. *J. Chem. Phys.* **2019,** *151* (17), 174504.

249.   Hofer, T. S.; Hunenberger, P. H., Absolute proton hydration free energy, surface potential of water, and redox potential of the hydrogen electrode from first principles: QM/MM MD free-energy simulations of sodium and potassium hydration. *J. Chem. Phys.* **2018,** *148* (22), 222814.

250.   Voityuk, A. A.; Vyboishchikov, S. F., Fast and accurate calculation of hydration energies of molecules and ions. *Phys. Chem. Chem. Phys.* **2020,** *22* (26), 14591-14598.

251.   Basdogan, Y.; Groenenboom, M. C.; Henderson, E.; De, S.; Rempe, S. B.; Keith, J. A., Machine learning-guided approach for studying solvation environments. *J. Chem. Theory Comput.* **2019,** *16* (1), 633-642.

252.   Kalhor, P.; Xu, J.; Ashraf, H.; Cao, B.; Yu, Z.-W., Structural Properties and Hydrogen-Bonding Interactions in Binary Mixtures Containing a Deep-Eutectic Solvent and Acetonitrile. *J. Phys. Chem. B* **2020,** *124* (7), 1229-1239.

253.   Hu, Y.; Luo, P., Energy change mechanisms of HMX solute molecules in pure solvents and binary solvent mixtures. *J. Mol. Liq.* **2021,** *332,* 115898.

254.   Stein, C. J.; Herbert, J. M.; Head-Gordon, M., The Poisson--Boltzmann model for implicit solvation of electrolyte solutions: Quantum chemical implementation and assessment via Sechenov coefficients. *J. Chem. Phys.* **2019,** *151* (22), 224111.

255.   Wang, C.; Ren, P.; Luo, R., Ionic solution: what goes right and wrong with continuum solvation modeling. *J. Phys. Chem. B* **2017,** *121* (49), 11169-11179.

256.   Abdel-Azeim, S., Revisiting OPLS-AA force field for the simulation of anionic surfactants in concentrated electrolyte solutions. *J. Chem. Theory Comput.* **2020,** *16* (2), 1136-1145.

257.   Clabaut, P.; Schweitzer, B.; Gotz, A. W.; Michel, C.; Steinmann, S. N., Solvation Free Energies and Adsorption Energies at the Metal/Water Interface from Hybrid Quantum-Mechanical/Molecular Mechanics Simulations. *J. Chem. Theory Comput.* **2020,** *16* (10), 6539-6549.

258.   Tesei, G.; Aspelin, V.; Lund, M., Specific Cation Effects on SCN–in Bulk Solution and at the Air–Water Interface. *J. Phys. Chem. B* **2018,** *122* (19), 5094-5105.

259.   McCaffrey, D. L.; Nguyen, S. C.; Cox, S. J.; Weller, H.; Alivisatos, A. P.; Geissler, P. L.; Saykally, R. J., Mechanism of ion adsorption to aqueous interfaces: Graphene/water vs. air/water. *PNAS* **2017,** *114* (51), 13369-13373.

260.   Benimam, H.; Si-Moussa, C.; Laidi, M.; Hanini, S., Modeling the activity coefficient at infinite dilution of water in ionic liquids using artificial neural networks and support vector machines. *Neural. Comput. Appl.* **2020,** *32* (12), 8635-8653.

261.   Bononi, F. C.; Chen, Z.; Rocca, D.; Andreussi, O.; Hullar, T.; Anastasio, C.; Donadio, D., Bathochromic Shift in the UV--Visible Absorption Spectra of Phenols at Ice Surfaces: Insights from First-Principles Calculations. *J. Phys. Chem. A* **2020,** *124* (44), 9288-9298.

262.   Zhao, X.; Zheng, W.; Miao, X.; Huang, W., Barbituric acid-based mono/bi-heterocyclic dyes showing distinct spectral behaviors induced by solvents and pH. *Dyes Pigm.* **2021,** *187,* 109087.

263.   Awoonor-Williams, E.; Walsh, A. G.; Rowley, C. N., Modeling covalent-modifier drugs. *Biochim. Biophys. Acta* **2017,** *1865* (11), 1664-1675.

264.   Lintuluoto, M.; Yamada, C.; Lintuluoto, J. M., QM/MM Calculation of the Enzyme Catalytic Cycle Mechanism for Copper-and Zinc-Containing Superoxide Dismutase. *J. Phys. Chem. B* **2017,** *121* (30), 7235-7246.

265.   Tu, Y.-J.; Njus, D.; Schlegel, H. B., A theoretical study of ascorbic acid oxidation and HOO˙/O2˙− radical scavenging. *Org. Biomol. Chem* **2017,** *15,* 4417-4431.

266.   Sales, A. L. R.; Silla, J. e., M.; Neto, J. L.; Anconi, C. P. A., Condensed-phase relative Gibbs free energy and E/Z descriptors for 2-acetylthiophene and 2-acetylthiophene-N1-phenyl thiosemicarbazones. *J. Mol. Model.* **2021,** *27* (4), 1-15.

267.   Grifoni, E.; Piccini, G.; Parrinello, M., Microscopic description of acid--base equilibrium. *PNAS* **2019,** *116* (10), 4054-4057.

268.   Slocum, J. D.; First, J. T.; Webb, L. J., Orthogonal Electric Field Measurements near the Green Fluorescent Protein Fluorophore through Stark Effect Spectroscopy and pK_a Shifts Provide a Unique Benchmark for Electrostatics Models. *J. Phys. Chem. B* **2017,** *121* (28), 6799-6812.

269.   Sánchez-Castellanos, M.; Flores-Leonar, M. M.; Mata-Pinzón, Z.; Laguna, H. G.; García-Ruiz, K. M.; Rozenel, S. S.; Ugalde-Saldívar, V. M.; Moreno-Esparza, R.; Pijpers, J. J. H.; Amador-Bedolla, C., Theoretical exploration of 2,2'-bipyridines as electro-active compounds in flow batteries. *Physical Chemistry Chemical Physics* **2019,** *21* (28), 15823-15832.

270.   King, E.; Qi, R.; Li, H.; Luo, R.; Aitchison, E., Estimating the Roles of Protonation and Electronic Polarization in Absolute Binding Affinity Simulations. *J. Chem. Theory Comput.* **2021**.

271.   Ho, J.; Coote, M. L., First-principles prediction of acidities in the gas and solution phase. *WIREs Comput. Mol. Sci.* **2011,** *1* (5), 649-660.

272.   Seybold, P. G.; Shields, G. C., Computational estimation of pK_a values. *WIREs Comput. Mol. Sci.* **2015,** *5* (3), 290-297.

273.   Casasnovas, R.; Ortega-Castro, J.; Frau, J.; Donoso, J.; Muñoz, F., Theoretical pKa calculations with continuum model solvents, alternative protocols to thermodynamic cycles. *Int. J. Quant. Chem.* **2014,** *114* (20), 1350-1363.

274.   Alexov, E.; Mehler, E. L.; Baker, N.; M. Baptista, A.; Huang, Y.; Milletti, F.; Erik Nielsen, J.; Farrell, D.; Carstensen, T.; Olsson, M. H. M.; Shen, J. K.; Warwicker, J.; Williams, S.; Word, J. M., Progress in the prediction of pK_a values in proteins. *Proteins: Struct., Funct., Bioinf.* **2011,** *79* (12), 3260-3275.

275.   Ho, J., Are thermodynamic cycles necessary for continuum solvent calculation of pK_as and reduction potentials? *Phys. Chem. Chem. Phys.* **2015,** *17* (4), 2859-2868.

276.   Jensen, J. H.; Swain, C. J.; Olsen, L., Prediction of pK_a Values for Druglike Molecules Using Semiempirical Quantum Chemical Methods. *J. Phys. Chem. A* **2017,** *121* (3), 699-707.

277.   Banerjee, S.; Bhanja, S. K.; Chattopadhyay, P. K., Quantum chemical predictions of aqueous pK_a values for OH groups of some α-hydroxycarboxylic acids based on ab initio and DFT calculations. *Comput. Theor. Chem.* **2018,** *1125*, 29-38.

278.   Malloum, A.; Fifen, J. J.; Conradie, J., Determination of the absolute solvation free energy and enthalpy of the proton in solutions. *J. Mol. Liq.* **2021,** *322*, 114919.

279.   Rossini, E.; Bochevarov, A. D.; Knapp, E. W., Empirical Conversion of pK_a Values between Different Solvents and Interpretation of the Parameters: Application to Water, Acetonitrile, Dimethyl Sulfoxide, and Methanol. *ACS omega* **2018,** *3* (2), 1653-1662.

280.   Pliego, J. R.; Riveros, J. M., Theoretical Calculation of pKa Using the Cluster–Continuum Model. *J. Phys. Chem. A* **2002,** *106* (32), 7434-7439.

281.   Adam, K. R., New Density Functional and Atoms in Molecules Method of Computing Relative pK_a Values in Solution. *J. Phys. Chem. A* **2002,** *106* (49), 11963-11972.

282.   Ho, J.; Coote, M. L., pKa Calculation of Some Biologically Important Carbon Acids - An Assessment of Contemporary Theoretical Procedures. *J. Chem. Theory Comput.* **2009,** *5* (2), 295-306.

283.   Thapa, B.; Schlegel, H. B., Improved pK_a Prediction of Substituted Alcohols, Phenols, and Hydroperoxides in Aqueous Medium Using Density Functional Theory and a Cluster-Continuum Solvation Model. *J. Phys. Chem. A* **2017,** *121* (24), 4698-4706.

284.   Thapa, B.; Schlegel, H. B., Calculations of pK_a's and Redox Potentials of Nucleobases with Explicit Waters and Polarizable Continuum Solvation. *J. Phys. Chem. A* **2015,** *119* (21), 5134-5144.

285.   Zhang, S., A reliable and efficient first principles-based method for predicting pK_a values. III. Adding explicit water molecules: Can the theoretical slope be reproduced and pK_a values predicted more accurately? *J. Comput. Chem.* **2012,** *33* (5), 517-526.

286.   Sham, Y. Y.; Chu, Z. T.; Warshel, A., Consistent Calculations of pK_a's of Ionizable Residues in Proteins: Semi-microscopic and Microscopic Approaches. *J. Phys. Chem. B* **1997,** *101* (22), 4458-4472.

287.   Chen, W.; Morrow, B. H.; Shi, C.; Shen, J. K., Recent development and application of constant pH molecular dynamics. *Mol. simul.* **2014,** *40* (10-11), 830-838.

288.   Mongan, J.; Case, D. A., Biomolecular simulations at constant pH. *Curr Opin Struct Biol* **2005,** *15* (2), 157-63.

289.   Baptista, A. M.; Teixeira, V. H.; Soares, C. M., Constant-pH molecular dynamics using stochastic titration. *J. Chem. Phys.* **2002,** *117* (9), 4184-4200.

290.   Bürgi, R.; Kollman, P. A.; Van Gunsteren, W. F., Simulating proteins at constant pH: An approach combining molecular dynamics and Monte Carlo simulation. *Proteins* **2002,** *47* (4), 469-80.

291.   Börjesson, U.; Hünenberger, P. H., Explicit-solvent molecular dynamics simulation at constant pH: Methodology and application to small amines. *J. Chem. Phys.* **2001,** *114* (22), 9706-9719.

292.   Wallace, J. A.; Shen, J. K., Continuous Constant pH Molecular Dynamics in Explicit Solvent with pH-Based Replica Exchange. *J. Chem. Theory Comput.* **2011,** *7* (8), 2617-2629.

293.   Wallace, J. A.; Shen, J. K., Charge-leveling and proper treatment of long-range electrostatics in all-atom molecular dynamics at constant pH. *J. Chem. Phys.* **2012,** *137* (18), 184105.

294.   Messer, B. M.; Roca, M.; Chu, Z. T.; Vicatos, S.; Kilshtain, A. V.; Warshel, A., Multiscale simulations of protein landscapes: using coarse-grained models as reference potentials to full explicit models. *Proteins* **2010,** *78* (5), 1212-27.

295.   Itoh, S. G.; Damjanović, A.; Brooks, B. R., pH replica-exchange method based on discrete protonation states. *Proteins* **2011,** *79* (12), 3420-36.

296.   Harris, R. C.; Liu, R.; Shen, J., Predicting reactive cysteines with implicit-solvent-based continuous constant pH molecular dynamics in amber. *J. Chem. Theory Comput.* **2020,** *16* (6), 3689-3698.

297.   Reis, P. B.; Vila-Viçosa, D.; Rocchia, W.; Machuqueiro, M., PypKa: A Flexible Python Module for Poisson–Boltzmann-Based pK_a Calculations. *J. Chem. Inf. Model* **2020,** *60* (10), 4442-4448.

298.   Sun, Z.; Wang, X.; Song, J., Extensive Assessment of Various Computational Methods for Aspartate's pK_a Shift. *J. Chem. Inf. Model* **2017,** *57* (7), 1621-1639.

299.   Aleksandrov, A.; Roux, B.; MacKerell Jr, A. D., pKa Calculations with the Polarizable Drude Force Field and Poisson--Boltzmann Solvation Model. *J. Chem. Theory Comput.* **2020,** *16* (7), 4655-4668.

300.   Sharma, I.; Kaminski, G. A., Using polarizable POSSIM force field and fuzzy-border continuum solvent model to calculate pK_a shifts of protein residues. *J. Comput. Chem.* **2017,** *38* (2), 65-80.

301.   Schilling, M.; Luber, S., Determination of pK_a Values via ab initio Molecular Dynamics and its Application to Transition Metal-Based Water Oxidation Catalysts. *Inorganics* **2019,** *7* (6), 73.

302.   Wang, R.; Carnevale, V.; Klein, M. L.; Borguet, E., First-Principles Calculation of Water pK_a Using the Newly Developed SCAN Functional. *J. Phys. Chem. Lett* **2019,** *11* (1), 54-59.

303.   Thomsen, B.; Shiga, M., Nuclear quantum effects on autoionization of water isotopologs studied by ab initio path integral molecular dynamics. *J. Chem. Phys.* **2021,** *154* (8), 084117.

304.   Spiegelman, F.; Tarrat, N.; Cuny, J.; Dontot, L.; Posenitskiy, E.; Martí, C.; Simon, A.; Rapacioli, M., Density-functional tight-binding: basic concepts and applications to molecules and clusters. *Adv. Phys. X* **2020,** *5* (1), 1710252.

305.   Sinha, V.; Laan, J. J.; Pidko, E. A., Accurate and rapid prediction of pK_a of transition metal complexes: semiempirical quantum chemistry with a data-augmented approach. *Phys. Chem. Chem. Phys.* **2021,** *23* (4), 2557-2567.

306.   Serpone, N., Photocatalysis. *Kirk-Othmer Encyclopedia of Chemical Technology* **2000**.

307.   Olivucci, M., *Computational photochemistry*. Elsevier: 2005.

308.   Hill, N. S.; Coote, M. L., Chapter Seven - A comparison of methods for theoretical photochemistry: Applications, successes and challenges. In *Annual Reports in Computational Chemistry*, Dixon, D. A., Ed. Elsevier: 2019; Vol. 15, pp 203-285.

309.   Chergui, M., Ultrafast photophysics and photochemistry of iron hexacyanides in solution: Infrared to X-ray spectroscopic studies. *Coord. Chem. Rev.* **2018,** *372*, 52-65.

310.   Reichardt, C., Solvatochromic dyes as solvent polarity indicators. *Chem. Rev.* **1994,** *94* (8), 2319-2358.

311.   Ciampi, S.; Eggers, P. K.; Haworth, N. L.; Darwish, N.; Wagner, P.; Coote, M. L.; Wallace, G. G.; Raston, C. L., Decoloration rates of a photomerocyanine dye as a visual probe into hydrogen bonding interactions. *Chem. Commun.* **2015,** *51* (23), 4815-4818.

312.   Turner, M. A. P.; Turner, R. J.; Horbury, M. D.; Hine, N. D. M.; Stavros, V. G., Examining solvent effects on the ultrafast dynamics of catechol. *J. Chem. Phys.* **2019,** *151* (8), 084305.

313.   Stout, M. J.; Skelton, B. W.; Sobolev, A. N.; Raiteri, P.; Massi, M.; Simpson, P. V., Synthesis and Photochemical Properties of Re (I) Tricarbonyl Complexes Bound to Thione and Thiazol-2-ylidene Ligands. *Organometallics* **2020,** *39* (17), 3202-3211.

314.   Yempally, V.; Moncho, S.; Hasanayn, F.; Fan, W. Y.; Brothers, E. N.; Bengali, A. A., Ancillary ligand effects upon the photochemistry of Mn (bpy)(CO) 3X complexes (X= Br--, PhCC--). *Inorg. Chem.* **2017,** *56* (18), 11244-11253.

315.   Koch, M.; Saphiannikova, M.; Santer, S.; Guskova, O., Photoisomers of azobenzene star with a flat core: Theoretical insights into multiple states from DFT and MD perspective. *J. Phys. Chem. B* **2017,** *121* (37), 8854-8867.

316.   Ugandi, M.; Roemelt, M., An Ab Initio Computational Study of Electronic and Structural Factors in the Isomerization of Donor--Acceptor Stenhouse Adducts. *J. Phys. Chem. A* **2020,** *124* (38), 7756-7767.

317.   Marazzi, M.; Francés-Monerris, A.; Mourer, M.; Pasc, A.; Monari, A., Trans-to-cis photoisomerization of cyclocurcumin in different environments rationalized by computational photochemistry. *Phys. Chem. Chem. Phys.* **2020,** *22* (8), 4749-4757.

318.   Raucci, U.; Chiariello, M. G.; Rega, N., Modeling Excited-State Proton Transfer to Solvent: A Dynamics Study of a Super Photoacid with a Hybrid Implicit/Explicit Solvent Model. *J. Chem. Theory Comput.* **2020,** *16* (11), 7033-7043.

319.   Rabe, E. J.; Corp, K. L.; Huang, X.; Ehrmaier, J.; Flores, R. G.; Estes, S. L.; Sobolewski, A. L.; Domcke, W.; Schlenker, C. W., Barrierless Heptazine-Driven Excited State Proton-Coupled Electron Transfer: Implications for Controlling Photochemistry of Carbon Nitrides and Aza-Arenes. *J. Phys. Chem. C* **2019,** *123* (49), 29580-29588.

320.   Cowan, D. O.; Drisko, R. L., Heavy-atom solvent effect on the photodimerization of acenaphthylene. *J. Am. Chem. Soc.* **1967,** *89* (12), 3068-3069.

321.   Ghidinelli, S.; Abbate, S.; Koshoubu, J.; Araki, Y.; Wada, T.; Longhi, G., Solvent effects and aggregation phenomena studied by vibrational optical activity and molecular dynamics: the case of pantolactone. *J. Phys. Chem. B* **2020,** *124* (22), 4512-4526.

322.   Marrazzini, G.; Giovannini, T.; Egidi, F.; Cappelli, C., Calculation of Linear and Non-linear Electric Response Properties of Systems in Aqueous Solution: A Polarizable Quantum/Classical Approach with Quantum Repulsion Effects. *J. Chem. Theory Comput.* **2020,** *16* (11), 6993-7004.

323.   Suydam, I. T.; Boxer, S. G., Vibrational Stark effects calibrate the sensitivity of vibrational probes for electric fields in proteins. *Biochemistry* **2003,** *42* (41), 12050-12055.

324.   Marcus, R. A., On the theory of oxidation-reduction reactions involving electron transfer. I. *J. Chem. Phys.* **1956,** *24* (5), 966-978.

325.   Marenich, A. V.; Cramer, C. J.; Truhlar, D. G.; Guido, C. A.; Mennucci, B.; Scalmani, G.; Frisch, M. J., Practical computation of electronic excitation in solution: vertical excitation model. *Chem. Sci.* **2011,** *2* (11), 2143-2161.

326.   You, Z.-Q.; Mewes, J.-M.; Dreuw, A.; Herbert, J. M., Comparison of the Marcus and Pekar partitions in the context of non-equilibrium, polarizable-continuum solvation models. *J. Chem. Phys.* **2015,** *143* (20), 204104.

327.   Caricato, M., A comparison between state-specific and linear-response formalisms for the calculation of vertical electronic transition energy in solution with the CCSD-PCM method. *J. Chem. Phys.* **2013,** *139* (4), 044116.

328.   Guido, C. A.; Mennucci, B.; Scalmani, G.; Jacquemin, D., Excited state dipole moments in solution: comparison between state-specific and linear-response TD-DFT values. *J. Chem. Theory Comput.* **2018,** *14* (3), 1544-1553.
329.   Xu, T.; Wang, W.; Yin, S., Explicit method to evaluate the external reorganization energy of charge-transfer reactions in oligoacene crystals using the state-specific polarizable force field. *J. Phys. Chem. A* **2018,** *122* (45), 8957-8964.
330.   Li, X.-Y., An overview of continuum models for nonequilibrium solvation: Popular theories and new challenge. *Int. J. Quantum Chem.* **2015,** *115* (11), 700-721.
331.   Bi, T.-J.; Xu, L.-K.; Wang, F.; Ming, M.-J.; Li, X.-Y., Solvent effects on excitation energies obtained using the state-specific TD-DFT method with a polarizable continuum model based on constrained equilibrium thermodynamics. *Phys. Chem. Chem. Phys.* **2017,** *19* (48), 32242-32252.
332.   Xu, L.-K.; Bi, T.-J.; Ming, M.-J.; Wang, J.-B.; Li, X.-Y., Photoinduced charge-transfer electronic excitation of tetracyanoethylene/tetramethylethylene complex in dichloromethane. *Chem. Phys. Lett.* **2017,** *679*, 158-163.
333.   Ming, M.-J.; Xu, L.-K.; Wang, F.; Bi, T.-J.; Li, X.-Y., Theoretical study on electronic excitation spectra: A matrix form of numerical algorithm for spectral shift. *Chem. Phys.* **2017,** *492*, 27-34.
334.   Bi, T.-J.; Xu, L.-K.; Wang, F.; Li, X.-Y., Solvent effects for vertical absorption and emission processes in solution using a self-consistent state specific method based on constrained equilibrium thermodynamics. *Phys. Chem. Chem. Phys.* **2018,** *20* (19), 13178-13190.
335.   Boruah, A.; Borpuzari, M. P.; Kawashima, Y.; Hirao, K.; Kar, R., Assessment of range-separated functionals in the presence of implicit solvent: Computation of oxidation energy, reduction energy, and orbital energy. *J. Chem. Phys.* **2017,** *146* (16), 164102.
336.   Vong, A.; Widmer, D. R.; Schwartz, B. J., Nonequilibrium Solvent Effects during Photodissociation in Liquids: Dynamical Energy Surfaces, Caging, and Chemical Identity. *J. Phys. Chem. Lett.* **2020,** *11* (21), 9230-9238.
337.   Biasin, E.; Fox, Z. W.; Andersen, A.; Ledbetter, K.; Kjær, K. S.; Alonso-Mori, R.; Carlstad, J. M.; Chollet, M.; Gaynor, J. D.; Glownia, J. M., Direct observation of coherent femtosecond solvent reorganization coupled to intramolecular electron transfer. *Nat. Chem.* **2021,** *13* (4), 343-349.
338.   Fujii, K.; Nakano, H.; Sato, H.; Kimura, Y., Experimental observation of the unique solvation process along multiple solvation coordinates of photodissociated products. *Phys. Chem. Chem. Phys* **2021,** *23* (8), 4569-4579.
339.   Chen, X.; Qiao, W.; Miao, W.; Zhang, Y.; Mu, X.; Wang, J., the Dependence of implicit Solvent Model parameters and electronic Absorption Spectra and photoinduced charge transfer. *Sci. Rep.* **2020,** *10* (1), 1-8.
340.   Bozkurt, E.; Gul, H. I.; Mete, E., Solvent and substituent effect on the photophysical properties of pyrazoline derivatives: A spectroscopic study. *J. Photochem. Photobiol. A* **2018,** *352*, 35-42.
341.   Ren, S.; Harms, J.; Caricato, M., An EOM-CCSD-PCM benchmark for electronic excitation energies of solvated molecules. *J. Chem. Theory Comput.* **2017,** *13* (1), 117-124.
342.   Chansen, W.; Kungwan, N., Theoretical Insights into Excited-State Intermolecular Proton Transfers of 2, 7-Diazaindole in Water Using a Microsolvation Approach. *J. Phys. Chem. A* **2021.**
343.   Mera-Adasme, R.; Rezende, M. C.; Dominguez, M., On the physical-chemical nature of solvent polarizability and dipolarity. *Spectrochim. Acta A Mol. Biomol. Spectrosc.* **2020,** *229*, 118008.
344.   An, S.; Meng, S.; Xue, J.; Wang, H.; Zheng, X.; Zhao, Y., UV–Vis, Raman spectroscopic and density functional theoretical studies on microsolvation 1, 2, 4-triazole-3-thione clusters. *Spectrochim. Acta A Mol. Biomol. Spectrosc.* **2021,** *258*, 119762.
345.   Raucci, U.; Perrella, F.; Donati, G.; Zoppi, M.; Petrone, A.; Rega, N., Ab-initio molecular dynamics and hybrid explicit-implicit solvation model for aqueous and nonaqueous solvents:

GFP chromophore in water and methanol solution as case study. *J. Comput. Chem.* **2020,** *41* (26), 2228-2239.

346.   Quant, M.; Hamrin, A.; Lennartson, A.; Erhart, P.; Moth-Poulsen, K., Solvent Effects on the Absorption Profile, Kinetic Stability, and Photoisomerization Process of the Norbornadiene--Quadricyclanes System. *J. Phys. Chem. C* **2019,** *123* (12), 7081-7087.

347.   De Vetta, M.; Baig, O.; Steen, D.; Nogueira, J. J.; Gonzalez, L., Assessing Configurational Sampling in the Quantum Mechanics/Molecular Mechanics Calculation of Temoporfin Absorption Spectrum and Triplet Density of States. *Molecules* **2018,** *23* (11), 2932.

348.   Díaz Mirón, G.; González Lebrero, M. C., Fluorescence quantum yields in complex environments from QM-MM TDDFT simulations: The case of indole in different solvents. *J. Phys. Chem. A* **2020,** *124* (46), 9503-9512.

349.   Zuehlsdorff, T. J.; Isborn, C. M., Modeling absorption spectra of molecules in solution. *Int. J. Quantum Chem.* **2019,** *119* (1), e25719.

350.   Boulanger, E.; Harvey, J. N., QM/MM methods for free energies and photochemistry. *Curr. Opin. Struct. Biol.* **2018,** *49*, 72-76.

351.   Donati, G.; Wildman, A.; Caprasecca, S.; Lingerfelt, D. B.; Lipparini, F.; Mennucci, B.; Li, X., Coupling real-time time-dependent density functional theory with polarizable force field. *J. Phys. Chem. Lett.* **2017,** *8* (21), 5283-5289.

352.   Bennie, S. J.; Curchod, B. F. E.; Manby, F. R.; Glowacki, D. R., Pushing the limits of EOM-CCSD with projector-based embedding for excitation energies. *J. Phys. Chem. Lett.* **2017,** *8* (22), 5559-5565.

353.   Wen, X.; Graham, D. S.; Chulhai, D. V.; Goodpaster, J. D., Absolutely localized projection-based embedding for excited states. *J. Chem. Theory Comput.* **2019,** *16* (1), 385-398.

354.   Zhang, K.; Ren, S.; Caricato, M., Multistate QM/QM Extrapolation of UV/Vis Absorption Spectra with Point Charge Embedding. *J. Chem. Theory Comput.* **2020,** *16* (7), 4361-4372.

355.   Rivera, M.; Dommett, M.; Crespo-Otero, R., ONIOM (QM: QM') Electrostatic Embedding Schemes for Photochemistry in Molecular Crystals. *J. Chem. Theory Comput.* **2019,** *15* (4), 2504-2516.

356.   Winget, P.; Weber, E. J.; Cramer, C. J.; Truhlar, D. G., Computational electrochemistry: aqueous one-electron oxidation potentials for substituted anilines. *Phys. Chem. Chem. Phys.* **2000,** *2* (6), 1231-1239.

357.   Yan, M.; Kawamata, Y.; Baran, P. S., Synthetic Organic Electrochemical Methods Since 2000: On the Verge of a Renaissance. *Chem. Rev.* **2017,** *117* (21), 13230-13319.

358.   Ho, J.; Coote, M.; Cramer, C.; Truhlar, D., Theoretical Calculation of Reduction Potentials. In *Organic Electrochemistry: Revised and Expanded*, Hammerich, O.; Speiser, B., Eds. CRC Press, Taylor and Francis Group: 2015; pp 229-259.

359.   Marenich, A. V.; Ho, J.; Coote, M. L.; Cramer, C. J.; Truhlar, D. G., Computational Electrochemistry: Prediction of Liquid-Phase Reduction Potentials. *Phys. Chem. Chem. Phys.* **2014,** *16*, 15068-15106.

360.   Åvall, G.; Mindemark, J.; Brandell, D.; Johansson, P., Sodium-Ion Battery Electrolytes: Modeling and Simulations. *Advanced Energy Materials* **2018,** *8* (17), 1703036.

361.   Schwarz, K.; Sundararaman, R., The electrochemical interface in first-principles calculations. *Surf. Sci. Rep.* **2020,** 100492.

362.   Borodin, O.; Ren, X.; Vatamanu, J.; von Wald Cresce, A.; Knap, J.; Xu, K., Modeling insight into battery electrolyte electrochemical stability and interfacial structure. *Acc. Chem. Res.* **2017,** *50* (12), 2886-2894.

363.   Zhang, K.; Noble, B. B.; Mater, A. C.; Monteiro, M. J.; Coote, M. L.; Jia, Z., Effect of heteroatom and functionality substitution on the oxidation potential of cyclic nitroxide radicals: role of electrostatics in electrochemistry. *Phys. Chem. Chem. Phys.* **2018,** *20* (4), 2606-2614.

364.   Rogers, F. J. M.; Coote, M. L., Computational Assessment of Verdazyl Derivatives for Electrochemical Generation of Carbon-Centered Radicals. *J. Phys. Chem. C* **2019,** *123* (33), 20174-20180.

365.   Rogers, F. J. M.; Coote, M. L., Computational Evaluation of the Oxidative Cleavage of Triazine Derivatives for Electrosynthesis. *J Phys. Chem. C* **2019,** *123* (16), 10306-10310.

366.   Guerard, J. J.; Arey, J. S., Critical evaluation of implicit solvent models for predicting aqueous oxidation potentials of neutral organic compounds. *J. Chem. Theory Comput.* **2013,** *9* (11), 5046-5058.

367.   Listyarini, R. V.; Gesto, D. S.; Paiva, P.; Ramos, M. J.; Fernandes, P. A., Benchmark of Density Functionals for the Calculation of the Redox potential of Fe^{3+}/Fe^{2+} within protein coordination shells. *Front. Chem.* **2019,** *7*, 391.

368.   Qiu, H.; Du, X.; Zhao, J.; Wang, Y.; Ju, J.; Chen, Z.; Hu, Z.; Yan, D.; Zhou, X.; Cui, G., Zinc anode-compatible in-situ solid electrolyte interphase via cation solvation modulation. *Nat. Commun.* **2019,** *10* (1), 1-12.

369.   Liu, S.; Mao, J.; Zhang, L.; Pang, W. K.; Du, A.; Guo, Z. J. A. m., Manipulating the Solvation Structure of Nonflammable Electrolyte and Interface to Enable Unprecedented Stability of Graphite Anodes beyond 2 Years for Safe Potassium-Ion Batteries. *Adv. Mater.* **2021,** *33* (1), 2006313.

370.   Park, J.; Xu, Z.-L.; Kang, K., Solvated ion intercalation in graphite: sodium and beyond. *Front. Chem.* **2020,** *8*, 432.

371.   Seidl, L.; Bucher, N.; Chu, E.; Hartung, S.; Martens, S.; Schneider, O.; Stimming, U., Intercalation of solvated Na-ions into graphite. *Energy Environ. Sci.* **2017,** *10* (7), 1631-1642.

372.   Hou, T.; Yang, G.; Rajput, N. N.; Self, J.; Park, S.-W.; Nanda, J.; Persson, K. A., The influence of FEC on the solvation structure and reduction reaction of $LiPF_6$/EC electrolytes and its implication for solid electrolyte interphase formation. *Nano Energy* **2019,** *64*, 103881.

373.   Falbo, E.; Penfold, T. J., Redox Potentials of Polyoxometalates from an Implicit Solvent Model and QM/MM Molecular Dynamics. *J. Phys. Chem. C* **2020,** *124* (28), 15045-15056.

374.   Wylie, L.; Oyaizu, K.; Karton, A.; Yoshizawa-Fujita, M.; Izgorodina, E. I., Toward Improved Performance of All-Organic Nitroxide Radical Batteries with Ionic Liquids: A Theoretical Perspective. *ACS Sustainable Chemistry & Engineering* **2019,** *7* (5), 5367-5375.

375.   Wylie, L.; Blesch, T.; Freeman, R.; Hatakeyama-Sato, K.; Oyaizu, K.; Yoshizawa-Fujita, M.; Izgorodina, E. I., Reversible Reduction of the TEMPO Radical: One Step Closer to an All-Organic Redox Flow Battery. *ACS Sustain. Chem. Eng.* **2020,** *8* (49), 17988-17996.

376.   Wylie, L.; Hakatayama-Sato, K.; Go, C.; Oyaizu, K.; Izgorodina, E. I., Electrochemical characterization and thermodynamic analysis of TEMPO derivatives in ionic liquids. *Phys. Chem. Chem. Phys* **2021,** *23* (17), 10205-10217.

377.   Zhang, L.; Vogel, Y. B.; Noble, B. B.; Goncales, V. R.; Darwish, N.; Le Brun, A.; Gooding, J. J.; Wallace, G. G.; Coote, M. L.; Ciampi, S., TEMPO Monolayers on 51(100) Electrodes: Electrostatic Effects by the Electrolyte and Semiconductor Space-Charge on the Electroactivity of a Persistent Radical. *J. Am. Chem. Soc.* **2016,** *138* (30), 9611-9619.

378.   Bird, M. J.; Iyoda, T.; Bonura, N.; Bakalis, J.; Ledbetter, A. J.; Miller, J. R., Effects of electrolytes on redox potentials through ion pairing. *J. Electroanal. Chem.* **2017,** *804*, 107-115.

379.   Wang, Z.; Yan, L.; Yue, B.; Jiang, T.; Peng, S.; Lv, W.; Zhang, D., Density Functional Theory Calculations of Redox Potentials of Neptunium Complexes in Ionic Liquid. *J. Electrochem. Soc.* **2020,** *167* (13), 136503.

380.   Qu, X.; Persson, K. A., Toward Accurate Modeling of the Effect of Ion-Pair Formation on Solute Redox Potential. *J. Chem. Theory Comput.* **2016,** *12* (9), 4501-4508.

51

381.   Noble, B. B.; Norcott, P. L.; Hammill, C. L.; Ciampi, S.; Coote, M. L., Mechanism of Oxidative Alkoxyamine Cleavage: The Surprising Role of the Solvent and Supporting Electrolyte. *J. Phys. Chem. C* **2019,** *123* (16), 10300-10305.

382.   Tazhigulov, R. N.; Gurunathan, P. K.; Kim, Y.; Slipchenko, L. V.; Bravaya, K. B., Polarizable embedding for simulating redox potentials of biomolecules. *Phys. Chem. Chem. Phys.* **2019,** *21* (22), 11642-11650.

383.   Sterling, C. M.; Bjornsson, R., Multistep explicit solvation protocol for calculation of redox potentials. *J. Chem. Theory Comput.* **2018,** *15* (1), 52-67.

384.   Wang, L.-P.; Van Voorhis, T., A polarizable QM/MM explicit solvent model for computational electrochemistry in water. *J. Chem. Theory Comput.* **2012,** *8* (2), 610-617.

385.   Vogel, Y. B.; Evans, C. W.; Belotti, M.; Xu, L.; Russell, I. C.; Yu, L.-J.; Fung, A. K. K.; Hill, N. S.; Darwish, N.; Goncales, V. R.; others, The corona of a surface bubble promotes electrochemical reactions. *Nat. Commun.* **2020,** *11* (1), 1-8.

386.   Menzel, J. P.; Kloppenburg, M.; Belić, J.; de Groot, H. J.; Visscher, L.; Buda, F., Efficient workflow for the investigation of the catalytic cycle of water oxidation catalysts: Combining GFN-xTB and density functional theory. *J. Comput. Chem.* **2021,** *42* (26), 1885-1894.

387.   Neugebauer, H.; Bohle, F.; Bursch, M.; Hansen, A.; Grimme, S., Benchmark Study of Electrochemical Redox Potentials Calculated with Semiempirical and DFT Methods. *J. Phys. Chem. A* **2020,** *124* (35), 7166-7176.

388.   Varghese, J. J.; Mushrif, S. H., Origins of complex solvent effects on chemical reactivity and computational tools to investigate them: a review. *React. Chem. Eng.* **2019,** *4* (2), 165-206.

389.   Dyson, P. J.; Jessop, P. G., Solvent effects in catalysis: rational improvements of catalysts via manipulation of solvent interactions. *Catal. Sci. Technol.* **2016,** *6* (10), 3302-3316.

390.   Li, H.; Smith, R. L., Solvents take control. *Nat. Catal.* **2018,** *1* (3), 176-177.

391.   Shrivastav, G.; Khan, T. S.; Agarwal, M.; Haider, M. A., Elucidating the role of solvents in acid catalyzed dehydration of biorenewable hydroxy-lactones. *React. Chem. Eng.* **2020,** *5* (4), 651-662.

392.   Brea, O.; Daver, H.; Rebek Jr, J.; Himo, F., Mechanism (s) of thermal decomposition of N-Nitrosoamides: A density functional theory study. *Tetrahedron* **2019,** *75* (8), 929-935.

393.   Roytman, V. A.; Singleton, D. A., Solvation Dynamics and the Nature of Reaction Barriers and Ion-Pair Intermediates in Carbocation Reactions. *J. Am. Chem. Soc.* **2020,** *142* (29), 12865-12877.

394.   Yu, L.-J.; Cullen, D. A.; Morshedi, M.; Coote, M. L.; White, N. G., Room Temperature Hydrolysis of Benzamidines and Benzamidiniums in Weakly Basic Water. *J. Org. Chem.* **2021,** *86* (19), 13762-13767.

395.   Xie, J.; Hase, W. L., Rethinking the SN2 reaction. *Science* **2016,** *352* (6281), 32-33.

396.   Liu, X.; Zhang, J.; Yang, L.; Hase, W. L., How a solvent molecule affects competing elimination and substitution dynamics. Insight into mechanism evolution with increased solvation. *J. Am. Chem. Soc.* **2018,** *140* (35), 10995-11005.

397.   Gara, R.; Zouaghi, M. O.; ALshandoudi, L. M. H.; Arfaoui, Y., DFT investigation of solvent, substituent, and catalysis effects on the intramolecular Diels-Alder reaction. *J. Mol. Model.* **2021,** *27* (5), 1-12.

398.   Benchouk, W.; Mekelleche, S. M.; Silvi, B.; Aurell, M. J.; Domingo, L. R., Understanding the kinetic solvent effects on the 1,5 dipolar cycloaddition of benzonitrile N oxide: a DFT study. *J. Phys. Org. Chem.* **2011,** *24*, 611-618.

399.   Mehranfar, A.; Izadyar, M.; Khavani, M.; Housaindokht, M. R., Understanding the role of noncovalent interactions on the rate of some Diels-Alder reactions in different solvents. *Int. J. Quantum Chem.* **2019,** *119* (9), e25878.

400.   Silva, N. M.; Deglmann, P.; Pliego Jr, J. R., CMIRS solvation model for methanol: parametrization, testing, and comparison with SMD, SM8, and COSMO-RS. *J. Phys. Chem. B* **2016,** *120* (49), 12660-12668.

401.   Weiß, M.; Brehm, M., Exploring Free Energy Profiles of Enantioselective Organocatalytic Aldol Reactions under Full Solvent Influence. *Molecules* **2020,** *25* (24), 5861.

402.   Yu, L.-J.; Blyth, M. T.; Coote, M. L., Re-Examination of Proline-Catalyzed Intermolecular Aldol Reactions: An Ab Initio Kinetic Modelling Study. *Top. Catal.* **2021**, 1-12.

403.   Li, G.; Wang, B.; Resasco, D. E., Water-mediated heterogeneously catalyzed reactions. *ACS Catal.* **2019,** *10* (2), 1294-1309.

404.   Yan, Z.; Lian, J.; Li, M.; Meng, L.; Zhang, Y.; Ge, C.; Lu, J., Deeper insight into hydrolysis mechanisms of polyester/cotton blended fabrics for separation by explicit solvent models. *Int. J. Biol. Macromol.* **2020,** *154*, 596-605.

405.   Zhou, Y.; Xue, R.-C.; Feng, Y.; Zhang, L., How does HOTf/HFIP Cooperative System Catalyze the Ring-Opening Reaction of Cyclopropanes? A DFT Study. *Asian J. Org. Chem.* **2020,** *9* (2), 311-316.

406.   Zhang, Y.-Q.; Bohle, F.; Bleith, R.; Schnakenburg, G.; Grimme, S.; Gansäuer, A., Synthesis of 1, 3-Amino Alcohols by Hydroxy-Directed Aziridination and Aziridine Hydrosilylation. *Angew. Chem.* **2018,** *130* (41), 13716-13720.

407.   Bang, Y.; Kim, S.-H.; Kim, Y., Direct dynamics calculations of multiple proton transfer through hydrogen-bonded wire and the role of micro-solvation in $ClONO_2 + H_2O \rightarrow HNO_3 + HOCl$ reactions. *Theor. Chem. Acc.* **2017,** *136* (11), 1-13.

408.   Tachikawa, H., Effects of micro-solvation on the reaction dynamics of biphenyl cations following hole capture. *Chem. Phys.* **2017,** *490*, 12-18.

409.   Tachikawa, H.; Iyama, T., Hydration effects on proton transfer reactions in the catalytic triad Ser-His-Glu. *Chem. Phys.* **2021,** *540*, 111003.

410.   Sure, R.; El Mahdali, M.; Plajer, A.; Deglmann, P., Towards a converged strategy for including microsolvation in reaction mechanism calculations. *J. Comput. Aided Mol. Des.* **2021,** *35* (4), 473-492.

411.   Tripathi, R.; Durán Caballero, L.; Pérez de Tudela, R.; Hölzl, C.; Marx, D., Unveiling Zwitterionization of Glycine in the Microhydration Limit. *ACS omega* **2021,** *6* (19), 12676-12683.

412.   Arnaboldi, S.; Mezzetta, A.; Grecchi, S.; Longhi, M.; Emanuele, E.; Rizzo, S.; Arduini, F.; Micheli, L.; Guazzelli, L.; Mussini, P. R., Natural-based chiral task-specific deep eutectic solvents: a novel, effective tool for enantiodiscrimination in electroanalysis. *Electrochim. Acta* **2021**, 138189.

413.   Boereboom, J. M.; Fleurat-Lessard, P.; Bulo, R. E., Explicit solvation matters: Performance of QM/MM solvation models in nucleophilic addition. *J. Chem. Theory Comput.* **2018,** *14* (4), 1841-1852.

414.   Acevedo, O., Simulating Chemical Reactions in Ionic Liquids Using QM/MM Methodology. *J. Phys. Chem. A* **2014,** *118* (50), 11653-11666.

415.   Vázquez-Montelongo, E. A.; Vázquez-Cervantes, J. E.; Cisneros, G. A., Polarizable ab initio QM/MM Study of the Reaction Mechanism of N-tert-Butyloxycarbonylation of Aniline in [EMIm][BF4]. *Molecules* **2018,** *23* (11), 2830.

416.   Chew, A. K.; Walker, T. W.; Shen, Z.; Demir, B.; Witteman, L.; Euclide, J.; Huber, G. W.; Dumesic, J. A.; Van Lehn, R. C., Effect of mixed-solvent environments on the selectivity of acid-catalyzed dehydration reactions. *ACS Catal.* **2019,** *10* (3), 1679-1691.

417.   Hansen, B. B.; Spittle, S.; Chen, B.; Poe, D.; Zhang, Y.; Klein, J. M.; Horton, A.; Adhikari, L.; Zelovich, T.; Doherty, B. W.; Gurkan, B.; Maginn, E. J.; Ragauskas, A.; Dadmun, M.; Zawodzinski, T. A.; Baker, G. A.; Tuckerman, M. E.; Savinell, R. F.; Sangoro, J. R., Deep Eutectic Solvents: A Review of Fundamentals and Applications. *Chem. Rev.* **2021,** *121* (3), 1232-1285.

418.   Grajciar, L.; Heard, C. J.; Bondarenko, A. A.; Polynski, M. V.; Meeprasert, J.; Pidko, E. A.; Nachtigall, P., Towards operando computational modeling in heterogeneous catalysis. *Chem. Soc. Rev.* **2018,** *47* (22), 8307-8348.

419.   Keil, F. J., Multiscale modelling in computational heterogeneous catalysis. *Top Curr Chem* **2012,** *307*, 69-107.

420.   Bruix, A.; Margraf, J. T.; Andersen, M.; Reuter, K., First-principles-based multiscale modelling of heterogeneous catalysis. *Nat. Catal.* **2019,** *2* (8), 659-670.

421.   Ruiz-Lopez, M. F.; Francisco, J. S.; Martins-Costa, M. T.; Anglada, J. M., Molecular reactions at aqueous interfaces. *Nat. Rev. Chem.* **2020,** *4* (9), 459-475.

422.   Roldan, A., Frontiers in first principles modelling of electrochemical simulations. *Curr. Opin. Electrochem.* **2018,** *10*, 1-6.

423.   Leung, K., DFT modelling of explicit solid–solid interfaces in batteries: methods and challenges. *Phys. Chem. Chem. Phys.* **2020,** *22* (19), 10412-10425.

424.   Le, J.-B.; Yang, X.-H.; Zhuang, Y.-B.; Wang, F.; Cheng, J., Ab initio modeling of electrochemical interfaces and determination of electrode potentials. In *Atomic-Scale Modelling of Electrochemical Systems*, 2021; pp 173-200.

425.   Groß, A., Molecular Dynamics of the Electrochemical Interface and the Double Layer. In *Atomic-Scale Modelling of Electrochemical Systems*, 2021; pp 201-220.

426.   Hirano, T.; Morita, A., Electron Transfer Mechanism at the Oil/Water Interface Revealed by Multidimensional Free Energy Calculations. *J. Phys. Chem. B* **2020,** *124* (18), 3811-3827.

427.   Xu, L.; Izgorodina, E. I.; Coote, M. L., Ordered Solvents and Ionic Liquids Can Be Harnessed for Electrostatic Catalysis. *J. Am. Chem. Soc.* **2020,** *142* (29), 12826-12833.

428.   Acevedo, O.; Jorgensen, W. L., Exploring solvent effects upon the Menshutkin reaction using a polarizable force field. *J. Phys. Chem. B* **2010,** *114* (25), 8425-8430.

429.   Muzdalo, A.; Saalfrank, P.; Vreede, J.; Santer, M., Cis-to-Trans Isomerization of Azobenzene Derivatives Studied with Transition Path Sampling and Quantum Mechanical/Molecular Mechanical Molecular Dynamics. *J. Chem. Theory Comput.* **2018,** *14* (4), 2042-2051.

430.   Yang, Z.; Houk, K. N., The dynamics of chemical reactions: atomistic visualizations of organic reactions, and homage to van't Hoff. *Chem. Eur. J.* **2018,** *24* (16), 3916-3924.

2.3 Summary

In this chapter, different computational models for solvation modelling and their applications in studying pK_a, redox potential, photochemical properties, reaction mechanims and catalysis were reviewed. This chapter introduced an overview of the extensive databases for solvation free energies. We highlighted the recommended parameters for both implicit and explicit solvent simulations with theoretical methods at different scales. These parameters include the choice of theoretical levels, electrostatic scaling factors, atomic radii in both implicit and explicit solvent simulations, partial charge schemes and atomic polarizability values in force field methods. The conclusions from benchmark works in this chapter provides insights into the design of future computational protocols. A part of the important works published recently in related fields were introduced. Finally an outlook was given for future works in the development and applications of solvation modelling techniques from our perspective. The computational theory in this chapter underpins the approach undertaken in the subsequent chapters.

Bibliography

[1] A. V Marenich, C. J Cramer, and D. G Truhlar, "Universal solvation model based on solute electron density and on a continuum model of the solvent defined by the bulk dielectric constant and atomic surface tensions", *The Journal of Physical Chemistry B* **113**(18), pp. 6378–6396 (2009).

[2] J Tomasi, B Mennucci, and R Cammi, "Quantum mechanical continuum solvation models", *Chemical Reviews* **105**(8), pp. 2999–3094 (2005).

[3] A Klamt, V Jonas, T Bürger, and J. C Lohrenz, "Refinement and parametrization of COSMO-RS", *The Journal of Physical Chemistry A* **102**(26), pp. 5074–5085 (1998).

[4] V Barone and M Cossi, "Quantum calculation of molecular energies and energy gradients in solution by a conductor solvent model", *The Journal of Physical Chemistry A* **102**(11), pp. 1995–2001 (1998).

[5] M Cossi, G Scalmani, N Rega, and V Barone, "Energies, gradients, and harmonic frequencies for molecules in solution by the C-PCM solvation model", *J. Comput. Chem* **24**, pp. 669 (2003).

[6] A Klamt, "The COSMO and COSMO-RS solvation models", *Wiley Interdisciplinary Reviews: Computational Molecular Science* **1**(5), pp. 699–709 (2011).

[7] S Ehlert, M Stahn, S Spicher, and S Grimme, "Robust and efficient implicit solvation model for fast semiempirical methods", *Journal of Chemical Theory and Computation* **17**(7), pp. 4250–4261 (2021).

[8] Y Okiyama, T Nakano, C Watanabe, K Fukuzawa, Y Mochizuki, and S Tanaka, "Fragment molecular orbital calculations with implicit solvent based on the Poisson–Boltzmann equation: Implementation and DNA study", *The Journal of Physical Chemistry B* **122**(16), pp. 4457–4471 (2018).

[9] M Garcia-Ratés, U Becker, and F Neese, "Implicit solvation in domain based pair natural orbital coupled cluster (DLPNO-CCSD) theory", *Journal of Computational Chemistry* **42**(27), pp. 1959–1973 (2021).

[10] R Di Remigio, A. H Steindal, K Mozgawa, V Weijo, H Cao, and L Frediani, "PCM-Solver: An open-source library for solvation modeling", *International Journal of Quantum Chemistry* **119**(1), pp. e25685 (2019).

[11] P Štěpánek and P Bouř, "Multi-scale modeling of electronic spectra of three aromatic amino acids: Importance of conformational averaging and explicit solute–solvent interactions", *Physical Chemistry Chemical Physics* **16**(38), pp. 20639–20649 (2014).

[12] A Wang, S Kadam, H Li, S Shi, and Y Qi, "Review on modeling of the anode solid electrolyte interphase (SEI) for lithium-ion batteries", *npj Computational Materials* **4**(1), pp. 1–26 (2018).

[13] D Kundu, P. S Rao, and T Banerjee, "First-principles prediction of Kamlet–Taft solvatochromic parameters of deep eutectic solvent using the COSMO-RS model", *Industrial & Engineering Chemistry Research* **59**(24), pp. 11329–11339 (2020).

[14] V. S Bernales, A. V Marenich, R Contreras, C. J Cramer, and D. G Truhlar, "Quantum mechanical continuum solvation models for ionic liquids", *The Journal of Physical Chemistry B* **116**(30), pp. 9122–9129 (2012).

[15] E. I Izgorodina, Z. L Seeger, D. L Scarborough, and S. Y Tan, "Quantum chemical methods for the prediction of energetic, physical, and spectroscopic properties of ionic liquids", *Chemical Reviews* **117**(10), pp. 6696–6754 (2017).

[16] Y Cong, C Du, Y Zhang, Y Xue, B Qiao, T Ye, and M Wang, "Solubility modelling, solvent effect, preferential solvation and solution thermodynamic of thymine form AH A° in ten mono solvents and two solvent mixtures", *Journal of Molecular Liquids* **300**, pp. 112257 (2020).

[17] J Chocholoušová, J Vacek, and P Hobza, "Acetic acid dimer in the gas phase, nonpolar solvent, microhydrated environment, and dilute and concentrated acetic acid: Ab initio quantum chemical and molecular dynamics simulations", *The Journal of Physical Chemistry A* **107**(17), pp. 3086–3092 (2003).

[18] F Camerin, N Gnan, L Rovigatti, and E Zaccarelli, "Modelling realistic microgels in an explicit solvent", *Scientific Reports* **8**(1), pp. 1–12 (2018).

[19] J. J Prompers and R Brüschweiler, "General framework for studying the dynamics of folded and nonfolded proteins by NMR relaxation spectroscopy and MD simulation", *Journal of the American Chemical Society* **124**(16), pp. 4522–4534 (2002).

[20] W. D Cornell, P Cieplak, C. I Bayly, I. R Gould, K. M Merz, D. M Ferguson, D. C Spellmeyer, T Fox, J. W Caldwell, and P. A Kollman, "A second generation force field for the simulation of proteins, nucleic acids, and organic molecules", *Journal of the American Chemical Society* **117**(19), pp. 5179–5197 (1995).

[21] A. D MacKerell Jr, D Bashford, M Bellott, R. L Dunbrack Jr, J. D Evanseck, M. J Field, S Fischer, J Gao, H Guo, and S Ha, "All-atom empirical potential for molecular modeling and dynamics studies of proteins", *The Journal of Physical Chemistry B* **102**(18), pp. 3586–3616 (1998).

[22] W. L Jorgensen, D. S Maxwell, and J Tirado-Rives, "Development and testing of the OPLS all-atom force field on conformational energetics and properties of organic liquids", *Journal of the American Chemical Society* **118**(45), pp. 11225–11236 (1996).

[23] C Liu, J.-P Piquemal, and P Ren, "Implementation of geometry-dependent charge flux into the polarizable AMOEBA+ potential", *The Journal of Physical Chemistry Letters* **11**(2), pp. 419–426 (2019).

[24] V. M Anisimov, G Lamoureux, I. V Vorobyov, N Huang, B Roux, and A. D MacKerell, "Determination of electrostatic parameters for a polarizable force field based on the classical Drude oscillator", *Journal of Chemical Theory and Computation* **1**(1), pp. 153–168 (2005).

[25] T. P Senftle, S Hong, M. M Islam, S. B Kylasa, Y Zheng, Y. K Shin, C Junkermeier, R Engel-Herbert, M. J Janik, and H. M Aktulga, "The ReaxFF reactive force-field: development, applications and future directions", *npj Computational Materials* **2**(1), pp. 1–14 (2016).

[26] S. J Marrink, A. H De Vries, and A. E Mark, "Coarse grained model for semiquantitative lipid simulations", *The Journal of Physical Chemistry B* **108**(2), pp. 750–760 (2004).

[27] T Hou, J Wang, Y Li, and W Wang, "Assessing the performance of the molecular mechanics/Poisson Boltzmann surface area and molecular mechanics/generalized Born surface area methods. II. the accuracy of ranking poses generated from docking", *Journal of Computational Chemistry* **32**(5), pp. 866–877 (2011).

[28] W. L Jorgensen and L. L Thomas, "Perspective on free-energy perturbation calculations for chemical equilibria", *Journal of Chemical Theory and Computation* **4**(6), pp. 869–876 (2008).

[29] M. J Mitchell and J. A McCammon, "Free energy difference calculations by thermodynamic integration: difficulties in obtaining a precise value", *Journal of Computational Chemistry* **12**(2), pp. 271–275 (1991).

[30] A Barducci, M Bonomi, and M Parrinello, "Metadynamics", *Wiley Interdisciplinary Reviews: Computational Molecular Science* **1**(5), pp. 826–843 (2011).

[31] J Kästner, "Umbrella sampling", *Wiley Interdisciplinary Reviews: Computational Molecular Science* **1**(6), pp. 932–942 (2011).

[32] J. S Smith, O Isayev, and A. E Roitberg, "ANI-1: an extensible neural network potential with DFT accuracy at force field computational cost", *Chemical Science* **8**(4), pp. 3192–3203 (2017).

[33] A. N Beyer, J. O Richardson, P. J Knowles, J Rommel, and S. C Althorpe, "Quantum tunneling rates of gas-phase reactions from on-the-fly instanton calculations", *The Journal of Physical Chemistry Letters* **7**(21), pp. 4374–4379 (2016).

[34] M Dračínský̀ and P Hodgkinson, "Effects of quantum nuclear delocalisation on NMR parameters from path integral molecular dynamics.", *Chemistry: A European Journal.* **20**(8), pp. 2201–2207 (2014).

[35] K. I Assaf, M Florea, J Antony, N. M Henriksen, J Yin, A Hansen, Z.-W Qu, R Sure, D Klapstein, and M. K Gilson, "Hydrophobe challenge: A joint experimental and computational study on the host–guest binding of hydrocarbons to cucurbiturils, allowing explicit evaluation of guest hydration free-energy contributions", *The Journal of Physical Chemistry B* **121**(49), pp. 11144–11162 (2017).

[36] J Chen, Y Shao, and J Ho, "Are explicit solvent models more accurate than implicit solvent models? A case study on the menschutkin reaction", *The Journal of Physical Chemistry A* **123**(26), pp. 5580–5589 (2019).

[37] R Car and M Parrinello, "Unified approach for molecular dynamics and density-functional theory", *Physical Review Letters* **55**(22), pp. 2471 (1985).

[38] V Chaban, "Solvation of lithium ion in dimethoxyethane and propylene carbonate", *Chemical Physics Letters* **631**, pp. 1–5 (2015).

[39] H.-J Qian, A. C van Duin, K Morokuma, and S Irle, "Reactive molecular dynamics simulation of fullerene combustion synthesis: ReaxFF vs DFTB potentials", *Journal of Chemical Theory and Computation* **7**(7), pp. 2040–2048 (2011).

[40] S Spicher and S Grimme, "Efficient computation of free energy contributions for association reactions of large molecules", *The Journal of Physical Chemistry Letters* **11**(16), pp. 6606–6611 (2020).

[41] Y Komeiji, T Nakano, K Fukuzawa, Y Ueno, Y Inadomi, T Nemoto, M Uebayasi, D. G Fedorov, and K Kitaura, "Fragment molecular orbital method: application to molecular dynamics simulation,'ab initio FMO-MD"', *Chemical Physics Letters* **372**(3-4), pp. 342–347 (2003).

[42] M. S Gordon, L Slipchenko, H Li, and J. H Jensen, "The effective fragment potential: a general method for predicting intermolecular interactions", *Annual Reports in Computational Chemistry* **3**, pp. 177–193 (2007).

[43] M. A Collins and R. P Bettens, "Energy-based molecular fragmentation methods", *Chemical Reviews* **115**(12), pp. 5607–5642 (2015).

[44] S Li, W Li, and J Ma, "Generalized energy-based fragmentation approach and its applications to macromolecules and molecular aggregates", *Accounts of Chemical Research* **47**(9), pp. 2712–2720 (2014).

[45] D. P Geerke, S Thiel, W Thiel, and W. F van Gunsteren, "Combined QM/MM molecular dynamics study on a condensed-phase SN_2 reaction at nitrogen: The effect of explicitly including solvent polarization", *Journal of Chemical Theory and Computation* **3**(4), pp. 1499–1509 (2007).

[46] D Loco, L Lagardère, S Caprasecca, F Lipparini, B Mennucci, and J.-P Piquemal, "Hybrid QM/MM molecular dynamics with AMOEBA polarizable embedding", *Journal of Chemical Theory and Computation* **13**(9), pp. 4025–4033 (2017).

[47] F Himo, "Recent trends in quantum chemical modeling of enzymatic reactions", *Journal of the American Chemical Society* **139**(20), pp. 6780–6786 (2017).

[48] M. H Cardenuto, H. M Cezar, K. V Mikkelsen, S. P Sauer, K Coutinho, and S Canuto, "A QM/MM study of the conformation stability and electronic structure of the photochromic switches derivatives of DHA/VHF in acetonitrile solution", *Spectrochimica Acta Part A: Molecular and Biomolecular Spectroscopy* **251**, pp. 119434 (2021).

[49] Q Cui, T Pal, and L Xie, "Biomolecular QM/MM simulations: What are some of the "burning issues"?", *The Journal of Physical Chemistry B* **125**(3), pp. 689–702 (2021).

[50] F Ding, D. B Lingerfelt, B Mennucci, and X Li, "Time-dependent non-equilibrium dielectric response in QM/continuum approaches", *The Journal of Chemical Physics* **142**(3), pp. 034120 (2015).

[51] M Newton, M Basilevsky, and I Rostov, "A frequency-resolved cavity model (FRCM) for treating equilibrium and non-equilibrium solvation energies: 2: Evaluation of solvent reorganization energies", *Chemical Physics* **232**(1-2), pp. 201–210 (1998).

[52] T.-J Bi, L.-K Xu, F Wang, M.-J Ming, and X.-Y Li, "Solvent effects on excitation energies obtained using the state-specific TD-DFT method with a polarizable continuum model based on constrained equilibrium thermodynamics", *Physical Chemistry Chemical Physics* **19**(48), pp. 32242–32252 (2017).

[53] L.-K Xu, T.-J Bi, M.-J Ming, J.-B Wang, and X.-Y Li, "Photoinduced charge-transfer electronic excitation of tetracyanoethylene/tetramethylethylene complex in dichloromethane", *Chemical Physics Letters* **679**, pp. 158–163 (2017).

[54] T. E Markland and M Ceriotti, "Nuclear quantum effects enter the mainstream", *Nature Reviews Chemistry* **2**(3), pp. 1–14 (2018).

[55] J Lobaugh and G. A Voth, "The quantum dynamics of an excess proton in water", *The Journal of Chemical Physics* **104**(5), pp. 2056–2069 (1996).

[56] M. B Oviedo and B. M Wong, "Real-time quantum dynamics reveals complex, many-body interactions in solvated nanodroplets", *Journal of Chemical Theory and Computation* **12**(4), pp. 1862–1871 (2016).

[57] S. T Hutchinson and R Kobayashi, "Solvent-specific featurization for predicting free energies of solvation through machine learning", *Journal of Chemical Information and Modeling* **59**(4), pp. 1338–1346 (2019).

[58] H Lim and Y Jung, "MLSolv-A: A novel machine learning-based prediction of solvation free energies from pairwise atomistic interactions", *arXiv preprint arXiv:2005.06182* (2020).

[59] H Lim and Y Jung, "Delfos: deep learning model for prediction of solvation free energies in generic organic solvents", *Chemical Science* **10**(36), pp. 8306–8315 (2019).

[60] J Scheen, W Wu, A. S Mey, P Tosco, M Mackey, and J Michel, "Hybrid alchemical free energy/machine-learning methodology for the computation of hydration free energies", *Journal of Chemical Information and Modeling* **60**(11), pp. 5331–5339 (2020).

[61] Y Basdogan, M. C Groenenboom, E Henderson, S De, S. B Rempe, and J. A Keith, "Machine learning-guided approach for studying solvation environments", *Journal of Chemical Theory and Computation* **16**(1), pp. 633–642 (2019).

[62] D Lu, H Wang, M Chen, L Lin, R Car, E Weinan, W Jia, and L Zhang, "86 PFLOPS deep potential molecular dynamics simulation of 100 million atoms with ab initio accuracy", *Computer Physics Communications* **259**, pp. 107624 (2021).

[63] F Liu, N Luehr, H. J Kulik, and T. J Martínez, "Quantum chemistry for solvated molecules on graphical processing units using polarizable continuum models", *Journal of Chemical Theory and Computation* **11**(7), pp. 3131–3144 (2015).

[64] A Peramo, "Solvated and generalised Born calculations differences using GPU CUDA and multi-CPU simulations of an antifreeze protein with AMBER", *Molecular Simulation* **42**(15), pp. 1263–1273 (2016).

[65] W Huang, N Blinov, and A Kovalenko, "Octanol–water partition coefficient from 3D-RISM-KH molecular theory of solvation with partial molar volume correction", *The Journal of Physical Chemistry B* **119**(17), pp. 5588–5597 (2015).

[66] K Coutinho, S Canuto, and M Zerner, "A Monte Carlo-quantum mechanics study of the solvatochromic shifts of the lowest transition of benzene", *The Journal of Chemical Physics* **112**(22), pp. 9874–9880 (2000).

[67] P Suppan, "Invited review solvatochromic shifts: The influence of the medium on the energy of electronic states", *Journal of Photochemistry and Photobiology A: Chemistry* **50**(3), pp. 293–330 (1990).

Chapter 3

Improving the Accuracy of Implicit Solvent Models

3.1 Introduction

Continuum solvent models are widely used in the accurate prediction of solution-phase properties and reactions. While gas-phase single-point energies and free energies can be treated with sophisticated methods, solvation free energies, especially those of ions are one of the largest error sources in computational chemistry today.[1, 2]

Currently most implicit solvent models are based on the ASC scheme[3] and the SCRF method.[4] With these methods the solute is placed in a vacuum cavity, which is immersed in the polarizable continuum medium where the dielectric constant of solvent and other parameters are used to model the bulk properties of the solvent environment. When the electrostatic potential generated by the solute charge polarizes the solvent medium, the polarized solvent medium can further polarize the solute in an iterative process until a convergence is reached. The solute-solvent interaction is added to the gas-phase Hamiltonian of the solute. One key factor of these implicit solvent models is the construction of the solute cavity. A simple scheme of a solute cavity construction is illustrated in Figure 3.1.

In Figure 3.1, we use a water molecule as the example. The three spheres in red represent the vdW spheres of each atom. The surface of overlapped vdW spheres of the water molecule is vdW surface. The two spheres in purple are the solvent probe molecules, which moves along the vdW surface of the molecule and generates two types of surface, one is SES which is also called the Connolly surface. The other is SAS, and the SAS area, i.e., SASA is frequently used in MD simulations[5]. More details about these concepts can be found in the work of Quan and Stamm.[6, 7] It needs to be noted that, for some environments, for example, solvent mixtures, ionic liquids and large solvent molecules, the size of solvent probe is often less well-defined and explicit solute-solvent interactions are often important. Thus, implicit solvent models are often not good enough, and a few explicit solvent molecules near solute molecules should be modelled explicitly instead of using fully continuum model. An example for modelling reactions in ionic liquids using a few explicit ion pairs and implicit solvent model can be found in the work of Wylie and co-workers.[8]

The size of solute cavity dramatically influences the computed solvation free energy.[9]
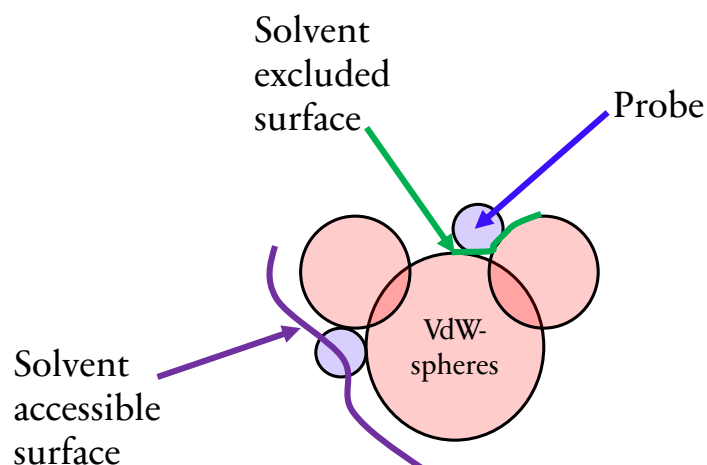
Figure 3.1: The scheme of cavity construction in implicit solvent models.

It is mainly affected by three factors: atomic radii, cavity surface type and ESF value. Atomic radii are key parameters for continuum solvent models, with different sets available according to the solvation models and software packages. Generally speaking, the cavity size should be set to exclude the solvent molecules and include the largest part of solute charge distribution.[10] Although some simple models, e.g., sphere cavities have been designed,[11] they are far from real shape of most solute molecules. This is the reason why atomic radii interlocked superposition of atomic spheres was introduced to reproduce solute shape and exclude solvent molecules. Atomic radii can be evaluated by different ways. For example, Bondi introduced a set of atomic radii based hard volume values of molecules,[12] these atomic radii were confirmed by the data from the Cambridge Structural Database.[10] Some atomic radii, for example, the UFF atomic radii were taken from corresponding force fields.[13] It was reported by Rahm and co-workers that the decay of electron density are different for neutral and charged species, so for the same element, cationic radii are usually smaller than neutral radii while anionic radii are usually larger.[14] Besides giving different radii for a element with different net charges, ESF values are often used to scale all atomic radii of a charged molecule with an uniform value. An application of this strategy can be found in Ref.[15] Besides the dependence of atomic radii on net charge, atomic radii are also influenced by the polarity of solvent. Some atomic radii, e.g., those used in SMD,[16] are solvent-dependent, while others (e.g., UAHF radii[17]) are not. UAHF radii were designed by Barone and co-workers in 1997. It is a type of united atomic radii for which atomic radii of hydrogen atom are not explicitly defined while they are emerged to the radii of heavy atoms that hydrogen atoms are attached to.[17] All UAHF atomic radii were obtained with HF calculations using reference data in water. Another set of atomic radii, i.e., UAKS radii were later developed in a similar way while using DFT instead of HF calculations. ESF value, again, is introduced to scale atomic radii to make them more transferable in different solvents, so ESF values themselves are usually solvent-dependent and charge-dependent, the default ESF value for both UAHF and UAKS radii is 1.2. These parameters are often optimized to reproduce accurate solvation free energies or/and solution-phase properties (e.g., pK_a and redox potential) with implicit solvent models.

When a solute is placed in the vacuum cavity, its position-dependent electrostatic potential $\phi(r)$ can be determined. The Green function inside the cavity is $G_i(r)$. The source electron density $\rho(r)$, total electrostatic potential $\Phi(r)$ and the position-dependent permittivity $\epsilon(r)$ can be connected by the Poisson equation:

$$\nabla \cdot [\epsilon(r)\nabla\Phi(r)] = -4\pi\rho(r) \tag{3.1}$$

where $\Phi(r)$ is the sum of solute potential $\phi_m(r)$ and the apparent potential $\phi_s(r)$. With the boundary conditions, the equation can be solved by many strategies, and further details can be found in Ref.[10, 18]. For the case of the ASC method, the polarized charge $\sigma(s)$ is assumed to be located at the cavity surface, and the surface is separated into different segments using different algorithms (e.g., GEPOL.[19]). The polarized charge in each part is usually assumed as either a constant or solute electron density (i.e., SMD). The interaction between solute and solvent can be expressed as the interaction between solute charge and polarized surface charge. $\phi_s(r)$ can be computed as:

$$\phi_s(r) = \int \frac{\sigma(s)}{|r-s|}ds \tag{3.2}$$

Within this framework, the solution-phase free energy of species A, $G_{A,sol}$ can be expressed as:

$$G_{A,sol} = G_{A,gas} + \Delta G_{A,solv} + 1.89 \tag{3.3}$$

where $G_{A,gas}$ is the gas-phase free energy and $\Delta G_{A,solv}$ is the solvation free energy, and 1.89 kcal/mol is the correction for the change of standard states from gas-phase to solution-phase at room temperature and pressure. The correct use of continuum solvent models has been frequently discussed.[20–22] Many factors including the theoretical levels and the cavity construction schemes can dramatically affect the final accuracy of $\Delta G_{A,solv}$ and related chemical properties, for example, see a discussion about redox potential.[23]

Although implicit solvent models have achieved great success in the past decades, efforts to further improve the accuracy of implicit solvent models are still meaningful because the accuracy of solvation modelling directly determines the computed properties and energies. In this thesis, we mainly focus on two types of implicit solvent models: SMD[16] and PCM (specifically CPCM and IEFPCM with united atom schemes)[10]. Here we choose these two solvation models as they are the most used PCM variants in the community. Details about the development of SMD can be found in Ref.[16] and the main parts can be illustrated by Figure 3.2. Essentially, SMD solvation free energy can be separated into two parts: electrostatic components and non-electrostatic components. The latter is also called CDS term, i.e., the contributions from cavitation, dispersion and repulsion. For the electrostatic component, SMD was developed based on the framework of IEFPCM using the electron density of the solute with the solvent-dependent atomic radii (atomic Coulomb radii). Non-electrostatic components were calculated using a set of parameters including atomic surface tension coefficient. These parameters, along with the atomic Coulomb radii and the theoretical levels used for solvation free energies were systematically optimized using the data in the MNSOL-v2012 database.[24]

Since reported in 2009, SMD has gained popularity and is widely used in the community of quantum chemistry. Different attempts have been made to improve the accuracy in
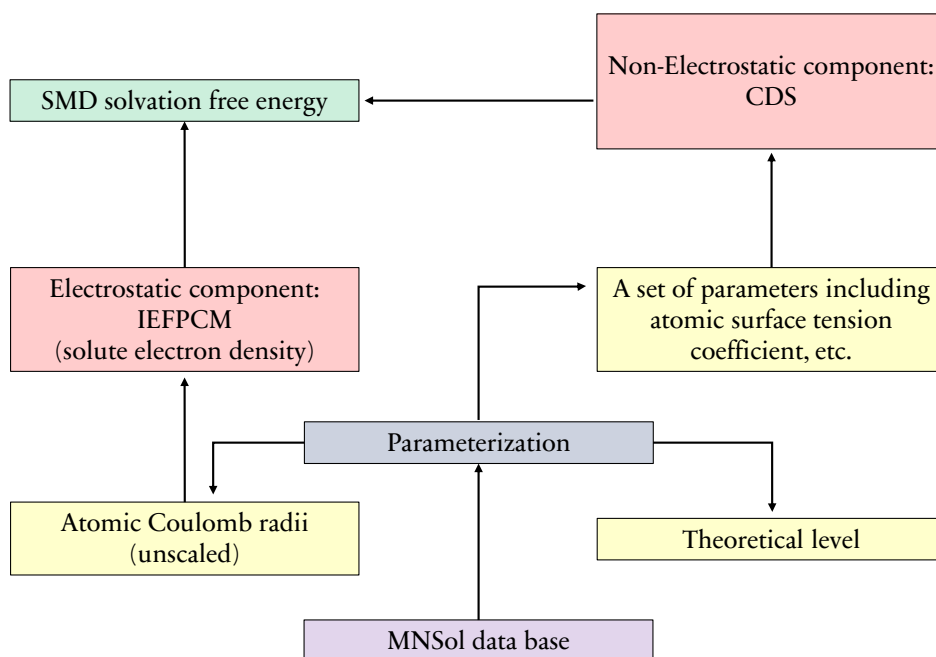
Figure 3.2: Main parts in the development of SMD.

the predictions of SMD solvation free energies. The first method is tuning the theoretical level (usually the combinations of different DFT functionals and basis sets) used for solvation free energies.[20, 25] The second method is to include a few explicit solvent molecules near the solute molecule, which is also called cluster model or mixed discrete–continuum solvation model.[26–28] The third method is to scale the solute cavity, i.e., to change the atomic radii, cavity surface type, or/and the ESF.[29, 30]

Although these methods can improve the accuracy of SMD for some cases, some open questions remain unsolved:

(1) What is the best theoretical level for SMD solvation free energy? Many works including our previous work[20] propose using M052X/6-31G(d), while a closer look at the results from Ref.[16] suggests M052X/6-31G(d) is not the best choice for ions, which can introduce errors when this theoretical level is applied to model chemical properties where ions are involved, e.g., pK_a and redox potential. For cations containing only C, H, N, O atoms, using M052X/6-31+G(d,p) can produce smaller mean unsigned error than M052X/6-31G(d) by 0.5 kcal/mol. While for anions, surprisingly using HF/6-31G(d) is more accurate than M052X/6-31G(d) by over 1 kcal/mol.

(2) Whether using explicit solvent molecules is always helpful? Although it's widely recognized that introducing explicit solute-solvent interactions can be helpful, the fact that SMD was developed using explicit solvent molecules for only few species raises the concern that whether the explicit interactions have been, at least partially, included already implicitly in the parameterization of SMD. Thus, double counting could possibly introduce additional errors.

(3) Is cavity scaling really necessary? Several studies have reported the use of cavity scaling to improve the results of SMD. In a study by Schlegel and Thapa, the cavity size was only slightly changed from its default settings (i.e., ESF = 1).[29] While in a study by Smith and co-workers, the cavity was re-constructed using a different cavity surface

type and direct method (instead of the thermodynamic cycle method), and the ESF value used significantly deviated from the default value of SMD[30]. This raises the question that if a suitable theoretical level is used and the explicit solvent molecules are properly included, whether cavity scaling is still useful? A good example to highlight this is that different optimized ESF values were obtained when different theoretical levels were used for gas-phase free energies in Ref.[29] Furthermore, the generality of these cavity scaling methods is also a concern.

To answer these questions, in Section 3.2, we conducted pK_a calculations on a wide range of solute molecules in water with the thermodynamic cycle method described in Figure. 3.3.
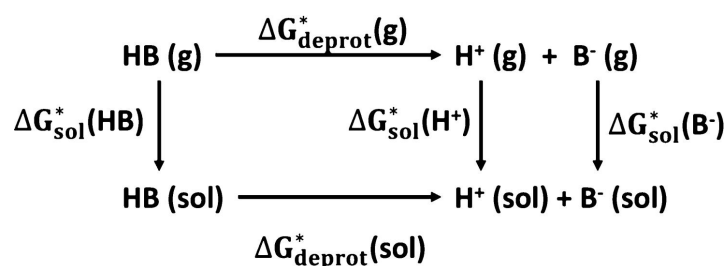
Figure 3.3: Thermodynamic cycle method for pK_a calculations in solution phase.

SMD was developed on the basis of IEFPCM, so it can be regarded as one specific case of the PCM model. More generally, there are many variants of PCM, as shown in Figure. 3.4.
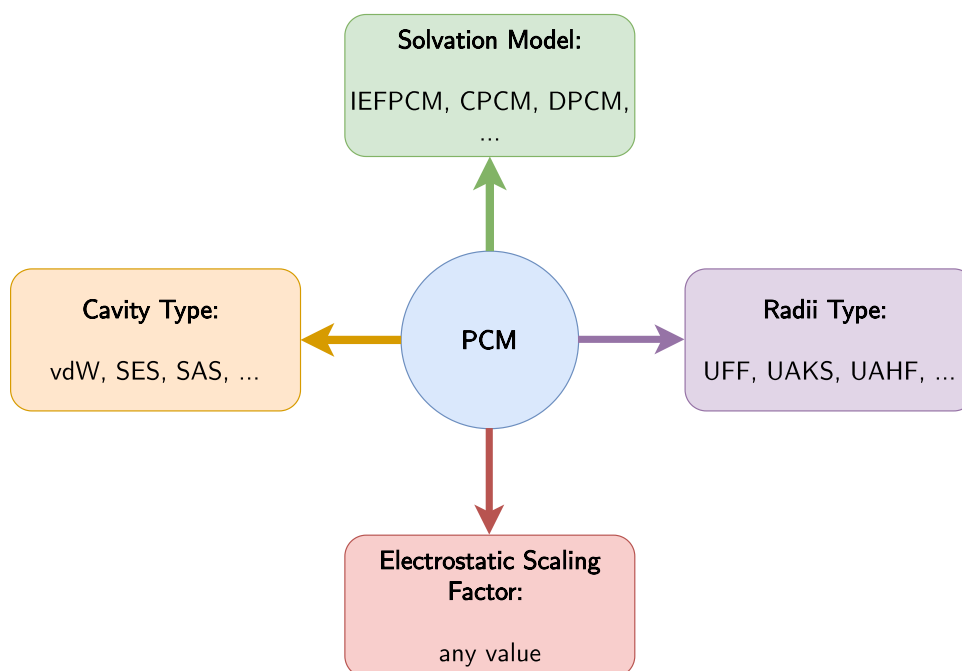
Figure 3.4: Factors for different variants of the polarizable continuum model.

In Section 3.3, we specifically investigate the CPCM and IEFPCM solvation model with UAHF and UAKS radii. Among all PCM methods, CPCM and IEFPCM are the

two most used, thus improving their accuracy is highly important.UAHF and UAKS radii were developed by Barone, Cossi and Tomasi in 1997.[17] The advantage of these two radii types is that they were designed using an optimal theoretical level, so users do not need to further benchmark theoretical levels. The disadvantage is that they were designed for hydration free energy only, so if these radii are used in non-aqueous solutions, their parameters need to be re-designed. Currently, the most widely used method is to optimize the ESF value (also called α value) to improve their accuracy in non-aqueous solution. Most quantum chemical programs, e.g., Gaussian[31] and Q-Chem[32] provide options for users to specify their own ESF values. Specifying ESF values is much easier than designing and implementing a new surface type or a new set of atomic radii. Although cavity scaling does improve the accuracy of solvation free energies for PCM-UAHF and PCM-UAKS, there are still some problems:

(1) First of all, in most studies on scaling solute cavities, usually only a small number of solute molecules in limited types of solvents were investigated, which means the optimal ESF values reported in these works might be less useful for other solute/solvent combinations.

(2) Most studies scaled the solute cavity via reproducing experimental pK_a values and/or redox potential in solution phase, usually with an less accurate but cheaper theoretical level for the gas-phase free energies. This means that the obtained optimal ESF value and associated solvation free energies actually implicitly included the components used to correct the errors of gas-phase free energies. The optimized ESF values are dependent on the theoretical level used for gas-phase free energies, which limits the use of this method.

(3) Most studies presented only an overall optimal ESF value for all species types. Considering the fact that the optimal cavity size of ions and neutral species could be very different, whether it is meaningful to use different ESF values for ions and neutrals species (i.e., mixed ESF method) remains an open question, especially for pK_a and redox potential caluclations where both neutral and charged species exist.

Accordingly, a systematic optimization of the ESF values is performed in Section 3.3 where:

(1) An extensive and large data base of solute/solvent combinations (i.e., the MNSOL-v2012 database[24]) is used.

(2) ESF values are optimized directly using the solvation free energy instead of solution-phase properties.

(3) ESF values of neutral and ionic species are optimized separately.

A scheme for our optimization is shown in Figure 3.5.

Here we set the initial choices of ESF values for all cases as 1.1, 1.2, 1.3 with the interval as 0.1. If the optimal ESF value is within this initial range, then the optimization process is finished. If the optimal ESF value is not found, then extra ESF values are added to the side towards smaller error, e.g., if the error of 1.3 is smaller than that of 1.2 and 1.1, then we further try 1.4. The loop is repeated until the optimal ESF values with the smallest error are obtained for all solute/solvent combinations, which generates a final ESF range from 0.9 to 2.1, with the interval as 0.1.

The performance of the optimized ESF values are tested by pK_a calculations in both water and acetonitrile using the thermodynamic cycle method as described in Figure 3.3.
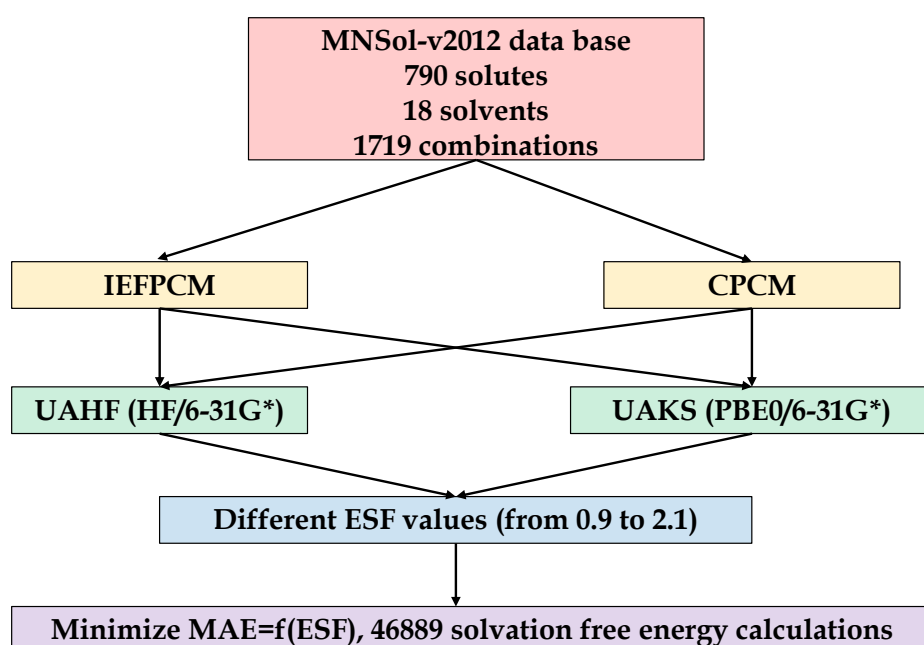
Figure 3.5: Method for our optimization of ESF values.

3.2   Publication 2

Methods To Improve the Calculations of Solvation Model Density Solvation Free Energies and Associated Aqueous pK_a Values: Comparison between Choosing an Optimal Theoretical Level, Solute Cavity Scaling, and Using Explicit Solvent Molecules

Longkun Xu, Michelle L. Coote
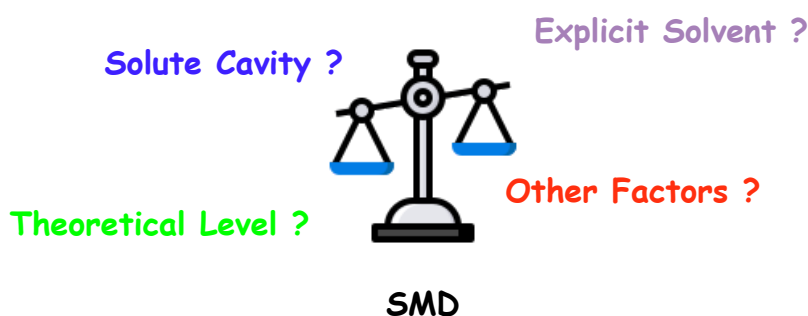
This publication is a peer-reviewed manuscript published in *The Journal of Physical Chemistry A*. All computational results and subsequent discussion were my own work under the supervision of Prof. Michelle Coote, who edited the manuscript. Supporting information is available online (https://pubs.acs.org/doi/10.1021/acs.jpca.9b04920). The document for the statement of contributions is placed in the Appendix.

Methods To Improve the Calculations of Solvation Model Density Solvation Free Energies and Associated Aqueous pK_a Values: Comparison between Choosing an Optimal Theoretical Level, Solute Cavity Scaling, and Using Explicit Solvent Molecules

Longkun Xu and Michelle L. Coote*

ARC Centre of Excellence for Electromaterials Science, Research School of Chemistry, Australian National University, Canberra, Australian Capital Territory 2601, Australia

Ⓢ *Supporting Information*

ABSTRACT: Many approaches have been used to improve the accuracy of implicit solvent models including solute cavity scaling, introducing explicit solvent molecules, and changing the level of theory for the solvation calculations. Here, we compare these strategies using a large test set of aqueous pK_a values for amines, nucleobases, carboxylic acids, thiols, peptide carbon acids, alcohols, and anilines for the specific case of solvation model density (SMD) within the framework of a thermodynamic cycle in which the gas-phase component is consistently calculated via the accurate CBS-QB3 method. We show that the choice of theoretical level for solvation energies should be based on the original parameterization of the solvent model, with separate levels of theory for the solvation energies of neutrals, anions, or cations, outperforming the best compromise level of theory. However, when explicit solvent molecules are introduced, a higher level of theory is needed to describe the solute−solvent interactions. For the systems studied here, explicit solvation improved the results for acids (and hence anions) but not for bases, for which results deteriorated. Importantly, we find that solute cavity scaling does not significantly improve the SMD results for the CHNO compounds tested when the correct theoretical level is employed and explicit solvent effects are correctly treated.
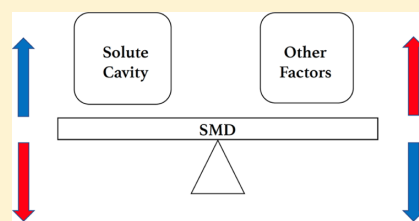
■ INTRODUCTION

Continuum solvent models are crucial for making quantum chemical studies of practical chemical systems tractable.[1−5] At the same time, they are usually the largest source of error in any calculation and the most difficult part of the calculation to systematically improve.[6−9] Apart from developing new models, strategies for improving the accuracy of continuum solvent calculations include changing the level of theory at which the calculations are applied,[9] scaling the solute cavity via electrostatic scaling factor (ESF) and/or surface type,[10−21] and including one or more explicit solvent molecules in the calculation.[22−25]

However, all of these approaches can have problems. For instance, because solvent models are parameterized at a specific level of theory, improving the level of theory can sometimes increase rather than decrease the errors. A classic example is when UAHF radii, which were parameterized with HF/6-31G(d), are used with correlated methods. Hartree−Fock is known to overpolarize the solute, which is empirically corrected by the UAHF parameters. As a result, when these parameters are used with correlated levels of theory, they then overcorrect for polarization and have larger errors.[9]

Likewise, it is intuitive that inclusion of explicit solvent molecules should improve the accuracy of solvation calculations, and indeed, many studies have shown them to be necessary when direct solute−solvent interactions occur.[3,15,21,22,24−29] Nonetheless, because solvent models were parameterized without explicit solvent molecules, indiscriminate inclusion of multiple explicit solvent molecules can often lead to double counting and increased errors in other aspects of the calculation such as the cavitation free energies.[30]

Finally, a number of studies[10−21,31−45] have shown that the scaling of cavities by an ESF and/or surface type can help to minimize errors, particularly on changing solvents or from neutrals to cations to anions. However, recommended values of the ESF can vary considerably even for the same solvent model and solvent. Hence, this raises the question as to whether they are physical or not or whether they can help beyond the systems to which they were fitted.

The present work aims to explore these issues and help to identify the best method(s) for improving the accuracy of solvation energies and solution-phase properties. We have limited our focus to the popular solvation model density (SMD) solvent model[46] as this allows us to eliminate some but not all of the variables. For instance, this model has in-built intrinsic atomic Coulomb radii working with the default van der Waals

Scheme 1. Test Set Used in This Work, Which Includes Aqueous pK_a Values of 5 Methyl-Substituted Nucleic Acid Bases (M1−M5), 17 Carboxylic Acids (C1−C17), 10 Aliphatic Amines (A1−A10), 5 Thiols (T1−T5), 13 Neutral (N1−N13) and 10 Cationic (H1−H10) Carbon Acids, 5 Alcohols (AL1−AL5), and 5 Anilines (AN1−AN5)[a]
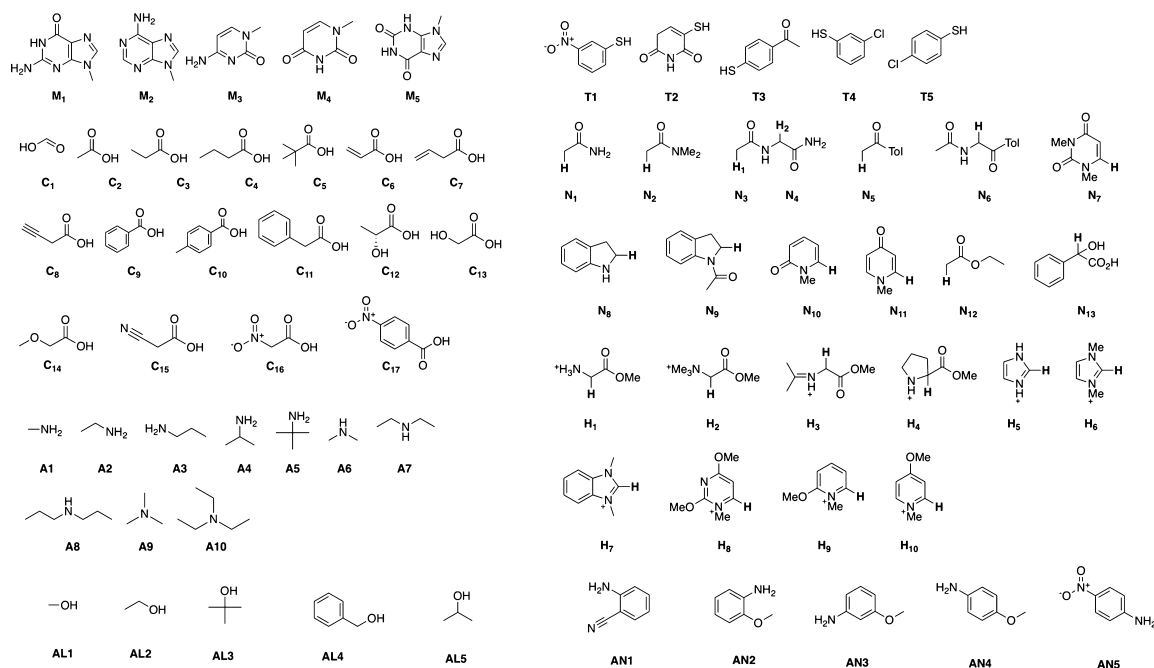
[a]For bases (pK_{a1} of M1−M5, A1−A10, AN1−AN5), the pK_a of the conjugate acid was calculated. For M1, M4, and M5 pK_{a2} (i.e., deprotonation of the neutral species) was also calculated. For carbon acids, the hydrogen that is deprotonated is bolded for clarity. Species M1−M5 were originally studied in ref 47, C1−C17, A1−A10, and T1−T5 in ref 48, N1−N13 and H1−H10 in ref 28, AL1−AL5 in ref 30, and AN1−AN5 in ref 23.

(vdW) surface, which were optimized in the design of SMD, and thus, we use these for the present work. This model was parameterized for a large test set of neutral, cationic, and anionic solvation energies across several solvents, and its recommended ESF is 1 (i.e., no scaling is necessary any more). The model was benchmarked over six levels of theory, but, of these, different levels of theory were shown to perform better for neutral versus anionic versus cationic species and with different solvents. Hence, we have the option to compare the effects of using the recommended level of theory for a given solvent and type of species rather than other levels of theory.

However, despite its recommended ESF value of 1, recently, Schlegel and co-workers[47] showed that pK_a predictions using SMD could be further improved by ESF optimization. They studied methyl-substituted nucleobases in aqueous solution using accurate CBS-QB3 gas-phase energies in conjunction with SMD solvation energies at the B3LYP/6-31+G(d,p) level of theory in a thermocycle so as to minimize other sources of error. They showed that the highest accuracy pK_a results were obtained with an ESF of 0.975 for cations (used for pK_{a1} calculations), 0.925 for anions (used for pK_{a2} calculations), and 1 for neutrals in both cases. Alternatively, if less accurate B3LYP gas-phase energies are used, the optimal ESF values are 1.00 for neutrals and cations and 0.90 for anions. This highlights that ESF values can sometimes implicitly correct other errors in the calculation, beyond merely the solvation energies.

In an independent study by Smith et al.,[48] more dramatic ESF scaling of SMD was recommended using the solvent accessible surface (SAS) instead of the default vdW surface. In that work,

aqueous pK_a values of several carboxylic acids and aliphatic amines were computed with M062X/6-31+G(d,p) via the direct method (i.e., entropies and thermal corrections were calculated using gas-phase partition functions applied to solution-phase geometries and frequencies). An optimal ESF value of 0.485 was obtained with the use of SAS, so both atomic radii of the solute and the solvent radius were tuned. Unlike the work of Schlegel,[47] this study included a number of thiols. Sulfur-containing compounds had been shown previously to perform very poorly with SMD compared with C, H, N, and O species.[46] With the inclusion of an ESF scaling, the thiol results improved dramatically.[48]

Although these three strategies are widely employed, comparison of their efficacy is scarce. In the present work, we compare them so as to address three key questions: (1) is solute cavity scaling still necessary for SMD when suitable theoretical procedures are used? (2) Does using explicit solvent molecules always improve the accuracy of solvation free energies? (3) Which one of these approaches is more general for various solute types and thus the one to use for a new system for which there may not be experimental data for fitting or testing?

To this end, we use the above-mentioned two prior studies as a basis to compare the effectiveness of solute cavity scaling against the use of explicit solvent molecules and/or simply use the optimal level of theory for the solvation energies. At the same time, we control other sources of error using the in-built SMD parameters and using a thermocycle in conjunction with a high level of theory in the gas-phase electronic energies as the parameterization and benchmarking in original SMD design was

for solvation free energies rather than for solution-phase Gibbs free energies.[46] As our test set (Scheme 1), we consider a subset of molecules from these previous two studies for which accurate experimental data are available. Although we mainly focus on compounds only containing C, H, N, and/or O in this work, we include five thiols to show how SMD accuracy differs significantly for these sulfur-containing species. To test the wider applicability of the various protocols, we also employ an independent test set to which none of the literature ESF values have been fitted, comprising neutral and cationic carbon acids taken from ref 28 (N1−N13 and H1−N10), alcohols (AL1−AL5) taken from ref 30, and anilines (AN1−AN5) taken from ref 23.

■ COMPUTATIONAL METHODS

Unless noted otherwise, we used the thermocycle method (Scheme 2) for pK_a calculations in this work. It should be noted

Scheme 2. Thermodynamic Cycle Method for pK_a Calculations in the Solution Phase
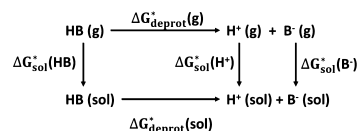
that according to convention, pK_a values of the bases studied here are expressed as the deprotonation of their conjugate acid. Using the thermocycle method, the total Gibbs free energy of a species in solution is given as[9]

$$G*(sol) = G^0(g) + \Delta G^*_{solv} + \Delta G^{1atm \rightarrow 1M} \quad (1)$$

where $G^0(g)$ is the standard gas-phase Gibbs free energy, ΔG^*_{solv} is the solvation Gibbs free energy, and $\Delta G^{1atm \rightarrow 1M}$ (which equals 1.89 kcal/mol) is the Gibbs free energy change resulting from the different standard states in the gas and solution phase. The pK_a value can then be computed as

$$pK_a = \frac{\Delta G^*_{deprot}(sol)}{2.303RT} \quad (2)$$

where $\Delta G^*_{deprot}(sol)$ is the standard state free energy change of the deprotonation reaction in the solution phase, R is the universal gas constant, and T is the temperature in kelvin. The aqueous solvation free energy of proton $\Delta G^*_{sol}(H^+)$ is taken as −265.9 kcal/mol to remain consistent with Schlegel's work.[47]

For species M1−M5, there are multiple tautomers, and thus, following the method of Schlegel and co-workers,[47] we calculate the ensemble pK_a considering contributions from multiple tautomers as

$$pK_a = pK_a^{ij} + \log \frac{f'_j}{f_i} \quad (3)$$

where pK_a^{ij} is the tautomer-specific pK_a related with the tautomer j of the deprotonated species and the tautomer i of the protonated species and f'_j and f_i are, respectively, the population of tautomer j and tautomer i. This treatment was applied except in cases where explicit solvent molecules were also required; in those cases, the dominant tautomer was considered. Moreover, where the methods used were identical, the optimized structures of M1−M5 were taken directly from ref 47.

All quantum chemical calculations were performed with either Gaussian 16[49] or Molpro 2015.[50] For cases without explicit solvent molecules, the default CBS-QB3 method was used for gas-phase free energies. In cases with explicit solvent molecules, gas-phase Gibbs free energies were calculated using the complete basis set method CBS-QB3[51]//M062X/6-31+G(d,p) so as to take dispersion into account in the geometry optimizations and to minimize other sources of error. To provide additional confidence in the accuracy of CBS-QB3, results obtained with this level were compared with otherwise identical results obtained with an alternative type of composite ab initio method G3(MP2, CC), as well as the lower cost density functional theory (DFT) procedures employed in some of the literature protocols tested here. Results in the Supporting Information (Table S1) show that the mean unsigned deviations of G3(MP2, CC), M062X/6-31+G(d,p), and B3LYP/aug-cc-PVTZ gas-phase reaction electronic energy are, respectively, 0.75, 0.88, and 0.89 kcal/mol compared with CBS-QB3 results. However, the maximum unsigned deviations are, respectively, 1.45, 3.50, and 3.05 kcal/mol. Thus, CBS-QB3 and G3(MP2, CC), both of which have been independently benchmarked on large test sets, mutually support each other, while the two DFT procedures also perform almost on average but show that large random deviations are not reliable. Between the two composite ab initio methods, we select CBS-QB3 for consistency with ref 47.

Gas-phase thermal corrections to enthalpies and entropies were calculated using an in-house script that implemented the quasi-harmonic oscillator (QHO) approximation. Frequencies were scaled by their literature scale factors.[52] Testing in the Supporting Information (Tables S2−S11) using the below protocols 1−4 showed that the results were relatively unaffected by the QHO cutoff value over the range of 0−100 cm^{-1}. Unsurprisingly, the largest differences occurred when an explicit solvent molecule was included because of the introduction of additional low-frequency torsional modes. In those cases, 100 cm^{-1} provided the best agreement with the experiment. For calculations without explicit solvent molecules, we use 25 cm^{-1} as it produces minimum overall mean absolute errors (MAEs) with both protocol 1 and protocol 2.

To calculate the Gibbs free energies of solvation, solution-phase geometries were consistently optimized in solution using M062X/6-31+G(d,p). However, for calculating the Gibbs free energies of solvation, four different protocols were considered.

(1) Mixed levels of theory: ΔG_{solv} values were calculated as single point energies using M052X/6-31G(d) for neutrals, M052X/6-31+G(d,p) for cations, and HF/6-31G(d) for anions. These are (counterintuitively) the best-performing levels of theory for each of these CHNO species in aqueous solution in the original SMD study.[46]

(2) M052X/6-31G(d) level of theory: ΔG_{solv} values were calculated as single points using M052X/6-31G(d) for all species. M052X/6-31G(d) was the best overall average performer for aqueous solvation energies in the original SMD study.[46]

(3) Explicit solvent M052X/cc-pVTZ level: ΔG_{solv} values were calculated as single points using the M052X/cc-pVTZ level for all species, which is the level of theory suggested in ref 22. One explicit solvent molecule is used.

(4) Explicit solvent M062X/6-31G(d): ΔG_{solv} values were calculated as single points using the M062X/6-31G(d) level for all species. One explicit solvent molecule is used.

M062X/6-31G(d) was recommended by Truhlar and Cramer when using SMD with an explicit solvent molecule.[27]

For cases with an explicit solvent molecule, that is, protocols 3 and 4, the explicit solvent molecule is placed near the (de)protonation site as this is the complex which most influences the reaction (see Figure 1 for an example).[24,25]
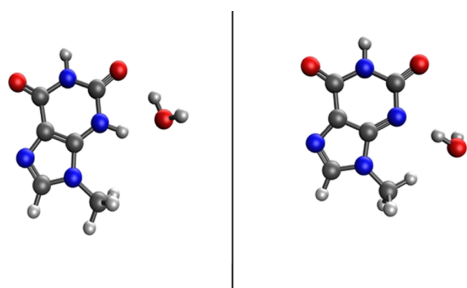

Figure 1. Optimized structures of neutral (left) and anion (right) forms of 9-methylxanthine (M5) with one explicit solvent in aqueous solution in pK_{a2} calculation.

Having placed the molecule there, a complete conformational search about the rotatable covalent and noncovalent bonds is then performed. This strategy is widely used for solute−solvent complexes, for example, see refs.[15,22] Note that the positions of the explicit solvent molecule are different for the pK_{a1} and pK_{a2} calculations of the same molecule as different hydrogen atoms are involved.

Finally, in addition to using our unscaled SMD protocols, the scaled SMD methods of Schlegel and co-workers[47] and Smith and co-workers[48] were also evaluated for comparison. Where the systems were identical to their original papers, data were taken directly from those works, for all additional system calculations were performed exactly as per their protocols except where otherwise noted. These protocols are outlined below for convenience.

In the methods of Schlegel and co-workers, denoted here as CBS-QB3_S and B3LYP_S, a thermocycle is used where gas-phase geometries and frequencies are obtained with default CBS-QB3 and B3LYP/6-31+G(d,p), respectively, and energies are calculated using default CBS-QB3 and B3LYP/aug-cc-PVTZ, respectively. The gas-phase thermal corrections and entropic corrections are calculated using the harmonic oscillator approximation. In both methods, solvation energies are then calculated using SMD/B3LYP/6-31+G(d,p), with ESFs applied. ESF values for CBS-QB3_S are 1.00 for neutrals, 0.975 for cations, and 0.925 for anions; for B3LYP_S, they are 1.00 for cations and neutrals and 0.90 for anions.

In their paper, Smith and co-workers[48] used the direct method (i.e., directly computed the total free energy in the solution phase) rather than the thermodynamic cycle method (i.e., separately calculated gas-phase free energy and solvation free energy). They also scaled the SAS rather than the vdW surface. They used three different approaches to calculate the Gibbs free energies in solution: (a) the direct method using the SMD model based on a SAS scaled by 0.485 (SMD-sSAS); (b) the same direct method but using an ESF of 1 (SMD-default); (c) the direct method but with the intrinsic atomic Coulombic radii used in the SMD model replaced by Bondi radii and other parameters unchanged (SMD-Bondi). Figure S2 in the

Supporting Information of ref 48 provides a good comparison between different radii types. The theoretical level used by Smith and co-workers for the above three models is M062X/6-31+G(d,p). Thermal and entropic corrections were calculated using QHO approximation with a 30 cm^{-1} QHO cutoff. Testing in the Supporting Information showed that the results obtained were relatively unaffected by this value over the range of 0−100 cm^{-1} (Tables S12−S17). For comparison, we also introduce a variant of SMD-sSAS, denoted SMD-sSAS-C, which is identical to the former except that a thermocycle is used and the gas-phase energies are calculated using the higher-level CBS-QB3 method.

■ RESULTS AND DISCUSSION

Default Solute Cavities. We initially considered the substituted nucleic acid bases (M1−M5), carboxylic acids (C1−C17), aliphatic amines (A1−A10), and thiols (T1−T5) of Scheme 1 as these were previously subjected to solute cavity scaling in either ref.[47,48] To assess whether an unscaled method could achieve similar or better accuracy, ΔG^{*}_{solv} values were calculated via our four different protocols described above and then combined with high-level gas-phase Gibbs free energies so as to obtain pK_a values. Complete pK_a results with their absolute errors (AEs), as obtained via each protocol, are provided in the Supporting Information (Tables S5, S6, S10, and S11); MAE and maximum absolute errors (MAXs) of each subtest set are shown in Figure 2. All results in Figure 2 are obtained without solute cavity scaling, that is, using the default SMD ESF = 1.0 and default vdW surface for all species.
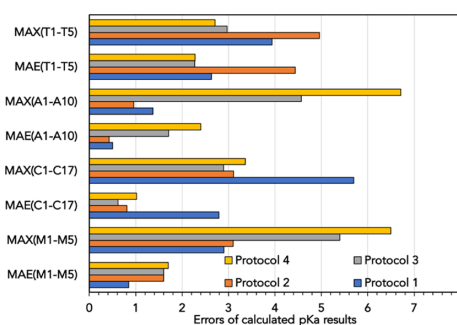

Figure 2. MAEs and MAXs calculated for the thiols, amines, carboxylic acids, and nucleobases of Scheme 1 with default solute cavity.

From Figure 2, it can be seen that the magnitude of the error varies considerably among the subtest sets and that the relative performance of the different protocols also varies. Generally, it is seen that the protocols without explicit solvent molecules (1 and 2) outperform those that include them (3 and 4) for nucleobases and aliphatic amines. However, for carboxylic acids and thiols, the reverse is true. Additionally, within M1−M5, the explicit solvent increases the errors for pK_{a1} and decreases the errors for pK_{a2}, especially comparing protocol 3 with protocol 1 (Table 1). Where explicit solvents are not required, protocol 1 outperforms protocol 2, especially for M1−M5, and hence, using the best possible level of theory for each solvation energy in the Hess cycle, as recommended in the original SMD paper,[46] is preferable to using the best compromise level of theory from that work.[46] Where explicit solvents are needed, protocol 3 outperforms protocol 4, especially for C1−C17 presumably

Table 1. MAE and MAXs of the M1−M5 Subset, Separated into pK_{a1} and pK_{a2} Values[a]

	protocol			
	1	2	3	4
pK_{a1} MAE	0.2	2.1	2.2	2.2
pK_{a1} MAX	0.4	3.1	5.3	6.5
pK_{a2} MAE	1.7	0.9	0.9	1.1
pK_{a2} MAX	2.9	1.4	1.7	1.9

[a]For individual data, see Tables S5, S6, S10, and S11 of the Supporting Information.

because a higher level of theory is needed to model the noncovalent interactions between the solute and solvent.

The results in Figure 2 and Table 1 show that when the recommended theoretical level is respectively used for both calculations with and without an explicit solvent, explicit solvents do not always improve the accuracy of SMD, presumably because of the possibility of double counting effects that are implicitly accounted for through parameterization. On the basis of the present results, it appears that explicit solvents are necessary for reactions involving anions but not for neutrals and cations. This is consistent with other studies. For instance, Zhang[23] showed that the errors in the pK_{a1} values of the amines and anilines increased after adding one solvent molecule to both the neutral and cationic species. More generally, Schlegel and co-workers concluded that the improvement resulting from explicit solvent molecules in pK_a values involving neutrals and cations was modest while that in pK_a values involving neutrals and anions was quite significant.[24] Cramer, Truhlar, and co-workers also concluded that an explicit solvent molecule is especially required for anions concentrating charge on a single exposed heteroatom.[26] Other studies have also highlighted the need for explicit solvent correction for pK_a calculations of carboxylic acids.[53] Hence, the poor performance of protocol 1 in Figure 2 for carboxylic acids, compared with protocol 3, is in many ways more physical.

For thiols, adding an explicit solvent is generally helpful. Indeed, an earlier study has shown that as many as three explicit solvent molecules are required for such compounds.[25] While we attempted to include three explicit molecules for the present work, problems finding reasonable stable geometries forced us to abandon this approach. In any case, it is worth noting that none of the protocols used here delivers an optimal MAE for the thiols of comparable accuracy to the CHNO species studied. For these latter species, the best protocol delivers average errors of the order of around 0.5 pK_a unit and maximum errors between 1 and 3 pK_a units. In the case of thiols, the average errors exceed 2 pK_a units. The poor performance of thiols is consistent with that reported in the original SMD paper, which also showed larger errors for compounds containing sulfur, and suggests that SMD itself contains greater errors in this case.[46] Because the levels of theory used in protocols 3 and 4 are taken from papers benchmarking CHNO compounds only, performing bench-marking on other molecules such as thiols may help to solve this problem. Indeed, ref 25 suggested using ωB97XD in place of M06-2X for these particular compounds, in conjunction with the three explicit solvent molecules. Clearly, molecules containing atoms other than CHNO require special consideration and are beyond the scope of the present work.

Effect of Scaling Solute Cavities. Having teased out the differing roles of the theoretical level and explicit solvents, we can now study the effect of solute cavity scaling on the results

and also compare our methods with the results obtained using scaled solute cavities. For the rest of this work, we use protocol 1 for bases (pK_{a1} of M1−M5 and A1−A10) and protocol 3 for acids (pK_{a2} of M1−M5 and C1−C17). We exclude the thiols (T1−T5), which, as noted above, perform poorly with SMD. In other words, one uses the recommended levels of theory without an explicit solvent and then includes explicit solvent molecules where physically necessary. When including explicit solvent molecules, use of a higher level of theory is then needed to better describe the interactions with the solvent molecule. The questions then arise: does this approach outperform approaches based on a scaled solute cavity and can our approach be itself improved with solute cavity scaling?

Figure 3 shows the MAE of pK_a values of M1−M5 calculated with our above strategy, compared with CBS-QB3_S and
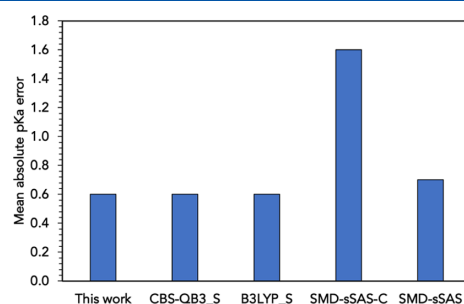

Figure 3. MAE of calculated pK_a values of M1−M5 calculated in this work (with default solute cavity) and obtained with four solute cavity scaling methods (see text).

B3LYP_S results taken from Schlegel and co-workers,[47] the result obtained with the SMD-sSAS method of Smith and co-workers,[48] and our variant SMD-sSAS-C. Details of all methods are described in the methods section; all individual data are provided in the Supporting Information. For M1−M5, both CBS-QB3_S and B3LYP_S were fitted directly to the data and as such perform well. The difference in accuracy between CBS-QB3 and B3LYP for the gas-phase reaction energies is clearly compensated by different values of the ESFs in the two protocols, at least for the systems to which these methods were fitted. Importantly, Figure 3 shows that the unscaled SMD protocols of the current work perform equally well, despite not benefitting from the same direct fitting. Although the SMD-sSAS method was not fitted to this data set, it gave good results (MAE = 0.7 pK_a unit). However, SMD-sSAS-C performs much worse than SMD-sSAS, despite the former using a higher level of theory. This indicates that the scale factor is correcting both solvation errors and DFT errors in the reaction energies.

To test if tuning the solute cavity, or more specifically, tuning ESF values, would lower errors of our results in Figure 3, ESF values of the ions were optimized while those of neutral species were unchanged, as in the work of Schlegel.[47] The considered range of ESF values is from 0.925 to 1.025 for cations and from 0.950 to 1.050 for anions. The dependence of AE and MAE on ESF is plotted in Figure 4a,b for pK_{a1} and pK_{a2}, respectively. It is clear that 1.00 is the optimal ESF for both the pK_{a1} and pK_{a2} values and that for these systems, the extra computational cost associated with determining an optimal ESF value can be avoided if accurate gas-phase free energies are combined with solvation energies calculated using the recommended levels of theory for solvation free energies.
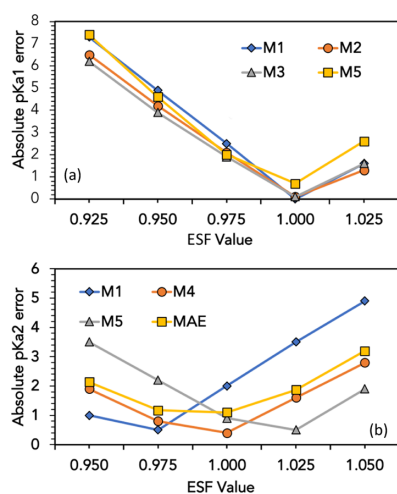
Figure 4. Dependence of AE and MAE of (a) pK_{a1} and (b) pK_{a2} values of methyl-substituted nucleic acid bases produced in this work on ESF value change.

The results for C1−C17 and A1−A10 are considered together as the two test sets are from the same literature and used the same solute cavity scaling method.[48] Figure 5 shows the MAE of
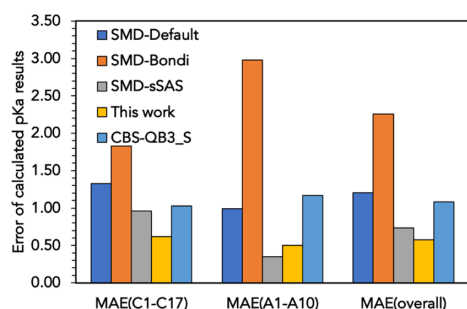

Figure 5. MAE of C1−C17 and A1−A10 pK_a results calculated via our method (no solute cavity scaling) and four solute cavity scaling methods (see the text for details).

pK_a values for the three methods investigated by Smith et al.[48] (SMD-sSAS, SMD-default, SMD-Bondi), the CBS-QB3_S method of Schlegel et al.,[47] and our unscaled SMD method for pK_a calculations using protocol 1 involving amines (i.e., the bases) and protocol 3 (explicit solvent) involving carboxylic acids (i.e., the acids). The MAE for each method is collected in Figure 5, and individual data can be found in the Supporting Information (Table S18). The average errors produced with our unscaled SMD protocol are smaller than those computed with other four methods for carboxylic acids, comparable to the best method for amines, and smallest overall. Overall, these results suggest that again solute cavity scaling is not required for SMD calculations on CHNO compounds if appropriate levels of theory are used and explicit solvent molecules are included when physically required.

To investigate whether the errors in our method can be further decreased through tuning the ESF values, we considered ESF values of 0.96−1.01 for C1−C17 and 0.99−1.02 for A1−A10 (Figure 6). For more consistent comparison with the work
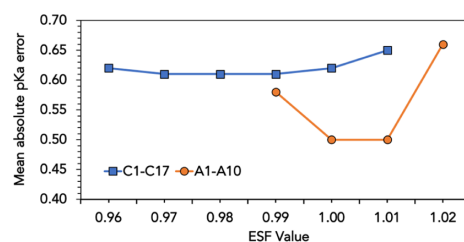
Figure 6. Dependence of MAE of pK_a values of C1−C17 and A1−A10 on the change of ESF value.

of Smith and co-workers,[48] here ESF optimization is conducted on all species including neutrals, although we scale only the vdW surface. For the pK_a values of the amines of A1−A10, the MAE reaches its minimum (0.50) at the ESF values of 1.00−1.01, and hence, scaling does not improve results. For carboxylic acids, C1−C17, the minimum of the MAE (0.61) is located at ESF = 0.97−0.99. However, the decrease in MAE (from 0.62 pK_a units with ESF = 1.0 to 0.61 pK_a units) via ESF optimization is minimal and is much smaller than that in the work of Smith and co-workers (MAE from 1.33 or even 1.83 to 0.96). In other words, for these CHNO compounds, if the recommended theoretical level and default vdW surface are used, along with explicit solvent molecules when required, the errors are small to begin with and ESF optimization has only minimal effects.

Performance on an Independent Test Set: Carbon Acids, Alcohols, and Anilines. From Figures 3 and 5, we can, respectively, see that the accuracy of our results and those obtained with ESF optimization by Smith[48] and Schlegel[47] are actually very close, despite the fact that we do not tune solute cavity by fitting to the experimental data we are predicting. Although neither Schlegel nor Smith claimed that their solute cavity scaling methods can be applied to other systems, an ESF value is only useful if it can make some independent predictions. To fully explore whether these scaled solute cavities are useful beyond the systems to which they were optimized and to further test the unscaled SMD protocols of this work, we considered an additional independent test set of neutral and cationic carbon acids (taken from ref 28), alcohols (taken from ref 30), and anilines (taken from ref 23) (respectively, N1−N13, H1−H10, AL1−AL5, and AN1−AN5 of Scheme 1). These test sets were not used in either ESF optimization training sets of Smith[48] or Schlegel.[47]

The pK_a values for the neutral carbon acids and alcohols are studied with protocol 3 (as anions are involved), while protocol 1 is used for the cationic carbon acids and anilines (which are bases). For comparison, we used the SMD-sSAS direct method of Smith and co-workers[48] and the CBS-QB3_S protocol employed by Schlegel and co-workers.[47] Note that for molecule N6 and N6-base (see Scheme 1), we use the gas-phase free energies from ref 28 in place of CBS-QB3 because of computational cost; however, this does not influence the conclusions below. Figure 7 shows the MAEs obtained via the three methods for carbon acids, split between the neutral and cationic species, anilines, and alcohols; full data are given in the Supporting Information (Tables S12−S17 and S27−S30).

For the neutral carbon acids, N1−N13, the errors in our method are significantly smaller than those produced by the SMD-sSAS method[48] and CBS-QB3_S method.[47] This further reinforces the need for an explicit solvent molecule when anions are involved and shows that this need cannot be fully addressed
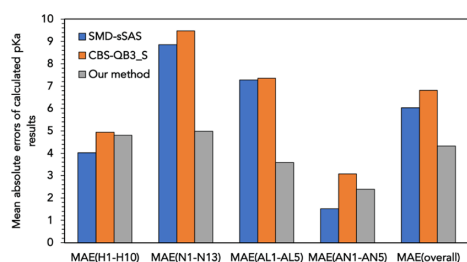
Figure 7. MAE of pK_a calculations of 10 cationic (H1−10) and 13 neutral (N1−13) carbon acids, 5 alcohols (AL1−5), and 5 anilines (AN1−5), as obtained with our recommended unscaled SMD protocol and the SMD-sSAS and CBS-QB3_S methods.

by solute cavity scaling. For the cationic carbon acids, the results by all three methods are very similar, and the SMD-sSAS method slightly outperforms the other two. Our method also produces the best results among all the three methods for alcohols. For anilines, the MAE of the SMD-sSAS method is the smallest, while the CBS-QB3_S method performs worst. This latter result is surprising, as anilines have similar structures to methyl nucleobases, which is the test set used to fit the ESF values for the CBS-QB3_S method. This indicates that even for very similar molecules within CHNO compounds, a solute cavity scaled for a specific solute type cannot necessarily be directly used to another one, which limits the application of solute cavity scaling methods. Our method shows intermediate behavior. Overall, our unscaled SMD method significantly outperforms the other two protocols by 1.7 and 2.5 pK_a unit, significantly outperforms them in two categories, and deviates in an average error by less than a pK_a unit from the best performer in the other two categories.

Across these new test sets and the original ones, the unscaled SMD was found to provide either equivalent or significantly better performance than the scaled procedures. Nonetheless for some test sets, particularly the carbon acids, the errors remain very large, even with the best-performing protocols. This was also noted in the original study of these systems, where it was suggested that using a proton exchange approach, and potentially other solvent models, could help to ameliorate these problems.[28] To test whether solute cavity scaling could also be effective, we recalculated the results using a range of ESF values. Figure 8a shows the results for carbon acids, and Figure 8b shows the results for alcohols and anilines. In Figure 8a, we only show MAE values at several key ESF values; more details can be found in the Supporting Information (Tables S31−S34).

It is seen that for anilines, the optimal ESF values are 0.97− 0.98, which produce a minimum MAE of 1.84 pK_a unit, compared with the default value (MAE = 2.39 pK_a unit). This 23% decrease is less than a pK_a unit. For alcohols, the difference resulted from ESF optimization is smaller, and optimal ESF (0.96) results in a 3.44 pK_a unit MAE, which is smaller than MAE (3.58 pK_a unit) with the default ESF by a 0.14 pK_a unit (only around 4% decrease). ESF optimization can decrease the MAE of H1−H10 from 4.80 (ESF = 1) to 3.94 (ESF = 1.17). This 18% decrease is still less than 1 pK_a unit, despite the results benefitting from fitting to data. The only MAE change exceeding 1 pK_a unit resulted from ESF optimization in this work is for N1−N13; its minimum MAE is 3.89, with an ESF of 1.12, compared with the MAE of 4.98 at the default ESF value. Even here, the change is 1.09 pK_a unit or around 22%. Thus, while
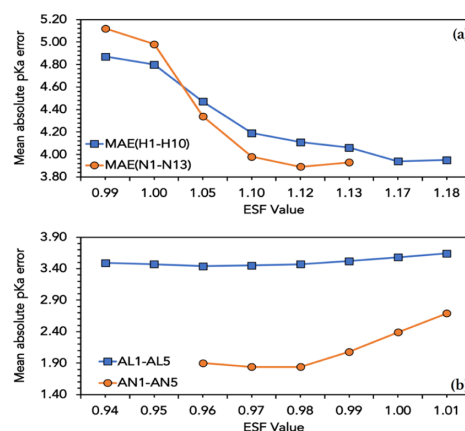
Figure 8. Dependence of the MAE of the pK_a values upon the ESF value for the (a) neutral and cationic carbon acids and (b) alcohols and anilines.

fitting to the data one is trying to predict can sometimes help to reduce the errors, the optimal ESF values obtained vary with the chemical system and for the results herein affect pK_a errors by less than or close to a single pK_a unit.

■ CONCLUSIONS

Implicit solvent models are important tools for using quantum chemistry to study solution-phase chemical reactions. Widely used approaches to improve the results of solvation free energies and solution-phase properties such as pK_a values include choosing the best theoretical level for the various components of the calculation using explicit solvent molecules and solute cavity scaling. In this work, we compared the above three methods for SMD solvation on a broad test set of aqueous pK_a values for methyl-substituted nucleic acid bases, carboxylic acids, aliphatic and aromatic amines, carbon acids, alcohols, and anilines.

We show that the unscaled SMD can give better or comparable performance to solute cavity scaling procedures provided one uses a thermocycle method with high levels of theory for the gas-phase component, the default surface type and parameters, the recommended[46] levels of theory for the solvation energy, and an explicit solvent molecule when physically necessary (e.g., for reactions involving anions). While in some cases ESF optimization on the basis of our method could in principle further reduce the errors for the data to which the ESF value is fitted, we show that the improvement in results is less than or close to a single pK_a unit and any ESF value obtained is not universal and would need to be reconsidered on a case-by-case basis. This limits their application to systems where experimental results are already available.

In drawing this conclusion, we stress that it is limited to the SMD model, which was parameterized for 2821 solvation energies of a wide range of neutral, anionic, and cationic species across a range of different solvents. It is also limited to compounds containing C, H, N, and O, as other compounds with other heteroatoms (e.g., S, F, Cl, and Br) have been shown to perform relatively poorly with SMD and may need modifications to their parameters or extra benchmarking. Nonetheless, within these limits, we suggest that using

The Journal of Physical Chemistry A   Article

appropriate theoretical levels together with the intuitive use of explicit solvent effects is a more universal approach to accurate solvation compared with relying on tuning the solute cavity to eliminate all errors, particularly as experimental values of investigated solute−solvent combinations are not always available. This conclusion is echoed by Cramer, Truhlar, and co-workers who have suggested that adding a small number of explicit water molecules to a continuum solvation calculation is much more straightforward than making large adjustments to the boundary between the solute and the continuum solvent (i.e., making large adjustments in the values used for the empirical atomic radii).[26]

■ ASSOCIATED CONTENT

ⓢ Supporting Information

The Supporting Information is available free of charge on the ACS Publications website at DOI: 10.1021/acs.jpca.9b04920.

> Raw data of gas-phase free energies, solvation free energies, calculated pK_a results, AEs, MAE, and MAX and Gaussian archive entries (PDF)

■ AUTHOR INFORMATION

Corresponding Author

*E-mail: michelle.coote@anu.edu.au. Phone: 61 2 6125 3771.

ORCID ⊙

Michelle L. Coote: 0000-0003-0828-7053

Author Contributions

The manuscript was written through contributions of all authors. All authors have given approval to the final version of the manuscript.

Notes

The authors declare no competing financial interest.

■ ACKNOWLEDGMENTS

■ REFERENCES

(1) Tomasi, J.; Mennucci, B.; Cammi, R. Quantum Mechanical Continuum Solvation Models. *Chem. Rev.* **2005**, *105*, 2999−3094.

(2) Guerard, J. J.; Arey, J. S. Critical Evaluation of Implicit Solvent Models for Predicting Aqueous Oxidation Potentials of Neutral Organic Compounds. *J. Chem. Theory Comput.* **2013**, *9*, 5046−5058.

(3) Haworth, N. L.; Wang, Q.; Coote, M. L. Modeling Flexible Molecules in Solution: A pK_a Case Study. *J. Phys. Chem. A* **2017**, *121*, 5217−5225.

(4) Ho, J.; Ertem, M. Z. Calculating Free Energy Changes in Continuum Solvation Models. *J. Phys. Chem. B* **2016**, *120*, 1319−1329.

(5) Klamt, A. The COSMO and COSMO-RS Solvation Models. *Wiley Interdiscip. Rev.: Comput. Mol. Sci.* **2011**, *1*, 699−709.

(6) Dhillon, S.; East, A. L. L. Challenges in Predicting ΔrxnG in Solution: Hydronium, Hydroxide, and Water Autoionization. *Int. J. Quantum Chem.* **2018**, *118*, No. e25703.

(7) Wen, M.; Jiang, J.; Wang, Z.-X.; Wu, C. How Accurate Are the Popular PCM/GB Continuum Solvation Models for Calculating the Solvation Energies of Amino Acid Side-Chain Analogs? *Theor. Chem. Acc.* **2014**, *133*, 1471.

(8) Sviatenko, L.; Isayev, O.; Gorb, L.; Hill, F.; Leszczynski, J. Toward Robust Computational Electrochemical Predicting the Environmental Fate of Organic Pollutants. *J. Comput. Chem.* **2011**, *32*, 2195−2203.

(9) Ho, J.; Klamt, A.; Coote, M. L. Comment on the Correct Use of Continuum Solvent Models. *J. Phys. Chem. A* **2010**, *114*, 13442−13444.

(10) Shen, K.; Fu, Y.; Li, J.-N.; Liu, L.; Guo, Q.-X. What Are the pK_a Values of C−H Bonds in Aromatic Heterocyclic Compounds in DMSO? *Tetrahedron* **2007**, *63*, 1568−1576.

(11) Barone, V.; Carnimeo, I.; Scalmani, G. Computational Spectroscopy of Large Systems in Solution: The DFTB/PCM and TD-DFTB/PCM Approach. *J. Chem. Theory Comput.* **2013**, *9*, 2052−2071.

(12) Long, M. R. P.; Isborn, C. M. Combining Explicit Quantum Solvent with a Polarizable Continuum Model. *J. Phys. Chem. B* **2017**, *121*, 10105−10117.

(13) Preat, J.; Loos, P.-F.; Assfeld, X.; Jacquemin, D.; Perpète, E. A. DFT and TD-DFT Investigation of IR and UV Spectra of Solvated Molecules: Comparison of Two SCRF Continuum Models. *Int. J. Quantum Chem.* **2007**, *107*, 574−585.

(14) Lee, T. B.; McKee, M. L. Dependence of pK_a on Solute Cavity for Diprotic and Triprotic Acids. *Phys. Chem. Chem. Phys.* **2011**, *13*, 10258−10269.

(15) Khalili, F.; Henni, A.; East, A. L. L. Entropy Contributions in pK_a Computation: Application to Alkanolamines and Piperazines. *J. Mol. Struct.: THEOCHEM* **2009**, *916*, 1−9.

(16) Close, D. M.; Wardman, P. Calculations of the Energetics of Oxidation of Aqueous Nucleosides and the Effects of Prototropic Equilibria. *J. Phys. Chem. A* **2016**, *120*, 4043−4048.

(17) Close, D. M.; Wardman, P. Calculation of Standard Reduction Potentials of Amino Acid Radicals and the Effects of Water and Incorporation into Peptides. *J. Phys. Chem. A* **2018**, *122*, 439−445.

(18) Cammi, R.; Verdolino, V.; Mennucci, B.; Tomasi, J. Towards the Elaboration of a QM Method to Describe Molecular Solutes under the Effect of a Very High Pressure. *Chem. Phys.* **2008**, *344*, 135−141.

(19) Amovilli, C.; Floris, F. M. Solubility of Water in Liquid Hydrocarbons: A Bridge between the Polarizable Continuum Model and the Mobile Order Theory. *Phys. Chem. Chem. Phys.* **2002**, *5*, 363−368.

(20) Brinck, T.; Larsen, A. G.; Madsen, K. M.; Daasbjerg, K. Solvation of Carbanions in Organic Solvents: A Test of the Polarizable Continuum Model. *J. Phys. Chem. B* **2000**, *104*, 9887−9893.

(21) Hebert, S. P.; Schlegel, H. B. Computational Study of the pH-Dependent Competition between Carbonate and Thymine Addition to the Guanine Radical. *Chem. Res. Toxicol.* **2019**, *32*, 195−210.

(22) Sutton, C. C. R.; Franks, G. V.; da Silva, G. First Principles pK_a Calculations on Carboxylic Acids Using the Smd Solvation Model: Effect of Thermodynamic Cycle, Model Chemistry, and Explicit Solvent Molecules. *J. Phys. Chem. B* **2012**, *116*, 11999−12006.

(23) Zhang, S. A Reliable and Efficient First Principles-Based Method for Predicting pK_a Values. Iii. Adding Explicit Water Molecules: Can the Theoretical Slope Be Reproduced and pK_a Values Predicted More Accurately? *J. Comput. Chem.* **2012**, *33*, 517−526.

(24) Thapa, B.; Schlegel, H. B. Calculations of pK_a's and Redox Potentials of Nucleobases with Explicit Waters and Polarizable Continuum Solvation. *J. Phys. Chem. A* **2015**, *119*, 5134−5144.

(25) Thapa, B.; Schlegel, H. B. Density Functional Theory Calculation of pK_a's of Thiols in Aqueous Solution Using Explicit Water Molecules and the Polarizable Continuum Model. *J. Phys. Chem. A* **2016**, *120*, 5726−5735.

(26) Kelly, C. P.; Cramer, C. J.; Truhlar, D. G. Adding Explicit Solvent Molecules to Continuum Solvent Calculations for the Calculation of Aqueous Acid Dissociation Constants. *J. Phys. Chem. A* **2006**, *110*, 2493−2499.

(27) Marenich, A. V.; Ding, W.; Cramer, C. J.; Truhlar, D. G. Resolution of a Challenge for Solvation Modeling: Calculation of

Dicarboxylic Acid Dissociation Constants Using Mixed Discrete−Continuum Solvation Models. *J. Phys. Chem. Lett.* **2012**, *3*, 1437−1442.

(28) Ho, J.; Coote, M. L. pK_a Calculation of Some Biologically Important Carbon Acids - an Assessment of Contemporary Theoretical Procedures. *J. Chem. Theory Comput.* **2009**, *5*, 295−306.

(29) Ghosh, D.; Roy, A.; Seidel, R.; Winter, B.; Bradforth, S.; Krylov, A. I. First-Principle Protocol for Calculating Ionization Energies and Redox Potentials of Solvated Molecules and Ions: Theory and Application to Aqueous Phenol and Phenolate. *J. Phys. Chem. B* **2012**, *116*, 7269−7280.

(30) Ho, J.; Coote, M. L. A Universal Approach for Continuum Solvent pKa Calculations: Are We There Yet? *Theor. Chem. Acc.* **2010**, *125*, 3−21.

(31) Luque, F. J.; Negre, M. J.; Orozco, M. An AM1-SCRF Approach to the Study of Changes in Molecular Properties Induced by Solvent. *J. Phys. Chem.* **1993**, *97*, 4386−4391.

(32) Orozco, M.; Luque, F. J. Optimization of the Cavity Size for ab Initio MST-SCRF Calculations of Monovalent Ions. *Chem. Phys.* **1994**, *182*, 237−248.

(33) Luque, F. J.; Zhang, Y.; Alemán, C.; Bachs, M.; Gao, J.; Orozco, M. Solvent Effects in Chloroform Solution: Parametrization of the MST/SCRF Continuum Model. *J. Phys. Chem.* **1996**, *100*, 4269−4276.

(34) Luque, F. J.; Bachs, M.; Alemn, C.; Orozco, M. Extension of MST/SCRF Method to Organic Solvents: Ab Initio and Semiempirical Parametrization for Neutral Solutes in CCl4. *J. Comput. Chem.* **1996**, *17*, 806−820.

(35) Curutchet, C.; Orozco, M.; Luque, F. J. Solvation in Octanol: Parametrization of the Continuum MST Model. *J. Comput. Chem.* **2001**, *22*, 1180−1193.

(36) Curutchet, C.; Bidon-Chanal, A.; Soteras, I.; Orozco, M.; Luque, F. J. MST Continuum Study of the Hydration Free Energies of Monovalent Ionic Species. *J. Phys. Chem. B* **2005**, *109*, 3565−3574.

(37) Soteras, I.; Forti, F.; Orozco, M.; Luque, F. J. Performance of the IEF-MST Solvation Continuum Model in a Blind Test Prediction of Hydration Free Energies. *J. Phys. Chem. B* **2009**, *113*, 9330−9334.

(38) Pliego, J. R.; Riveros, J. M. Parametrization of the PCM Model for Calculating Solvation Free Energy of Anions in Dimethyl Sulfoxide Solutions. *Chem. Phys. Lett.* **2002**, *355*, 543−546.

(39) Fu, Y.; Liu, L.; Li, R.-Q.; Liu, R.; Guo, Q.-X. First-Principle Predictions of Absolute pK_a's of Organic Acids in Dimethyl Sulfoxide Solution. *J. Am. Chem. Soc.* **2004**, *126*, 814−822.

(40) Fu, Y.; Liu, L.; Yu, H.-Z.; Wang, Y.-M.; Guo, Q.-X. Quantum-Chemical Predictions of Absolute Standard Redox Potentials of Diverse Organic Molecules and Free Radicals in Acetonitrile. *J. Am. Chem. Soc.* **2005**, *127*, 7227−7234.

(41) Böes, E. S.; Livotto, P. R.; Stassen, H. Solvation of Monovalent Anions in Acetonitrile and N,N-Dimethylformamide: Parameterization of the IEF-PCM Model. *Chem. Phys.* **2006**, *331*, 142−158.

(42) Kim, H.; Park, J.; Lee, Y. S. A Protocol to Evaluate One Electron Redox Potential for Iron Complexes. *J. Comput. Chem.* **2013**, *34*, 2233−2241.

(43) Verdolino, V.; Cammi, R.; Munk, B. H.; Schlegel, H. B. Calculation of pK_a Values of Nucleobases and the Guanine Oxidation Products Guanidinohydantoin and Spiroiminodihydantoin Using Density Functional Theory and a Polarizable Continuum Model. *J. Phys. Chem. B* **2008**, *112*, 16860−16873.

(44) Psciuk, B. T.; Schlegel, H. B. Computational Prediction of One-Electron Reduction Potentials and Acid Dissociation Constants for Guanine Oxidation Intermediates and Products. *J. Phys. Chem. B* **2013**, *117*, 9518−9531.

(45) Gryn'ova, G.; Barakat, J. M.; Blinco, J. P.; Bottle, S. E.; Coote, M. L. Computational Design of Cyclic Nitroxides as Efficient Redox Mediators for Dye-Sensitized Solar Cells. *Chem.—Eur. J.* **2012**, *18*, 7582−7593.

(46) Marenich, A. V.; Cramer, C. J.; Truhlar, D. G. Universal Solvation Model Based on Solute Electron Density and on a Continuum Model of the Solvent Defined by the Bulk Dielectric Constant and Atomic Surface Tensions. *J. Phys. Chem. B* **2009**, *113*, 6378−6396.

(47) Psciuk, B. T.; Lord, R. L.; Munk, B. H.; Schlegel, H. B. Theoretical Determination of One-Electron Oxidation Potentials for Nucleic Acid Bases. *J. Chem. Theory Comput.* **2012**, *8*, 5107−5123.

(48) Lian, P.; Johnston, R. C.; Parks, J. M.; Smith, J. C. Quantum Chemical Calculation of pK_as of Environmentally Relevant Functional Groups: Carboxylic Acids, Amines, and Thiols in Aqueous Solution. *J. Phys. Chem. A* **2018**, *122*, 4366−4374.

(49) Frisch, M. J.; Trucks, G. W.; Schlegel, H. B.; Scuseria, G. E.; Robb, M. A.; Cheeseman, J. R.; Scalmani, G.; Barone, V.; Petersson, G. A.; Nakatsuji, H.; et al. *Gaussian 16*, Revision A.03; Gaussian, Inc.: Wallingford, CT, 2016.

(50) Werner, H. J.; Knowles, P. J.; Knizia, G.; Manby, F. R.; Schütz, M.; Celani, P.; Györffy, W.; Kats, D.; Korona, T.; Lindh, R.; et al. *MOLPRO*, version 2015.1: Stuttgart, 2015.

(51) Montgomery, J. A.; Frisch, M. J.; Ochterski, J. W.; Petersson, G. A. A Complete Basis Set Model Chemistry. VI Use of Density Functional Geometries and Frequencies. *J. Chem. Phys.* **1999**, *110*, 2822−2827.

(52) Merrick, J. P.; Moran, D.; Radom, L. An Evaluation of Harmonic Vibrational Frequency Scale Factors. *J. Phys. Chem. A* **2007**, *111*, 11683−11700.
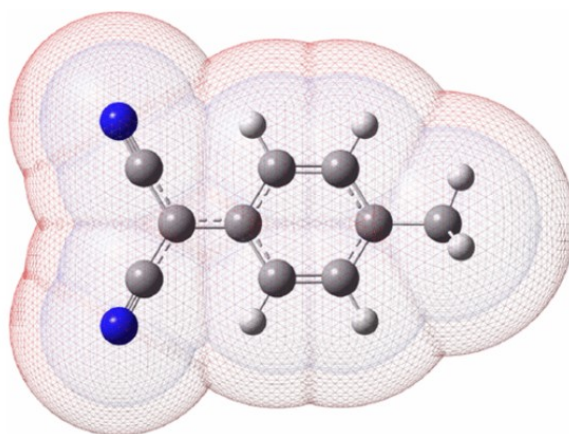
(53) Adam, K. R. New Density Functional and Atoms in Molecules Method of Computing Relative pK_a Values in Solution. *J. Phys. Chem. A* **2002**, *106*, 11963−11972.

3.3   Publication 3

Improving the Accuracy of PCM-UAHF and PCM-UAKS Calculations Using Optimized Electrostatic Scaling Factors

Longkun Xu, Michelle L. Coote

This publication is a peer-reviewed manuscript published in *Journal of Chemical Theory and Computation*. All computational results and subsequent discussion were my own work under the supervision of Prof. Michelle Coote, who edited the manuscript. Supporting information is available online (https://pubs.acs.org/doi/10.1021/acs.jctc.9b00888). The document for the statement of contributions is placed in the Appendix.

Improving the Accuracy of PCM-UAHF and PCM-UAKS Calculations Using Optimized Electrostatic Scaling Factors

Longkun Xu and Michelle L. Coote*

ARC Centre of Excellence for Electromaterials Science, Research School of Chemistry, Australian National University, Canberra, Australian Capital Territory 2601, Australia

Ⓢ *Supporting Information*

ABSTRACT: The optimal electrostatic scaling factor (ESF) for the calculation of solvation Gibbs free energies with the polarizable continuum model (PCM) was determined via extensive benchmarking against 1719 experimental solvation Gibbs free energies and transfer free energies taken from the MNSol-v2012 database, as well as 45 aqueous pK_a values covering nine solute types (amines, thiols, carbon acid cations, pyridines, alcohols, anilines, carboxylic acids, carbon acid neutrals, phenols) and 20 pK_a values in acetonitrile covering four solute types (phenols, carbon acids, carboxylic acids, pyridines). Optimal values for the ESF in a range of solvents are reported. For example, in water, the optimal ESF value is 1.2 and this does not vary with solute charge, radius type, or method. For acetonitrile, we recommend 1.1 for neutrals, 1.0 and 1.1 respectively for cations with UAHF and UAKS radii types, 1.3 for anions for IEFPCM-UAHF, and 1.4 for other anions. At the same time, we show that ESF optimization does not address all errors in PCM, and is thus not a substitute for the appropriate use of explicit solvent molecules, nor for the use of isodesmic methods to enhance systematic error cancellation. For a representative subset of the data we show that the errors in PCM are somewhat larger than in SMD and somewhat smaller than in COSMO-RS, although the latter has not benefited from cavity scaling.
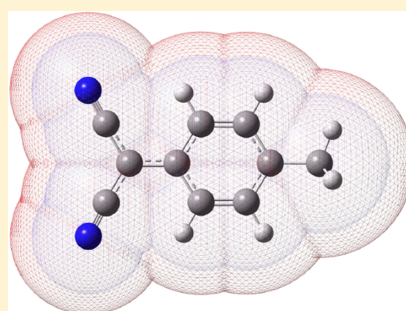
INTRODUCTION

The development of implicit solvent models has made it possible to model chemical reactions and properties in solution phase using quantum chemical methods with reasonable accuracy. Among the various available continuum solvation models, the two most widely used are the universal solvation model based on solute electron density (SMD)[1] and the polarizable continuum model (PCM).[2] While SMD can generally achieve excellent accuracy in modeling common organic molecules, PCM also remains important. One reason is that PCM is more suitable for "self-defined" solvation calculations as it needs fewer parameters than SMD. More generally, PCM remains a popular choice as is evident in the wide range of recent studies in which it has been employed, including modeling of NMR chemical shifts,[3] excited state properties of solvated molecules,[4] redox potentials,[5] relative reactivities,[6] catalysis mechanisms,[7] lipophilicity properties,[8] infrared and Raman spectra,[9] nonequilibrium solvation,[10] quantum chemical calculations on graphical processing units (GPUs),[11] and combining solvation modeling with various theoretical methods and programs.[12−14]

Many variables can be altered to improve the accuracy of PCM calculations, for example, the theoretical level, surface type, radius type, and electrostatic scaling factor (ESF). The latter three determine how to construct the solute cavity immersed in continuum medium. The most widely used surface type is van der Waals surface (VDW). The most widely used radius types include UFF, UAHF, and UAKS radii. ESF values determine how much the atomic radii are scaled to produce most accurate solvation Gibbs free energies. The importance of theoretical level choice has been pointed out in many works.[15,16] Given the semiempirical nature of solvation models, the optimal theoretical level is usually that at which the model and radii were originally parametrized. For instance, for the PCM solvation Gibbs free energy calculations with UAHF and UAKS radii types, the parametrization levels are HF/6-31G(d) and PBE1PBE/6-31G(d), respectively. If these method/radii combinations are swapped (i.e., UAHF with PBE1PBE and UAKS with HF), the accuracy deteriorates.

While it is relatively difficult to design and implement a new surface type or a new set of atomic radii, the ESF is the easiest parameter to change at will in quantum chemical programs. That is why ESF optimization has been widely employed to improve solvation calculations in recent years.[21,23−31] However, the optimal ESF values reported often differ significantly, and inevitably are affected by many factors including solvation models, theoretical level, atomic radius type, surface type, solute type, and solvent type (see Table 1).

To address this problem, here we define a standard set of protocols for calculating the solvation energy and use a broad test set of experimental solvation and transfer energies from

Table 1. Some Examples of ESF Optimization with PCM

ref	solute type and property	solvent(s)[a]	theoretical level	radius type	ESF[b]
17	ΔG_{solv} of anions	DMSO	IEF-PCM/HF/6-31+G(d,p)	GAMESS[c]	not reported (1.35)
18	ΔG_{solv} of neutral and anionic compounds	DMSO	PCM/HF/6-31+G(d,p)	Bondi	1.20–1.45 (1.35)
19	pK_a of organic acids	MeCN	PCM/B3LYP/6-31+G(d,p)	Bondi	1.10–1.35 (1.20)
20	ΔG_{solv} of organic univalent anions	MeCN and DMF	IEF-PCM/HF/6-31+G(d,p)	GAMESS	1.0–2.0 (1.36 in MeCN, 1.39 DMF)
21	redox potentials of nitroxides	MeCN	PCM/B3-LYP/6-31G(d)	UAKS	1.1–1.5 (1.45)
22	ΔG_{solv} of amino acid side-chain analogues	H_2O	IEFPCM/6 theoretical levels[d]	UAKS	1.1 and 1.2 (1.2)

[a]DMSO = dimethyl sulfoxide; MeCN = acetonitrile; DMF = dimethyl formamide. [b]Studied ESF range and the optimal one (in parentheses). [c]Radius type implemented in GAMESS software package. [d]See Figure 1 in ref 22.

the latest Minnesota Solvation Database, MNSol-v2012,[32] to determine optimal ESF values as a function of radius type (UAHF and UAKS), solvent, and/or solute charge. By focusing on solvation and transfer energies, rather than properties such as pK_a values or redox potentials, the resulting ESF corrects only for solvation energy errors and is disconnected from any error in reaction energies, allowing one the freedom to change this (as part of a thermocycle) when needed, without changing the ESF. Our recommended ESF values are then tested for the prediction of pK_a values of a test set of amines, thiols, carbon acid cations, pyridines, alcohols, anilines, carboxylic acids, carbon acid neutrals, and phenols in water (Scheme 1), and phenols, carbon acids, carboxylic acids, and pyridines in acetonitrile (Scheme 2). For a subset of the solvation energies, the relative accuracies of PCM, SMD, and COSMO-RS are also studied.

■ **COMPUTATIONAL DETAILS**

The MNSol-v2012[32] database contains 3037 experimental free energies of solvation or transfer free energies for 790 solutes in 92 solvents. However, in the present work we consider a subset of 1719 experimental free energies of solvation or transfer free energies because we have to remove the following:

1. Remove all solutes containing iodine because the 6-31G(d) basis set needs to be used consistently throughout this work so as to use the parametrization level.

2. Remove solvents in which the nonelectrostatics solvation components (cavitation, dispersion, and repulsion) are not supported in Gaussian 16.[43] This leaves the following 18 solvents for the solvation Gibbs free energy calculations of neutrals: acetonitrile, aniline, benzene, carbon tetrachloride, chlorobenzene, chloroform, cyclohexane, dichloroethane, diethyl ether, dimethyl sulfoxide, ethanol, heptane, methylene chloride, nitromethane, octanol, tetrahydrofuran, toluene, and water. For the benchmarking of transfer free energies, the following nine nonaqueous solvents are used: benzene, carbon tetrachloride, chlorobenzene, chloroform, cyclohexane, dichloroethane, diethyl ether, heptane, and octanol. For the benchmarking of solvation Gibbs free energies of ions, the following three solvents are used: acetonitrile, dimethyl sulfoxide, and water.

For each experimental free energy of solvation or transfer, two solvation models (IEF-PCM and C-PCM) combining two radius types (UAHF and UAKS) at their optimal theoretical level, i.e., HF/6-31G(d) for UAHF and PBE1PBE/6-31G(d) for UAKS, multiple ESF values are used for each solvation Gibbs free energy or transfer free energy so as to identify the optimal value. All solvation Gibbs free energies are calculated with gas-phase optimized geometries at the M062X/MG3S[44] theoretical level provided in the MNSol-v2012 database. All
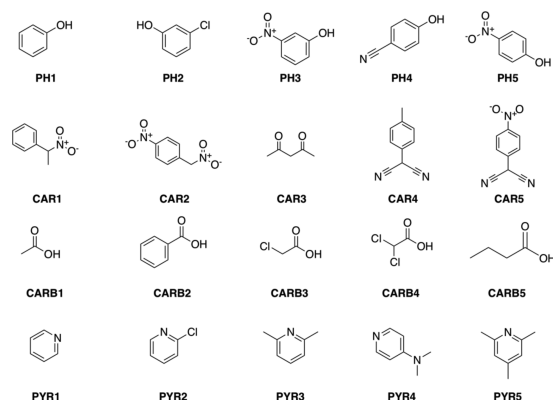
Scheme 1. Test Set Used in This Work for pK_a Calculations in Aqueous Solution[a]
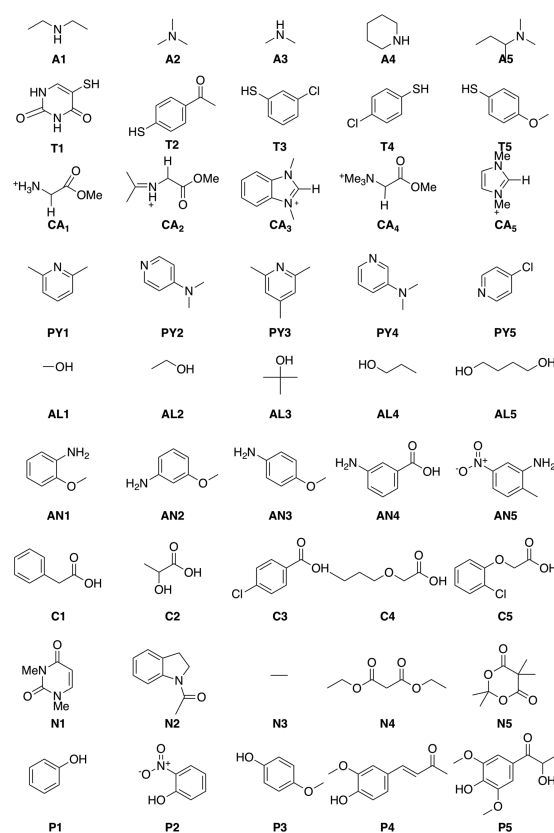
[a]Test set includes five amines (A1–A5), five thiols (T1–T5), five carbon acid cations (CA1–CA5), five pyridines (PY1–PY5), five alcohols (AL1–AL5), five anilines (AN1–AN5), five carboxylic acids (C1–C5), five carbon acid neutrals (N1–N5), and five phenols (P1–P5). For the bases (A1–A5, CA1–CA5, PY1–PY5) the pK_a of the conjugate acid was calculated. A1–A5 were taken from refs 16 and 33, T1–T5 were taken from refs 16 and 34, CA1–CA5 were taken from ref 16, PY1–PY5 were taken from refs 35 and 36, AL1–AL5 were taken from refs 16 and 37, AN1–AN5 were taken from refs 16 and 38, C1–C5 were taken from refs 16 and 39, N1–N5 were taken from refs 16 and 40, and P1–P5 were taken from refs 16 and 41.
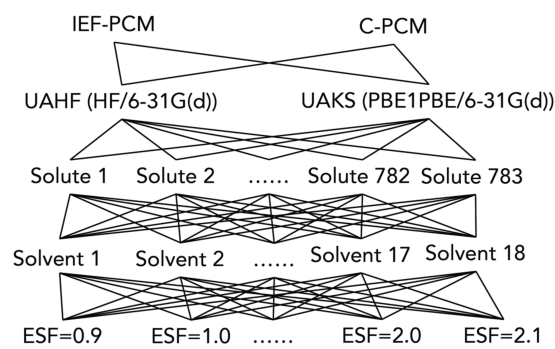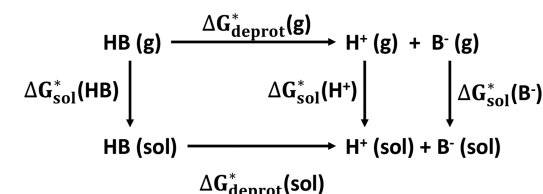
combinations used for benchmarking are included in Scheme 3.

The thermocycle method (Scheme 4) was used for pK_a calculations in this work. It should be noted that, according to

Scheme 2. Test Set Used for pK_a Calculations in Acetonitrile[a]

PH1 PH2 PH3 PH4 PH5

CAR1 CAR2 CAR3 CAR4 CAR5

CARB1 CARB2 CARB3 CARB4 CARB5

PYR1 PYR2 PYR3 PYR4 PYR5

[a]Twenty molecules include five phenols (PH1−PH5) taken from ref 19, five carbon acids (CAR1−CAR5) taken from refs 19 and 42, five carboxylic acids (CARB1−CARB5) taken from ref 19, and five pyridines (PYR1−PYR5) taken from ref 35. For the bases (PYR1−PYR5), the pK_a of the conjugate acid was calculated.

Scheme 3. All Combinations Used for Benchmarking in This Work

IEF-PCM   C-PCM

UAHF (HF/6-31G(d))   UAKS (PBE1PBE/6-31G(d))

Solute 1   Solute 2   ......   Solute 782   Solute 783

Solvent 1   Solvent 2   ......   Solvent 17   Solvent 18

ESF=0.9   ESF=1.0   ......   ESF=2.0   ESF=2.1

Scheme 4. Thermodynamic Cycle Method for pK_a Calculations in Solution Phase

$$HB\ (g) \xrightarrow{\Delta G_{deprot}^*(g)} H^+\ (g)\ +\ B^-\ (g)$$

with vertical arrows $\Delta G_{sol}^*(HB)$, $\Delta G_{sol}^*(H^+)$, $\Delta G_{sol}^*(B^-)$

$$HB\ (sol) \xrightarrow{\Delta G_{deprot}^*(sol)} H^+\ (sol)\ +\ B^-\ (sol)$$

convention, pK_a values of the bases studied here are expressed as the deprotonation of their conjugate acids. Using the thermocycle method, the total Gibbs free energy of a species in solution is given as[15]

$$G^*(sol) = G^\circ(g) + \Delta G_{solv}^* + \Delta G^{1\,atm \to 1\,M} \qquad (1)$$

where $G^\circ(g)$ is the standard gas-phase Gibbs free energy, ΔG_{solv}^* is the solvation Gibbs free energy, and $\Delta G^{1\,atm \to 1\,M}$ (which equals 1.89 kcal/mol) is the Gibbs free energy change

resulting from the different standard states in gas and solution phases. The pK_a value can then be computed as

$$pK_a = \frac{\Delta G_{deprot}^*(sol)}{2.303 RT} \qquad (2)$$

where $\Delta G_{deprot}^*(sol)$ is the standard state free energy change of the deprotonation reaction in solution phase, R is the universal gas constant, and T is the temperature in Kelvin. The aqueous solvation Gibbs free energy of proton $\Delta G_{sol}^*(H^+)$ is taken as −265.9 kcal/mol.[45,46]

All gas-phase free energies in this work were conducted using the high-level G3 (MP2, CC) method so as to minimize errors from this component. All quantum chemical calculations were performed with Gaussian 16[43] except for CCSD(T) calculations, which were performed using Molpro 2015,[47] and solvation Gibbs free energy calculations with COSMO-RS,[48,49] which were performed with COSMOtherm.[50]

■ RESULTS AND DISCUSSION

ESF Benchmarking. Optimal ESF values for neutral species in the 18 solvents are provided in Table 2. Details of gas-phase and solution-phase electronic energies, absolute errors (AEs), and mean absolute errors (MAEs) of solvation Gibbs free energy calculations can be found in Tables S1−S6 and the Supporting Information spreadsheet. While 1.2 instead of 1.1 (the default value in Gaussian 16[43]) is the overall optimal ESF for IEFPCM and CPCM calculations with UAHF and UAKS radii types, the optimal ESF is indeed dependent on solvent type. This is not surprising, as, for example, the UAHF radii were designed using solvation data in water only,[51] and adjustments for nonaqueous solvents might reasonably be expected. At the same time, due to the limited data available for some specific nonaqueous solvents (for example, only seven molecules in acetonitrile are used here), some solvent-specific ESF values may need further adjustment as more data becomes available. One way to provide this extra data is through indirect sources, such as pK_a values, which we examine below (vide infra).

Comparing UAHF and UAKS radii types with other factors fixed, the optimal ESF values for UAHF and UAKS radii are the same in most solvents (Table 2). Moreover, we can see from Tables S1 and S2 that two different radius types produce very similar errors for solvation Gibbs free energy calculations. Although the exact details of how the UAKS radii were designed are not clear,[52] it is highly possible that, like the UAHF radii, UAKS radii were designed in water only. Comparing IEFPCM and CPCM, it is clear that these two solvation models produce very close MAEs and their optimal ESF is the same in most solvents.

Comparing different solvents, water is the solvent affected most by the ESF: for example, the MAE produced with ESF = 1.0 is 14.37 kcal/mol using the IEFPCM solvation model, which can be decreased massively to 1.39 kcal/mol with ESF = 1.2. As a contrast, heptane basically is not influenced by an ESF change. It is easy to understand that this is related to the polarity of solvent as ESF change mainly affects the electrostatics contribution to solvation Gibbs free energies; the dielectric constant of water is 78.36 while that of heptane is only 1.91. Therefore, ESF optimization plays a more important role in strong polar solvents.

Finally, optimal ESFs in Table 2 are located in the range from 1.0 to 1.4, which shows that ESF only needs to be slightly

Table 2. Optimal ESFs and Mean Absolute Errors (MAEs, in kcal/mol) of Neutral Species in 18 Solvents[a]

solvent	N	IEFPCM-UAHF		IEFPCM-UAKS		CPCM-UAHF		CPCM-UAKS	
		optimal ESF	optimal MAE	optimal ESF	optimal MAE	optimal ESF	optimal MAE	optimal ESF	optimal MAE
acetonitrile	7	1.2	2.62	1.2	2.83	1.2	2.59	1.2	2.76
aniline	10	1.1	3.20	1.1	2.85	1.1	3.55	1.1	3.05
benzene	75	1.1	2.41	1.0	2.34	1.1	1.99	1.1	2.00
carbon tetrachloride	78	1.0	2.45	1.0	2.40	1.1	2.23	1.1	2.23
chlorobenzene	38	1.1	1.99	1.1	1.82	1.2	1.91	1.2	2.00
chloroform	108	1.1	2.31	1.1	2.30	1.1	2.54	1.1	2.51
cyclohexane	91	1.1	1.44	1.1	1.40	1.2	1.50	1.2	1.51
dichloroethane	39	1.2	1.38	1.2	1.56	1.2	1.30	1.2	1.41
diethyl ether	70	1.1	2.06	1.1	1.99	1.2	2.11	1.2	2.17
dimethyl sulfoxide	7	1.3	2.35	1.2	2.16	1.3	2.33	1.2	2.18
ethanol	8	1.4	1.57	1.3	1.51	1.4	1.57	1.3	1.51
heptane	68	1.1	1.29	1.1	1.21	1.2	1.30	1.2	1.29
methylene chloride	11	1.2	2.02	1.2	1.95	1.2	2.11	1.2	1.88
nitromethane	7	1.3	1.86	1.3	1.94	1.3	1.85	1.3	1.91
octanol	241	1.1	3.33	1.1	3.53	1.1	3.20	1.1	3.36
tetrahydrofuran	7	1.2	1.98	1.2	1.81	1.3	2.04	1.2	1.81
toluene	51	1.1	1.55	1.1	1.57	1.1	1.64	1.1	1.50
water	381	1.2	1.39	1.2	1.36	1.2	1.38	1.2	1.35
all	1297	1.2	2.72	1.2	2.79	1.2	2.50	1.2	2.56

[a]N is the number of experimental solvation Gibbs free energies.

Table 3. Optimal ESFs and Optimal Mean Absolute Errors (MAEs, in kcal/mol) for Transfer Free Energies of Neutral Species in Nine Solvent/Water Combinations[a]

solvent	N	IEFPCM-UAHF		IEFPCM-UAKS		CPCM-UAHF		CPCM-UAKS	
		optimal ESF	optimal MAE	optimal ESF	optimal MAE	optimal ESF	optimal MAE	optimal ESF	optimal MAE
carbon tetrachloride	2	2.1	0.91	2.1	0.82	2.1	0.88	2.1	0.80
benzene	4	1.6	0.74	1.6	0.60	1.5	0.70	1.6	0.60
chlorobenzene	1	1.4	0.10	1.4	0.08	1.3	0.09	1.3	0.07
chloroform	7	1.5	0.81	1.5	0.81	1.4	0.80	1.4	0.80
cyclohexane	5	1.2	1.18	1.2	1.14	1.2	1.13	1.2	1.24
dichloroethane	3	1.2	0.50	1.1	0.43	1.1	0.47	1.1	0.51
diethyl ether	8	1.5	1.29	1.5	1.27	1.4	1.25	1.4	1.22
heptane	6	1.2	1.70	1.2	1.86	1.2	1.54	1.2	1.71
octanol	103	2.1	5.05	2.1	5.04	2.1	5.00	2.1	4.99
all	139	2.0−2.1	4.32	2.1	4.03	1.8−2.1	4.30	1.7−2.1	4.29

[a]N is the number of experimental data.

changed, although this slight change of ESF can sometimes produce massive change in solvation Gibbs free energies. This supports the observation in our prior study[16] of SMD solvation energies, that an overlarge change of ESF usually corrects errors from other sources, for example, inaccurate gas-phase free energies or (and) an unsuitable choice of theoretical level.

Table 3 shows the optimal ESF values for transfer Gibbs free energies, with full details in Tables S3 and S4. Optimal ESFs for transfer free energies are much more variable and at times much larger than those of solvation Gibbs free energies, especially for carbon tetrachloride−water and octanol−water. For these two cases, the MAE had still not reached its minimum with ESF = 2.1, although the decrease of MAE with 0.1 ESF increment after 1.7 is ca. 0.05 kcal/mol. While these are extreme cases, the larger and more variable ESF values result in part from low overall energies for transfer free energies (generally less than 1 kcal/mol) that in turn are due to the opportunity for systematic error cancellation between hydration free energies and solvation Gibbs free energies. Again, UAHF and UAKS radii produce very close results. For example, for all nine solvent−water combinations, MAEs for

UAHF and UAKS differ by less than 0.16 kcal/mol, further supporting our above assumption that, like UAHF, UAKS radii were designed in water only.

In the calculations of solution-phase properties, the quantities affecting the accuracy most are the solvation Gibbs free energies of ions. The lack of systematic error cancellation in reactions involving different ion types is well-known,[53] and this may be due in part to systematic differences in their optimal radii. To examine the effect of solute charge on the ESF value, in Table 4, we optimized the ESFs of neutrals, cations, and anions separately in acetonitrile, dimethyl sulfoxide, and water, respectively. In doing this we also distinguish between molecules containing CHNO atoms only, and all other types, as their errors differ significantly in the original SMD paper.[1]

Examining Table 4, it is clear that in water the optimal ESF value is consistently 1.2 for neutrals, cations, and anions, which makes sense if the parameters were optimized across all solute types in this solvent. In the nonaqueous solvents, the optimal ESF values for cations are smaller than this and ESF values for anions are larger. This is also intuitive as the electron density in

Table 4. Optimal ESFs and Optimal Mean Absolute Errors (MAEs, in kcal/mol) for Solvation Gibbs Free Energies of Ions[a]

solute class	N	IEFPCM-UAHF		IEFPCM-UAKS		CPCM-UAHF		CPCM-UAKS	
		optimal ESF	optimal MAE	optimal ESF	optimal MAE	optimal ESF	optimal MAE	optimal ESF	optimal MAE
Acetonitrile									
CHNO cations	36	1.1	5.97	1.1	6.38	1.1	6.04	1.1	6.43
other cations	3	1.1	10.14	1.1	10.72	1.1	10.15	1.1	10.74
all cations	39	1.1	6.29	1.1	6.72	1.1	6.35	1.1	6.76
CHNO anions	19	1.5	2.42	1.4	2.40	1.5	2.35	1.4	2.36
other anions	11	1.4	2.47	1.4	2.59	1.4	2.58	1.4	2.54
all anions	30	1.4	2.46	1.4	2.47	1.5	2.45	1.4	2.43
Dimethyl Sulfoxide									
CHNO cations	4	1.1	3.35	1.1	2.87	1.1	3.22	1.1	2.73
other cations	0	N/A	N/A	N/A	N/A	N/A	N/A	N/A	N/A
all cations	4	1.1	3.35	1.1	2.87	1.1	3.22	1.1	2.73
CHNO anions	52	1.5	4.05	1.5	4.25	1.5	4.06	1.5	4.25
other anions	15	1.5	3.59	1.5	3.75	1.5	3.61	1.5	3.75
all anions	67	1.5	3.94	1.5	4.14	1.5	3.96	1.5	4.14
Water									
CHNO cations	56	1.2	4.73	1.2	4.97	1.2	4.64	1.2	4.88
other cations	4	1.2	7.92	1.2	8.64	1.2	7.92	1.2	8.65
all cations	60	1.2	4.94	1.2	5.21	1.2	4.86	1.2	5.13
CHNO anions	60	1.2	8.69	1.2	10.17	1.2	8.64	1.2	10.13
other anions	23	1.2	3.47	1.2	4.07	1.2	3.48	1.2	4.04
all anions	83	1.2	7.25	1.2	8.48	1.2	7.21	1.2	8.44

[a]N is the number of experimental solvation Gibbs free energies.

anions is more diffuse than neutrals and the reverse is true for cations. Thus, using individually optimized ESF values for cations and anions can further improve the accuracy compared with using one uniform ESF value for all. For example, in acetonitrile with IEFPCM-UAHF calculations, when using the overall optimal ESF (i.e., 1.2) for CHNO cations, the MAE is 10.22 kcal/mol, which can be decreased to 5.97 kcal/mol with ESF = 1.1 (optimal ESF for cations in acetonitrile). More dramatically, using the CHNO anion specific optimal ESF in acetonitrile, i.e., 1.5, can decrease MAE to 2.42 kcal/mol compared with using ESF = 1.2, which gives MAE as 10.86 kcal/mol. Similarly, for IEFPCM-UAHF calculations in dimethyl sulfoxide, the MAEs for CHNO cations and anions can be reduced by 6.27 and 17.49 kcal/mol compared with using 1.2 for all. The change can be even larger for calculations with non-CHNO ions. This trend is common in all four types of calculations, i.e., IEFPCM-UAHF, IEFPCM-UAKS, CPCM-UAHF, and CPCM-UAKS calculations. Details of data can be seen in Tables S5 and S6.

Comparison with the Literature. In the original work designing UAHF radii types,[51] 1.2 was specified as the overall optimal ESF value which is consistent with our benchmarking results, both for the overall optimal value and for the optimal value for water, and thus reconfirms our results are reasonable. In 2014, Wu and co-workers conducted an extensive benchmarking study and concluded that changing the ESF value from 1.1 to 1.2 can dramatically improve the accuracy of PCM-UAKS aqueous solvation Gibbs free energies of amino acid side chain analogues,[22] which is consistent with the results in this work. Similarly, Pacureanu and co-workers also noted that the van der Waals radii of the solute atoms should be scaled by a factor of 1.2 with the PCM-UAHF model in their study on Watson–Crick-type bases in aqueous solutions.[54]

For the more polar solvents, and particularly for the anions, higher values have generally been reported in the literature,[17,18,20,21,55] and this is also seen here. For example, in

Table 1, the ESF for DMSO had been previously reported as 1.35 for test sets of solvation Gibbs free energies of anions[17] or neutrals and anions,[18] albeit with different radius types. This is close to the values of 1.4–1.5 (depending on the radius type) reported in Table 3. The acetonitrile values reported in Table 1 are variable,[19−21] in part because only one of the three studies[20] employed the solvation energies of anions rather than properties such as pK_a values and redox potentials, for which solvation energies of neutrals and ions are contributing together. In the study of anion solvation energies, the value reported, 1.36, is again similar to our values of 1.4–1.5 (depending on the radius type) reported in Table 3. Bryantsev[56] pointed out that atomic radii of ions developed in water need to be scaled in acetonitrile and using ESF = 1.4 in acetonitrile to minimize errors, which also agrees well with our results.

Effect of Level of Theory for the Solvation Model. Solvation models are semiempirical and perform best when used at the level of theory at which they were originally parametrized, which in the case of PCM was HF/6-31G(d) and PBE1PBE/6-31G(d), which is what is used here. For convenience, all solvation Gibbs free energies were calculated using the gas-phase M062X/MG3S optimized geometries provided in the MNSol-v2012[32] database. As such, the reported ESF values here should be employed in conjunction with these theoretical levels for the solvation model. However, by focusing on solvation energies, the ESF values can be employed as part of a thermocycle with any gas-phase level of theory for reaction energies, as appropriate to the problem at hand.

Nonetheless, one can envisage situations, such as when explicit solvent molecules might be required, where use of an improved level of theory for the solvation energies might be required to, for example, treat dispersion interactions. To test how robust the ESF values are to the theoretical level, we conducted an additional set of calculations on a representative

Article

Table 5. Optimal ESFs and MAEs (in kcal/mol) of 82 Solute/Solvent Combinations Obtained with Default Theoretical Levels and ωB97X-D/6-31+G(d,p)[a]

solute class	N	IEFPCM-UAHF		IEFPCM-UAKS		CPCM-UAHF		CPCM-UAKS	
		optimal ESF	optimal MAE	optimal ESF	optimal MAE	optimal ESF	optimal MAE	optimal ESF	optimal MAE
					Acetonitrile				
neutrals	7	1.2/1.2	2.62/2.79	1.2/1.2	2.83/2.50	1.2/1.2	2.59/2.79	1.2/1.2	2.76/2.50
CHNO cations	4	1.2/1.2	7.52/6.93	1.2/1.2	7.89/6.93	1.2/1.2	7.28/6.72	1.2/1.2	7.65/6.72
other cations	1	0.9/0.9	1.79/1.39	0.9/0.9	0.18/1.39	0.9/0.9	2.16/1.76	0.9/0.9	0.52/1.76
all cations	5	1.1/1.1	10.09/10.62	1.1/1.1	9.99/10.62	1.1/1.1	10.25/10.78	1.1/1.1	10.15/10.78
other anions	1	1.4/1.4	2.45/1.26	1.4/1.4	0.27/1.26	1.5/1.4	1.37/1.40	1.4/1.4	0.39/1.40
all anions	1	1.4/1.4	2.45/1.26	1.4/1.4	0.27/1.26	1.5/1.4	1.37/1.40	1.4/1.4	0.39/1.40
					Water				
neutrals	58	1.2/1.2	1.16/1.74	1.2/1.2	1.04/1.48	1.2/1.2	1.16/1.69	1.2/1.2	1.04/1.45
CHNO cations	5	1.2/1.1	6.59/6.48	1.2/1.1	6.90/6.48	1.2/1.1	6.50/6.71	1.2/1.1	6.82/6.71
other cations	1	1.2/1.3	0.50/0.03	1.2/1.2	0.38/0.03	1.2/1.2	0.76/0.65	1.2/1.2	0.65/0.65
all cations	6	1.2/1.3	5.57/7.23	1.2/1.2	5.82/7.23	1.2/1.2	5.54/7.17	1.2/1.2	5.79/7.17
CHNO anions	3	1.2/1.1	2.42/2.17	1.2/1.1	2.01/2.25	1.2/1.1	2.43/1.94	1.2/1.1	2.02/2.00
other anions	2	1.1/1.1	2.16/2.69	1.1/1.1	2.95/2.69	1.1/1.1	2.08/2.62	1.1/1.1	2.88/2.62
all anions	5	1.2/1.1	4.13/2.38	1.2/1.1	4.08/2.42	1.2/1.1	4.12/2.21	1.2/1.1	4.07/2.49

[a]ESFs and MAEs obtained with default theoretical levels and ωB97X-D/6-31+G(d,p) are respectively placed before and after the slash.

subset of 82 solute/solvent combinations (see the Supporting Information). For this set, geometries and solvation energies were calculated using a modern dispersion-corrected functional, ωB97X-D/6-31+G(d,p), and optimal ESF values were redetermined (Table 5).

It can be seen from Table 5 that changing the theoretical level has a small effect on the optimal ESF values and minimum MAEs of solvation Gibbs free energies. Replacing the default theoretical level with ωB97X-D/6-31+G(d,p) can improve the calculations of some solvation Gibbs free energies while not improving others. The overall accuracy of these theoretical levels is pretty close for the 82 solute/solvent combinations. In acetonitrile, the effect of teh theoretical level is rather minimal: all optimal ESFs obtained with the default theoretical level and ωB97X-D/6-31+G(d,p) are the same except for the anions with the CPCM-UAHF method. In contrast, the difference in water is larger: optimal ESF values obtained with all theoretical levels are all 1.2 for neutral species; however, optimal ESF values of ions are different. Thus, while the ESF values are relatively robust, they should be reoptimized if different levels of theory are to be used for the solvation calculations. The values presented here offer a starting point for ωB97X-D/6-31+G(d,p).

Protocol. This brings us to the recommended protocol for PCM solvation energy calculations.

• Where possible, the recommended ESF values in Table 4 should be used according to solute charge, solvent type and method/radii combination. With these specified, solvation energies should be calculated with HF/6-31G(d)//M062X/MG3S and PBE1PBE/6-31G(d)//M062X/MG3S, for UAHF and UAKS radii, respectively.

• If a different level of theory for the solvation energy is required, ESF values should be reoptimized and Table 5 provides examples for ωB97X-D/6-31+G(d,p).

• For solvents other than those in Table 4, values of neutral species are provided as a function of solvent type and method/radii combination in Table 2. However, these should be used cautiously for charged species in polar solvents, as it is likely that anions require higher values and cations require smaller values than neutrals.

Having obtained solvation Gibbs free energies, these can be used in a thermocycle in conjunction with accurate gas-phase-reaction Gibbs free energies, as calculated at any appropriate level of theory, to obtain reaction energies in solution.

Comparing the Performances of CPCM-UAHF, SMD, and COSMO-RS. Following the above protocol, the same test set of 82 solute/solvent combinations was used to compare the best-performing PCM variant (CPCM-UAHF) with two other popular solvent models, SMD and COSMO-RS. For SMD, we used the optimal protocol established in our recent study of cavity scaling for this model.[16] In that work we showed that the optimal ESF is 1, provided the recommended levels of theory in the original SMD study are used.[1] Thus, here we use (for both water and acetonitrile) M052X/6-31G(d) for neutrals and M052X/6-31+G(d,p) for cations, while for anions, HF/6-31G(d) is used in water while B3LYP/6-31G(d) is used in acetonitrile. As in PCM, all geometries were taken from the M062X/MG3S structures in the MNSol-v2012, consistent with ref 1. For solvation Gibbs free energies, calculations with COSMO-RS,[48,49] in which the screening charge densities of solutes and solvents are first generated by a CPCM/BVP86/TZVP/DGA1 calculation in Gaussian 16,[43] these are then exported as .cosmo files to COSMOtherm,[50] where solvation energies are calculated using COSMO-RS with TZVP parametrization. Cavity scaling was not applied to COSMO-RS.

Figure 1 shows the mean absolute errors of solvation Gibbs free energies of the 82 solute/solvent combinations as calculated with CPCM-UAHF, SMD, and COSMO-RS. Overall, SMD gives the smallest error (1.75 kcal/mol) while COSMO-RS produces the largest error (3.43 kcal/mol); our optimized CPCM-UAHF performs slightly worse than SMD and gives the MAE as 2.36 kcal/mol. It should be noted that, unlike PCM and SMD, optimal ESF values have not been determined for COSMO-RS. While this method is much more complex, it is possible that scaling the cavities for the initial CPCM calculation may help to address these errors, though this may need to be done in conjunction with a reparametrization of the COSMO-RS calculation as well. The main take-home message is that, when appropriately
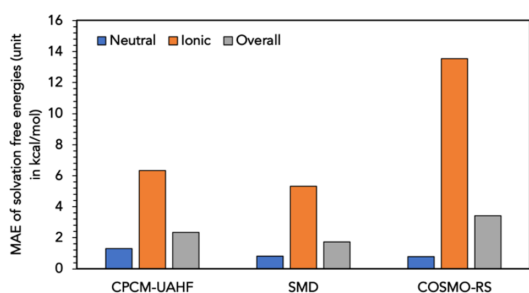
Figure 1. Mean absolute errors (MAEs) of solvation Gibbs free energies of neutral and ionic solutes calculated with different solvation models.

scaled, PCM shows marginally larger errors than SMD, and all methods show large errors for ions.

pK_a Tests. To test the optimal PCM ESF values in a practical setting, we next considered test sets of aqueous (Scheme 1) and nonaqueous (in acetonitrile, Scheme 2) pK_a values. The aqueous pK_a values (Figure 2) were calculated
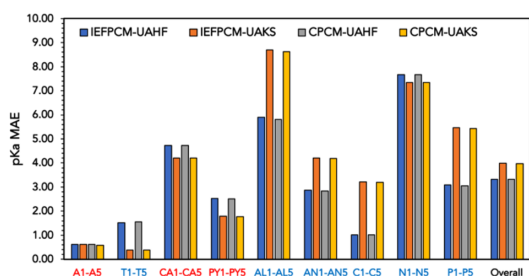

Figure 2. Mean absolute errors (MAEs) of the aqueous pK_a values in Scheme 1, as calculated using an ESF value of 1.2. pK_a values of solute types labeled in red (A1–A5, CA1–CA5, and PY1–PY5) are calculated with cations and neutrals, while those in blue are calculated with neutrals and anions. For all other computations, see Computational Details.

using ESF = 1.2. The acetonitrile values (Figure 3) were calculated using mixed ESF values, i.e., using optimal ESF
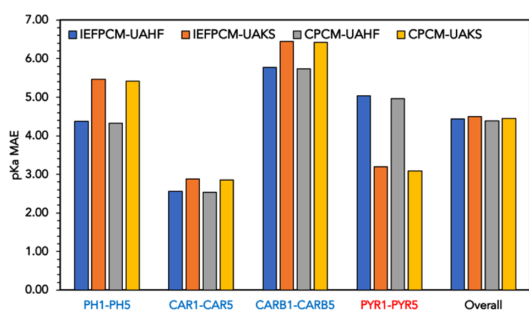
Figure 3. Mean absolute errors (MAEs) in the nonaqueous (acetonitrile) pK_a values of Scheme 2, as calculated using mixed ESF values. pK_a values of solute types labeled in red (PYR1–PYR5) are calculated with cations and neutrals, while those in blue are calculated with neutrals and anions. For all other computations, see Computational Details.

values obtained in Tables 2 and 4 for each one of the neutrals, anions, and cations. For example, for IEFPCM-UAHF calculations, we use 1.2 for neutrals, 1.1 for cations, 1.5 for CHNO anions, and 1.4 for other anions. All individual data are provided in Tables S7 and S8.

From Figures 2 and 3, it can be seen the errors in the pK_a values are large for some species and vary considerably with the solute and solvent type. This is not surprising given the size of the mean absolute errors in the solvation energies of neutrals, anions, and cations reported in Tables 2 and 4, even after ESF optimization. For instance, on average, CHNO cations contribute at least 6 kcal mol^{-1} (4.4 pK_a units) to the errors in pK_a values of cations in acetonitrile, which, when combined with an additional MAE of 2.7 kcal mol^{-1} (2 pK_a units) for neutrals in acetonitrile, can go a long way toward explaining the errors in these systems, even before any uncertainty in the solvation energy of the proton[45,46] is considered. Similar analysis can account for most of the errors here. Although error cancellation between neutrals and ions can help produce excellent pK_a results for some species, for example, pK_a MAEs of amines (A1–A5 in Figure 2), the error cancellation is not systematic. This is why the use of explicit solvent molecules and isodesmic methods are usually required for accurate pK_a calculations.[53]

The key question here is whether the underlying errors in the solvent model can be improved by further optimization of the ESF value. That is, is it helpful to include indirect measures of the solvation energy from pK_a values, particularly in the case of acetonitrile where the available data is limited? In this respect it is worth noting that, while the choice of method (IEFPCM vs CPCM) has little effect on the errors in Figures 2 and 3, the radius type (UAHF vs UAKS) does, although the results are not systematic across all solute types. Obviously using pK_a values rather than solvation energies presupposes that the gas-phase reaction energies are accurate and any errors arise from the solvation calculations. Here we use a high level of theory which has been shown to reproduce gas-phase proton acidities to within 1 kcal mol^{-1}.[53]

Figure 4 shows the effect on the errors in the aqueous pK_a values of varying the ESF value away from its optimized value;
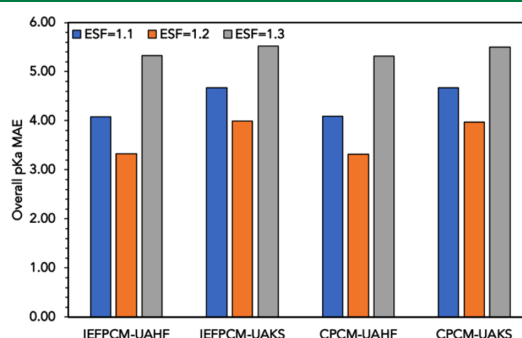
Figure 4. Mean absolute errors (MAEs) of 45 aqueous pK_a calculations obtained with ESF = 1.1, 1.2, and 1.3.

Figure 5 shows the same results for the nonaqueous values. For the aqueous pK_a values in Figure 4, the same values of ESF were used for neutrals, anions, and cations, as there was no variability in the optimal values in Tables 2 and 4. However, in acetonitrile anions, cations and neutrals had different optimal
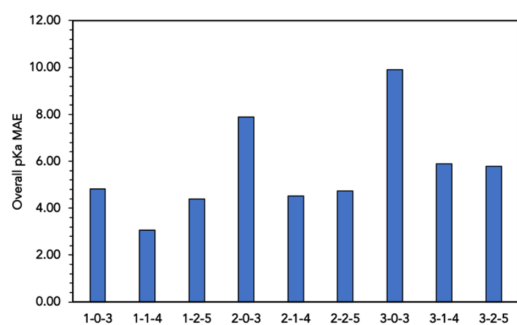
Figure 5. Mean absolute errors (MAEs) of 20 pK_a calculations in acetonitrile obtained with different ESF combinations using the IEFPCM-UAKS method. For example, 1−0−3 means using ESF = 1.1, 1.0, and 1.3 respectively for neutrals, cations, and anions.

ESF values; hence, we studied various combinations to see how they affect the pK_a. For simplicity, only the results for IEFPCM-UAKS are shown in Figure 5; results for the other solvent models are available in Table S11 and show identical trends to the IEFPCM-UAKS results below.

From Figure 4, we can see that, in water, ESF = 1.2 is optimal, with errors increasing as its value is adjusted up or down. This further confirms the optimization results above. From Figure 5, the optimal combination in acetonitrile for IEFPCM-UAKS is 1.1 for neutrals, 1.1 for cations, and 1.4 for anions. This differs slightly from the optimal results in Tables 2−4 of 1.2 for neutrals, 1.1 for cations, and 1.4 for anions which is equal to second best but gives an increase in error of just over 1 pK_a unit. This error is the same as the likely uncertainty that the gas-phase acidity calculations contribute to the pK_a values is thus not significant. Thus, the initial benchmarking gives close to the best results, the values for the anions and cations are confirmed, and the change in the neutrals is within the noise. Importantly, using our mixed ESF values for pK_a calculations can dramatically improve the accuracy compared with using one uniform ESF value for both neutrals and ions, especially compared with results using ESF = 1.1 (the default ESF value in the Gaussian 16[43] program) for all species. For example, for five carboxylic acids (CARB1−CARB5), the accuracy of pK_a values can be improved by around 9 pK_a units via using our mixed ESF values compared with using ESF = 1.1 for all. Related data can be seen in Table S12. This justifies the needs of using both our optimized ESF values and mixed ESF values in calculating solution-phase properties.

■ CONCLUSION

Herein we have determined optimal values of the electrostatic scaling factor for IEFPCM and CPCM with both UAHF and UAKS radii types in a variety of solvents as a function of solute charge. For this purpose, we considered over 1719 experimental solvation Gibbs free energies and transfer free energies of neutrals and ions from the MNSol-v2012 database, as well as 45 aqueous pK_a values including nine solute types (amines, thiols, carbon acid cations, pyridines, alcohols, anilines, carboxylic acids, carbon acid neutrals, and phenols) and 20 pK_a values in acetonitrile molecules covering four solute types (phenols, carbon acids, carboxylic acids, pyridines). Our key findings are as follows.

In water, the optimal ESF value is 1.2 and this does not vary with solute charge, radius type, or whether PCM or IEF-PCM is used, nor does it vary according to whether we consider the MNSol-v2012 database or the prediction of a range of pK_a values. This robustness in water is likely the result of the large amount of data available and the fact that the original parametrization of the model was carried out in this solvent.

In acetonitrile, the optimal value of the ESF is different for neutrals, cations, and anions, and their variation with charge is physically intuitive. Based on the data available here, we recommend ESF values of 1.1 for neutrals, 1.0 and 1.1 respectively for cations with UAHF and UAKS radii types, and 1.3 for anions for IEFPCM-UAHF and 1.4 for other anions. These values are also largely consistent with those determined from pK_a calculations. Optimal ESF values in further solvents can be found in Tables 2−4.

With 82 solute/solvent combinations taken from MNSol-v2012 database, our calculations show that the changing theoretical level for the solvation calculations has a small effect on the optimal ESF values, and thus the optimal ESF values in this work should be used according to the protocol used for ESF benchmarking. Comparison between different solvation models over the 82 solute/solvent combinations indicates that our optimized CPCM-UAHF method performs slightly worse than SMD and better than COSMO-RS, especially for solvation of ions. However, unlike the others, optimal ESF values (in this case for the initial CPCM calculation) have not been determined for COSMO-RS and this may be worth future investigation.

Despite ESF optimization, the accuracy of continuum solvation calculations remains poor, especially for ions, and this translates into large errors in pK_a predictions. ESF optimization is not a substitute for the appropriate use of explicit solvent molecules when solute−solvent interactions are important, nor the use of isodesmic methods to enhance systematic error cancellation. Rather, one should optimize the ESF on a very broad database of solvation energies, and treat remaining system specific errors using these other system-specific strategies. Considering the numerous combinations of solvation model, surface type, radius type, theoretical level, and solute and solvent types available, machine learning might be useful for future works finding the suitable set of parameters for accurate solvation modeling.

■ ASSOCIATED CONTENT

ⓢ Supporting Information

The Supporting Information is available free of charge on the ACS Publications Web site. The Supporting Information is available free of charge on the ACS Publications website at DOI: 10.1021/acs.jctc.9b00888.

Main results of ESF benchmarking; raw data of pK_a calculations; optimized structures of 65 molecules (PDF)

Detailed data of ESF benchmarking, comparison between CPCM-UAHF, SMD, and COSMO-RS; calculation results at ωB97X-D/6-31+G(d,p) theoretical level (XLSX)

■ AUTHOR INFORMATION

Corresponding Author
*E-mail: michelle.coote@anu.edu.au. Phone: 61 2 6125 3771.

ORCID ●

Michelle L. Coote: 0000-0003-0828-7053

■ **REFERENCES**

(1) Marenich, A. V.; Cramer, C. J.; Truhlar, D. G. Universal Solvation Model Based on Solute Electron Density and on a Continuum Model of the Solvent Defined by the Bulk Dielectric Constant and Atomic Surface Tensions. *J. Phys. Chem. B* **2009**, *113*, 6378−6396.

(2) Tomasi, J.; Mennucci, B.; Cammi, R. Quantum mechanical continuum solvation models. *Chem. Rev.* **2005**, *105* (8), 2999−3094.

(3) Lacerda, E. G., Jr.; Kamounah, F. S.; Coutinho, K.; Sauer, S. P. A.; Hansen, P. E.; Hammerich, O. Computational Prediction of 1H and 13C NMR Chemical Shifts for Protonated Alkylpyrroles: Electron Correlation and Not Solvation is the Salvation. *ChemPhysChem* **2018**, *20*, 78−91.

(4) Giovannini, T.; Macchiagodena, M.; Ambrosetti, M.; Puglisi, A.; Lafiosca, P.; Lo Gerfo, G.; Egidi, F.; Cappelli, C. Simulating vertical excitation energies of solvated dyes: From continuum to polarizable discrete modeling. *Int. J. Quantum Chem.* **2019**, *119*, No. e25684.

(5) Vakulin, I. V.; Bugaets, D. V.; Zilberg, R. A.; Maistrenko, V. N. Semi-empirical methods in RedOx potential calculations of substituted aromatic compounds: Parameterizations, solvation models, approximation by frontier molecular orbital energies. *Electrochim. Acta* **2019**, *294*, 423−430.

(6) Hoang, K. M.; Lees, N. R.; Herzon, S. B. Programmable Synthesis of 2-Deoxyglycosides. *J. Am. Chem. Soc.* **2019**, *141*, 8098− 8103.

(7) Zhang, Q.; Asthagiri, A. Solvation effects on DFT predictions of ORR activity on metal surfaces. *Catal. Today* **2019**, *323*, 35−43.

(8) Zamora, W. J.; Campanera, J. M.; Luque, F. J. Development of a Structure-Based, pH-Dependent Lipophilicity Scale of Amino Acids from Continuum Solvation Calculations. *J. Phys. Chem. Lett.* **2019**, *10*, 883−889.

(9) Nakata, H.; Fedorov, D. G. Simulations of infrared and Raman spectra in solution using the fragment molecular orbital method. *Phys. Chem. Chem. Phys.* **2019**, *21*, 13641−13652.

(10) Bi, T. J.; Xu, L. K.; Wang, F.; Li, X. Y. Solvent effects for vertical absorption and emission processes in solution using a self-consistent state specific method based on constrained equilibrium thermodynamics. *Phys. Chem. Chem. Phys.* **2018**, *20*, 13178−13190.

(11) Liu, F.; Sanchez, D. M.; Kulik, H. J.; Martínez, T. J. Exploiting graphical processing units to enable quantum chemistry calculation of large solvated molecules with conductor-like polarizable continuum models. *Int. J. Quantum Chem.* **2019**, *119*, No. e25760.

(12) Caricato, M. Coupled cluster theory with the polarizable continuum model of solvation. *Int. J. Quantum Chem.* **2019**, *119*, No. e25710.

(13) Vuong, V. Q.; Nishimoto, Y.; Fedorov, D. G.; Sumpter, B. G.; Niehaus, T. A.; Irle, S. The Fragment Molecular Orbital Method Based on Long-Range Corrected Density-Functional Tight-Binding. *J. Chem. Theory Comput.* **2019**, *15*, 3008−3020.

(14) Di Remigio, R.; Steindal, A. H.; Mozgawa, K.; Weijo, V.; Cao, H.; Frediani, L. PCMSolver: An open-source library for solvation modeling. *Int. J. Quantum Chem.* **2019**, *119*, e25685.

(15) Ho, J.; Klamt, A.; Coote, M. L. Comment on the Correct Use of Continuum Solvent Models. *J. Phys. Chem. A* **2010**, *114*, 13442− 13444.

(16) Xu, L.; Coote, M. L. Methods To Improve the Calculations of Solvation Model Density Solvation Free Energies and Associated Aqueous pK_a Values: Comparison between Choosing an Optimal Theoretical Level, Solute Cavity Scaling, and Using Explicit Solvent Molecules. *J. Phys. Chem. A* **2019**, *123*, 7430−7438.

(17) Pliego, J. R.; Riveros, J. M. Parametrization of the PCM model for calculating solvation free energy of anions in dimethyl sulfoxide solutions. *Chem. Phys. Lett.* **2002**, *355*, 543−546.

(18) Fu, Y.; Liu, L.; Li, R.-Q.; Liu, R.; Guo, Q.-X. First-Principle Predictions of Absolute pK_a's of Organic Acids in Dimethyl Sulfoxide Solution. *J. Am. Chem. Soc.* **2004**, *126*, 814−822.

(19) Fu, Y.; Liu, L.; Yu, H. Z.; Wang, Y. M.; Guo, Q. X. Quantum-chemical predictions of absolute standard redox potentials of diverse organic molecules and free radicals in acetonitrile. *J. Am. Chem. Soc.* **2005**, *127*, 7227−7234.

(20) Böes, E. S.; Livotto, P. R.; Stassen, H. Solvation of monovalent anions in acetonitrile and N,N-dimethylformamide: Parameterization of the IEF-PCM model. *Chem. Phys.* **2006**, *331*, 142−158.

(21) Gryn'ova, G.; Barakat, J. M.; Blinco, J. P.; Bottle, S. E.; Coote, M. L. Computational Design of Cyclic Nitroxides as Efficient Redox Mediators for Dye-Sensitized Solar Cells. *Chem. - Eur. J.* **2012**, *18*, 7582−7593.

(22) Wen, M.; Jiang, J.; Wang, Z.-X.; Wu, C. How accurate are the popular PCM/GB continuum solvation models for calculating the solvation energies of amino acid side-chain analogs? *Theor. Chem. Acc.* **2014**, *133*, 1471.

(23) Barone, V.; Carnimeo, I.; Scalmani, G. Computational Spectroscopy of Large Systems in Solution: The DFTB/PCM and TD-DFTB/PCM Approach. *J. Chem. Theory Comput.* **2013**, *9*, 2052− 2071.

(24) Provorse Long, M. R.; Isborn, C. M. Combining Explicit Quantum Solvent with a Polarizable Continuum Model. *J. Phys. Chem. B* **2017**, *121*, 10105−10117.

(25) Preat, J.; Loos, P.-F.; Assfeld, X.; Jacquemin, D.; Perpète, E. A. DFT and TD-DFT Investigation of IR and UV Spectra of Solvated Molecules: Comparison of Two SCRF Continuum Models. *Int. J. Quantum Chem.* **2007**, *107*, 574−585.

(26) Lee, T. B.; McKee, M. L. Dependence of pK_a on solute cavity for diprotic and triprotic acids. *Phys. Chem. Chem. Phys.* **2011**, *13*, 10258−10269.

(27) Khalili, F.; Henni, A.; East, A. L. L. Entropy contributions in pK_a computation: Application to alkanolamines and piperazines. *J. Mol. Struct.: THEOCHEM* **2009**, *916*, 1−9.

(28) Close, D. M.; Wardman, P. Calculation of Standard Reduction Potentials of Amino Acid Radicals and the Effects of Water and Incorporation into Peptides. *J. Phys. Chem. A* **2018**, *122*, 439−445.

(29) Cammi, R.; Verdolino, V.; Mennucci, B.; Tomasi, J. Towards the elaboration of a QM method to describe molecular solutes under the effect of a very high pressure. *Chem. Phys.* **2008**, *344*, 135−141.

(30) Amovilli, C.; Floris, F. M. Solubility of water in liquid hydrocarbons: a bridge between the polarizable continuum model and the mobile order theory. *Phys. Chem. Chem. Phys.* **2003**, *5*, 363−368.

(31) Luque, F. J.; Bachs, M.; Alemán, C.; Orozco, M. Extension of MST/SCRF method to organic solvents: Ab initio and semiempirical parametrization for neutral solutes in CCl4. *J. Comput. Chem.* **1996**, *17*, 806−820.

(32) Marenich, A. V.; Kelly, C. P.; Thompson, J. D.; Hawkins, G. D.; Chambers, C. C.; Giesen, D. J.; Winget, P.; Cramer, C. J.; Truhlar, D. G. *Minnesota Solvation Database*, version 2012; University of Minnesota: Minneapolis, 2012.

Journal of Chemical Theory and Computation   Article

(33) Rebollar-Zepeda, A. M.; Galano, A. First principles calculations of pK_a values of amines in aqueous solution: Application to neurotransmitters. *Int. J. Quantum Chem.* **2012**, *112*, 3449−3460.

(34) Thapa, B.; Schlegel, H. B. Density Functional Theory Calculation of pK_a's of Thiols in Aqueous Solution Using Explicit Water Molecules and the Polarizable Continuum Model. *J. Phys. Chem. A* **2016**, *120*, 5726−5735.

(35) Muckerman, J. T.; Skone, J. H.; Ning, M.; Wasada-Tsutsui, Y. Toward the accurate calculation of pK_a values in water and acetonitrile. *Biochim. Biophys. Acta, Bioenerg.* **2013**, *1827*, 882−891.

(36) Lee, I.; Kim, C. K.; Han, I. S.; Lee, H. W.; Kim, W. K.; Kim, Y. B. Theoretical studies of solvent effect on the basicity of substituted pyridines. *J. Phys. Chem. B* **1999**, *103*, 7302−7307.

(37) Klicic, J. J.; Friesner, R. A.; Liu, S. Y.; Guida, W. C. Accurate prediction of acidity constants in aqueous solution via density functional theory and self-consistent reaction field methods. *J. Phys. Chem. A* **2002**, *106*, 1327−1335.

(38) Tehan, B. G.; Lloyd, E. J.; Wong, M. G.; Pitt, W. R.; Montana, J. G.; Manallack, D. T.; Gancia, E. Estimation of pK_a Using Semiempirical Molecular Orbital Methods. Part 1: Application to Phenols and Carboxylic Acids. *Quant. Struct.-Act. Relat.* **2002**, *21*, 457−472.

(39) Namazian, M.; Halvani, S. Calculations of pK_a values of carboxylic acids in aqueous solution using density functional theory. *J. Chem. Thermodyn.* **2006**, *38*, 1495−1502.

(40) Charif, I. E.; Mekelleche, S. M.; Villemin, D.; Mora-Diez, N. Correlation of aqueous pK_a values of carbon acids with theoretical descriptors: A DFT study. *J. Mol. Struct.: THEOCHEM* **2007**, *818*, 1−6.

(41) Ragnar, M.; Lindgren, C. T.; Nilvebrant, N.-O. pK_a-Values of Guaiacyl and Syringyl Phenols Related to Lignin. *J. Wood Chem. Technol.* **2000**, *20*, 277−305.

(42) Eckert, F.; Leito, I.; Kaljurand, I.; Kütt, A.; Klamt, A.; Diedenhofen, M. Prediction of acidity in acetonitrile solution with COSMO-RS. *J. Comput. Chem.* **2009**, *30*, 799−810.

(43) Frisch, M. J.; Trucks, G. W.; Schlegel, H. B.; Scuseria, G. E.; Robb, M. A.; Cheeseman, J. R.; Scalmani, G.; Barone, V.; Petersson, G. A.; Nakatsuji, H.; et al. *Gaussian 16*; Gaussian, Inc.: Wallingford, CT, 2016.

(44) Lynch, B. J.; Zhao, Y.; Truhlar, D. G. Effectiveness of diffuse basis functions for calculating relative energies by density functional theory. *J. Phys. Chem. A* **2003**, *107*, 1384−1388.

(45) Kelly, C. P.; Cramer, C. J.; Truhlar, D. G. Aqueous solvation free energies of ions and ion-water clusters based on an accurate value for the absolute aqueous solvation free energy of the proton. *J. Phys. Chem. B* **2006**, *110*, 16066−16081.

(46) Alongi, K. S.; Shields, G. C. Chapter 8 - Theoretical Calculations of Acid Dissociation Constants: A Review Article. In *Annual Reports in Computational Chemistry*, Wheeler, R. A., Ed. Elsevier: 2010; Vol. 6, pp 113−138.

(47) Werner, H.-J.; Knowles, P. J.; Knizia, G.; Manby, F. R.; Schütz, M.; Celani, P.; Györffy, W.; Kats, D.; Korona, T.; Lindh, R.; et al. *Molpro, A Package of Ab Initio Programs*, version 2015.1; TTI − Technologie-Transfer-Initiative GmbH an der Universität Stuttgart (TTI GmbH): Stuttgart, 2015.

(48) Klamt, A. Conductor-Like Screening Model for Real Solvents - a New Approach to the Quantitative Calculation of Solvation Phenomena. *J. Phys. Chem.* **1995**, *99*, 2224−2235.

(49) Klamt, A.; Jonas, V.; Burger, T.; Lohrenz, J. C. W. Refinement and parametrization of COSMO-RS. *J. Phys. Chem. A* **1998**, *102*, 5074−5085.

(50) Eckert, F.; Klamt, A. Fast solvent screening via quantum chemistry: COSMO-RS approach. *AIChE J.* **2002**, *48*, 369−385.

(51) Barone, V.; Cossi, M.; Tomasi, J. A new definition of cavities for the computation of solvation free energies by the polarizable continuum model. *J. Chem. Phys.* **1997**, *107*, 3210−3221.

(52) Kongsted, J.; Soderhjelm, P.; Ryde, U. How accurate are continuum solvation models for drug-like molecules? *J. Comput.-Aided Mol. Des.* **2009**, *23*, 395−409.

(53) Ho, J.; Coote, M. L. A universal approach for continuum solvent pK_a calculations: are we there yet? *Theor. Chem. Acc.* **2010**, *125*, 3−21.

(54) Pacureanu, L.; Simon, Z. DFT Plus PCM Calculation for Pairing Specificity of Watson-Crick-Type Bases in Aqueous Solutions. *Int. J. Quantum Chem.* **2009**, *110*, 1295−1305.

(55) Böes, E. S.; de Andrade, J.; Stassen, H.; Goncalves, P. F. B. Computational study of anion solvation in nitrobenzene. *Chem. Phys. Lett.* **2007**, *436*, 362−367.

(56) Bryantsev, V. S. Calculation of solvation free energies of Li+ and O-2(−) ions and neutral lithium-oxygen compounds in acetonitrile using mixed cluster/continuum models. *Theor. Chem. Acc.* **2012**, *131*, 1250.

JCTC
Journal of Chemical Theory and Computation

Correction to Improving the Accuracy of PCM-UAHF and PCM-UAKS Calculations Using Optimized Electrostatic Scaling Factors

Longkun Xu and Michelle L. Coote*

Ⓢ *Supporting Information*

During the preparation of the manuscript, we inadvertently made two mistakes: (1) We used aqueous solvation free energy of proton for pK_a calculations in acetonitrile, and (2) in the comparison between the accuracy of SMD, our revised CPCM-UAHF and COSMO-RS, we forgot to use the keyword *radii = klamt* in generating cosmo files of 11 ions in water. Thus, several figures and tables need to be changed; however, the conclusions reached in the Article remain unchanged.

1. Correction to pK_a Values in Acetonitrile. We inadvertently used the aqueous solvation free energy of proton in pK_a calculations in acetonitrile in the original version. Here we recalculate all pK_as in acetonitrile using the experimental value of the solvation free energy of proton as −260.2 kcal/mol as taken from ref 1. All calculated pK_a values in tab "pK_a calculations" in our original Supporting Information have been corrected; see the corrected Supporting Information. It can be seen that the accuracy of pK_a calculations in acetonitrile reported previously is underestimated. When using the correct solvation free energy of the proton in acetonitrile, our calculated pK_a results are much improved compared that reported previously. Figures 3 and 5 and Supporting Information Tables S11 and S12 have been changed.

In our original work, based on the results in the original Figure 5, we concluded the optimal ESF value of neutrals in acetonitrile might need a slight change. While here, 2-1-4 gives the smallest overall MAE, which proves using the ESF values obtained from our benchmarking gives the best results among all possible ESF combinations and does not need further change.
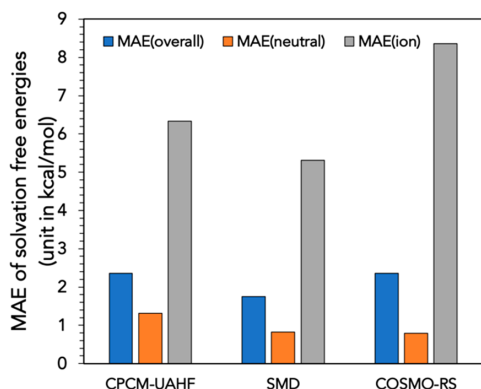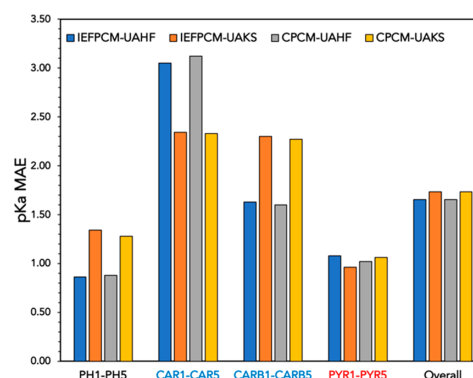
Figure 3. Mean absolute errors (MAEs) in the nonaqueous (acetonitrile) pK_a values of Scheme 2, as calculated using mixed ESF values. pK_a values of solute types labeled in red (PYR1−PYR5) are calculated with cations and neutrals, while those in blue are calculated with neutrals and anions. For all other computations, see Computational Details.

Figure 5. Mean absolute errors (MAEs) of 20 pK_a calculations in acetonitrile obtained with different ESF combinations using the IEFPCM-UAKS method. For example, 1-0-3 means using ESF = 1.1, 1.0, and 1.3, respectively, for neutrals, cations, and anions.

2. Correction to COSMO-RS Solvation Free Energies of Ions in Water. In the comparison between the accuracy of SMD, our revised CPCM-UAHF and COSMO-RS, we inadvertently forgot to use the keyword *radii = klamt* in generating cosmo files

Figure 1. Mean absolute errors (MAEs) of solvation Gibbs free energies of neutral and ionic solutes calculated with different solvation models.

Journal of Chemical Theory and Computation

of the 11 ions in water, which makes the error of COSMO-RS quite large. Related data in the "CPCM-UAHF VS SMD VS COSMO-RS" tab in the Supporting Information and Figure 1 in the main text need to be changed. Note that only COSMO-RS solvation free energies of ions in water need to be changed, and based on the new results, our revised CPCM-UAHF model still outperforms COSMO-RS but not SMD, thus the main conclusion and discussion in comparing these three solvation models in our original paper does not change.

The "CPCM-UAHF VS SMD VS COSMO-RS" tab in the Supporting Information now contains the correct solvation free energies of 11 ions.

Thus, in Figure 1 of the publication, the mean absolute error of the COSMO-RS solvation free energies of ions should be 8.36 kcal/mol, and that of all 82 solute/solvent combinations should be 2.36 kcal/mol.

■ ASSOCIATED CONTENT

Ⓢ Supporting Information

The Supporting Information is available free of charge at https://pubs.acs.org/doi/10.1021/acs.jctc.9b01191.

> Detailed data of ESF benchmarking, comparison between CPCM-UAHF, SMD, and COSMO-RS; calculation results at ωB97X-D/6-31+G(d,p) theoretical level (XLSX)
>
> Main results of ESF benchmarking; raw data of pKa calculations; optimized structures of 65 molecules (PDF)

■ REFERENCES

(1) Kelly, C. P.; Cramer, C. J.; Truhlar, D. G. Single-Ion Solvation Free Energies and the Normal Hydrogen Electrode Potential in Methanol, Acetonitrile, and Dimethyl Sulfoxide. *J. Phys. Chem. B* **2007**, *111*, 408−422.

3.4 Summary

Implicit solvent models are widely used in the study of chemical properties and reactions in solution phase, and their accuracy can be affected by many factors. In this chapter, we investigate several different protocols to improve the accuracy of the widely used SMD, PCM-UAKS and PCM-UAHF solvation models.

For SMD, we compare three strategies including the choice of theoretical level, scaling the solute cavity and using explicit solvent molecules. To test these different strategies, we explore their effects on the accuracy of aqueous pK_a calculations of a wide range of solute types including methyl-substituted nucleic acid bases, carboxylic acids, aliphatic and aromatic amines, carbon acids, alcohols, and anilines. The results suggest that the choice of theoretical level is important for SMD, with the use of the mixed theoretical levels for pK_a calculations of cations and neutral species gives the best performance. In contrast, the use of explicit solvent molecules does not further improve the results. While for pK_a calculations with anions involved, the use of explicit solvent molecules is necessary. For molecules containing only C, H, O, N atoms, the cavity scaling is not really necessary when the theoretical level and the explicit solvent molecules are dealt with properly. Compared with the cavity scaling methods, our method is easier to use, more versatile and more accurate.

For PCM-UAKS and PCM-UAHF, we systematically optimize the ESF values in both aqueous and non-aqueous solution for a wide range of solute types. Using over 1719 experimental solvation Gibbs free energies and transfer free energies of neutral species and ions from the MNSol-v2012 database, we present the optimized ESF values for the solvation free energies of neutral species in 18 solvents, the solvation free energy of ions in 3 solvents, and the transfer free energies of neutral species in 9 solvents/water combinations. The performance of the optimized ESF values are tested by pK_a calculations of amines, thiols, carbon acid cations, pyridines, alcohols, anilines, carboxylic acids, carbon acid neutrals, and phenols in water and acetonitrile. It is found ESF=1.2 should be used for hydration free energies. The mixed ESF method in non-aqueous solution that we present can significantly improves the accuracy of pK_a predictions. The tests using 82 solute/solvent combinations suggest CPCM-UAHF with our optimized parameters can approach the accuracy of SMD.

These two publications are expected to be useful for future studies on the prediction of solvation free energies and solution-phase properties (pK_a and redox potential) of small molecules.

Bibliography

[1] S Dhillon and A. L East, "Challenges in predicting ΔrxnG in solution: Hydronium, hydroxide, and water autoionization", *International Journal of Quantum Chemistry* **118**(19), pp. e25703 (2018).

[2] R. A Mata and M. A Suhm, "Benchmarking quantum chemical methods: Are we heading in the right direction?", *Angewandte Chemie International Edition* **56**(37), pp. 11011–11018 (2017).

[3] R Cammi and J Tomasi, "Remarks on the use of the apparent surface charges (ASC) methods in solvation problems: Iterative versus matrix-inversion procedures and the renormalization of the apparent charges", *Journal of Computational Chemistry* **16**(12), pp. 1449–1458 (1995).

[4] O Tapia and O Goscinski, "Self-consistent reaction field theory of solvent effects", *Molecular Physics* **29**(6), pp. 1653–1661 (1975).

[5] J Wang and T Hou, "Develop and test a solvent accessible surface area-based model in conformational entropy calculations", *Journal of Chemical Information and Modeling* **52**(5), pp. 1199–1212 (2012).

[6] C Quan and B Stamm, "Meshing molecular surfaces based on analytical implicit representation", *Journal of Molecular Graphics and Modelling* **71**, pp. 200–210 (2017).

[7] M. L Connolly, "Analytical molecular surface calculation", *Journal of Applied Crystallography* **16**(5), pp. 548–558 (1983).

[8] L Wylie, K Oyaizu, A Karton, M Yoshizawa-Fujita, and E. I Izgorodina, "Toward improved performance of all-organic nitroxide radical batteries with ionic liquids: a theoretical perspective", *ACS Sustainable Chemistry & Engineering* **7**(5), pp. 5367–5375 (2019).

[9] F Lipparini and B Mennucci, "Perspective: Polarizable continuum models for quantum-mechanical descriptions", *The Journal of Chemical Physics* **144**(16), pp. 160901 (2016).

[10] J Tomasi, B Mennucci, and R Cammi, "Quantum mechanical continuum solvation models", *Chemical Reviews* **105**(8), pp. 2999–3094 (2005).

[11] L Onsager, "Electric moments of molecules in liquids", *Journal of the American Chemical Society* **58**(8), pp. 1486–1493 (1936).

[12] A. v Bondi, "van der waals volumes and radii", *The Journal of physical chemistry* **68**(3), pp. 441–451 (1964).

[13] A. K Rappé, C. J Casewit, K Colwell, W. A Goddard III, and W. M Skiff, "UFF, a full periodic table force field for molecular mechanics and molecular dynamics simulations", *Journal of the American chemical society* **114**(25), pp. 10024–10035 (1992).

[14] M Rahm, R Hoffmann, and N Ashcroft, "Atomic and ionic radii of elements 1–96", *Chemistry–A European Journal* **22**(41), pp. 14625–14632 (2016).

[15] J.-N Li, L Liu, Y Fu, and Q.-X Guo, "What are the pK_a values of organophosphorus compounds?", *Tetrahedron* **62**(18), pp. 4453–4462 (2006).

[16] A. V Marenich, C. J Cramer, and D. G Truhlar, "Universal solvation model based on solute electron density and on a continuum model of the solvent defined by the bulk dielectric constant and atomic surface tensions", *The Journal of Physical Chemistry B* **113**(18), pp. 6378–6396 (2009).

[17] V Barone, M Cossi, and J Tomasi, "A new definition of cavities for the computation of solvation free energies by the polarizable continuum model", *The Journal of Chemical Physics* **107**(8), pp. 3210–3221 (1997).

[18] R Di Remigio, A. H Steindal, K Mozgawa, V Weijo, H Cao, and L Frediani, "PCM-Solver: An open-source library for solvation modeling", *International Journal of Quantum Chemistry* **119**(1), pp. e25685 (2019).

[19] J. L Pascual-Ahuir and E Silla, "GEPOL: An improved description of molecular surfaces. I. Building the spherical surface set", *Journal of Computational Chemistry* **11**(9), pp. 1047–1060 (1990).

[20] J Ho, A Klamt, and M. L Coote, "Comment on the correct use of continuum solvent models", *The Journal of Physical Chemistry A* **114**(51), pp. 13442–13444 (2010).

[21] C. J Cramer and D. G Truhlar, "A universal approach to solvation modeling", *Accounts of Chemical Research* **41**(6), pp. 760–768 (2008).

[22] C. J Cramer and D. G Truhlar, "Reply to comment on "a universal approach to solvation modeling"", *Accounts of Chemical Research* **42**(4), pp. 493–497 (2009).

[23] G Gryn'Ova, J. M Barakat, J. P Blinco, S. E Bottle, and M. L Coote, "Computational design of cyclic nitroxides as efficient redox mediators for dye-sensitized solar cells", *Chemistry: A European Journal* **18**(24), pp. 7582–7593 (2012).

[24] A. V Marenich, C. P Kelly, J. D Thompson, G. D Hawkins, C. C Chambers, D. J Giesen, P Winget, C. J Cramer, and D. G Truhlar, "Minnesota solvation database", *Minnesota Solvation Database* **20** (2012).

[25] R. F Ribeiro, A. V Marenich, C. J Cramer, and D. G Truhlar, "Use of solution-phase vibrational frequencies in continuum models for the free energy of solvation", *The Journal of Physical Chemistry B* **115**(49), pp. 14556–14562 (2011).

[26] A. V Marenich, W Ding, C. J Cramer, and D. G Truhlar, "Resolution of a challenge for solvation modeling: calculation of dicarboxylic acid dissociation constants using mixed discrete–continuum solvation models", *The Journal of Physical Chemistry Letters* **3**(11), pp. 1437–1442 (2012).

[27] C. P Kelly, C. J Cramer, and D. G Truhlar, "Adding explicit solvent molecules to continuum solvent calculations for the calculation of aqueous acid dissociation constants", *The Journal of Physical Chemistry A* **110**(7), pp. 2493–2499 (2006).

[28] M. R Provorse Long and C. M Isborn, "Combining explicit quantum solvent with a polarizable continuum model", *The Journal of Physical Chemistry B* **121**(43), pp. 10105–10117 (2017).

[29] B Thapa and H. B Schlegel, "Density functional theory calculation of pK_a's of thiols in aqueous solution using explicit water molecules and the polarizable continuum model", *The Journal of Physical Chemistry A* **120**(28), pp. 5726–5735 (2016).

[30] P Lian, R. C Johnston, J. M Parks, and J. C Smith, "Quantum chemical calculation of pK_as of environmentally relevant functional groups: Carboxylic acids, amines, and thiols in aqueous solution", *The Journal of Physical Chemistry A* **122**(17), pp. 4366–4374 (2018).

[31] M. J Frisch, G. W Trucks, H. B Schlegel, G. E Scuseria, M. A Robb, J. R Cheeseman, G Scalmani, V Barone, G. A Petersson, H Nakatsuji, X Li, M Caricato, A. V Marenich, J Bloino, B. G Janesko, R Gomperts, B Mennucci, H. P Hratchian, J. V Ortiz, A. F Izmaylov, J. L Sonnenberg, D Williams-Young, F Ding, F Lipparini, F Egidi, J Goings, B Peng, A Petrone, T Henderson, D Ranasinghe, V. G Zakrzewski, J Gao, N Rega, G Zheng, W Liang, M Hada, M Ehara, K Toyota, R Fukuda, J Hasegawa, M Ishida, T Nakajima, Y Honda, O Kitao, H Nakai, T Vreven, K Throssell, J. A Montgomery, Jr., J. E Peralta, F Ogliaro, M. J Bearpark, J. J Heyd, E. N Brothers, K. N Kudin, V. N Staroverov, T. A Keith, R Kobayashi, J Normand, K Raghavachari, A. P Rendell, J. C Burant, S. S Iyengar, J Tomasi, M Cossi, J. M Millam, M Klene, C Adamo, R Cammi, J. W Ochterski, R. L Martin, K Morokuma, O Farkas, J. B Foresman, and D. J Fox, "Gaussian16 Revision C.01" (2016), Gaussian Inc. Wallingford CT.

[32] Y Shao, Z Gan, E Epifanovsky, A. T Gilbert, M Wormit, J Kussmann, A. W Lange, A Behn, J Deng, and X Feng, "Advances in molecular quantum chemistry contained in the Q-Chem 4 program package", *Molecular Physics* **113**(2), pp. 184–215 (2015).

Chapter 4

Ordered Solvents and Ionic Liquids for Electrostatic Catalysis

4.1 Introduction

Chemical reactivity can be dramatically influenced by electrostatic interactions. While this was already known for redox reactions,[1] recently it was shown that external electric fields can also influence the rates and selectivity of non-redox reactions.[2] More generally, electrostatic catalysis, which catalysts are designed by tuning electrostatic interactions, has become an important research field.[2–5] Electrostatic interactions arise in a variety of scenarios,[6] for example, STM-BJ,[2] ionic aggregates,[7] reactant-ion interactions,[8] the air-water interface,[9–11] solid-liquid interface,[12–14] and pH-switchable charged functional groups[15, 16].

Electrostatic catalysis has been widely explored by computational techniques.[17] The pioneering works of Shaik and co-workers provided the first simulation of a reaction (in the gas phase) in an electric field, showing how the electric field affected the reaction.[18] A series of works has investigated the effects of CFG embedded on substrates or catalysts[15, 19–22]. These works highlight the impact of electrostatic catalysis on the fields of electrochemistry, photochemistry and polymer chemistry. One common point of the above works is that the reactions were in gas phase or pure organic solvents,[19, 23, 24] and implicit solvent models were used to model the bulk solvent environment. For modelling of the electrostatic catalysis in complex solvent environments, the effects of electric field and electrostatic interactions usually require MD simulation techniques for dynamic simulations at different time scales.[25–27]

Although electrostatic interaction shows promise in achieving efficient catalysis, and the laboratory experiments at single-molecule level already demonstrated the effects of external electric field[2], so far, its widespread implementation is limited by the scalability of platforms.[6] Further, polar solvents attenuate electric fields, which is another bottleneck to achieve large-scale electrostatic catalysis. Chemical synthesis frequently requires polar solvent environments, and the solubility of charged species in low-polarity solvents is often low.[28]

Things that we explicitly highlight here are the effects of the solute-solvent and reactant-enzyme interactions. Solvent reorganization and the associated change in solute-solvent interactions are the driving force for outer-shell electron-transfer reactions in so-

lution, according to Marcus theory.[29, 30] It is is widely recognised that electrostatic effects play an important role in the catalytic power of Enzymes, Nature's catalysts. As discussed in the works of Warshel[31] and Boxer[32, 33], the relationship between electrostatic field from enzyme and reactants dramatically determines the kinetics of reactions. In summary, these works showed that both the solvent and enzyme environments could be engineered as both reaction media and catalysts, which offers a strategy to address the above issues and to achieve large-scale electrostatic catalysis in polar solvent media.

It is also known that the degree of order in organic solvents can be influenced by many factors. For example, water can become ordered in an external electric field. Foroutan-Nejad and co-workers found the magnitude and directions of the external electric field could change the orientation of water molecules to form hydrogen-up or hydrogen-down configurations, which further influenced the ion-receptor interactions in the system.[34] Laird and co-workers reported a decrease in dielectric constant of solvents within an external electric field.[35] Li, Cheng and co-workers reported the changes in the orientation of electrified interfacial water structures.[36] In addition to electrochemical interfaces, the ordered structure of water has also been observed at the calcite-water interface.[37] The relationship between solvent orientation and the reaction rate of the Menshutkin reaction under an external electric field has been investigated by Shaik and co-workers.[38]

Compared with conventional organic solvents, RTILs have their advantages. For example, RTILs hold properties including high conductivity, low volatility and low melting temperature. These properties are important factors in designing solvents for practical applications.[39] RTILs are widely recognized as *green solvents* in comparison with conventional organic solvents[40]. RTILs have been applied to a wide range of fields including synthesis, catalysis, clean technology and most commonly, electrochemistry.[40–46] Unlike traditional organic solvents, the properties of ionic liquids can be tailored by various combinations of the cation and anion components.[40]

For the applications of RTILs in electrochemistry, an important consideration is the ordered structure near the charged electrodes and under external electric fields.[47, 48] This is closely related to the electrochemical double-layer structure. Different theoretical models have been proposed to understand the double-layer structure[49–51] and associated electrocatalysis and the design of batteries and supercapacitors.[52, 53] Besides the Gouy-Chapman-Stern model[54] and mean-field theory,[51], self-consistent field theory and DFT methods have also been used.[55–57]

Many other factors in addition to external electric field can affect the ordering of ionic liquids. For example, Padua and co-workers found that interactions between the metal surface and ionic liquids can influence the population of ionic liquids at the surface.[58] It was reported by Slattery and co-workers that temperature could significantly affect the ordering of LCILs, which was shown an ordered reaction medium to change the endo/exo ratio of the Diels–Alder reactions.[59]

Computational techniques have been applied to quantitatively investigate the ordered structures of ionic liquids. For example, Wang employed the average reduced heterogeneity order parameters and average second Legendre polynomials to quantify the cationic orientation with respect to the direction of the external electric field.[48] Although many efforts have been made to understand the ordered structure of ionic liquids, some questions remain unclear, such as the time scale for the relaxation of ordered ionic liquids.[60] This time scale is important to understand the dynamic details in applying ordered ionic

liquids to electrostatic catalysis and comparing the time scales of the relaxation of ordered ionic liquids and that of chemical reactions.[61]

In experiments, fast and staightforward measurement of ionic liquids has not been performed yet to directly relate experimental observations with the time scale of ordered ionic liquids. Moreover, it is meaningful to determine the correlation between the observed quantities and calculated results.

Motivated by the above works, studies in this chapter were conducted to understand two points:

(1) Exploring the feasibility of using ordered solvent and ionic liquids for electrostatic catalysis.

Modelling ionic liquids is harder than pure organic solvent, and is usually beyond the capacity of implicit solvent models. It is challenging to obtain accurate parameters such as the dielectric constant for ionic liquids. However, this is true not only for ionic liquids, but also for solvent mixtures, interfaces, and ordered environments. In this thesis, all solvent environments except for pure organic solvent are called *complex solvent environment*. To model electrostatic catalysis in complex solvent environments, especially in ordered solvent environments, two factors are important. The first is system sampling as solvent environment is hard to describe by a continuum, and hence explicit solvents are required. The other factor is accuracy of the calculations of electrostatic interactions between solute and the complex solvent environment, especially the mutual polarization. In this chapter, we employ multi-scale methods. Specifically, we used a relatively cheaper method for the MD simulation of the systems in combination with an accurate method for the calculations of electrostatic interactions for a set of representative configurations taken from the MD simulations. On the basis of this multi-scale protocol, a further ONIOM multi-scale energy calculation scheme is used to more accurately describe electrostatic interactions.

To model ordered solvent environments under an external electric field, a polarizable force field should be used to include polarization effects. There are three main types of polarizable force field, namely the fluctuating point charge method,[62] induced dipole method (for example, the AMOEBA force field)[63] and Drude oscillator method[64]. In this chapter, we use the Drude oscillator method, a simple scheme of which is illustrated in Figure 4.1. We choose this type of polarizable force field as it achieves good accuracy while still preserving the simple particle-particle Coulomb electrostatic interactions as those in non-polarizable force fields. Especially CL&Pol force field, which is an open-source method developed on the basis of OPLS-AA force field. It can produce structures, static and dynamic properties of ionic liquids under external electric field very accurately, which has been confirmed by many works including the recent one of Kirchner, Welton and co-workers.[65]
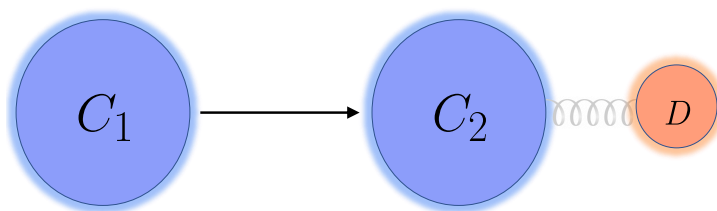
Figure 4.1: The Drude oscillator based polarizable force field.

In Drude polarizable force field, the particle *C1* in Figure 4.1 can be separated into an particle *C2* and *D*, which is an auxiliary particle attached to the polarizable atom via a harmonic spring. The half-stiffness K_D, the Drude charge q_D and the atomic polarizability α are connected as:

$$K_D = \frac{1}{2}\frac{q_D^2}{\alpha} \tag{4.1}$$

There are two different implementations of Drude polarizable force field, including that proposed by Lamoureux and Roux[64] and that by Schroder and Steinhauser.[66] Details about the difference between the two schemes and usage in LAMMPS can be found in Ref.[67].

In this thesis, we used the ONIOM(QM:QM') method to calculate the electrostatic interactions between solute and solvent molecules in the systems. The energy of a full system $E_{full}^{QM:QM'}$ is calculated as:

$$E_{full}^{QM:QM'} = E_{core}^{QM} + E_{full}^{QM'} - E_{core}^{QM'} \tag{4.2}$$

where E_{core}^{QM} is the energy of the core area (usually the isolated solute molecule) using a high-level QM method, $E_{full}^{QM'}$ is the energy of the full system (both solute and solvent molecules) using a low-level QM' method, and $E_{core}^{QM'}$ is the energy of the core area using the low-level QM' method. Although more advanced and accurate QM/QM' embedding methods exist[68–71], the accuracy of the energy obtained with this ONIOM(QM:QM') scheme is well accepted, as can be seen in the discussions in Section 4.2 and Section 5.2.

(2) With the above point, the central question is how the ordered solvent environments influence reaction kinetics. Besides, several questions remain unanswered. For example, how to characterize and compare the order degree of different ionic liquids using both computed and experimental techniques? How to correlate the computed and observed quantities? Thus, the second aim of this chapter is developing both experimental and computational methods to characterize the degree of order in ionic liquids. In short, OCP is utilized to characterize the lifetime and degree of order of ionic liquids. The measured OCP result is correlated with calculated quantities including ion dipole projections, diffusion coefficient of cation, and its volume from the trajectory of our polarizable molecular dynamic simulations of RTILs, for each of [EMIM][PF$_6$], [HMIM][PF$_6$], [EMIM][EtSO$_4$] and [BMIM][NTf$_2$].

In summary, the two works in this chapter focus on structures and properties of ordered solvent environments as well as their potential use in electrostatic catalysis. Bubble surface, as another type of complex solvent environment for electrostatic catalysis, will be introduced in the next chapter. Modelling these complex solvent environments beyonds the capability of implicit solvent models mentioned in Chapter 3. Studies in this field are useful not only for understanding catalysis effects, but also useful as a test for further development of accurate multi-scale methods for MD simulations and energy calculations.

4.2 Publication 4

Ordered Solvents and Ionic Liquids Can Be Harnessed for Electrostatic Catalysis

Longkun Xu, Ekaterina I. Izgorodina, Michelle L. Coote

Order Is Power
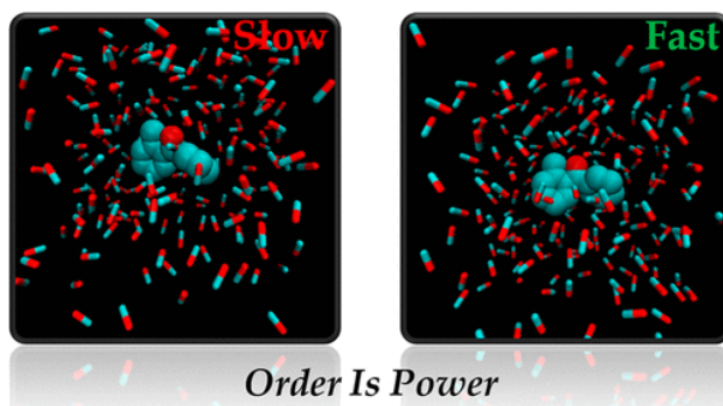
This publication is a peer-reviewed manuscript published in *Journal of the American Chemical Society*. All computational results and subsequent discussion were my own work under the supervision of Prof. Ekaterina I. Izgorodina and Prof. Michelle Coote, who co-edited the manuscript. Supporting information is available online (https://pubs.acs.org/doi/10.1021/jacs.0c05643). The document for the statement of contributions is placed in the Appendix. This research was highlighted in Chemistry in Australia.

J|A|C|S

JOURNAL OF THE AMERICAN CHEMICAL SOCIETY

Article

Ordered Solvents and Ionic Liquids Can Be Harnessed for Electrostatic Catalysis

Longkun Xu, Ekaterina I. Izgorodina,* and Michelle L. Coote*

Cite This: *J. Am. Chem. Soc.* 2020, 142, 12826−12833

Read Online

ACCESS | Metrics & More | Article Recommendations | Supporting Information

ABSTRACT: Herein, we employ classical molecular dynamics simulations using the Drude oscillator-based polarizable force field, quantum chemical calculations, and ONIOM multiscale calculations to study (a) how an external field orders the solvent environment in a chemical reaction and then (b) whether in the absence of this same applied field the ordered solvent environment alone can electrostatically catalyze a chemical reaction when compared with the corresponding disordered solvent. Our results show that a 0.2 V/Å external electric field, which is below the threshold for bond breaking of solvent molecules, leads to significant ordering of bulk methanol solvent and the ionic liquid $[EMIM][BF_4]$. Importantly, in the absence of this same field, the ordered solvent lowers the activation energy of the hydrogen-transfer reaction of *o*-alkylphenyl ketones in excess of 20 kcal/mol when the solvent is methanol and by over 30 kcal/mol for $[EMIM][BF_4]$. Even a 0.1 V/Å external field has effects of ca. 10 and 20 kcal/mol, respectively. This work suggests a possible strategy for scaling electrostatic catalysis by applying a pulsed external field to the reaction medium to maintain solvent ordering while allowing the reaction to proceed largely in the absence of an external field.

Order Is Power
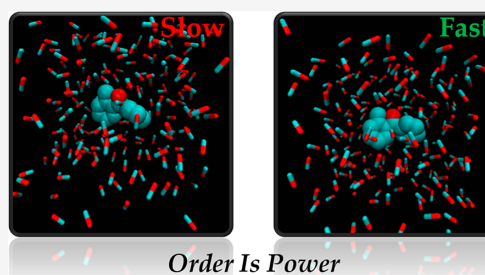
INTRODUCTION

The role of the electrostatic environment in catalyzing chemical reactions has long been an important research field. Two classical examples are Marcus theory[1,2] and enzyme catalysis.[3−6] In Marcus theory, solvent reorganization is the driving force for electron-transfer reactions, though internal reorganization can also be large. One of the explanations for enzyme catalysis is that the enzyme can stabilize the polar transition state via electrostatic interactions.[3,4,7]

In recent years, much research has been directed at harnessing electric fields for catalyzing and manipulating chemical reactions beyond enzymes.[8−10] While much of this work has been computational, experiments have shown that external electric fields (EEFs) delivered via scanning tunneling microscopy (STM) can catalyze bond-forming[11] and bond-breaking reactions.[12] While these experiments are difficult to scale for chemical synthesis, we have shown that the electric fields from remote charged functional groups, embedded on the substrate or a catalyst, can be used to catalyze chemical reactions and alter their outcome.[13−25] The charged group can be a Lewis acid or Bronsted acid or base whose charge and hence electric field can be altered with pH. While again much of the work to date has been computational, experiments have validated these predictions in a growing number of systems.[17−20,26,27] Others have shown that electrostatic effects are responsible for the catalytic effect of metal-ion clusters on gas-phase reactions[28−30] and that electrostatic effects are of general importance in heterogeneous catalysis.[31]

Despite these advances, there remain fundamental barriers to taking full advantage of electrostatic catalysis. On one hand, use of charged groups is an effective and scalable way to exert very precise electrostatic control over chemical reactions. However, the magnitude of such effects can be compromised by solvent attenuation, particularly as the solubility of the charged species in low-polarity solvents is often low. Use of external electric fields avoids solubility issues, but STM experiments are very small in scale, while scale up using electrodes has thus far resulted in electrochemical reactions.[12] While these may be useful in their own right[32] and while the electric fields undoubtedly influence the electrochemical processes themselves,[33,34] use of external fields to afford significant electrostatic catalysis in solution is yet to be realized.

To use external electric fields for electrostatic catalysis alternative approaches are required. One such approach is to use external fields to orient the solvent environment. The ordering of the solvent and ionic liquids (ILs) induced by an external electric field has already been reported by several groups. For example, Foroutan-Nejad and co-workers found

12826

EEFs can break the solvation shell and thus affect the ion–receptor interactions.[35] Laird and co-workers reported that the structure of the solvent framework and associated dielectric properties can be changed by an electric field.[36] Matta and co-workers showed that the electric field of a laser pulse can be used to eliminate (or even invert) a potential energy barrier of a reaction.[37,38] The ordering of the network of ionic liquids, which offer many advantages,[39−41] can also be changed by factors including the electric field, temperature, and length of the side chain of cations and metal surfaces, as shown by Wang, Voth, and Pádua.[42−45]

Recent computational work has shown that external fields can both order the solvent environment and catalyze chemical reactions.[46−50] However, given the propensity for external electric fields to trigger electrochemical reactions, a more practical question is whether, in the absence of a field, local electric fields within the ordered solvent environment itself are sufficient to catalyze a chemical reaction. Thus, solvents could be preordered with a field, and then reactions would be allowed to proceed without the external electric present. This could be carried out by pulsing the applied potential, thereby minimizing exposure to the external potential. While in a normal electrochemical cell the potential beyond the double layer is negligible, bipolar cells[51] could address this problem. Indeed, solvents could be preordered in other ways such as using microfluidics.

In this work, we use both Drude oscillator-based polarizable classical molecular dynamic (MD) simulations and multiscale quantum chemical calculations to determine if an ordered solvent environment is enough to catalyze a chemical reaction in the absence of an applied electric field. As a case study, we examine a hydrogen-transfer reaction of o-alkylphenyl ketones taken from our recent work (Figure 1).[24] We consider two solvent environments, methanol and the ionic liquid [EMIM]-[BF$_4$], where EMIM is the 1-ethyl-3-methylimidazolium cation.

■ RESULTS AND DISCUSSION

Classical molecular dynamics simulations using the Drude oscillator-based polarizable force field,[53−55] quantum chemical calculations, and ONIOM multiscale calculations were used to
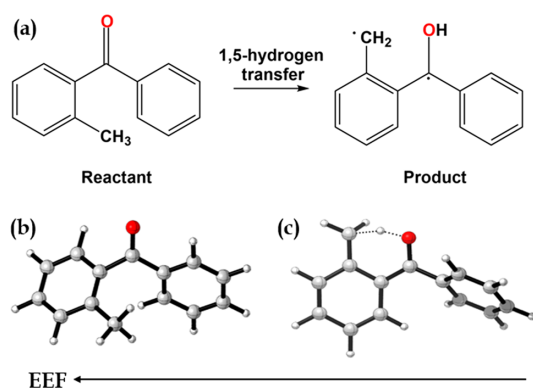
Figure 1. (a) Hydrogen-transfer reaction of o-alkylphenyl ketones. Optimized structures of the reactant (b) and transition state (c) of this reaction and the direction of the EEF. For more details of the reaction, see ref 24. Structures are rendered using the CYLview program.[52]

study the ordering effect of an external field on the solvent environment in a chemical reaction and the effect of this solvent environment in the absence of the applied field. Figure 2 shows the general workflow used to order the solvent in the electric field and simulate its effects on the reaction in Figure 1. Full computational procedures and parameters are provided in the Supporting Information.

Effect of External Fields on the Solvent Environment. To visualize how the environment is ordered under the influence of an external electric field, the representative snapshots obtained with MD simulation of TS solute in methanol solvent and [EMIM][BF$_4$] ionic liquids under 0 and 0.2 V/Å electric fields are shown in Figure 3.

It can be seen from Figure 3 that the distribution of methanol solvent molecules in the simulation box changes obviously after a 0.2 V/Å external electric field is applied. In Figure 3a, methanol solvent molecules are distributed randomly, while in Figure 3b, most O atoms of methanol point to the right because the external electric field is pointing to the left and the O atoms have negative partial charge. Conversely, the methyl groups which have a positive partial charge point in the opposite direction. Thus, the internal electric field runs from left to right, opposite to that of the external electric field.

In contrast, the change of the distribution of [EMIM][BF$_4$] resulting from the external electric field is less obvious. One possible reason is that the ionic liquids environment has two types of molecules (cations and anions). Unlike methanol molecules, the cations and anions move independently of one another. Besides, the cations and anions can form strong electrostatic interactions with their near neighbors that drown out higher level ordering. This competition between the external electric field and the electrostatic interactions between ions can also be found in the work of Wang.[44] Use of stronger fields can overcome this;[44] however, because the bonds of the methanol solvent might be broken under a higher electric field,[77] as reported by Saitta and co-workers, we do not consider electric fields larger than 0.2 V/Å for all environments.

Although the ordering of ionic liquids is less obvious, it can be confirmed by the results of the radial distribution function (RDF) in Figure 4. The RDFs in normal and ordered ionic liquids are obtained using the Travis program.[67] Only the distances from 0 to 1700 pm are shown here. Full details can be found in Table S8. The distance between the cation and the nearest anion is around 500 pm, but the radial distribution function $g(r)$ obtained in normal ionic liquids is much larger than that in ordered ionic liquids. This can be explained by comparing the simplified structures of normal and ordered ionic liquids in Figure 4b and 4c. In normal ionic liquids, the cations and anions usually form the alternative charge structures, like Figure 4b, as shown in Figure 2 of the work of Izgorodina and co-workers.[78] When an external electric field is applied, the structure can be changed to Figure 4c, where closer cation−cation and anion−anion distances become possible. The most classical example for this is probably the electrochemical double layer, for example, see Figure 3 in the work of Sharma and co-worker[79] This point has been also discussed in the works of Kaneko[80] and Kornyshev.[81] With the change from normal ionic liquids to ordered ionic liquids, the closer cation−cation and anion−anion pairs become possible; thus, the number of nearest cation−anion pairs decreases. As a result, our calculated RDF in Figure 4a indicates the ordering
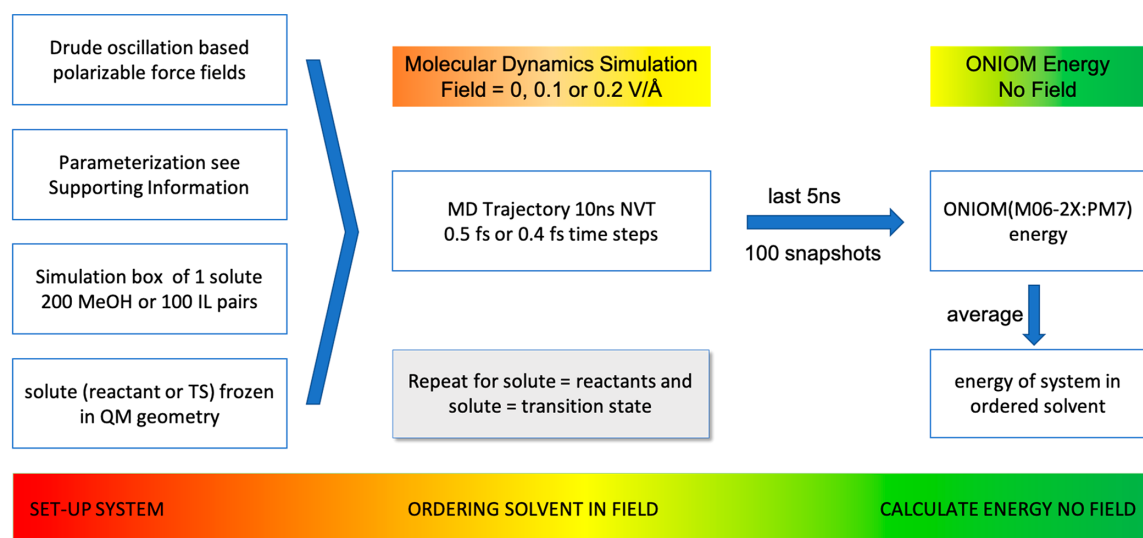
Figure 2. Workflow to calculate the activation energies. CL&Pol (KSDrude) force field[56−58] was used for the ionic liquid (IL) and OPLS-AA force field[59] for the methanol and solute. Force-field parameters and polarizabilities were taken from the literature and/or calculated using published methods[60−66] and are provided in Tables S1−S6 of the Supporting Information. The simulation box, with periodic boundary conditions, initially has a size of 25 and 34 Å for methanol and the IL, respectively. Molecular dynamics simulations are performed using the Nosé−Hoover thermostat and barostat with time steps of 0.5 and 0.4 fs for simulations in methanol and [EMIM][BF$_4$], respectively. From the last 5 ns the NVT simulations we extract 100 snapshots using the cut function of the Travis program.[67] Energy in each snapshot is calculated with ONIOM[68](M062X[69]/def2-TZVPP:[70]PM7[71]). Number of snapshots required to obtain an accurate barrier height is determined by benchmarking using high-level quantum chemical results obtained with the methods presented in refs 72−75. Full details of all calculations are in the Supporting Information.
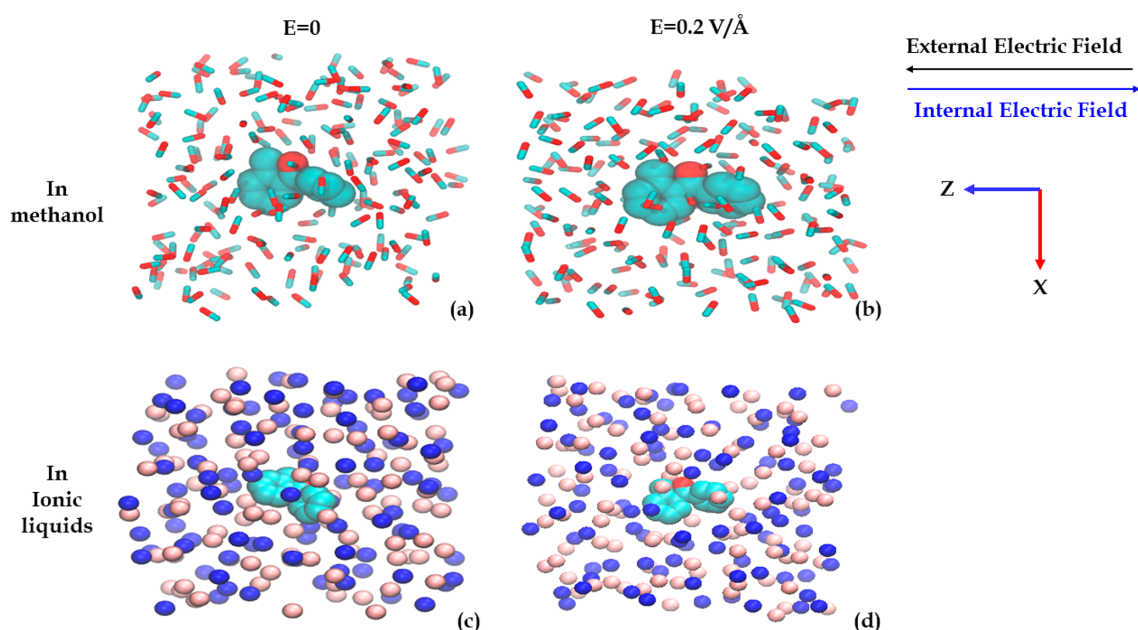
Figure 3. Snapshots obtained without and with a 0.2 V/Å external electric field of the TS solute molecule in methanol (a and b) and in [EMIM][BF$_4$] ionic liquids (c and d). For clarity, only non-hydrogen atoms of the solute molecule are shown in the VDW drawing method. Only C (in green) and O (in red) atoms of the methanol molecules (a and b) are shown. Only N (in blue, atom N3 in Figure 4d) and B (in pink) atoms representing the mass centers of the cations and anions, respectively, of [EMIM][BF$_4$] ionic liquids (c and d) are shown. All pictures are rendered using the VMD program.[76] External electric field is applied along the z direction.
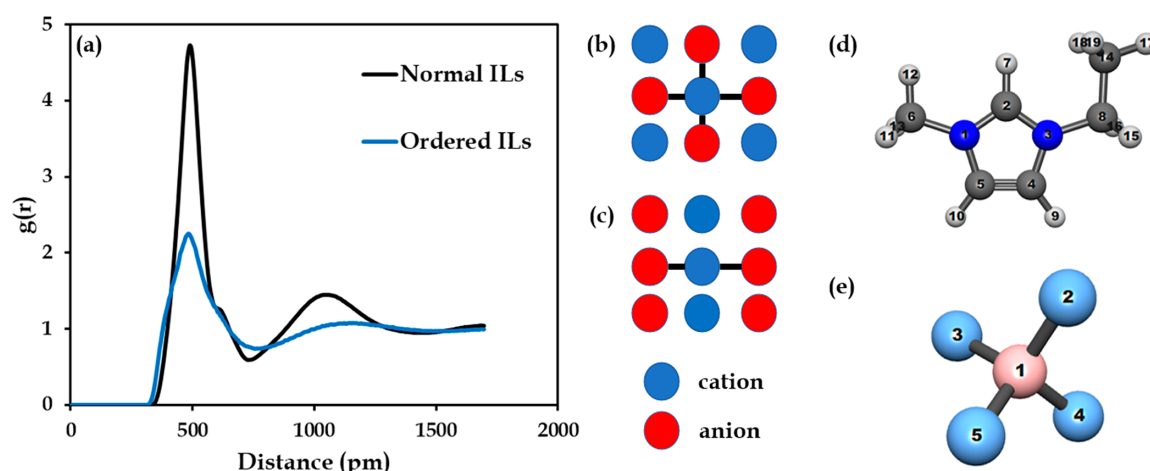
Figure 4. (a) Radial distribution function (RDF) between [EMIM] C2 atoms and [BF$_4$] B1 atoms in normal and ordered ionic liquids. (b and c) Simplified model of normal ionic liquids and ordered ionic liquids, respectively, where the interactions between the center cation and the nearest anion are labeled. (d and e) Structure of the cation and anion and their atomic index, respectively; pictures are rendered using the IQmol program.[82]

of ionic liquids does happen, although it is less obvious in Figure 3d.

Effect of Ordered Solvent Environment on Reactions. Figure 5 shows the activation energy in normal and ordered
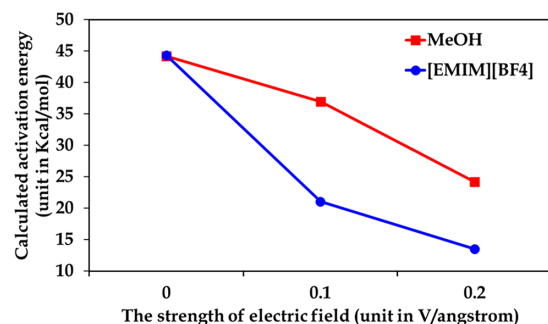
Figure 5. Calculated activation energy obtained in methanol solvent and the ionic liquid [EMIM][BF$_4$] without an external electric field as a function of the field strength used to order the surrounding solvent environment.

environments. We again stress that these species are calculated without the external field present; the field strength refers to that used to order the solvent environment. The energy used to calculate the activation energy is obtained by averaging the ensemble of snapshots (full details can be found in Tables S9 and S10).

From Figure 5 we can see the activation energy in both methanol and [EMIM][BF$_4$] is decreased in the presence of the ordered solvent environment. In methanol, the activation energy changes substantially from 44.20 kcal mol^{-1} in normal methanol solvent to 36.96 kcal mol^{-1} in ordered methanol solvent formed by a 0.1 V Å^{-1} electric field and then changes to 24.19 kcal/mol in ordered methanol solvent formed by a 0.2 V Å^{-1} electric field. Similarly, the obtained activation energy decreases from 44.34 kcal mol^{-1} in normal disordered ionic liquids to 21.03 and 13.49 kcal mol^{-1} in ordered ionic liquids

formed by, respectively, 0.1 and 0.2 V Å^{-1} external electric field.

The electrostatic origin of the barrier lowering is evident in Figure 6, which shows representative snapshots from the MD simulation without and with the 0.2 V Å^{-1} electric field. Also shown are the corresponding dipole moments of the system and the reaction axis.[9] The reaction axis is the direction along which the electrons reorganize from reactant-like to product-like bonding (in this case, the local dipole moment across the forming and breaking bonds). A field aligned parallel with the reaction axis stabilizes the transition state. Without an external electric field, solvent molecules are randomly distributed and the dipole moment is almost is perpendicular to the reaction axis. With the external electric field, the dipole moment is larger, its direction is nearly parallel to the reaction axis, and its polarity is primed to stabilize transition state, hence accounting for the barrier lowering observed.

We note that the actual activation barrier decrease measured from experiment might be smaller than what we calculate. The reasons are 2-fold. First, in our MD simulation, the external electric field is identically applied to all particles in the system while the electric field strength felt by different particles in the experimental electrochemical cell should be different and depend on the distance from the charged electrodes. However, as noted in the Introduction, use of bipolar electrochemical cells could address this problem.

Second, we assume the solvent remains ordered through the whole reaction process. The relaxation from ordered solvent to normal disordered solvent is ignored. Thus, a time-dependent nonequilibrium simulation should give more accurate results. However, these are beyond the scope of the present work. Instead, we note that experimental studies report that liquid solvents such as methanol relax on the order of 0.1−10 ps,[83] which is faster than the time scale of our reaction. However, for ionic liquids relaxation times are slower and can be tuned through cation and anion choice. Typically, relaxation times on the order of 1 s are observed over temperature ranges of 300−330 K,[84,85] but longer times of up to 100s are frequently reported.[86] These are longer than the corresponding half-life of
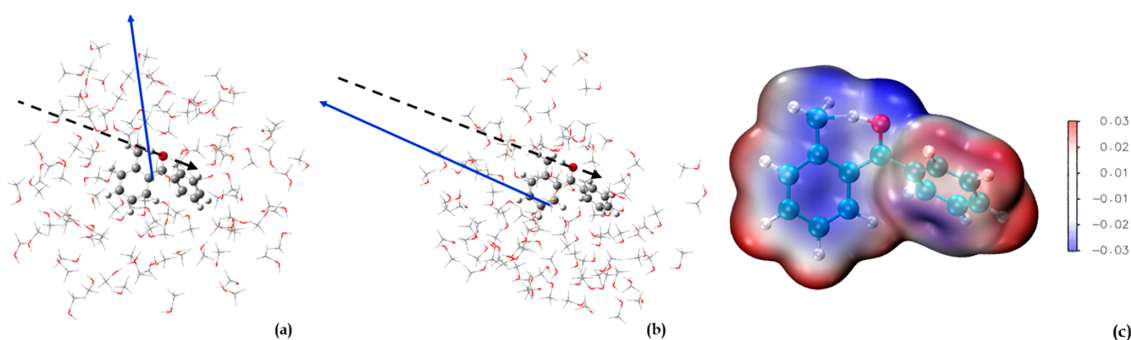
Figure 6. Representative snapshots from the MD simulation (a) without and (b) with 0.2 V Å^{-1} electric field. Dipole moment direction is in blue, while black dashed line represents the reaction axis.[9] Note that the length of the blue line in b has been scaled; magnitude of the dipole moment in b, 146.46 D, is around four times of that of a, 37.06 D. (c) Electrostatic potential (unit in au) within the isolated transition state, as calculated in continuum water.

the reaction studied here in the ordered ionic liquid (10^2-10^1 s at 0.1 V Å^{-1} and $10^{-3}-10^{-4}$ s at 0.2 V Å^{-1} for 300 and 330 K, respectively).

CONCLUSION

In summary, we propose a new strategy for electrostatic catalysis. Using ordered solvent and ionic liquids to catalyze reactions is environmentally friendly and can effectively solve the solvent-attenuation problem in current electrostatic catalysis. Results of the hydrogen-transfer reaction of o-alkylphenyl ketones obtained by combining polarizable classical MD simulation with ONIOM energy calculation indicate that both ordered methanol solvent and [EMIM]-[BF$_4$] ionic liquids can help decrease the activation energy significantly. Using larger electric field strengths can make the environment more ordered, which provides stronger electrostatic catalysis effects. Currently, we are undertaking experimental work in our group to validate the computational predictions. However, tentative experimental support for our work comes from the results of Slattery and co-workers, who showed that liquid-crystalline ionic liquids (ICILs) can work as an ordered reaction medium driven by the temperature change to change the exo/endo ratio of the Diels−Alder reaction.[87] More generally, our work suggests that electrostatic effects on solution-phase catalysis should not be ignored when studying other ordered environments such as at electrochemical interfaces or in nanoconfined environments.

ASSOCIATED CONTENT

ⓈⒾ Supporting Information

The Supporting Information is available free of charge at https://pubs.acs.org/doi/10.1021/jacs.0c05643.

> All computational procedures along with details of the parameters, determination of the suitable number of snapshots, benchmarking, raw data used in calculating RDF, energy calculated in each snapshot (PDF)

AUTHOR INFORMATION

Corresponding Authors

Michelle L. Coote − *ARC Centre of Excellence for Electromaterials Science, Research School of Chemistry, Australian National University, Canberra, Australian Capital Territory 2601, Australia;* ⓞ orcid.org/0000-0003-0828-7053; Email: michelle.coote@anu.edu.au

Ekaterina I. Izgorodina − *Monash Computational Chemistry Group, School of Chemistry, Monash University, Clayton, Victoria 3800, Australia;* ⓞ orcid.org/0000-0002-2506-4890; Email: katya.pas@monash.edu

Author

Longkun Xu − *ARC Centre of Excellence for Electromaterials Science, Research School of Chemistry, Australian National University, Canberra, Australian Capital Territory 2601, Australia;* ⓞ orcid.org/0000-0001-7314-2913

Complete contact information is available at:
https://pubs.acs.org/10.1021/jacs.0c05643

Author Contributions

The manuscript was written through contributions of all authors. All authors have given approval to the final version of the manuscript.

Notes

The authors declare no competing financial interest.

REFERENCES

(1) Marcus, R. A. On the Theory of Oxidation-Reduction Reactions Involving Electron Transfer I. *J. Chem. Phys.* **1956**, *24*, 966−978.

(2) Ghosh, S.; Horvath, S.; Soudackov, A. V.; Hammes-Schiffer, S. Electrochemical Solvent Reorganization Energies in the Framework of the Polarizable Continuum Model. *J. Chem. Theory Comput.* **2014**, *10*, 2091−2102.

(3) Warshel, A.; Sussman, F. Toward computer-aided site-directed mutagenesis of enzymes. *Proc. Natl. Acad. Sci. U. S. A.* **1986**, *83*, 3806−3810.

(4) Warshel, A.; Sharma, P. K.; Kato, M.; Xiang, Y.; Liu, H.; Olsson, M. H. Electrostatic basis for enzyme catalysis. *Chem. Rev.* **2006**, *106*, 3210−3235.

(5) Fried, S. D.; Boxer, S. G. Electric Fields and Enzyme Catalysis. *Annu. Rev. Biochem.* **2017**, *86*, 387−415.

(6) Romei, M. G.; Lin, C. Y.; Mathews, I. I.; Boxer, S. G. Electrostatic control of photoisomerization pathways in proteins. *Science* **2020**, *367*, 76−79.

(7) Wu, Y.; Fried, S. D.; Boxer, S. G. A Preorganized Electric Field Leads to Minimal Geometrical Reorientation in the Catalytic Reaction of Ketosteroid Isomerase. *J. Am. Chem. Soc.* **2020**, *142*, 9993−9998.

(8) Ciampi, S.; Darwish, N.; Aitken, H. M.; Díez-Pérez, I.; Coote, M. L. Harnessing electrostatic catalysis in single molecule, electrochemical and chemical systems: a rapidly growing experimental tool box. *Chem. Soc. Rev.* **2018**, *47*, 5146−5164.

(9) Shaik, S.; Ramanan, R.; Danovich, D.; Mandal, D. Structure and reactivity/selectivity control by oriented-external electric fields. *Chem. Soc. Rev.* **2018**, *47*, 5125−5145.

(10) Shaik, S.; Mandal, D.; Ramanan, R. Oriented electric fields as future smart reagents in chemistry. *Nat. Chem.* **2016**, *8*, 1091−1098.

(11) Aragones, A. C.; Haworth, N. L.; Darwish, N.; Ciampi, S.; Bloomfield, N. J.; Wallace, G. G.; Diez-Perez, I.; Coote, M. L. Electrostatic catalysis of a Diels-Alder reaction. *Nature* **2016**, *531*, 88−91.

(12) Zhang, L.; Laborda, E.; Darwish, N.; Noble, B. B.; Tyrell, J. H.; Pluczyk, S.; Le Brun, A. P.; Wallace, G. G.; Gonzalez, J.; Coote, M. L.; Ciampi, S. Electrochemical and electrostatic cleavage of alkoxyamines. *J. Am. Chem. Soc.* **2018**, *140*, 766−774.

(13) Gryn'ova, G.; Coote, M. L. Origin and Scope of Long-Range Stabilizing Interactions and Associated SOMO-HOMO Conversion in Distonic Radical Anions. *J. Am. Chem. Soc.* **2013**, *135*, 15392−15403.

(14) Blyth, M. T.; Coote, M. L. A pH-Switchable Electrostatic Catalyst for the Diels-Alder Reaction: Progress toward Synthetically Viable Electrostatic Catalysis. *J. Org. Chem.* **2019**, *84*, 1517−1522.

(15) Hill, N. S.; Coote, M. L. Internal Oriented Electric Fields as a Strategy for Selectively Modifying Photochemical Reactivity. *J. Am. Chem. Soc.* **2018**, *140*, 17800−17804.

(16) Yu, L. J.; Coote, M. L. Electrostatic Switching between S_N1 and S_N2 Pathways. *J. Phys. Chem. A* **2019**, *123*, 582−589.

(17) Gryn'Ova, G.; Marshall, D. L.; Blansby, S. J.; Coote, M. L. Switching radical stability by pH-induced orbital conversion. *Nat. Chem.* **2013**, *5*, 474.

(18) Noble, B. B.; Smith, L. M.; Coote, M. L. The effect of $LiNTf_2$ on the propagation rate coefficient of methyl methacrylate. *Polym. Chem.* **2014**, *5*, 4974−4983.

(19) Noble, B. B.; Mater, A. C.; Smith, L. M.; Coote, M. L. The effects of Lewis acid complexation on type I radical photoinitiators and implications for pulsed laser polymerization. *Polym. Chem.* **2016**, *7*, 6400−6412.

(20) Gryn'ova, G.; Smith, L. M.; Coote, M. L. Computational design of pH-switchable control agents for nitroxide mediated polymerization. *Phys. Chem. Chem. Phys.* **2017**, *19*, 22678−22683.

(21) Gryn'ova, G.; Coote, M. L. Directionality and the role of polarization in electric field effects on radical stability. *Aust. J. Chem.* **2017**, *70*, 367−372.

(22) Aitken, H. M.; Coote, M. L. Can electrostatic catalysis of Diels−Alder reactions be harnessed with pH-switchable charged functional groups? *Phys. Chem. Chem. Phys.* **2018**, *20*, 10671−10676.

(23) Hill, N. S.; Coote, M. L. Strategies for Red-Shifting Type I Photoinitiators: Internal Electric Fields versus Lewis Acids versus Increasing Conjugation. *Aust. J. Chem.* **2019**, *72*, 627−632.

(24) Blyth, M. T.; Noble, B. B.; Russell, I. C.; Coote, M. L. Oriented Internal Electrostatic Fields Cooperatively Promote Ground- and Excited-State Reactivity: A Case Study in Photochemical CO2 Capture. *J. Am. Chem. Soc.* **2020**, *142*, 606−613.

(25) Joy, J.; Stuyver, T.; Shaik, S. Oriented External Electric Fields and Ionic Additives Elicit Catalysis and Mechanistic Crossover in Oxidative Addition Reactions. *J. Am. Chem. Soc.* **2020**, *142*, 3836−3850.

(26) Klinska, M.; Smith, L. M.; Gryn'ova, G.; Banwell, M. G.; Coote, M. L. Experimental demonstration of pH-dependent electrostatic catalysis of radical reactions. *Chem. Sci.* **2015**, *6*, 5623−5627.

(27) Jiang, J. Y.; Smith, L. M.; Tyrell, J. H.; Coote, M. L. Pulsed laser polymerisation studies of methyl methacrylate in the presence of AlCl 3 and ZnCl 2−evidence of propagation catalysis. *Polym. Chem.* **2017**, *8*, 5948−5953.

(28) Yue, L.; Li, J.; Zhou, S.; Sun, X.; Schlangen, M.; Shaik, S.; Schwarz, H. Control of product distribution and mechanism by ligation and electric field in the thermal activation of methane. *Angew. Chem., Int. Ed.* **2017**, *56*, 10219−10223.

(29) Geng, C.; Li, J.; Schlangen, M.; Shaik, S.; Sun, X.; Wang, N.; Weiske, T.; Yue, L.; Zhou, S.; Schwarz, H. Oriented external electric fields as mimics for probing the role of metal ions and ligands in the thermal gas-phase activation of methane. *Dalton Trans.* **2018**, *47*, 15271−15277.

(30) Yue, L.; Wang, N.; Zhou, S.; Sun, X.; Schlangen, M.; Schwarz, H. The electric field as a "smart" ligand in controlling the thermal activation of methane and molecular hydrogen. *Angew. Chem., Int. Ed.* **2018**, *57*, 14635−14639.

(31) Che, F.; Gray, J. T.; Ha, S.; Kruse, N.; Scott, S. L.; McEwen, J.-S. Elucidating the roles of electric fields in catalysis: A perspective. *ACS Catal.* **2018**, *8*, 5153−5174.

(32) Norcott, P. L.; Hammill, C. L.; Noble, B. B.; Robertson, J. C.; Olding, A.; Bissember, A. C.; Coote, M. L. TEMPO−Me: An Electrochemically Activated Methylating Agent. *J. Am. Chem. Soc.* **2019**, *141*, 15450−15455.

(33) Vogel, Y. B.; Zhang, L.; Darwish, N.; Goncales, V. R.; Le Brun, A.; Gooding, J. J.; Molina, A.; Wallace, G. G.; Coote, M. L.; Gonzalez, J.; Ciampi, S. Reproducible flaws unveil electrostatic aspects of semiconductor electrochemistry. *Nat. Commun.* **2017**, *8*, 1−9.

(34) Zhang, L.; Vogel, Y. B.; Noble, B. B.; Goncales, V. R.; Darwish, N.; Brun, A. L.; Gooding, J. J.; Wallace, G. G.; Coote, M. L.; Ciampi, S. TEMPO monolayers on Si (100) electrodes: electrostatic effects by the electrolyte and semiconductor space-charge on the electroactivity of a persistent radical. *J. Am. Chem. Soc.* **2016**, *138*, 9611−9619.

(35) Novak, M.; Foroutan-Nejad, C.; Marek, R. Solvent effects on ion-receptor interactions in the presence of an external electric field. *Phys. Chem. Chem. Phys.* **2016**, *18*, 30754−30760.

(36) Daniels, I. N.; Wang, Z. X.; Laird, B. B. Dielectric Properties of Organic Solvents in an Electric Field. *J. Phys. Chem. C* **2017**, *121*, 1025−1031.

(37) Bandrauk, A. D.; Sedik, E.-W. S.; Matta, C. F. Effect of absolute laser phase on reaction paths in laser-induced chemical reactions. *J. Chem. Phys.* **2004**, *121*, 7764−7775.

(38) Bandrauk, A. D.; Sedik, E. L. W. S.; Matta, C. F. Laser control of reaction paths in ion−molecule reactions. *Mol. Phys.* **2006**, *104*, 95−102.

(39) Hallett, J. P.; Welton, T. Room-temperature ionic liquids: solvents for synthesis and catalysis. 2. *Chem. Rev.* **2011**, *111*, 3508−3576.

(40) Izgorodina, E. I.; Seeger, Z. L.; Scarborough, D. L.; Tan, S. Y. Quantum chemical methods for the prediction of energetic, physical, and spectroscopic properties of ionic liquids. *Chem. Rev.* **2017**, *117*, 6696−6754.

(41) Halat, P.; Seeger, Z. L.; Barrera Acevedo, S.; Izgorodina, E. I. Trends in two-and three-body effects in multiscale clusters of ionic liquids. *J. Phys. Chem. B* **2017**, *121*, 577−588.

(42) Wang, Y. T.; Izvekov, S.; Yan, T. Y.; Voth, G. A. Multiscale coarse-graining of ionic liquids. *J. Phys. Chem. B* **2006**, *110*, 3564−3575.

(43) Wang, Y.; Jiang, W.; Yan, T.; Voth, G. A. Understanding ionic liquids through atomistic and coarse-grained molecular dynamics simulations. *Acc. Chem. Res.* **2007**, *40*, 1193−1199.

(44) Wang, Y. T. Disordering and Reordering of Ionic Liquids under an External Electric Field. *J. Phys. Chem. B* **2009**, *113*, 11058−11060.

(45) Mendonca, A. C. F.; Malfreyt, P.; Padua, A. A. H. Interactions and ordering of ionic liquids at a metal surface. *J. Chem. Theory Comput.* **2012**, *8*, 3348−3355.

(46) Dutta Dubey, K.; Stuyver, T.; Kalita, S.; Shaik, S. Solvent-Organization and Rate-Regulation of a Menshutkin Reaction by Oriented-External Electric Fields are Revealed by Combined MD and QM/MM Calculations. *J. Am. Chem. Soc.* **2020**, *142*, 9955−9965.

(47) Herron, J. A.; Morikawa, Y.; Mavrikakis, M. Ab initio molecular dynamics of solvation effects on reactivity at electrified interfaces. *Proc. Natl. Acad. Sci. U. S. A.* **2016**, *113*, E4937−E4945.

(48) Cassone, G.; Pietrucci, F.; Saija, F.; Guyot, F.; Saitta, A. M. One-step electric-field driven methane and formaldehyde synthesis from liquid methanol. *Chem. Sci.* **2017**, *8*, 2329−2336.

(49) Cassone, G.; Pietrucci, F.; Saija, F.; Guyot, F.; Sponer, J.; Sponer, J. E.; Saitta, A. M. Novel electrochemical route to cleaner fuel dimethyl ether. *Sci. Rep.* **2017**, *7*, 1−9.

(50) Arabi, A. A.; Matta, C. F. Effects of external electric fields on double proton transfer kinetics in the formic acid dimer. *Phys. Chem. Chem. Phys.* **2011**, *13*, 13738−13748.

(51) Shida, N.; Zhou, Y.; Inagi, S. Bipolar Electrochemistry: A Powerful Tool for Electrifying Functional Material Synthesis. *Acc. Chem. Res.* **2019**, *52*, 2598−2608.

(52) Legault, C. Y., *CYLview, 1.0b*; Université de Sherbrooke, 2009; http://www.cylview.org (accessed May 21, 2020).

(53) Lemkul, J. A.; Huang, J.; Roux, B.; MacKerell, A. D., Jr An empirical polarizable force field based on the classical drude oscillator model: development history and recent applications. *Chem. Rev.* **2016**, *116*, 4983−5013.

(54) Lamoureux, G.; Roux, B. Modeling induced polarization with classical Drude oscillators: Theory and molecular dynamics simulation algorithm. *J. Chem. Phys.* **2003**, *119*, 3025−3039.

(55) Dequidt, A.; Devemy, J.; Padua, A. A. Thermalized Drude oscillators with the LAMMPS molecular dynamics simulator. *J. Chem. Inf. Model.* **2016**, *56*, 260−268.

(56) Goloviznina, K.; Canongia Lopes, J. N.; Costa Gomes, M.; Pádua, A. A. Transferable, Polarizable Force Field for Ionic Liquids. *J. Chem. Theory Comput.* **2019**, *15*, 5858−5871.

(57) Canongia Lopes, J. N.; Deschamps, J.; Padua, A. A. H. Modeling ionic liquids using a systematic all-atom force field. *J. Phys. Chem. B* **2004**, *108*, 2038−2047.

(58) Canongia Lopes, J. N.; Padua, A. A. H. Molecular force field for ionic liquids III: Imidazolium, pyridinium, and phosphonium cations; Chloride, bromide, and dicyanamide anions. *J. Phys. Chem. B* **2006**, *110*, 19586−19592.

(59) Jorgensen, W. L.; Maxwell, D. S.; TiradoRives, J. Development and testing of the OPLS all-atom force field on conformational energetics and properties of organic liquids. *J. Am. Chem. Soc.* **1996**, *118*, 11225−11236.

(60) Jorgensen, W. L.; Tirado-Rives, J. Potential energy functions for atomic-level simulations of water and organic and biomolecular systems. *Proc. Natl. Acad. Sci. U. S. A.* **2005**, *102*, 6665−6670.

(61) Dodda, L. S.; Vilseck, J. Z.; Tirado-Rives, J.; Jorgensen, W. L. 1.14*CM1A-LBCC: Localized Bond-Charge Corrected CM1A Charges for Condensed-Phase Simulations. *J. Phys. Chem. B* **2017**, *121*, 3864−3870.

(62) Dodda, L. S.; Cabeza de Vaca, I.; Tirado-Rives, J.; Jorgensen, W. L. LigParGen web server: an automatic OPLS-AA parameter generator for organic ligands. *Nucleic Acids Res.* **2017**, *45*, W331−W336.

(63) Heid, E.; Szabadi, A.; Schröder, C. Quantum mechanical determination of atomic polarizabilities of ionic liquids. *Phys. Chem. Chem. Phys.* **2018**, *20*, 10992−10996.

(64) *fftool*; https://github.com/agiliopadua/fftool (accessed Apr 7, 2020).

(65) Zeman, J.; Uhlig, F.; Smiatek, J.; Holm, C. A coarse-grained polarizable force field for the ionic liquid 1-butyl-3-methylimidazolium hexafluorophosphate. *J. Phys.: Condens. Matter* **2017**, *29*, 504004.

(66) *pol_il*; https://github.com/agiliopadua/pol_il (accessed Apr 7, 2020).

(67) Brehm, M.; Kirchner, B. TRAVIS-a free analyzer and visualizer for Monte Carlo and molecular dynamics trajectories. *J. Chem. Inf. Model.* **2011**, *51*, 2007−2023.

(68) Chung, L. W.; Sameera, W. M. C.; Ramozzi, R.; Page, A. J.; Hatanaka, M.; Petrova, G. P.; Harris, T. V.; Li, X.; Ke, Z.; Liu, F.; Li, H.-B.; Ding, L.; Morokuma, K. The ONIOM method and its applications. *Chem. Rev.* **2015**, *115*, 5678−5796.

(69) Zhao, Y.; Truhlar, D. G. The M06 suite of density functionals for main group thermochemistry, thermochemical kinetics, non-covalent interactions, excited states, and transition elements: two new functionals and systematic testing of four M06-class functionals and 12 other functionals. *Theor. Chem. Acc.* **2008**, *120*, 215−241.

(70) Weigend, F.; Ahlrichs, R. Balanced basis sets of split valence, triple zeta valence and quadruple zeta valence quality for H to Rn: Design and assessment of accuracy. *Phys. Chem. Chem. Phys.* **2005**, *7*, 3297−3305.

(71) Stewart, J. J. Optimization of parameters for semiempirical methods VI: more modifications to the NDDO approximations and re-optimization of parameters. *J. Mol. Model.* **2013**, *19*, 1−32.

(72) Xu, L.; Coote, M. L. Methods To Improve the Calculations of Solvation Model Density Solvation Free Energies and Associated Aqueous p K a Values: Comparison between Choosing an Optimal Theoretical Level, Solute Cavity Scaling, and Using Explicit Solvent Molecules. *J. Phys. Chem. A* **2019**, *123*, 7430−7438.

(73) Xu, L.; Coote, M. L. Improving the Accuracy of PCM-UAHF and PCM-UAKS Calculations Using Optimized Electrostatic Scaling Factors. *J. Chem. Theory Comput.* **2019**, *15*, 6958−6967.

(74) Riplinger, C.; Neese, F. An efficient and near linear scaling pair natural orbital based local coupled cluster method. *J. Chem. Phys.* **2013**, *138*, 034106.

(75) Wylie, L.; Oyaizu, K.; Karton, A.; Yoshizawa-Fujita, M.; Izgorodina, E. I. Toward improved performance of all-organic nitroxide radical batteries with ionic liquids: a theoretical perspective. *ACS Sustainable Chem. Eng.* **2019**, *7*, 5367−5375.

(76) Humphrey, W.; Dalke, A.; Schulten, K. VMD: visual molecular dynamics. *J. Mol. Graphics* **1996**, *14*, 33−38.

(77) Cassone, G.; Giaquinta, P. V.; Saija, F.; Saitta, A. M. Liquid methanol under a static electric field. *J. Chem. Phys.* **2015**, *142*, 054502.

(78) Seeger, Z. L.; Kobayashi, R.; Izgorodina, E. I. Cluster approach to the prediction of thermodynamic and transport properties of ionic liquids. *J. Chem. Phys.* **2018**, *148*, 193832.

(79) Sharma, P.; Bhatti, T. A review on electrochemical double-layer capacitors. *Energy Convers. Manage.* **2010**, *51*, 2901−2912.

(80) Futamura, R.; Iiyama, T.; Takasaki, Y.; Gogotsi, Y.; Biggs, M. J.; Salanne, M.; Segalini, J.; Simon, P.; Kaneko, K. Partial breaking of the Coulombic ordering of ionic liquids confined in carbon nanopores. *Nat. Mater.* **2017**, *16*, 1225−1232.

(81) Kondrat, S.; Kornyshev, A. Superionic state in double-layer capacitors with nanoporous electrodes. *J. Phys.: Condens. Matter* **2011**, *23*, 022201.

(82) *IQmol*; http://iqmol.org/ (accessed May 23, 2020).

(83) Lakowicz, J. R. Dynamics of Solvent and Spectral Relaxation. In *Principles of Fluorescence Spectroscopy*; Lakowicz, J. R., Ed.; Springer: Boston, MA, 2006; pp 237−276.

(84) Driver, G. W.; Huang, Y.; Laaksonen, A.; Sparrman, T.; Wang, Y. L.; Westlund, P. O. Correlated/non-correlated ion dynamics of charge-neutral ion couples: the origin of ionicity in ionic liquids. *Phys. Chem. Chem. Phys.* **2017**, *19*, 4975−4988.

(85) Green, S. M.; Ries, M. E.; Moffat, J.; Budtova, T. NMR and Rheological Study of Anion Size Influence on the Properties of Two Imidazolium-based Ionic Liquids. *Sci. Rep.* **2017**, *7*, 8968.

(86) Nishi, N.; Hirano, Y.; Motokawa, T.; Kakiuchi, T. Ultraslow relaxation of the structure at the ionic liquid|gold electrode interface to a potential step probed by electrochemical surface plasmon resonance measurements: asymmetry of the relaxation time to the potential-step direction. *Phys. Chem. Chem. Phys.* **2013**, *15*, 11615−11619.

(87) Bruce, D. W.; Gao, Y.; Canongia Lopes, J. N.; Shimizu, K.; Slattery, J. M. Liquid-Crystalline Ionic Liquids as Ordered Reaction Media for the Diels-Alder Reaction. *Chem. - Eur. J.* **2016**, *22*, 16113–16123.

4.3   Publication 5

Experimental Evidence of Long-Lived Electric Fields of Ionic Liquid Bi-layers

Mattia Belotti, Xin Lyu, <u>Longkun Xu</u>, Peter Halat, Nadim Darwish, Debbie S. Silvester,
Ching Goh, Ekaterina I. Izgorodina, Michelle L. Coote, Simone Ciampi
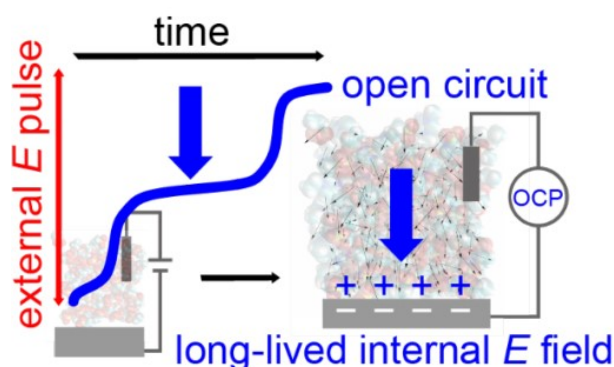
This publication is a manuscript published in *Journal of the American Chemical Society.* I am the first computational chemistry author of this work. I performed all preliminary calculations and wrote the initial discussion. These formed the basis for improved calculations that were performed by Peter Halat, whose results were the final ones included in the manuscript. Prof. Michelle L. Coote and Prof. Ekaterina I. Izgorodina supervised and co-wrote up the computational work, and the rest of the authors contributed to the experimental part of this work. Supporting information is available online (https://pubs.acs.org/doi/10.1021/jacs.1c06385). The document for the statement of contributions is placed in the Appendix. This research was highlighted in Chemistry in Australia.

J|A|C|S
JOURNAL OF THE AMERICAN CHEMICAL SOCIETY

Article

Experimental Evidence of Long-Lived Electric Fields of Ionic Liquid Bilayers

Mattia Belotti, Xin Lyu, Longkun Xu, Peter Halat, Nadim Darwish, Debbie S. Silvester, Ching Goh, Ekaterina I. Izgorodina,* Michelle L. Coote,* and Simone Ciampi*

Cite This: https://doi.org/10.1021/jacs.1c06385

Read Online

ACCESS | 📊 Metrics & More | 📖 Article Recommendations | 🔵 Supporting Information

ABSTRACT: Herein we demonstrate that ionic liquids can form long-lived double layers, generating electric fields detectable by straightforward open circuit potential (OCP) measurements. In imidazolium-based ionic liquids an external negative voltage pulse leads to an exceedingly stable near-surface dipolar layer, whose field manifests as long-lived (∼1−100 h) discrete plateaus in OCP versus time traces. These plateaus occur within an ionic liquid-specific and sharp potential window, defining a simple experimental method to probe the onset of interfacial ordering phenomena, such as overscreening and crowding. Molecular dynamics modeling reveals that the OCP arises from the alignment of the individual ion dipoles to the external electric field pulse, with the magnitude of the resulting OCP correlated with the product of the projected dipole moment of cation with the ratio of predicted diffusion coefficient of cation and its volume. Our findings also reveal that a stable overscreened structure is more likely to form if the interface is first forced through crowding, possibly accounting for the scattered literature data on relaxation kinetics of near-surface structures in ionic liquids.
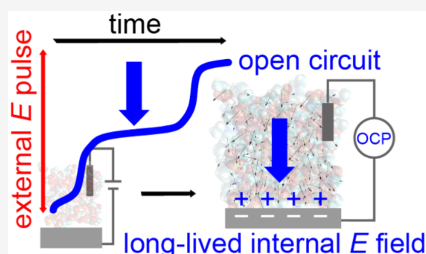
■ INTRODUCTION

Room-temperature ionic liquids (RTILs) are liquids with melting points below 100 °C, composed solely of anions and cations.[1,2] They have been known for over a century[3] but entered mainstream electrochemical research only in the middle of the 1990s with the discovery of RTILs with stable anions.[4] Several such RTILs are now commercially available, and unlike conventional solvent-based electrolytes they can have exceedingly large electrochemical windows.[1,4,5] This makes them valuable in applications ranging from energy generation and storage to electrocatalysis.[6−9]

RTILs typically comprise large unsymmetrical ions[10] that form what can be approximated as a coordinated network of ions,[11,12] with intermolecular forces tunable through changes in the molecular structure of the ions.[13,14] The unique nature of RTILs has important implications for the structure and dynamics of their interface with solid electrodes. While large molecular sizes and conformational flexibility prevent the formation of an ordered solid in the bulk,[15] RTILs at interfaces are inherently ordered.[16] Specifically, RTIL double-layer structures[17−19] formed in the proximity of charged electrodes are of great practical importance as this phase boundary governs charge transport, energy storage, and lubricating properties of electrode−RTIL systems.[9,20,21] As the electrode is charged away from its potential of zero charge (PZC hereafter) in response to an external bias, counterions are enriched in the first ionic layer, where their lateral diffusivity is lower than in bulk.[22] This charged first layer induces a second ionic layer of opposite charges and so on, causing the potential profile to decay with damped oscillations.

Despite a general consensus on the presence of an alternating out-of-plane arrangement of cation- and anion-rich layers,[23,24] the exact short-range ordering of RTILs near electrodes remains unclear.[16,25−28] To date, experimental insights on the interface between RTILs and electrodes have relied on technically demanding atomic force microscopy,[24,29] X-ray reflectometry (XRR) experiments, and Raman spectroscopy.[17,30] The lack of routine and straightforward measurements, suitable to probe the electrode−ionic liquid interface, is part of the reason why details of the near-electrode structure are still unclear. In the present work we address this problem by introducing open-circuit potentiometry as a rapid and technically simple method to probe the interface between RTILs and electrodes.

First, quantitative data on RTIL double layer dynamics, as well as data on the magnitude of the potential required to trigger the formation of ordered layers, are scattered. While solvation dynamics of bulk RTILs have a time scale between picoseconds
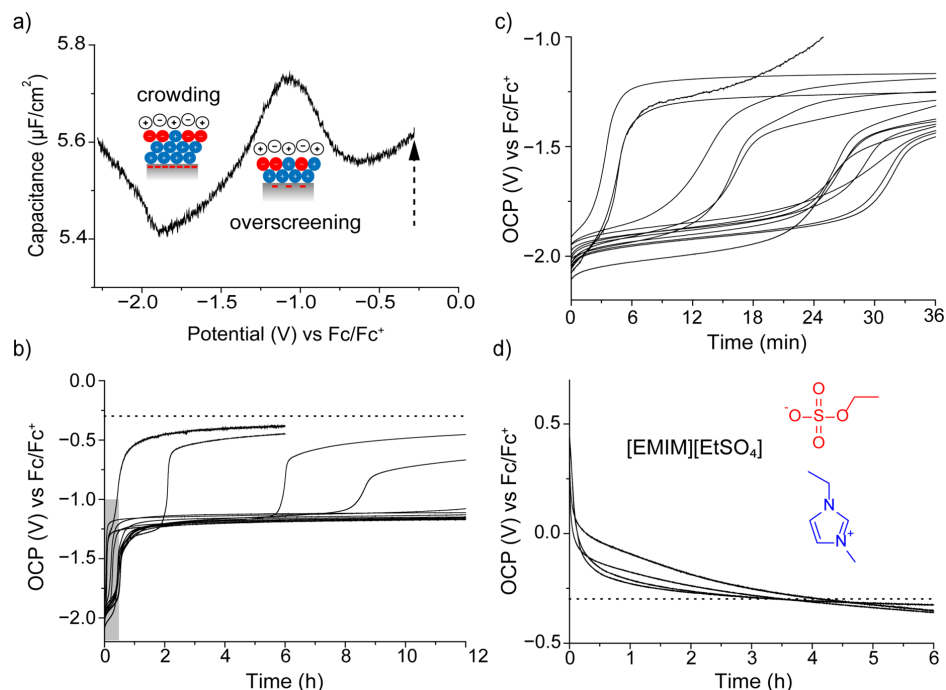
Figure 1. (a) Representative electrochemical impedance spectroscopy (EIS) capacitance−potential plot, with a schematic depiction of the onset of overscreening and crowding in correspondence of local capacitance maximum and minimum, respectively (platinum disk in [EMIM][EtSO$_4$]). The vertical arrow indicates the system initial OCP value, prior to any external biasing. Representative OCP−time measurements for platinum electrodes immersed in [EMIM][EtSO$_4$] were recorded after the application of negative (b, c) and positive (d) potential steps (60 s, ±2.0 V relative to the initial OCP). Dotted horizontal lines represent the average initial OCP. (b) Negative bias excursions lead to very stable OCP plateaus located between −1.1 V and −1.3 V vs Fc/Fc$^+$. (c) A relatively short-lived and more negative OCP plateau, found between −1.9 V and −2.0 V, is evident upon close inspection of the first 30 min of the OCP relaxation data. The gray shaded area in (b) indicates the data region shown in (c).

67 and nanoseconds,[31] the relaxation of RTILs at interfaces is
68 significantly slower.[32−35] But how slow is unclear, with available
69 data indicating relaxation times varying between a few seconds
70 to several minutes.[32,35]
71   Second, while some authors argue that at potentials close to
72 the PZC counterions will already overscreen electrode
73 charges,[26,36] others advocate for such features occurring only
74 at larger biases and persisting over large potential windows.[37−39]
75 For instance Yamamoto and co-workers put forward data in
76 favor of RTILs overscreening at biases around +1.5 V,[18] while
77 Uysal and co-workers observed this already at −0.4 V.[40]
78 Moreover, there is also the hypothesis of electrode "crowding" at
79 large anodic and cathodic excursions,[26,41] as well as a debate
80 around whether the thickness of the first ionic layer drops with
81 increasing electrode charges[42−44] or whether it remains
82 essentially unchanged.[45] Addressing these issues is important
83 because the phase boundary ultimately governs how energy is
84 stored in the electric field of electrochemical devices, such as
85 capacitors,[9,46,47] and how accessible the electrode surface is
86 toward charge-transfer reactions. The latter is emerging as a
87 viable strategy for controlling the balance between inner- and
88 outer-sphere competing electron transfer reactions for both
89 electrocatalysis and electrosynthesis.[48,49] Moreover, recent
90 computational work has shown that ionic liquids that are
91 ordered as a result of exposure to external electric fields can

generate strong internal electric fields that electrostatically 92
catalyze chemical reactions, even when the external field is 93
removed.[50] Experimental confirmation of these fields, and 94
measurements of their lifetime, would be the first step toward 95
harnessing these electrostatic effects in chemical synthesis.[51−54] 96
     By means of open-circuit potentiometry, we demonstrate that 97
at electrode surfaces RTILs assume stable ordered structures 98
and generate significant endogenous electric fields that persist 99
for days after an external potential is removed. 100

■ RESULTS AND DISCUSSSION   101

Interfacial Dynamics of [EMIM][EtSO$_4$]. Prior to studying 102
the response of RTILs to an applied potential, we conducted a 103
search of the minimum of the electrode−RTIL capacitance as a 104
function of the electrode potential. This minimum provides a 105
baseline reading for the disordered RTILs against which the 106
ordered RTILs could be compared, and it was obtained through 107
electrochemical impedance spectroscopy (EIS). The potential 108
where capacitance reaches a minimum generally coincides with 109
the electrode PZC,[43] and EIS measurements with platinum 110
electrodes indicate that this is close to −0.6 V vs Fc/Fc$^+$ (Figure 111 fl
1a). The accumulation of counterions at the electrode surface is 112 fl
likely to occur in both bias directions,[27] implying that the 113
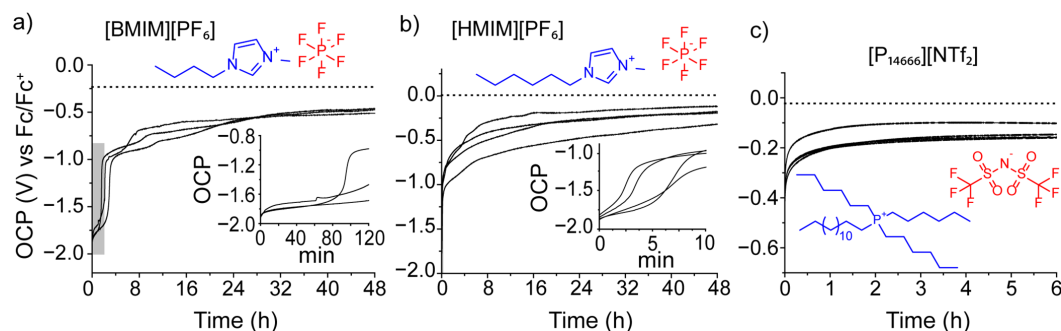positive and negative branches of the capacitance−potential 114

Figure 2. Representative OCP−time measurements acquired with platinum electrodes immersed in $[\text{BMIM}][\text{PF}_6]$ (a), $[\text{HMIM}][\text{PF}_6]$ (b), and $[\text{P}_{14666}][\text{NTf}_2]$ (c) after a negative potential step (60 s). The potential step was −2 V away from the electrode initial rest OCP (dotted horizontal lines). The gray shaded areas in (a, b) indicate the data plotted as figure insets. Data in (a) reveal the onset of crowding in $[\text{BMIM}][\text{PF}_6]$ as an OCP vertical step located between −1.7 V and −1.8 V. The overscreening OCP signature is found between −0.9 V and −1.0 V. (b) OCP−time data for $[\text{HMIM}][\text{PF}_6]$ with evidence of discernible OCP plateaus at approximately −1.7 V and poorly defined plateaus between −1.0 V and −0.75 V.

curve around the PZC are delimiting bias regions where the liquid side of the interface is enriched of either anions or cations.

Prior to exposure to an applied potential, the rest open circuit potential (OCP) was generally only slightly positive of the PZC. After a short (60 s) potential step equal to or smaller than ±1.0 V away from this initial OCP (dashed arrow and dashed horizontal lines in Figure 1) we were only able to record a rapid, <30 min, equilibration of the electrode potential back to its initial rest value (Supporting Information, Figure S1). In this respect an electrode−RTIL interface, such as platinum immersed in $[\text{EMIM}][\text{EtSO}_4]$, behaves qualitatively similar to the interface formed between electrodes and conventional molecular solvent-based electrolytes, such as Bu_4NClO_4 in acetonitrile (Supporting Information, Figure S2). Surprisingly, the experimental OCP relaxation was rapid despite the magnitude of the cathodic step (−1.0 V) being more than sufficient for the interface to reach its capacitance maximum (approximately −1.1 V vs Fc/Fc⁺, Figure 1a). It is therefore probable that the −1.0 V step triggered the formation of an ordered overscreened interface,[41,55] but this structure did not persist once the external bias was removed. As ordering will progressively increase with bias[18] and since capacitance drops under fully occupied conditions,[23] the presence of a minimum in the negative branch of the capacitance−potential curve at approximately −1.9 V vs Fc/Fc⁺ (Figure 1a) suggests the possibility of a thicker first layer of counterions forming at this more negative bias. We consequently measured the OCP relaxation that followed a cathodic step of −1.5 V from the initial rest potential. Once again, this bias is sufficient for the system to reach its capacitance minimum (crowding), but OCPs still relaxed asymptotically and very slowly (∼3 h).

A remarkably different response was observed when the electrode potential was disturbed away from its rest potential by a potential step as large as −2.0 V. Applying such a large negative pulse was effective in locking the interface in a stable "cation-rich" configuration. This cation-rich ordered configuration manifested as an OCP plateau between −1.1 V and −1.3 V vs Fc/Fc⁺, which persisted rarely less than 6 h (Figure 1b) and occasionally up to 4 days (Supporting Information, Figures S3−S6). Importantly, the position of these long-lived OCP plateaus matches the onset of overscreening as assessed by EIS (Figure 1a). A closer inspection of the first part of the time-resolved

OCP measurements revealed the consistent presence of a more negative plateau between −1.9 V and −2.0 V (Figure 1c). The position of this initial plateau closely matches the onset of crowding in the EIS data (Figure 1a). These initial cation-rich surface structures persist only for short times, from a few seconds to ∼30 min, which is of the same order of magnitude of relaxation times obtained for ionic liquid systems through much more complex techniques.[32,40]

Chemisorption reactions, potentially triggered by the cathodic pulse, are an unlikely cause for the plateaus. For instance, while very gentle vibrations of the electrochemical cell did not disturb an overscreening OCP plateau, extracting and reimmersing the electrode in the liquid were enough to reset the initial OCP (Supporting Information, Figure S6). Molecules chemisorbed on surfaces are not so easily removed.[56] Further evidence against chemisorption is the lack of a change in electrode active area following the pulse (Supporting Information, Figure S7).

The existence of such negative plateaus is in accordance with the theory of Kornyshev and co-workers, where multiple layers of counterions balance surface charges (see schematics in Figure 1a).[26,57] Interestingly, only when the metal charge density has sufficiently decreased can the double layer then adjust to an overscreening organization, where just a monolayer of counterions balances the surface charge (Figure 1a). In brief, implicit from our data is that a stable overscreened arrangement forms if the system is first forced into crowding. On the other hand, OCP relaxation responses following positive potential steps were featureless: no plateaus were detected and OCPs relaxed asymptotically (Figure 1d). A similar conclusion was previously reached by AFM data, where the force required for an AFM tip to push through the first ionic liquid layer was significantly larger for negative biases.[27,45] It was therefore not surprising that the occurrence of these negative OCP signatures was largely independent of the nature of the anion, with for instance $[\text{EMIM}][\text{EtSO}_4]$ behaving very similarly to $[\text{EMIM}][\text{BF}_4]$ (Supporting Information, Figure S8). We have not tested $[\text{EMIM}][\text{PF}_6]$ because, in spite of its commercial availability, it is not liquid at room temperature.

Comparison of Different RTILs. To define the generality of OCP measurements in probing interfacial dynamics, we then proceeded to test a range of RTILs with different cations.

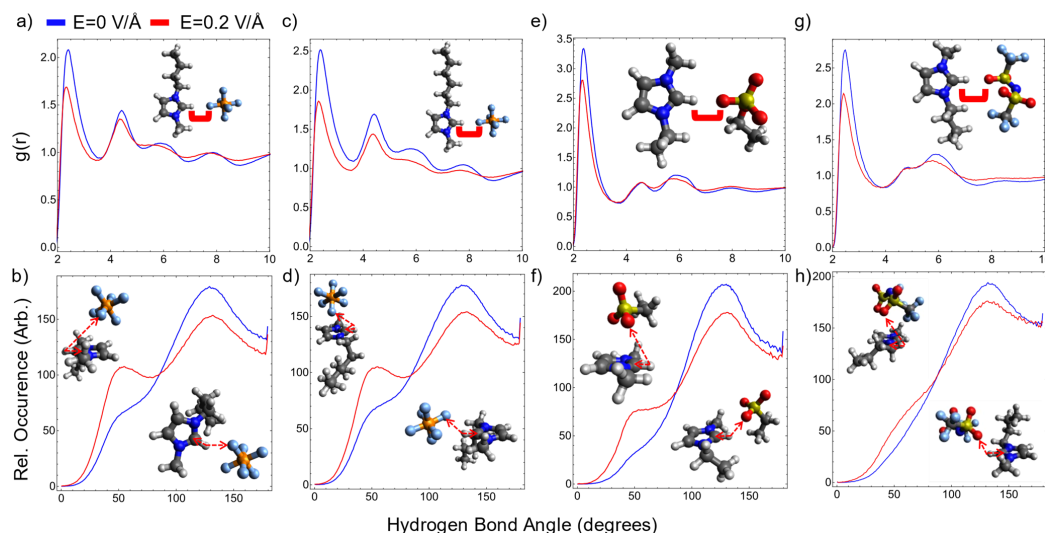**Figure 3.** Normalized radial distribution functions of $(C_2)H{-}F$ distances in (a) $[BMIM][PF_6]$ and (c) $[BMIM][PF_6]$ and $(C_2)H{-}O$ distances in (e) $[EMIM][EtSO_4]$ and (g) $[BMIM][NTf_2]$. Cone-corrected angular distribution functions of $C_2{-}H{\cdots}F$ angles in (b) $[BMIM][PF_6]$ and (d) $[HMIM][PF_6]$ and $C_2{-}H{\cdots}O$ distances in (f) $[EMIM][EtSO_4]$ and (h) $[BMIM][NTf_2]$. In all panels, blue lines denote behavior without an external field, and red lines denote behavior in an external 0.2 V/Å field. Insets in (b), (d), (f), and (h) are motifs representative of the two main peaks at 55° and 130°.

Imidazolium cations with longer alkyl side chains have higher permanent dipole moments, and this in turn increases the strength of their electrostatic interaction with the applied electric field. To illustrate this trend experimentally, we measured OCP relaxations in RTILs containing butyl and hexyl substituents on the imidazolium ring. Data in Figure 2a,b show that after an anodic step the relaxation behavior of $[BMIM][PF_6]$ and $[HMIM][PF_6]$ is asymptotic and indistinguishable from that of the smaller $[EMIM][EtSO_4]$ in Figure 1d. After a cathodic excursion, both $[BMIM][PF_6]$ and $[HMIM][PF_6]$ form negative plateaus, but especially in the case of $[HMIM][PF_6]$, these OCP signatures are not as long-lived and well-defined as those observed with $[EMIM][EtSO_4]$ (Figure 2a,b). OCP signatures for overscreening are still clearly visible for both $[BMIM][PF_6]$ and $[HMIM][PF_6]$, although shorter in the latter (insets in Figure 2). Crowding features in the OCP−time plot are clearly distinguishable only for $[BMIM]$-$[PF_6]$. Extending the duration of the cathodic step, from 1 to 6 min, did not alter the dynamics of the OCP relaxation (Supporting Information, Figure S9). The ability to form ordered dipolar structures disappears for larger cations, such as for example with $[P_{14666}][NTf_2]$ (Figure 2c), and despite previous reports suggesting that a more localized charge leads to stronger surface interactions,[58] pyrrolidinium-based RTILs did not generate clear OCP signatures ($[BMPyrr][NTf_2]$, Supporting Information, Figure S10).

Effect of Electrode Material. There is also experimental evidence of a relationship between ordering on the liquid side of the interface and the mobility of surface atoms of the electronic conductor. Similar to platinum, OCP plateaus were also observed on gold surfaces, but surprisingly they were not detected on covalent electrode materials of large self-diffusion activation energy,[59] such as silicon and carbon (Supporting Information, Figures S11−S13). Further, plateaus recorded with gold electrodes were located at less negative voltages than for platinum, between −0.6 V and −0.7 V, an observation for which we do not yet have a satisfactory explanation (Supporting Information, Figure S14). Differences in double-layer structures for a given RTIL between platinum and gold are not unprecedented,[60] but at present we can only speculate that a less negative OCP plateau for ordered dipolar structures on gold may relate to a difference in surface diffusivity between the two metals.[61]

Polarizable Molecular Dynamics Studies. To understand these results, we conducted polarizable molecular dynamics[39] simulations for $[BMIM][PF_6]$, $[EMIM][EtSO_4]$, and $[HMIM][PF_6]$ in the presence and absence of an applied electric field of 0.2 V/Å along the z-axis. Imidazolium-based ionic liquids are known to exhibit strong hydrogen bonding between the C_2−H bond on the imidazolium ring and electronegative atom on the anions.[62] Radial distribution functions (RDFs, Figure 3a,c) of the $(C_2)H{\cdots}F$ interionic distances indicate the significant changes in the short- and long-range order of both PF_6-based ionic liquids upon the application of the electric field. $[EMIM][EtSO_4]$ and $[BMIM][NTf_2]$ demonstrated smaller structural changes in the $(C_2)H{\cdots}O$ interionic distances (Figure 3e,g), suggesting that the constituent ions do not require a significant change in the bulk arrangement to align with the electric field. Angular distribution functions (ADFs) of the C_2−H$\cdots$X bond (where X is either F (PF_6^-) or O ($EtSO_4^-$ and NTf_2^-; Figure 3b,d,f,h) clearly identify that the hydrogen bond in all three ionic liquids undergoes a change from a more directional hydrogen-bond type (a peak at 130°) to a nondirectional interaction above the imidazolium ring (a peak at 55°). The occurrence of the latter strongly suggests that ionic liquid ions realign themselves in the electric field. Some anions become located right above the

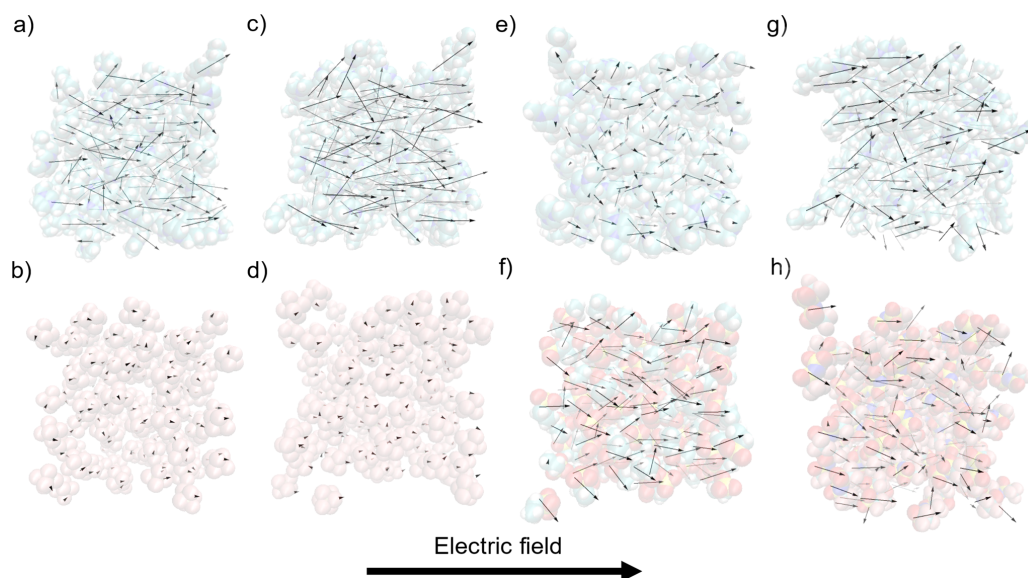**Figure 4.** Visualizations of dipole moments of ions (a) BMIM$^+$ and (b) PF$_6^-$ in [BMIM][PF$_6$], (c) HMIM$^+$ and (d) PF$_6^-$ in [HMIM][PF$_6$], (e) EMIM$^+$ and (f) EtSO$_4^-$ in [EMIM][EtSO$_4$], and (g) BMIM$^+$ and (h) NTf$_2^-$ in [BMIM][NTf$_2$] under a 0.2 V/Å electric field in molecular dynamics simulations. Dipole vector lengths are calibrated to 1 Å/D.
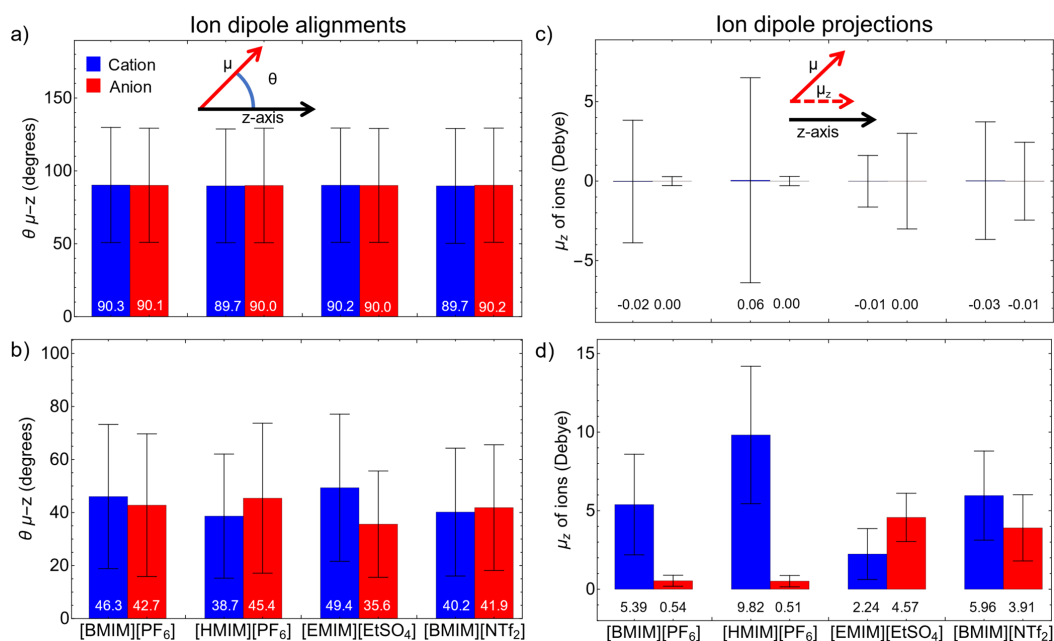

Figure 5. Average angles between ionic dipole moments and the z-axis (a) without an external electric field and (b) in an external field of 0.2 V/Å along the z-axis. (c) displays the mean ion dipole projections along the z-axis without an external electric field and (d) in an external field of 0.2 V/Å oriented along the z-axis. Error bars in (a)−(d) represent standard deviations.

266 imidazolium ring, which corresponds to a typical interionic
267 interaction mode in these ILs.

The strong alignment of the ion dipole moments with the field 268
is presented in Figure 4. Ion dipole moments were calculated 269 f4

with center-of-mass reference points, with magnitudes equivalent to the "charge arm" calculated with respect to center of charge.[63,64] The alignment is particularly stark for ions with nonzero dipole moments such as the imidazolium cations, EMIM$^+$, BMIM$^+$, and HMIM$^+$, and the EtSO$_4^-$ and NTf$_2^-$ anions. The PF$_6^-$ anion that does not have a nominal dipole moment, when calculated in isolation, becomes strongly polarized in the presence of other ions, with the dipole moment also becoming aligned in the field. The alignment of the individual ion dipole moments is not perfect due to strong intermolecular interactions between ionic liquid ions in the range of 320−420 kJ mol^{-1} per single ion pair.[65] The deviation from the field direction was estimated by calculating the average θ angle between the apparent dipole moment of each ion and the direction of the field (Figure 5a,b). It is not surprising and rather reassuring that, in the absence of the electric field, the average θ value was observed to be ∼90° for all ions. This indicates a random distribution, with cone-corrected angular distributions in the Supporting Information (Figure S15) serving as further proof.

The situation changes dramatically as the field is introduced, with the average θ value falling between 35.6° for EtSO$_4^-$ and 49.4° for EMIM$^+$. Further analysis reveals that θ only weakly correlates with the dipole moment of the ions, smaller θ values loosely corresponding to larger dipole moments. In addition to the dipole orientation, each ion dipole moment was projected along the external field axis, μ_Z, (Figure 5c,d). All ions besides PF$_6^-$ exhibit a strong projection ranging from 2.24 D for EMIM$^+$ to 9.82 D for HMIM$^+$. This is due to the strong permanent dipole moments present in the imidazolium cations, the EtSO$_4^-$ and the NTf$_2^-$, whereas the PF$_6^-$ anion does not have a permanent dipole moment due to symmetry. The projected induced dipole moment of PF$_6^-$ anions is not negligible, averaging 0.53 D for both [BMIM][PF$_6$] and [HMIM][PF$_6$].

The alignment of these ion dipoles to the applied electric field induces an opposing internal electric field that, we hypothesize, is responsible for the OCP observed when the external field is removed. The process of the ion realignment is also accompanied by cations moving to the cathode and anions moving to the cathode. In our MD simulations diffusion coefficients of cations and anions increased by 4 orders of magnitude on average when the field was applied (see Supporting Information, Tables S3 and S4). BMIM$^+$ and HMIM$^+$ cations in the PF$_6$-based ionic liquids were found to diffuse slightly faster than cations in [EMIM][EtSO$_4$] and [BMIM][NTf$_2$], which can be explained by stronger hydrogen bonding preventing ions from moving freely in the latter. We also confirmed that the NTf$_2^-$ anion maintained its *trans* configuration throughout the entire simulation in an external electric field (Supporting Information, Figure S16). The calculated diffusion coefficients, ranging from 3.7 × 10^{-7} to 2.5 × 10^{-6} m^2 s^{-1}, suggest that ions can easily move to electrodes, thus leading to crowding of cations at the anode as shown in Figure 1a. It was also noticed that the mobility of cations correlated with the projected dipole moment and the strength of intermolecular interactions within an ionic liquid. The ability of cations with a larger dipole moment and weak hydrogen bonding to anions to strongly realign with an electric field is reflected in their increased diffusion coefficient.

Since ions of opposite charge move in opposite directions in an electric field, it is not surprising that the projected dipole moment sum of the cation and anion did not correlate with the experimental OCP plateaus (Supporting Information, Figure S17). It is well-known that cations will form a crowding layer next to the anode, thus creating a medium of different viscosity at the interface compared to that of the bulk of an ionic liquid. The density of coverage also depends on the cation size, with larger cations creating less dense coverage. Therefore, it was hypothesized that the average projected dipole moment of cation corrected for changed viscosity at the electrode interface and cation size should correlate with the OCP. Since viscosity is inversely proportional to diffusion coefficient, the product of the projected dipole moment of cation with the ratio of predicted diffusion coefficient of cation and its volume gives a strong correlation to the observed OCP plateaus (Figure 6) with an R^2 of 0.907.
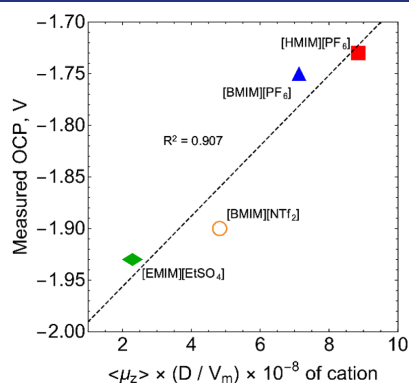

Figure 6. Correlation of measured OCP values (crowding) of ionic liquids against the product of average dipole moment projections and diffusion coefficients in the electric field, divided by cation molar volumes.

This correlation suggests that the mobility of cations in an electric field plays a key role in the formation of a stable crowding interface at the anode resulting in negative OCP plateaus. Lower mobility of EMIM$^+$ and BMIM$^+$ in an electric field in ionic liquids with strong hydrogen bonding, reflected in small structural changes, allows for cations to form a more stable crowding interface, thus exhibiting the lower OCP plateaus (Figures 1c and S18, Supporting Information). This conclusion is further reinforced by the absence of a clear plateau in [P$_{14666}$][NTf$_2$] (Figure 2c), in which the cation displays a negligible dipole moment and hence very low mobility.[63,66] The presented MD simulations thus confirmed that ionic liquid ions are able to reorient their dipole moments along the external electric field without sacrificing their bulk structure to a great extent.

■ CONCLUSIONS

We have described a simple and straightforward method to detect order and electric fields of organized and long-lived ionic liquid double layers by open circuit potentiometry. We show that overscreened and crowded near-electrode structures are detectable as negative open-circuit signatures occurring within sharp potential windows, validating ionic liquids double layer models proposed by Kornyshev and co-workers.[26] Crowding manifests as negative OCP plateaus, which survive up to several tens of minutes. This structure rearranges into an overscreened double layer lasting up to several days, where just a monolayer of

counterions balances the surface charge. These fields can potentially be harnessed for the electrostatic catalysis of chemical reactions,[50,67,68] for the development of safe supercapacitors, and can find applications in the emerging field of redox-enhanced electrochemical capacitors.[69,70] The presence of a stable blocking layer on the electrode may limit side reactions in electrosynthesis, such as reducing hydrogen evolution in the presence of trace water. Further, slow double layer dynamics in RTILs are known to manifest in voltammetry[32] and to introduce hysteresis in capacitance measurements;[34] here we show that RTILs forming dense dielectric layers can be rapidly identified by OCP measurements.

Polarizable molecular dynamics simulations demonstrated the loss of short- and long-range order in $[BMIM][PF_6]$, $[HMIM][PF_6]$, and to a lesser extent $[EMIM][EtSO_4]$ and $[BMIM][NTf_2]$ under an external electric field. The ionic liquid ions were confirmed to align their dipole moments with the external field. The alignment of ions was found to depend on the presence of strong hydrogen bonding in ionic liquids. Cations with larger projected dipole moments were also found to have increased mobility in an electric field. The projected dipole moment of the cation, corrected for its volume and mobility in an electric field, correlates well with the observed crowding OCP plateaus, suggesting that increased dipole moment strength and mobility prevent cations from forming a more stable crowding interface. This represents an excellent design parameter to predict the likelihood of forming stable ionic liquid bilayers having strong endogenous electric fields.

■ EXPERIMENTAL SECTION

Materials. Unless noted otherwise, all reagents were of analytical grade and utilized without further purification. Milli-Q water (>18.2 MΩ cm) was used for cleaning procedures and to prepare electrolytic solutions. 1-Ethyl-3-methylimidazolium ethyl sulfate (≥95%, Sigma, $[EMIM][EtSO_4]$), 1-butyl-3-methylimidazolium hexafluorophosphate (≥97% Sigma, $[BMIM][PF_6]$), 1-hexyl-3-methylimidazolium hexafluorophosphate (≥97%, Sigma, $[HMIM][PF_6]$), trihexyltetradecylphosphonium bis(trifluoromethylsulfonyl)imide (>98%, Iolitec, Germany, $[P_{14666}][NTf_2]$), 1-butyl-1-methylpyrrolidinium bis(trifluoromethylsulfonyl)imide (99.5%, Iolitec, Germany, $[BMPyrr][NTf_2]$), 1-ethyl-3-methylimidazolium tetrafluoroborate (>98%, Iolitec, Germany, $[EMIM][BF_4]$), 1-butyl-3-methylimidazolium bis(trifluoromethylsulfonyl)imide (99%, Iolitec, Germany, $[BMIM][NTf_2]$), acetonitrile (99.5%, VWR chemicals, USA, MeCN), and tetrabutylammonium perchlorate (≥98%, Sigma, Bu_4NClO_4) were used as received. The water content of all the ionic liquids used in this work was estimated by Karl Fisher titration (Mettler-Toledo C20S compact coulometer, Honeywell HYDRANAL Coulomat AG reagent, Merck Water Standard 0.1%, USA), and with at least three samples measured for each ionic liquid. The water content readings between samples of the same ionic liquid varied less than 50 ppm, and the average values were the following: $[EMIM][EtSO_4]$, 930 ppm; $[EMIM][BF_4]$, 500 ppm; $[BMIM][PF_6]$, 490 ppm; $[HMIM]-[PF_6]$, 745 ppm; $[BMPyrr][NTf_2]$, 125 ppm; $[P_{14666}][NTf_2]$, 1215 ppm; $[BMIM][NTf_2]$, 100 ppm.

Electrochemical Methods. All electrochemical measurements were carried out using a small (~4 mL) single-compartment three-electrode glass cell. Cyclic voltammetry (CV) and open circuit potentiometry (OCP) experiments were performed on an Emstat3 Blue potentiostat (PalmSens BV, Houten, The Netherlands). Electrochemical impedance spectroscopy (EIS) experiments were carried out using a CH 650D electrochemical analyzer (CH Instruments, Austin, USA), imposing an AC potential amplitude of 15 mV (root-mean-square) over the DC offset (E_{dc}) of the working electrode. The AC frequency was varied between 0.1 Hz and 0.1 MHz. Reproducibility of the EIS data was highest at 1 kHz, as also observed by others,[43,71,72] and

therefore capacitance−voltage data in this work refer only to this frequency. The E_{dc} offset of the working electrode was ramped starting from the system's initial OCP and moved toward the cathodic limit of the sweep. The sweep rate was 40 mV/s. This sampling approach is common practice for EIS experiments in molten salts.[73] The out-of-phase impedance (Z'') was used to estimate the electrode capacitance ($C = 1/(\omega Z'')^{-1}$). For all the electrochemical experiments the cell was loaded with a small sample (10 mL) of the ionic liquid, which was previous degassed by means of bubbling it with high-purity argon gas (99.997%, Coregas) for at least 20 min. Platinum wire was used as working and counter electrodes for both CV and OCP experiments (0.5 mm diameter wire, 99.99+%, Goodfellow Cambridge Limited), while EIS data were recorded at platinum disk electrodes (eDAQ, ET052, 3 mm diameter). The size of the counter electrode was in excess of 20 times that of the working electrode. A plastic body silver/silver chloride "leakless" setup was used as the reference electrode (eDAQ, part ET072-1, 3.4 M aqueous potassium chloride as filling solution). The active area of the platinum wire working electrodes was either 0.28 cm^2 or 0.63 cm^2, as determined from the refinement of a E model (DigiElch-Professional version 7, ElchSoft) against experimental voltammograms measured in 1.0×10^{-1} M MeCN/Bu_4NClO_4 and in the presence of 1.0×10^{-3} M ferrocene (Fc in shorthand hereafter, Supporting Information, Figures S19 and S20). The active surface area of the platinum disk was 0.08 cm^2 (Supporting Information, Figure S21). The size of the working electrode had no measurable effect on the OCP versus time results. The reference electrode was calibrated before and after each experiment against the apparent formal potential of the ferrocene/ferricenium couple (Fc/Fc^+) measured with the platinum disk using 1.0×10^{-3} M Fc in 2.0×10^{-1} M MeCN/Bu_4NClO_4, and unless specified otherwise, potentials are reported against the Fc/Fc^+ couple. Electrochemical experiments were performed at room temperature (23 ± 2 °C) inside a gastight acrylate box (Molecular Imaging, model GB306, USA) kept under nitrogen atmosphere. The nitrogen line was fitted with a Drierite gas drying unit (Sigma). Working and counter platinum electrodes were cleaned prior to the experiments by means of multiple cyclic voltammetry scans in aqueous 0.5 M sulfuric acid, ramping the potential between −0.2 and 1.0 V at a voltage sweep rate of 0.05 V s^{-1}. Control experiments with gold, carbon, and silicon surfaces were done using, respectively, gold wire of 0.25 mm diameter (99.999+%, Goodfellow), glassy carbon plates of 12.7 mm diameter (TED PELLA, Inc.), and highly doped monolayer-coated oxide-free silicon wafers (prime grade, CZ, 111-oriented (±0.5°), 500 μm thick, single-side polished, boron-doped, 0.007–0.013 Ω cm, from Siltronix S.A.S, Archamps, France). The gold wire was cleaned prior to the experiments by means of cyclic voltammetry in aqueous 50 mM sulfuric acid (sweeps in the −0.2 to 1.0 V range, at 0.05 V s^{-1}). Glassy carbon electrodes were polished to mirror-like finish with alumina slurry (0.05 μm, eDAQ, ET033) on a polishing cloth (Struers). After the polishing step, the electrodes were sonicated in water for 1 min.

Hydrogen-terminated silicon electrodes were modified with an organic monolayer of 1,8-nonadiyne (98%, Sigma-Aldrich) in order to passivate the oxide-free surface against anodic decomposition. The procedure follows minor modification of literature procedures.[74−76] In brief, silicon wafers (1 cm × 1 cm) were kept for 30 min in piranha solution (100 °C, a 3:1 (v/v) mixture of concentrated sulfuric acid and 30% hydrogen peroxide), then rinsed with water, and etched for 10 min in deoxygenated aqueous ammonium fluoride (40 wt %). A small amount of ammonium sulfite was added to the etching solution as oxygen scavenger. Hydrogen-terminated silicon samples were then rinsed with water, dichloromethane, dried under a flow of nitrogen, and then covered with a deoxygenated sample of 1,8-nonadiyne. The silicon sample was then kept under nitrogen for 2 h at a distance of approximately 200 nm from a 312 nm UV source (Vilber, VL-215.M). The chemically passivated silicon electrodes were rinsed with dichloromethane, rested for 24 h in a sealed vial under dichloromethane at +4 °C, and then blown dry under a nitrogen stream before being analyzed. The silicon electrodes were mounted in a three-electrode and single-compartment polytetrafluoroethylene (PTFE) custom cell where a circular Viton gasket defined the geometric area of the working electrode to 0.28 cm^2. Ohmic contact between the back of the silicon

sample and a copper plate was achieved by gently scribing the back of the electrode with emery paper before applying on it a small amount of gallium—indium eutectic. The topography of both silicon and carbon samples was estimated before the electrochemical experiments by atomic force microscopy (AFM). AFM data were acquired on a Park NX10 (Park Systems Corporation, Suwon, Korea). The scanning was conducted in True Non-Contact mode. The silicon sample was fixed on a steel plate using carbon tape and then mounted on the AFM magnetic sample holder. Imaging was done in air, at room temperature, using n-type silicon AFM probes (OCML-AC160TS, Olympus Corporation, Tokyo, Japan) with a nominal resonance frequency of 300 kHz and a spring constant of 26 N/m. The image size was set to 5 $\mu m \times 5\ \mu m$, the resolution to 256 points/line, and the scan rate to 1 Hz (Supporting Information, Figures S22 and S23). Prior to the OCP—time measurements, electrodes were left to equilibrate in contact with the ionic liquid sample until the first derivative of the OCP versus time traces (dV/dt) dropped below |0.0001|. This was normally achieved within 5 min of immersing the electrodes in the liquid (Supporting Information, Figures S24—S27). After this initial stabilization phase, a potential step of variable magnitude and sign was applied to the working electrode. Unless specified otherwise, the duration of this potential pulse was 60 s. OCP recording was resumed immediately after the pulse. The time that elapsed between the anodic, or cathodic, excursion and the resuming of the OCP measurement was less than 2 s.

Computational Methods. The CL&Pol[77−79] force field optimized for ionic liquids was enforced on periodic simulation boxes containing 125 ion pairs of [BMIM][PF$_6$], [HMIM][PF$_6$], and [EMIM][EtSO$_4$]. Where necessary, k_{ij} parameters were calculated (see Supporting Information Table S1). All systems had initial structures produced with PACKMOL[80] and were initially equilibrated for 5 ns in an NpT ensemble, proving to be ample time for each system's density to converge (Supporting Information, Figure S28). Average densities from the last nanosecond of equilibration were within 5% of experimental values (see Supporting Information, Table S2), with corresponding average volumes enforced for 10 ns NVT production runs. Separate NVT runs from identical restart files were performed, with the absence or presence of a 0.2 V/Å external field along the positive z-axis direction. Initially, all systems were allowed 0.1 ns to deform to the average box volume, and a further picosecond to align with the electric field where necessary before the production run. In all simulations, Nose—Hoover temperature grouped thermostats and barostats were used, with atoms thermalized to 353 K and drude particles thermalized to 1 K, and a 1 fs time step was used in all simulations. The LAMMPS[81] software package was used to run all simulations, utilizing the USER-DRUDE module. Trajectory analysis was performed using TRAVIS[82,83] software, with dipole moments calculated with force field charges, and each ion's center of mass as a reference point. The magnitude of these calculated dipole moments is also known as the ion's "charge arm". Volume of cations was calculated based on the previously published methodology.[66] The volume for EMIM$^+$ was taken from that work,[66] and the volumes of BMIM$^+$ and HMIM$^+$ cations are given in Supporting Information, Table S5. The diffusion coefficients were measured as the slope of the mean standard deviation (MSD) of each ion's center of mass. All contributions of each ion across the production runs were considered, with maximum correlation times set to 30% of the trajectory. Correlation times of 1.5−3.0 ns were sampled and produced linear fits of correlation coefficients of at least 0.99 in all cases. These analyses were performed with TRAVIS.

■ ASSOCIATED CONTENT

ⓢ Supporting Information

The Supporting Information is available free of charge at https://pubs.acs.org/doi/10.1021/jacs.1c06385.

■ AUTHOR INFORMATION

Corresponding Authors

Ekaterina I. Izgorodina — *School of Chemistry, Monash University, Clayton, Victoria 3800, Australia;* ◉ orcid.org/0000-0002-2506-4890; Email: katya.pas@monash.edu

Michelle L. Coote — *ARC Centre of Excellence for Electromaterials Science, Research School of Chemistry, Australian National University, Canberra, Australian Capital Territory 2601, Australia;* ◉ orcid.org/0000-0003-0828-7053; Email: michelle.coote@anu.edu.au

Simone Ciampi — *School of Molecular and Life Sciences, Curtin University, Bentley, Western Australia 6102, Australia;* ◉ orcid.org/0000-0002-8272-8454; Email: simone.ciampi@curtin.edu.au

Authors

Mattia Belotti — *School of Molecular and Life Sciences, Curtin University, Bentley, Western Australia 6102, Australia;* ◉ orcid.org/0000-0002-7382-337X

Xin Lyu — *School of Molecular and Life Sciences, Curtin University, Bentley, Western Australia 6102, Australia;* ◉ orcid.org/0000-0002-6506-0392

Longkun Xu — *ARC Centre of Excellence for Electromaterials Science, Research School of Chemistry, Australian National University, Canberra, Australian Capital Territory 2601, Australia;* ◉ orcid.org/0000-0001-7314-2913

Peter Halat — *School of Chemistry, Monash University, Clayton, Victoria 3800, Australia;* ◉ orcid.org/0000-0002-0878-6963

Nadim Darwish — *School of Molecular and Life Sciences, Curtin University, Bentley, Western Australia 6102, Australia;* ◉ orcid.org/0000-0002-6565-1723

Debbie S. Silvester — *School of Molecular and Life Sciences, Curtin University, Bentley, Western Australia 6102, Australia;* ◉ orcid.org/0000-0002-7678-7482

Ching Goh — *School of Molecular and Life Sciences, Curtin University, Bentley, Western Australia 6102, Australia;* ◉ orcid.org/0000-0002-3381-5316

Complete contact information is available at:
https://pubs.acs.org/10.1021/jacs.1c06385

Author Contributions

The manuscript was written through contributions of all the authors. All authors have given approval to the final version of the manuscript.

Notes

The authors declare no competing financial interest.

■ ACKNOWLEDGMENTS

■ REFERENCES

(1) Barrosse-Antle, L. E.; Bond, A. M.; Compton, R. G.; O'Mahony, A. M.; Rogers, E. I.; Silvester, D. S. Voltammetry in Room Temperature Ionic Liquids: Comparisons and Contrasts with Conventional Electrochemical Solvents. *Chem. - Asian J.* **2010**, *5*, 202−230.

(2) Ghandi, K. A Review of Ionic Liquids, Their Limits and Applications. *Green Sustainable Chem.* **2014**, *04*, 44−53.

(3) Gabriel, S.; Weiner, J. Ueber Einige Abkömmlinge Des Propylamins. *Ber. Dtsch. Chem. Ges.* **1888**, *21*, 2669−2679.

(4) Bonhôte, P.; Dias, A.-P.; Papageorgiou, N.; Kalyanasundaram, K.; Grätzel, M. Hydrophobic, Highly Conductive Ambient-Temperature Molten Salts. *Inorg. Chem.* **1996**, *35*, 1168−1178.

(5) De Vos, N.; Maton, C.; Stevens, C. V. Electrochemical Stability of Ionic Liquids: General Influences and Degradation Mechanisms. *ChemElectroChem* **2014**, *1*, 1258−1270.

(6) Zhong, C.; Deng, Y.; Hu, W.; Qiao, J.; Zhang, L.; Zhang, J. A Review of Electrolyte Materials and Compositions for Electrochemical Supercapacitors. *Chem. Soc. Rev.* **2015**, *44*, 7484−7539.

(7) Wu, J.; Lan, Z.; Lin, J.; Huang, M.; Huang, Y.; Fan, L.; Luo, G. Electrolytes in Dye-Sensitized Solar Cells. *Chem. Rev.* **2015**, *115*, 2136−2173.

(8) Osada, I.; de Vries, H.; Scrosati, B.; Passerini, S. Ionic-Liquid-Based Polymer Electrolytes for Battery Applications. *Angew. Chem., Int. Ed.* **2016**, *55*, 500−513.

(9) Watanabe, M.; Thomas, M. L.; Zhang, S.; Ueno, K.; Yasuda, T.; Dokko, K. Application of Ionic Liquids to Energy Storage and Conversion Materials and Devices. *Chem. Rev.* **2017**, *117*, 7190−7239.

(10) Li, H.; Kobrak, M. N. A Molecular Dynamics Study of the Influence of Ionic Charge Distribution on the Dynamics of a Molten Salt. *J. Chem. Phys.* **2009**, *131*, 194507.

(11) Gebbie, M. A.; Valtiner, M.; Banquy, X.; Fox, E. T.; Henderson, W. A.; Israelachvili, J. N. Ionic Liquids Behave as Dilute Electrolyte Solutions. *Proc. Natl. Acad. Sci. U. S. A.* **2013**, *110*, 9674−9679.

(12) Perkin, S.; Salanne, M.; Madden, P.; Lynden-Bell, R. Is a Stern and Diffuse Layer Model Appropriate to Ionic Liquids at Surfaces? *Proc. Natl. Acad. Sci. U. S. A.* **2013**, *110*, E4121−E4121.

(13) Welton, T. Room-Temperature Ionic Liquids. Solvents for Synthesis and Catalysis. *Chem. Rev.* **1999**, *99*, 2071−2084.

(14) Hallett, J. P.; Welton, T. Room-Temperature Ionic Liquids: Solvents for Synthesis and Catalysis. 2. *Chem. Rev.* **2011**, *111*, 3508−3576.

(15) Krossing, I.; Slattery, J. M.; Daguenet, C.; Dyson, P. J.; Oleinikova, A.; Weingärtner, H. Why Are Ionic Liquids Liquid? A Simple Explanation Based on Lattice and Solvation Energies. *J. Am. Chem. Soc.* **2006**, *128*, 13427−13434.

(16) Gong, X.; Kozbial, A.; Li, L. What Causes Extended Layering of Ionic Liquids on the Mica Surface? *Chem. Sci.* **2015**, *6*, 3478−3482.

(17) Mezger, M.; Schröder, H.; Reichert, H.; Schramm, S.; Okasinski, J. S.; Schöder, S.; Honkimäki, V.; Deutsch, M.; Ocko, B. M.; Ralston, J.; Rohwerder, M.; Stratmann, M.; Dosch, H. Molecular Layering of Fluorinated Ionic Liquids at a Charged Sapphire (0001) Surface. *Science* **2008**, *322*, 424−428.

(18) Yamamoto, R.; Morisaki, H.; Sakata, O.; Shimotani, H.; Yuan, H.; Iwasa, Y.; Kimura, T.; Wakabayashi, Y. External Electric Field Dependence of the Structure of the Electric Double Layer at an Ionic Liquid/Au Interface. *Appl. Phys. Lett.* **2012**, *101*, 053122.

(19) Perkin, S.; Crowhurst, L.; Niedermeyer, H.; Welton, T.; Smith, A. M.; Gosvami, N. N. Self-Assembly in the Electrical Double Layer of Ionic Liquids. *Chem. Commun.* **2011**, *47*, 6572−6574.

(20) Fedorov, M. V.; Kornyshev, A. A. Ionic Liquids at Electrified Interfaces. *Chem. Rev.* **2014**, *114*, 2978−3036.

(21) Li, H.; Rutland, M. W.; Atkin, R. Ionic Liquid Lubrication: Influence of Ion Structure, Surface Potential and Sliding Velocity. *Phys. Chem. Chem. Phys.* **2013**, *15*, 14616−14623.

(22) Sha, M.; Wu, G.; Dou, Q.; Tang, Z.; Fang, H. Double-Layer Formation of [Bmim][Pf6] Ionic Liquid Triggered by Surface Negative Charge. *Langmuir* **2010**, *26*, 12667−12672.

(23) Nishi, N.; Uchiyashiki, J.; Ikeda, Y.; Katakura, S.; Oda, T.; Hino, M.; Yamada, N. L. Potential-Dependent Structure of the Ionic Layer at the Electrode Interface of an Ionic Liquid Probed Using Neutron Reflectometry. *J. Phys. Chem. C* **2019**, *123*, 9223−9230.

(24) Zhang, X.; Zhong, Y.-X.; Yan, J.-W.; Su, Y.-Z.; Zhang, M.; Mao, B.-W. Probing Double Layer Structures of Au (111)−Bmipf6 Ionic Liquid Interfaces from Potential-Dependent Afm Force Curves. *Chem. Commun.* **2012**, *48*, 582−584.

(25) Gebbie, M. A.; Dobbs, H. A.; Valtiner, M.; Israelachvili, J. N. Long-Range Electrostatic Screening in Ionic Liquids. *Proc. Natl. Acad. Sci. U. S. A.* **2015**, *112*, 7432−7437.

(26) Bazant, M. Z.; Storey, B. D.; Kornyshev, A. A. Double Layer in Ionic Liquids: Overscreening Versus Crowding. *Phys. Rev. Lett.* **2011**, *106*, 046102.

(27) Li, H.; Endres, F.; Atkin, R. Effect of Alkyl Chain Length and Anion Species on the Interfacial Nanostructure of Ionic Liquids at the Au(111)−Ionic Liquid Interface as a Function of Potential. *Phys. Chem. Chem. Phys.* **2013**, *15*, 14624−14633.

(28) Bozzini, B.; Busson, B.; Humbert, C.; Mele, C.; Raffa, P.; Tadjeddine, A. Investigation of Au Electrodeposition from [Bmp]-[Tfsa] Room-Temperature Ionic Liquid Containing K[Au(Cn)2] by in Situ Two-Dimensional Sum Frequency Generation Spectroscopy. *J. Electroanal. Chem.* **2011**, *661*, 20−24.

(29) Atkin, R.; Warr, G. G. Structure in Confined Room-Temperature Ionic Liquids. *J. Phys. Chem. C* **2007**, *111*, 5162−5168.

(30) Toda, S.; Clark, R.; Welton, T.; Shigeto, S. Observation of the Pockels Effect in Ionic Liquids and Insights into the Length Scale of Potential-Induced Ordering. *Langmuir* **2021**, *37*, 5193−5201.

(31) Arzhantsev, S.; Jin, H.; Ito, N.; Maroncelli, M. Observing the Complete Solvation Response of Dcs in Imidazolium Ionic Liquids, from the Femtosecond to Nanosecond Regimes. *Chem. Phys. Lett.* **2006**, *417*, 524−529.

(32) Nishi, N.; Hirano, Y.; Motokawa, T.; Kakiuchi, T. Ultraslow Relaxation of the Structure at the Ionic Liquid|Gold Electrode Interface to a Potential Step Probed by Electrochemical Surface Plasmon Resonance Measurements: Asymmetry of the Relaxation Time to the Potential-Step Direction. *Phys. Chem. Chem. Phys.* **2013**, *15*, 11615−11619.

(33) Roling, B.; Drüschler, M.; Huber, B. Slow and Fast Capacitive Process Taking Place at the Ionic Liquid/Electrode Interface. *Faraday Discuss.* **2012**, *154*, 303−311.

(34) Zhou, W.; Xu, Y.; Ouchi, Y. Hysteresis Effects in the in Situ Sfg and Differential Capacitance Measurements on Metal Electrode/Ionic Liquids Interface. *ECS Trans.* **2013**, *50*, 339−348.

(35) Makino, S.; Kitazumi, Y.; Nishi, N.; Kakiuchi, T. Charging Current Probing of the Slow Relaxation of the Ionic Liquid Double Layer at the Pt Electrode. *Electrochem. Commun.* **2011**, *13*, 1365−1368.

(36) Fedorov, M. V.; Kornyshev, A. A. Ionic Liquid near a Charged Wall: Structure and Capacitance of Electrical Double Layer. *J. Phys. Chem. B* **2008**, *112*, 11868−11872.

(37) Baldelli, S. Probing Electric Fields at the Ionic Liquid−Electrode Interface Using Sum Frequency Generation Spectroscopy and Electrochemistry. *J. Phys. Chem. B* **2005**, *109*, 13049−13051.

(38) Baldelli, S. Surface Structure at the Ionic Liquid−Electrified Metal Interface. *Acc. Chem. Res.* **2008**, *41*, 421−431.

(39) Alam, M. T.; Islam, M. M.; Okajima, T.; Ohsaka, T. Measurements of Differential Capacitance at Mercury/Room-Temperature Ionic Liquids Interfaces. *J. Phys. Chem. C* **2007**, *111*, 18326−18333.

(40) Uysal, A.; Zhou, H.; Feng, G.; Lee, S. S.; Li, S.; Fenter, P.; Cummings, P. T.; Fulvio, P. F.; Dai, S.; McDonough, J. K.; Gogotsi, Y. Structural Origins of Potential Dependent Hysteresis at the Electrified Graphene/Ionic Liquid Interface. *J. Phys. Chem. C* **2014**, *118*, 569−574.

(41) Kornyshev, A. A. Double-Layer in Ionic Liquids: Paradigm Change? *J. Phys. Chem. B* **2007**, *111*, 5545−5557.

(42) Rivera-Rubero, S.; Baldelli, S. Surface Spectroscopy of Room-Temperature Ionic Liquids on a Platinum Electrode: A Sum Frequency Generation Study. *J. Phys. Chem. B* **2004**, *108*, 15133−15140.

(43) Lockett, V.; Sedev, R.; Ralston, J.; Horne, M.; Rodopoulos, T. Differential Capacitance of the Electrical Double Layer in Imidazolium-Based Ionic Liquids: Influence of Potential, Cation Size, and Temperature. *J. Phys. Chem. C* **2008**, *112*, 7486−7495.

(44) Aliaga, C.; Baldelli, S. Sum Frequency Generation Spectroscopy and Double-Layer Capacitance Studies of the 1-Butyl-3-Methylimidazolium Dicyanamide−Platinum Interface. *J. Phys. Chem. B* **2006**, *110*, 18481−18491.

768 (45) Jurado, L. A.; Espinosa-Marzal, R. M. Insight into the Electrical
769 Double Layer of an Ionic Liquid on Graphene. *Sci. Rep.* **2017**, *7*, 4225.
770 (46) Brandt, A.; Pohlmann, S.; Varzi, A.; Balducci, A.; Passerini, S.
771 Ionic Liquids in Supercapacitors. *MRS Bull.* **2013**, *38*, 554−559.
772 (47) Salanne, M. Ionic Liquids for Supercapacitor Applications. In
773 *Ionic Liquids II*; Kirchner, B., Perlt, E., Eds.; Springer International
774 Publishing: Cham, Switzerland, 2018; pp 29−53.
775 (48) Ramaswamy, N.; Mukerjee, S. Influence of Inner- and Outer-
776 Sphere Electron Transfer Mechanisms During Electrocatalysis of
777 Oxygen Reduction in Alkaline Media. *J. Phys. Chem. C* **2011**, *115*,
778 18015−18026.
779 (49) Bhat, M. A.; Ingole, P. P.; Chaudhari, V. R.; Haram, S. K. Outer
780 Sphere Electroreduction of Ccl4 in 1-Butyl-3-Methylimmidazolium
781 Tetrafluoroborate: An Example of Solvent Specific Effect of Ionic
782 Liquid. *J. Phys. Chem. B* **2009**, *113*, 2848−2853.
783 (50) Xu, L.; Izgorodina, E. I.; Coote, M. L. Ordered Solvents and Ionic
784 Liquids Can Be Harnessed for Electrostatic Catalysis. *J. Am. Chem. Soc.*
785 **2020**, *142*, 12826−12833.
786 (51) Shaik, S.; Mandal, D.; Ramanan, R. Oriented Electric Fields as
787 Future Smart Reagents in Chemistry. *Nat. Chem.* **2016**, *8*, 1091−1098.
788 (52) Meir, R.; Chen, H.; Lai, W.; Shaik, S. Oriented Electric Fields
789 Accelerate Diels-Alder Reactions and Control the Endo/Exo
790 Selectivity. *ChemPhysChem* **2010**, *11*, 301−310.
791 (53) Shaik, S.; Ramanan, R.; Danovich, D.; Mandal, D. Structure and
792 Reactivity/Selectivity Control by Oriented-External Electric Fields.
793 *Chem. Soc. Rev.* **2018**, *47*, 5125−5145.
794 (54) Ciampi, S.; Darwish, N.; Aitken, H. M.; Díez-Pérez, I.; Coote, M.
795 L. Harnessing Electrostatic Catalysis in Single Molecule, Electro-
796 chemical and Chemical Systems: A Rapidly Growing Experimental
797 Tool Box. *Chem. Soc. Rev.* **2018**, *47*, 5146−5164.
798 (55) Fedorov, M. V.; Kornyshev, A. A. Towards Understanding the
799 Structure and Capacitance of Electrical Double Layer in Ionic Liquids.
800 *Electrochim. Acta* **2008**, *53*, 6835−6840.
801 (56) Gooding, J. J.; Ciampi, S. The Molecular Level Modification of
802 Surfaces: From Self-Assembled Monolayers to Complex Molecular
803 Assemblies. *Chem. Soc. Rev.* **2011**, *40*, 2704−2718.
804 (57) Fedorov, M. V.; Georgi, N.; Kornyshev, A. A. Double Layer in
805 Ionic Liquids: The Nature of the Camel Shape of Capacitance.
806 *Electrochem. Commun.* **2010**, *12*, 296−299.
807 (58) Hayes, R.; Borisenko, N.; Tam, M. K.; Howlett, P. C.; Endres, F.;
808 Atkin, R. Double Layer Structure of Ionic Liquids at the Au(111)
809 Electrode Interface: An Atomic Force Microscopy Investigation. *J. Phys.*
810 *Chem. C* **2011**, *115*, 6855−6863.
811 (59) Peart, R. F. Self Diffusion in Intrinsic Silicon. *Phys. Status Solidi B*
812 **1966**, *15*, K119−K122.
813 (60) Gomes, C.; Costa, R.; Pereira, C. M.; Silva, A. F. The Electrical
814 Double Layer at the Ionic Liquid/Au and Pt Electrode Interface. *RSC*
815 *Adv.* **2014**, *4*, 28914−28921.
816 (61) Alonso, C.; Salvarezza, R. C.; Vara, J. M.; Arvia, A. J.; Vazquez, L.;
817 Bartolome, A.; Baro, A. M. The Evaluation of Surface Diffusion
818 Coefficients of Gold and Platinum Atoms at Electrochemical Interfaces
819 from Combined Stm-Sem Imaging and Electrochemical Techniques. *J.*
820 *Electrochem. Soc.* **1990**, *137*, 2161−2166.
821 (62) Low, K.; Wylie, L.; Scarborough, D. L. A.; Izgorodina, E. I. Is It
822 Possible to Control Kinetic Rates of Radical Polymerisation in Ionic
823 Liquids? *Chem. Commun.* **2018**, *54*, 11226−11243.
824 (63) Kobrak, M. N.; Sandalow, N. An Electrostatic Interpretation of
825 Structure-Property Relationships in Ionic Liquids. *Proc. - Electrochem.*
826 *Soc.* **2004**, *2004-24*, 417.
827 (64) Clark, R.; von Domaros, M.; McIntosh, A. J. S.; Luzar, A.;
828 Kirchner, B.; Welton, T. Effect of an External Electric Field on the
829 Dynamics and Intramolecular Structures of Ions in an Ionic Liquid. *J.*
830 *Chem. Phys.* **2019**, *151*, 164503.
831 (65) Rigby, J.; Izgorodina, E. I. New Scs- and Sos-Mp2 Coefficients
832 Fitted to Semi-Coulombic Systems. *J. Chem. Theory Comput.* **2014**, *10*,
833 3111−3122.
834 (66) Izgorodina, E. I.; Forsyth, M.; MacFarlane, D. R. On the
835 Components of the Dielectric Constants of Ionic Liquids: Ionic
836 Polarization? *Phys. Chem. Chem. Phys.* **2009**, *11*, 2452−2458.

837 (67) Aragonès, A.; Haworth, N.; Darwish, N.; Ciampi, S.; Bloomfield,
838 N.; Wallace, G.; Diez-Perez, I.; Coote, M. Electrostatic Catalysis of a
839 Diels−Alder Reaction. *Nature* **2016**, *531*, 88−91.
840 (68) Zhang, L.; Laborda, E.; Darwish, N.; Noble, B. B.; Tyrell, J. H.;
841 Pluczyk, S.; Le Brun, A. P.; Wallace, G. G.; Gonzalez, J.; Coote, M. L.;
842 Ciampi, S. Electrochemical and Electrostatic Cleavage of Alkoxy-
843 amines. *J. Am. Chem. Soc.* **2018**, *140*, 766−774.
844 (69) Evanko, B.; Boettcher, S. W.; Yoo, S. J.; Stucky, G. D. Redox-
845 Enhanced Electrochemical Capacitors: Status, Opportunity, and Best
846 Practices for Performance Evaluation. *ACS Energy Lett.* **2017**, *2*, 2581−
847 2590.
848 (70) Mourad, E.; Coustan, L.; Lannelongue, P.; Zigah, D.; Mehdi, A.;
849 Vioux, A.; Freunberger, S. A.; Favier, F.; Fontaine, O. Biredox Ionic
850 Liquids with Solid-Like Redox Density in the Liquid State for High-
851 Energy Supercapacitors. *Nat. Mater.* **2017**, *16*, 446−453.
852 (71) Gale, R. J.; Osteryoung, R. A. The Electrical Double Layer at
853 Mercury in Room Temperature Aluminum Chloride: 1-Butylpyridi-
854 nium Chloride Ionic Liquids. *Electrochim. Acta* **1980**, *25*, 1527−1529.
855 (72) Lockett, V.; Horne, M.; Sedev, R.; Rodopoulos, T.; Ralston, J.
856 Differential Capacitance of the Double Layer at the Electrode/Ionic
857 Liquids Interface. *Phys. Chem. Chem. Phys.* **2010**, *12*, 12499−12512.
858 (73) Graves, A. D.; Inman, D. Adsorption and the Differential
859 Capacitance of the Electrical Double-Layer at Platinum/Halide Metal
860 Interfaces. *Nature* **1965**, *208*, 481−482.
861 (74) Ciampi, S.; Böcking, T.; Kilian, K. A.; James, M.; Harper, J. B.;
862 Gooding, J. J. Functionalization of Acetylene-Terminated Monolayers
863 on Si(100) Surfaces: A Click Chemistry Approach. *Langmuir* **2007**, *23*,
864 9320−9329.
865 (75) Zhang, L.; Vogel, Y. B.; Noble, B. B.; Gonçales, V. R.; Darwish,
866 N.; Brun, A. L.; Gooding, J. J.; Wallace, G. G.; Coote, M. L.; Ciampi, S.
867 Tempo Monolayers on Si(100) Electrodes: Electrostatic Effects by the
868 Electrolyte and Semiconductor Space-Charge on the Electroactivity of
869 a Persistent Radical. *J. Am. Chem. Soc.* **2016**, *138*, 9611−9619.
870 (76) Ferrie, S.; Darwish, N.; Gooding, J. J.; Ciampi, S. Harnessing
871 Silicon Facet-Dependent Conductivity to Enhance the Direct-Current
872 Produced by a Sliding Schottky Diode Triboelectric Nanogenerator.
873 *Nano Energy* **2020**, *78*, 105210.
874 (77) Canongia Lopes, J. N.; Deschamps, J.; Pádua, A. A. H. Modeling
875 Ionic Liquids Using a Systematic All-Atom Force Field. *J. Phys. Chem. B*
876 **2004**, *108*, 2038−2047.
877 (78) Canongia Lopes, J. N.; Pádua, A. A. H.; Shimizu, K. Molecular
878 Force Field for Ionic Liquids Iv: Trialkylimidazolium and Alkox-
879 ycarbonyl-Imidazolium Cations; Alkylsulfonate and Alkylsulfate
880 Anions. *J. Phys. Chem. B* **2008**, *112*, 5039−5046.
881 (79) Goloviznina, K.; Canongia Lopes, J. N.; Costa Gomes, M.;
882 Pádua, A. A. H. Transferable, Polarizable Force Field for Ionic Liquids.
883 *J. Chem. Theory Comput.* **2019**, *15*, 5858−5871.
884 (80) Martínez, L.; Andrade, R.; Birgin, E. G.; Martínez, J. M. Packmol:
885 A Package for Building Initial Configurations for Molecular Dynamics
886 Simulations. *J. Comput. Chem.* **2009**, *30*, 2157−2164.
887 (81) Plimpton, S. Fast Parallel Algorithms for Short-Range Molecular
888 Dynamics. *J. Comput. Phys.* **1995**, *117*, 1−19.
889 (82) Brehm, M.; Kirchner, B. Travis - a Free Analyzer and Visualizer
890 for Monte Carlo and Molecular Dynamics Trajectories. *J. Chem. Inf.*
891 *Model.* **2011**, *51*, 2007−2023.
892 (83) Brehm, M.; Thomas, M.; Gehrke, S.; Kirchner, B. Travis—a Free
893 Analyzer for Trajectories from Molecular Simulation. *J. Chem. Phys.*
894 **2020**, *152*, 164105.

4.4 Summary

In this chapter, we presented two works studying ordered solvent and ionic liquids and their applications to electrostatic catalysis.

First, we reviewed the concept of electrostatic catalysis and previous works in this field. The bottlenecks in the practical applications of electrostatic catalysis and solvent attenuation were examined. Ordered solvent and ionic liquids and the factors influencing their ordering were introduced. Previous works studying the degree of order in ionic liquids and important factors in simulation techniques were highlighted.

Subsequently, we employed Drude polarizable force field based MD simulation, post-HF, ONIOM(DFT:PM7) and wave function analysis methods to investigate the role of the orientation of the solvent methanol and the ionic liquids [EMIM][BF$_4$] on the activation energy of the hydrogen transfer reaction of o-alkylphenyl ketones. The activation energy was decreased significantly due to the internal electric field arising from the ordered solvent environment.

Finally, we further analysed more details of the structures and properties of ordered ionic liquids under an external electric field, using both computational and experimental techniques. A plateau in the OCP was observed upon application of an external electric field and its removal, which persisted in some ionic liquids over several hours. We propose this method as an easy and straightforward technique to characterize and compare the degree of order of different ionic liquids. Several parameters were also calculated using the trajectory of the polarizable molecular dynamic simulations to characterise the ordering of different ionic liquids. Both the radial distribution function and angular distribution functions of ionic liquids were altered after the external electric field was applied. The alignment of the dipole moments of ions along the direction of the external electric field was visualized. The dipole moment of the ions were separated into the components from different directions. By considering ion dipole projection, the diffusion coefficient of the cation and its volume, a good correlation was found between the measured OCP and the calculated quantities for the ionic liquids [EMIM][PF$_6$], [HMIM][PF$_6$], [EMIM][EtSO$_4$] and [BMIM][NTf$_2$].

The findings in this chapter assist in the understanding electrostatic catalysis in complex solvent environment (e.g., electrochemical interfaces and nanoconfined environment) and will aid the design of future electrostatic catalysis. This work is the first step towards implementing efficient electrostatic catalysis in polar solvent environments. Finally, the findings will assist future studies on the degree of order of ionic liquids in electrochemical double-layer models and the design of electrochemical devices (e.g., batteries and supercapacitors) using ionic liquids.

Bibliography

[1] E Gileadi, *Electrode kinetics for chemists, chemical engineers, and materials scientists*, Capstone (1993).

[2] A. C Aragonès, N. L Haworth, N Darwish, S Ciampi, N. J Bloomfield, G. G Wallace, I Diez-Perez, and M. L Coote, "Electrostatic catalysis of a Diels–Alder reaction", *Nature* **531**(7592), pp. 88–91 (2016).

[3] P. K Sharma, Z. T Chu, M. H Olsson, and A Warshel, "A new paradigm for electrostatic catalysis of radical reactions in vitamin B12 enzymes", *Proceedings of the National Academy of Sciences* **104**(23), pp. 9661–9666 (2007).

[4] A. K Chakraborti, L Sharma, and R Gulhane, "Electrostatic catalysis by ionic aggregates: scope and limitations of Mg (ClO$_4$) $_2$ as acylation catalyst", *Tetrahedron* **59**(39), pp. 7661–7668 (2003).

[5] T Stuyver, D Danovich, J Joy, and S Shaik, "External electric field effects on chemical structure and reactivity", *Wiley Interdisciplinary Reviews: Computational Molecular Science* **10**(2), pp. e1438 (2020).

[6] S Ciampi, I Diez-Perez, M. L Coote, and N Darwish, "Experimentally harnessing electric fields in chemical transformations", In S Shaik and T Stuyver, editors, *Effects of Electric Fields on Structure and Reactivity*, pp. 71–118. Royal Society of Chemistry Publishing (2021).

[7] Y Pocker and R. F Buchholz, "Electrostatic catalysis of ionic aggregates. I. Ionization and dissociation of trityl chloride and hydrogen chloride in lithium perchlorate-diethyl ether solutions", *Journal of the American Chemical Society* **92**(7), pp. 2075–2084 (1970).

[8] L Zhang, Y. B Vogel, B. B Noble, V. R Goncales, N Darwish, A. L Brun, J. J Gooding, G. G Wallace, M. L Coote, and S Ciampi, "TEMPO monolayers on Si (100) electrodes: electrostatic effects by the electrolyte and semiconductor space-charge on the electroactivity of a persistent radical", *Journal of the American Chemical Society* **138**(30), pp. 9611–9619 (2016).

[9] M Chaplin, "Theory vs experiment: what is the surface charge of water", *Water* **1**(1), pp. 1–28 (2009).

[10] J. K Lee, K. L Walker, H. S Han, J Kang, F. B Prinz, R. M Waymouth, H. G Nam, and R. N Zare, "Spontaneous generation of hydrogen peroxide from aqueous microdroplets", *Proceedings of the National Academy of Sciences* **116**(39), pp. 19294–19298 (2019).

[11] C. F Chamberlayne and R. N Zare, "Simple model for the electric field and spatial distribution of ions in a microdroplet", *The Journal of Chemical Physics* **152**(18), pp. 184702 (2020).

[12] L Zhang, E Laborda, N Darwish, B. B Noble, J. H Tyrell, S Pluczyk, A. P Le Brun, G. G Wallace, J Gonzalez, and M. L Coote, "Electrochemical and electrostatic cleavage of alkoxyamines", *Journal of the American Chemical Society* **140**(2), pp. 766–774 (2018).

[13] C. F Gorin, E. S Beh, and M. W Kanan, "An electric field–induced change in the selectivity of a metal oxide–catalyzed epoxide rearrangement", *Journal of the American Chemical Society* **134**(1), pp. 186–189 (2012).

[14] C. F Gorin, E. S Beh, Q. M Bui, G. R Dick, and M. W Kanan, "Interfacial electric field effects on a carbene reaction catalyzed by Rh porphyrins", *Journal of the American Chemical Society* **135**(30), pp. 11257–11265 (2013).

[15] M. T Blyth and M. L Coote, "A pH-switchable electrostatic catalyst for the Diels–Alder reaction: Progress toward synthetically viable electrostatic catalysis", *The Journal of Organic Chemistry* **84**(3), pp. 1517–1522 (2019).

[16] M. T Blyth and M. L Coote, "Recent advances in designed local electric fields", In S Shaik and T Stuyver, editors, *Effects of Electric Fields on Structure and Reactivity* , pp. 119–146. Royal Society of Chemistry Publishing (2021).

[17] T Stuyver, J Joy, D Danovich, and S Shaik, "Computational generation and quantification of electric fields and electrostatics-mediated catalyst optimization", In S Shaik and T Stuyver, editors, *Effects of Electric Fields on Structure and Reactivity* , pp. 195–224. Royal Society of Chemistry Publishing (2021).

[18] R Meir, H Chen, W Lai, and S Shaik, "Oriented electric fields accelerate Diels–Alder reactions and control the endo/exo selectivity", *ChemPhysChem* **11**(1), pp. 301–310 (2010).

[19] G Gryn'ova and M. L Coote, "Origin and scope of long-range stabilizing interactions and associated SOMO–HOMO conversion in distonic radical anions", *Journal of the American Chemical Society* **135**(41), pp. 15392–15403 (2013).

[20] N. S Hill and M. L Coote, "Internal oriented electric fields as a strategy for selectively modifying photochemical reactivity", *Journal of the American Chemical Society* **140**(50), pp. 17800–17804 (2018).

[21] L.-J Yu and M. L Coote, "Electrostatic switching between SN_1 and SN_2 pathways", *The Journal of Physical Chemistry A* **123**(2), pp. 582–589 (2018).

[22] M. T Blyth, B. B Noble, I. C Russell, and M. L Coote, "Oriented internal electrostatic fields cooperatively promote ground-and excited-state reactivity: A case study in photochemical CO_2 capture", *Journal of the American Chemical Society* **142**(1), pp. 606–613 (2019).

[23] G Gryn'ova, D. L Marshall, S. J Blanksby, and M. L Coote, "Switching radical stability by pH-induced orbital conversion", *Nature Chemistry* **5**(6), pp. 474–481 (2013).

[24] M Klinska, L. M Smith, G Gryn'ova, M. G Banwell, and M. L Coote, "Experimental demonstration of pH-dependent electrostatic catalysis of radical reactions", *Chemical Science* **6**(10), pp. 5623–5627 (2015).

[25] R Reale, N. J English, J.-A Garate, P Marracino, M Liberti, and F Apollonio, "Human aquaporin 4 gating dynamics under and after nanosecond-scale static and alternating electric-field impulses: A molecular dynamics study of field effects and relaxation", *The Journal of Chemical Physics* **139**(20), pp. 11B616_1 (2013).

[26] G Cassone, J Sponer, and F Saija, "Ab initio molecular dynamics studies of the electric-field-induced catalytic effects on liquids", *Topics in Catalysis* , pp. 1–19 (2021).

[27] N. J English, "Molecular dynamics in the presence of external electric fields", In S Shaik and T Stuyver, editors, *Effects of Electric Fields on Structure and Reactivity* , pp. 263–316. Royal Society of Chemistry Publishing (2021).

[28] H. M Aitken and M. L Coote, "Can electrostatic catalysis of Diels–Alder reactions be harnessed with pH-switchable charged functional groups?", *Physical Chemistry Chemical Physics* **20**(16), pp. 10671–10676 (2018).

[29] R. A Marcus, "On the theory of oxidation-reduction reactions involving electron transfer. I.", *The Journal of Chemical Physics* **24**(5), pp. 966–978 (1956).

[30] S Ghosh, A. V Soudackov, and S Hammes-Schiffer, "Electrochemical electron transfer and proton-coupled electron transfer: Effects of double layer and ionic environment on solvent reorganization energies", *Journal of Chemical Theory and Computation* **12**(6), pp. 2917–2925 (2016).

[31] A Warshel, P. K Sharma, M Kato, Y Xiang, H Liu, and M. H Olsson, "Electrostatic basis for enzyme catalysis", *Chemical Reviews* **106**(8), pp. 3210–3235 (2006).

[32] S. D Fried and S. G Boxer, "Electric fields and enzyme catalysis", *Annual Review of Biochemistry* **86**, pp. 387–415 (2017).

[33] M. G Romei, C.-Y Lin, I. I Mathews, and S. G Boxer, "Electrostatic control of photoisomerization pathways in proteins", *Science* **367**(6473), pp. 76–79 (2020).

[34] M Novák, C Foroutan-Nejad, and R Marek, "Solvent effects on ion–receptor interactions in the presence of an external electric field", *Physical Chemistry Chemical Physics* **18**(44), pp. 30754–30760 (2016).

[35] I. N Daniels, Z Wang, and B. B Laird, "Dielectric properties of organic solvents in an electric field", *The Journal of Physical Chemistry C* **121**(2), pp. 1025–1031 (2017).

[36] C.-Y Li, J.-B Le, Y.-H Wang, S Chen, Z.-L Yang, J.-F Li, J Cheng, and Z.-Q Tian, "In situ probing electrified interfacial water structures at atomically flat surfaces", *Nature Materials* **18**(7), pp. 697–701 (2019).

[37] P Fenter, S Kerisit, P Raiteri, and J. D Gale, "Is the calcite–water interface understood? Direct comparisons of molecular dynamics simulations with specular X-ray reflectivity data", *The Journal of Physical Chemistry C* **117**(10), pp. 5028–5042 (2013).

[38] K Dutta Dubey, T Stuyver, S Kalita, and S Shaik, "Solvent organization and rate regulation of a Menshutkin reaction by oriented external electric fields are revealed by combined MD and QM/MM calculations", *Journal of the American Chemical Society* **142**(22), pp. 9955–9965 (2020).

[39] M Watanabe, M. L Thomas, S Zhang, K Ueno, T Yasuda, and K Dokko, "Application of ionic liquids to energy storage and conversion materials and devices", *Chemical Reviews* **117**(10), pp. 7190–7239 (2017).

[40] J. P Hallett and T Welton, "Room-temperature ionic liquids: Solvents for synthesis and catalysis. 2", *Chemical Reviews* **111**(5), pp. 3508–3576 (2011).

[41] S. A Forsyth, J. M Pringle, and D. R MacFarlane, "Ionic liquids—an overview", *Australian Journal of Chemistry* **57**(2), pp. 113–119 (2004).

[42] K. R Seddon, "Ionic liquids for clean technology", *Journal of Chemical Technology & Biotechnology: International Research in Process, Environmental And Clean Technology* **68**(4), pp. 351–356 (1997).

[43] H Ohno, *Electrochemical aspects of ionic liquids*, John Wiley & Sons (2005).

[44] R. D Rogers and K. R Seddon, "Ionic liquids–solvents of the future?", *Science* **302**(5646), pp. 792–793 (2003).

[45] T Tsuda and C. L Hussey, "Electrochemical applications of room-temperature ionic liquids", *The Electrochemical Society Interface* **16**(1), pp. 42 (2007).

[46] M. C Buzzeo, R. G Evans, and R. G Compton, "Non-haloaluminate room-temperature ionic liquids in electrochemistry-a review", *ChemPhysChem* **5**(8), pp. 1106–1120 (2004).

[47] Z Wang, Y Yang, D. L Olmsted, M Asta, and B. B Laird, "Evaluation of the constant potential method in simulating electric double-layer capacitors", *The Journal of Chemical Physics* **141**(18), pp. 184102 (2014).

[48] Y Wang, "Disordering and reordering of ionic liquids under an external electric field", *The Journal of Physical Chemistry B* **113**(32), pp. 11058–11060 (2009).

[49] B. B Damaskin and O. A Petrii, "Historical development of theories of the electrochemical double layer", *Journal of Solid State Electrochemistry* **15**(7), pp. 1317–1334 (2011).

[50] Z Stojek, *The electrical double layer and its structure*, Springer (2010).

[51] A. A Kornyshev, "Double-layer in ionic liquids: Paradigm change?", *The Journal of Physical Chemistry B* **111**(20), pp. 5545–5557 (2007).

[52] A Lewandowski and A Świderska-Mocek, "Ionic liquids as electrolytes for Li-ion batteries—An overview of electrochemical studies", *Journal of Power Sources* **194**(2), pp. 601–609 (2009).

[53] A Balducci, U Bardi, S Caporali, M Mastragostino, and F Soavi, "Ionic liquids for hybrid supercapacitors", *Electrochemistry Communications* **6**(6), pp. 566–570 (2004).

[54] A. J Bard and L. R Faulkner, "Fundamentals and applications", *Electrochemical Methods* **2**(482), pp. 580–632 (2001).

[55] A Maggs and R Podgornik, "General theory of asymmetric steric interactions in electrostatic double layers", *Soft Matter* **12**(4), pp. 1219–1229 (2016).

[56] J Forsman, C. E Woodward, and M Trulsson, "A classical density functional theory of ionic liquids", *The Journal of Physical Chemistry B* **115**(16), pp. 4606–4612 (2011).

[57] S.-M Lu, J.-F Chen, Y.-Y Peng, W Ma, H Ma, H.-F Wang, P Hu, and Y.-T Long, "Understanding the dynamic potential distribution at the electrode interface by stochastic collision electrochemistry", *Journal of the American Chemical Society* **143**(32), pp. 12428–12432 (2021).

[58] A. C Mendonça, P Malfreyt, and A. A Padua, "Interactions and ordering of ionic liquids at a metal surface", *Journal of Chemical Theory and Computation* **8**(9), pp. 3348–3355 (2012).

[59] J. M Slattery, D. W Bruce, Y Gao, K Shimizu, and J. N Canongia Lopes, "Liquid-crystalline ionic liquids as ordered reaction media for the Diels–Alder reaction", *Chemistry: A European Journal* , pp. 16113–16123 (2016).

[60] N Nishi, Y Hirano, T Motokawa, and T Kakiuchi, "Ultraslow relaxation of the structure at the ionic liquid| gold electrode interface to a potential step probed by electrochemical surface plasmon resonance measurements: Asymmetry of the relaxation time to the potential-step direction", *Physical Chemistry Chemical Physics* **15**(28), pp. 11615–11619 (2013).

[61] L Xu, E. I Izgorodina, and M. L Coote, "Ordered solvents and ionic liquids can be harnessed for electrostatic catalysis", *Journal of the American Chemical Society* **142**(29), pp. 12826–12833 (2020).

[62] S Patel and C. L Brooks III, "Fluctuating charge force fields: recent developments and applications from small molecules to macromolecular biological systems", *Molecular Simulation* **32**(3-4), pp. 231–249 (2006).

[63] J. W Ponder, C Wu, P Ren, V. S Pande, J. D Chodera, M. J Schnieders, I Haque, D. L Mobley, D. S Lambrecht, and R. A DiStasio Jr, "Current status of the AMOEBA polarizable force field", *The Journal of Physical Chemistry B* **114**(8), pp. 2549–2564 (2010).

[64] G Lamoureux, A. D MacKerell Jr, and B Roux, "A simple polarizable model of water based on classical Drude oscillators", *The Journal of Chemical Physics* **119**(10), pp. 5185–5197 (2003).

[65] R Clark, M von Domaros, A. J McIntosh, A Luzar, B Kirchner, and T Welton, "Effect of an external electric field on the dynamics and intramolecular structures of ions in an ionic liquid", *The Journal of Chemical Physics* **151**(16), pp. 164503 (2019).

[66] C Schröder and O Steinhauser, "Simulating polarizable molecular ionic liquids with Drude oscillators", *The Journal of Chemical Physics* **133**(15), pp. 154511 (2010).

[67] "Tutorial for thermalized Drude oscillators in LAMMPS", https://lammps.sandia.gov/doc/Howto_drude2.html, Accessed: 2021-01-19.

[68] K Zhang, S Ren, and M Caricato, "Multistate QM/QM extrapolation of UV/Vis absorption spectra with point charge embedding", *Journal of Chemical Theory and Computation* **16**(7), pp. 4361–4372 (2020).

[69] J. M. H Olsen, C Steinmann, K Ruud, and J Kongsted, "Polarizable density embedding: A new QM/QM/MM-based computational strategy", *The Journal of Physical Chemistry A* **119**(21), pp. 5344–5355 (2015).

[70] S. J Bennie, M. W van der Kamp, R. C Pennifold, M Stella, F. R Manby, and A. J Mulholland, "A projector-embedding approach for multiscale coupled-cluster calculations applied to citrate synthase", *Journal of Chemical Theory and Computation* **12**(6), pp. 2689–2697 (2016).

[71] S. J Bennie, B. F Curchod, F. R Manby, and D. R Glowacki, "Pushing the limits of EOM-CCSD with projector-based embedding for excitation energies", *The Journal of Physical Chemistry Letters* **8**(22), pp. 5559–5565 (2017).

Chapter 5

The Corona of A Surface Bubble Promotes Electrochemical Reactions

5.1   Introduction

Interfaces between different phases are important research fields as they often possess unique properties and play important roles in biological, environmental and atmospheric chemistry compared with that of bulk solid, liquid or air phases.[1] For example, solid-liquid interfaces influence outcomes of various electrochemical applications.[2–4]

Within the context of the electrochemistry, what matters is not only solid-liquid interface, the water-gas interface such as the bubble surface is also a unique electrostatic environment. Studies of the bubble surface have been undertaken. Similar with other interfaces, bubble surface also holds interesting characters. It was reported that bubbles were generated at nucleation sites due to the change of chemical potential of dissolved gas molecules near the electrode surface.[5] Bubbles can flow away from the electrodes, which can justify their negative net charge.[6] Additionally, bubbles can influence the energy transfer and electron transfer.[5] Cooksey and co-workers concluded that bubble surface can cause a potential drop of 0.09-0.35 V.[7] It was also reported that hydrogen-bonding interactions are altered at the bubble surface relative to bulk solution.[8]

Another interesting feature of air-water interfaces is that these systems are not neutral due to the accumulation of hydroxide ions.[9] Chaplin reported that the negatively charged bubbles migrated towards the positive electrode.[10] It is known that the electrostatic interactions resulting from ions in solution are important for both electrochemical reactions[11] and the design of electrolytes for sodium-metal batteries.[12] It is well known that reactions at water-air interfaces can be dramatically faster than that in the bulk solution.[13] For bubble surfaces, the local electric field from the net charges of accumulated anions can be as large as 1.4 V/nm, and is influenced by the water orientation and the ion distribution.[1] The local electric fields generated from bubble surface can significantly influence interfacial reactivity, transport and solvation thermodynamics of ions.[1, 8, 14] Similar with the ordered solvent environments discussed in the previous chapter, the large local electric field at the bubble surface is an excellent platform for making electrostatic catalysis.

In the work presented in this chapter, we studied how the concentration of hydroxide ions at the bubble surface affects its oxidation potential. Obviously, it is impractical

to model bubble surface using implicit solvent models discussed in Chapter 1, especially when different ions concentrations are involved. Thus, in this work, GFN-xTB MD simulation method is used. This method is based on semi-empirical QM methods, so it can relatively well describe the properties of both ions and radicals. In detail, (non-periodic) semi-empircal GFN-xTB MD simulations are conducted for different concentrations of hydroxide aqueous solution. As periodic condition and Ewald summation are not used, the simulation box is not necessarily neutral, so no charge compensation is performed. Note that non-periodic condition is often used for modelling reactions using AIMD and semi-empirical MD techniques, especially for charged systems. One example system is provided for AIMD simulation of proton transfer reactions of $[Al(H_2O)_6]^{3+}$ using ORCA.[15] From these MD simulation trajectories, several snapshots are extracted for further semi-empirical GFN2-xTB QM geometry optimizations and energy calculations. Configuration extraction was performed using TRAVIS program,[16] where closest molecules were determined by the distance between the central solute and O atoms of water molecules. For each condition, the most stable structure is used for further ONIOM energy calculations, where energy of core area (isolated OH anion/radical) is calculated using CCSD(T)/CBS level (via cc-pVTZ to QZ extrapolation) while energy of the rest is calculated with double hybrid DFT method (RI-PWPB95-D3(BJ)/def2-TZVPP). Finally, these energies are used for the calculations of oxidation potentials versus SHE.

Our simulation conclusion, which is confirmed by the experimental results from the OH radical induced polymerization of luminol, highlighted the importance of the ion concentration and local electric field at the bubble surface for electrostatic catalysis. This, together with ordered solvent environments in the previous chapter, could inspire the design of new strategies for electrostatic catalysis in the future. For example, the specific ion effects in salts and electrolyte solution, associated with energy decomposition analysis with QM methods, could be possibly harnessed in this regard.[17, 18]
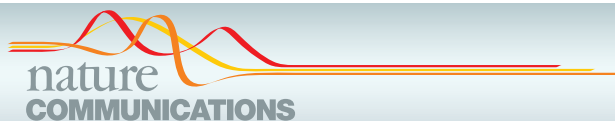
5.2 Publication 6

The Corona of A Surface Bubble Promotes Electrochemical Reactions

Yan B. Vogel, Cameron W. Evans, Mattia Belotti, Longkun Xu, Isabella C. Russell,
Li-Juan Yu, Alfred K. K. Fung, Nicholas S. Hill, Nadim Darwish, Vinicius R. Gonçales,
Michelle L. Coote, K. Swaminathan Iyer, Simone Ciampi
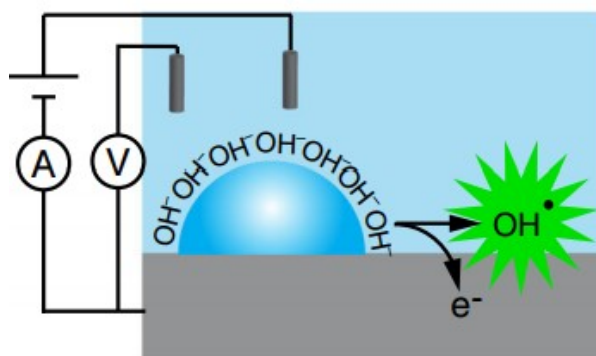
This publication is a peer-reviewed manuscript published in *Nature Communications*. I am the first computational chemistry author in this paper. All semi-empirical MD simulation and quantum chemistry computational results and subsequent discussion about the effect of OH anion repulsion on oxidation were my own work under the supervision of Prof. Michelle Coote. This constitutes Supplementary Note 1 of the supporting information which I wrote, the conclusion of which explained the central finding of the paper. All experimental sections and all other computational sections (e.g. the field effects on peroxide splitting and the polymerization mechanism) were the works of others, as is the writing of the manuscript. Supporting information is available online (https://www.nature.com/articles/s41467-020-20186-0Ack1). The document for the statement of contribution is placed in the Appendix. This research was highlighted in multiple news platforms including EurekAlert!, PHYS.ORG and Chemistry in Australia.

ARTICLE

Check for updates

The corona of a surface bubble promotes electrochemical reactions

Yan B. Vogel [1], Cameron W. Evans [2], Mattia Belotti [1], Longkun Xu [3], Isabella C. Russell[3], Li-Juan Yu[3], Alfred K. K. Fung[3], Nicholas S. Hill[3], Nadim Darwish [1], Vinicius R. Gonçales[4], Michelle L. Coote [3✉], K. Swaminathan Iyer[2✉] & Simone Ciampi [1✉]

The evolution of gaseous products is a feature common to several electrochemical processes, often resulting in bubbles adhering to the electrode's surface. Adherent bubbles reduce the electrode active area, and are therefore generally treated as electrochemically inert entities. Here, we show that this general assumption does not hold for gas bubbles masking anodes operating in water. By means of imaging electrochemiluminescent systems, and by studying the anisotropy of polymer growth around bubbles, we demonstrate that gas cavities adhering to an electrode surface initiate the oxidation of water-soluble species more effectively than electrode areas free of bubbles. The corona of a bubble accumulates hydroxide anions, unbalanced by cations, a phenomenon which causes the oxidation of hydroxide ions to hydroxyl radicals to occur at potentials at least 0.7 V below redox tabled values. The downhill shift of the hydroxide oxidation at the corona of the bubble is likely to be a general mechanism involved in the initiation of heterogeneous electrochemical reactions in water, and could be harnessed in chemical synthesis.

[1] School of Molecular and Life Sciences, Curtin Institute of Functional Molecules and Interfaces, Curtin University, Bentley, WA 6102, Australia. [2] School of Molecular Sciences, The University of Western Australia, Crawley, WA 6009, Australia. [3] ARC Centre of Excellence for Electromaterials Science, Research School of Chemistry, Australian National University, Canberra, ACT 2601, Australia. [4] School of Chemistry, Australian Centre for NanoMedicine and Australian Research Council Centre of Excellence in Convergent Bio-Nano Science and Technology, University of New South Wales, Sydney, NSW 2052, Australia. ✉email: michelle.coote@anu.edu.au; swaminatha.iyer@uwa.edu.au; simone.ciampi@curtin.edu.au

ARTICLE

M ajor industrial processes, such as the electrolysis of alumina[1], the chloralkali process[2], and the refining of copper[3], involve the evolution of gases, which are often accompanied by gas bubbles forming at the electrode. An adherent bubble masks a portion of the electrode; it resists the passage of electrical currents by disrupting ionic conduction at the solid–liquid interface. Surface gaseous cavities are therefore generally regarded as undesirable and electrochemically inactive entities[4].

The gas–water interface is, however, not electrically neutral[5], and the interface between water and gas carries electric fields as high as 1.4 V nm^{-1} [6–8]. Measurements of zeta potential for bubbles suspended in ultrapure water indicate that the corona of a bubble is electrified due to the accumulation of hydroxide ions (OH^-)[9]. This is most likely caused by the increased self-ionization constant of water at the gas–water interface[10], which coupled to the fast diffusion of protons by the Grotthuss mechanism[11], leaves the water surface with an OH^- excess. Adhesion of a bubble on a solid surface leads to two interfaces, the solid–gas and the gas–liquid, with the gas obviously acting as an electrically insulating cavity separating the electrode from the liquid[4,12]. However, with an analogy to a suspended gas cavity, at the point where the solid, the gas, and the liquid meet, a high concentration of unbalanced hydroxide ions is likely to exist. We, therefore, postulated that, due to mutual destabilization of hydroxide ions by electrostatic repulsion, the one-electron oxidation of hydroxides to hydroxyls could be significantly facilitated around bubbles adhering to an electrified support. The oxidizing power of hydroxyls $(HO^\bullet + e^- \rightleftharpoons OH^-, E^0 = +1.90$ V vs. SHE)[13] could then be harvested to trigger redox chemistry[14,15].

Results

Increase in electrochemical current densities in the presence of adherent bubbles. Starting with a simple experimental setup, current measurements and optical images in Fig. 1a, b show, unambiguously, that adherent oxygen bubbles (Fig. 1c) are not electrochemically inert entities. In an electrolytic solution containing only 0.1 M sodium hydroxide, the anodic current measured at an indium tin oxide (ITO) electrode, biased at +1.2 V vs. SHE, is surprisingly higher in the presence of macroscopic surface-adherent oxygen bubbles than it is in their absence. An increased electrochemical current is observed in the presence of bubbles, regardless of the gas composition (Supplementary Fig. 1), and the electrochemical current systematically increases by increasing the cumulative bubbles' perimeter (C, Fig. 1a, b, Supplementary Fig. 2, and Supplementary Table 1). Surface static bubbles favor the oxidation of hydroxides to hydroxyls, and this is a surprising result; a small increase in the gas–water interface outbalances the net loss of "wet" electrode area. We note that these macroscopic bubbles are stable over the time frame of the electrochemical measurements (Supplementary Fig. 3); hence, localized changes in redox reactivity are due to characteristics of the gas–water interface, rather than to energy released during the rapid collapse of the cavity, such as in sonochemistry[16–18], to convection enhancement[19], or the cavity absorbing dissolved gas products[20].

To confirm that the increase in anodic currents, shown in Fig. 1a, is arising from the oxidation of OH^- to $HO^\bullet$ around adherent gas cavities, we coupled electrochemical experiments to epifluorescence microscopy to visually detect the presence of $HO^\bullet$ in the corona of surface bubbles (Fig. 1d). Figure 1e, f (see also Supplementary Video 1) shows epifluorescence microscopy data of argon bubbles resting on an ITO electrode, with 3′-(p-hydroxyphenyl) fluorescein (HPF) present in the electrolytic solution. When the electrode is biased anodically (+1.2 V vs.

SHE), a sharp increase in the fluorescence contrast is observed between the bubble's surface and electrode regions away from the cavity. In our model system, made up of only sodium hydroxide, water, and gas, the plausible reactive oxygen species augmenting the fluorescence of HPF are $HO^\bullet$ and H_2O_2. HPF is ca. 400 times more selective toward $HO^\bullet$ than to H_2O_2[21], strongly suggesting that $HO^\bullet$ is being generated in the corona of the bubble. Confocal microscopy images, acquired at different z heights over the electrode surface (Fig. 1g, h), show that hydroxyl radicals are generated in proximity of the gas–water interface, but principally at a height close to the electrode substrate (Fig. 1i).

Hydroxyl radicals from the oxidation of hydroxide ions. We note that the increased electrochemical reactivity of surface bubbles observed here is not simply the manifestation of higher current densities observed at regions of an electrode that are partially masked by a dielectric object[4,22]. A local increase in current density implies a reaction rate increase for a favorable reaction, while the oxidation of OH^- to $HO^\bullet$ is thermodynamically unfavorable at +1.2 V vs SHE. Instead, the contra-thermodynamic shift experienced by the OH^- oxidation in the presence of surface-adherent bubbles is more likely linked to the high unbalanced concentration of OH^- at the gas–liquid interface (Fig. 2a). Based on Nernst considerations, the $HO^\bullet/OH^-$ redox potential, +1.9 V at standard conditions[13], will drop only by 59 mV every order of magnitude of increase in OH^- activity (Fig. 2b, dashed line). However, if largely unbalanced by cations, electrostatic repulsions between adjacent OH^- are likely to further lower their oxidation potential, as demonstrated by our quantum-chemical simulations (Fig. 2b, symbols, and Supplementary Note 1). It was, therefore, necessary to first estimate experimentally the OH^- excess concentration at the gas–water interface of bubbles. This excess was first determined by means of accelerating gas bubbles, suspended in ultrapure water, under an electric field (Supplementary Note 2)[9]. Selected video frames (Supplementary Video 2), reproduced in Fig. 2c, show a microscopic (50 μm) oxygen bubble in ultrapure water moving at a velocity of 1.3 mm s^{-1} toward the anode under a field of ca. 40 V cm^{-1}. Similar results were obtained for nitrogen bubbles suspended in water (Supplementary Fig. 4 and Supplementary Video 3). The gas–water interface carries an unbalanced population of OH^-, causing the electrical potential to drop away from the gas–liquid interface (Fig. 2a). A quantitative descriptor of this potential profile is the bubble's zeta potential ζ, that is, the potential difference between the shear plane and the bulk solution[23]. We obtained a ζ value of −526 ± 138 mV from the measured bubble velocities using the Smoluchowski equation[24]. The surface charge density of a spherical particle relates to ζ, and using the relationship proposed by Loeb et al.[25], we estimated a charge density of −52 μC cm^{-2} or the equivalent of 5.4×10^{-10} mol cm^{-2} of OH^-. To confirm that the negative charge of bubbles is linked to a local unbalanced excess of hydroxide ions, we resorted to direct pH measurements of gas/water emulsions (Fig. 2d). These experiments have strong conceptual analogies with the "pH-stat" experiments reported by Beattie and coworkers for oil emulsions in water[26]. Suspensions of fine nitrogen bubbles are a way to access a water sample characterized by the presence of a very large gas–liquid interface, and as such, a drop in pH would be expected if an excess of OH^- is trapped at the interface of water with the gas. By generating a large concentration of microscopic nitrogen bubbles (9.3×10^7 particles L^{-1}, Supplementary Video 4) in a water sample, such pH drop was in fact observed (Fig. 2e), indicating at pH ~7 (quiescent sample) a surface OH^- excess of 4.2×10^{-11} mol cm^{-2} (Supplementary Note 3). At pH ~12, such as where hydroxyl radicals are detected (Fig. 1), this excess rises to 1.3×10^{-7} mol cm^{-2} (Supplementary Fig. 5).
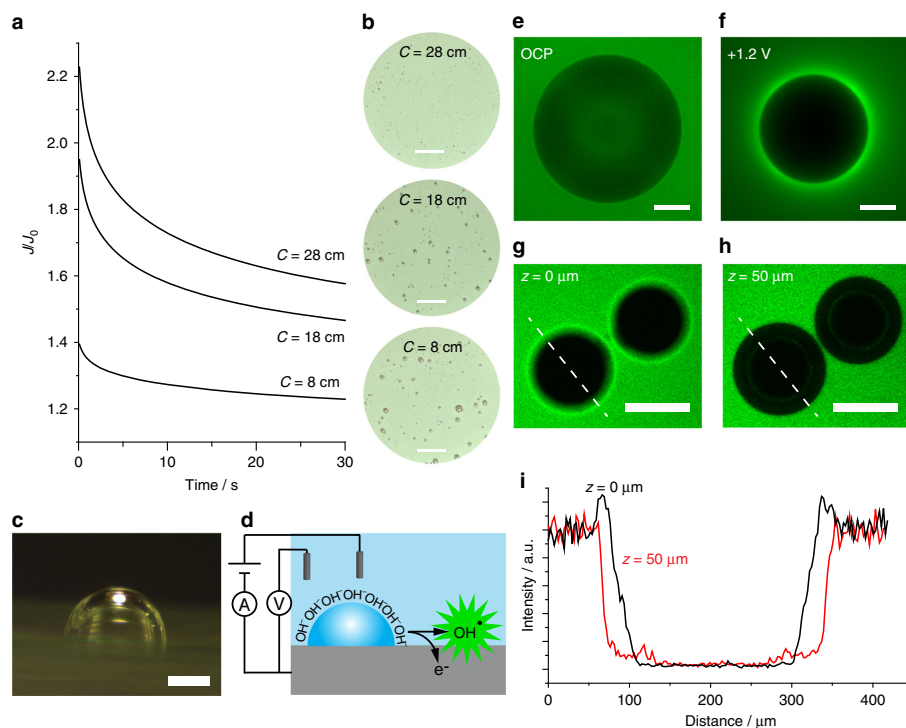
Fig. 1 Surface-adherent gas bubbles increase electrochemical current outputs. a Normalized amperometric curves acquired in aqueous 0.1 M sodium hydroxide using an ITO electrode, biased at +1.2 V vs. SHE, in the presence of surface-adherent oxygen cavities. The current density recorded in the presence of surface-adherent bubbles (J) is systematically higher than that found in the absence of bubbles (J_0). The experimental J/J_0 ratio scales with the total bubble corona length (C, data analysis in Supplementary Fig. 2, and Supplementary Table 1). **b** Optical images of the ITO electrode acquired during the current measurements reported in (**a**). Scale bars are 2 mm. Wide-field views of the entire electrode area are in Supplementary Fig. 2. **c** Representative bright-field image (side view) of an oxygen bubble on the ITO electrode. The scale bar is 200 μm. **d** Schematics of the electrochemical generation, and fluorescence detection, of HO• in the corona of an electrode-adherent bubble. **e, f** Epifluorescence microscopy images for the detection of HO• around an argon bubble adhering on an ITO electrode. The electrode is immersed in an aqueous solution of sodium hydroxide (0.1 M) and 3′-(p-hydroxyphenyl) fluorescein (10 μM), and it is either rested at its open-circuit potential (**e** OCP), or biased at +1.2 V vs. SHE (**f**). See also Supplementary Video 1. **g, h** Confocal microscopy images for the HO• detection around nitrogen bubbles supported on a biased (+1.2 V vs. SHE) ITO slide. The aqueous electrolyte contains dichlorodihydrofluorescein diacetate (100 μM) and sodium hydroxide (0.1 M). The z height above the electrode surface is specified in the figure. Scale bars in **e–h** are 200 μm. Emission intensities for the images (frames) in **e–h** are normalized to the highest-intensity value measured in each frame. **i** Fluorescence emission intensity profiles measured along the dashed lines of panels **g**, **h**, showing a larger emission at the gas–liquid interface closer to the electrode surface.

Anisotropic polymerization of luminol around surface bubbles. To demonstrate the scope and extent to which the surface of an adherent bubble enhances the oxidizing power of an electrode, we designed a detection scheme capable of imaging in real-time the 2D growth of a polymer around bubbles. We coupled an electrochemiluminescent reaction with a step polymerization, both being redox oxidative processes and both being initiated by reactive oxygen species. The surface electrochemiluminescent reaction allows generating a dim internal light source, while the polymer locally quenches it, generating a real-time 2D map of the polymer growth (Fig. 3a, see also Supplementary Videos 5 and 6). We used 5-amino-2,3-dihydrophthalazine-1,4-dione (hereafter luminol) as both the source of chemiluminescence[27,28] and polymerization reactant[29]. Because the formed polymer is non-conductive in its deprotonated state (Supplementary Note 4), as commonly observed in polyaniline analogs[30], it impedes electron transfer between the electrode and the electrolyte quenching the electrochemiluminescent reaction.

The anisotropic growth of the polymer filaments (Fig. 3a), linking neighboring bubbles rather than growing radially from the bubble, tracks the concentration gradient of reactive oxygen species away from the bubble. The luminol light path in water begins with the oxidation of the luminol monoanion[31], yielding a radical susceptible to nucleophilic attack by superoxide ($O_2^{•-}$). This intermediate collapses to a light emitter excited state of 3-aminophthalate (Supplementary Fig. 6)[15]. Superoxide forms upon the oxidation of hydrogen peroxide by HO• radicals ($HO_2^- + HO^• \rightarrow O_2^{•-} + H_2O$)[32], which is evident from the inspection of epifluorescence micrographs obtained around ITO-adherent oxygen (Fig. 3b, and Supplementary Video 7) and argon bubbles (Supplementary Fig. 7, Supplementary Video 8), showing that the presence of oxygen radicals (HO• and $O_2^{•-}$) at the gas–water interface is far more dramatic in peroxide-containing solutions. We discarded the possibility of homolytic cleavage of HO_2^- to form HO• under the strong electric field at the gas–water interface (Supplementary Note 5). Data in Fig. 3b (and
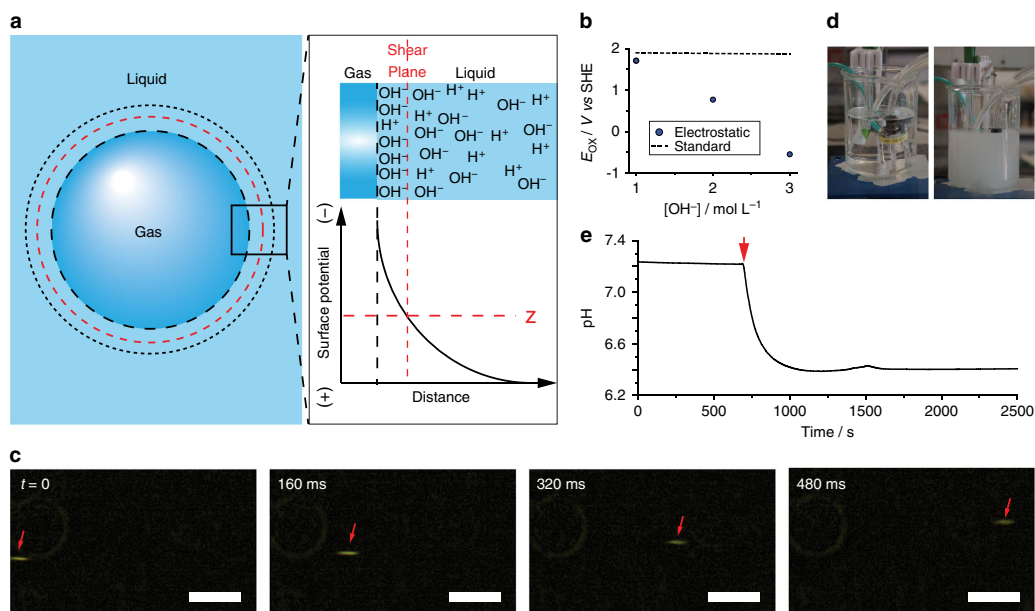
ARTICLE

Fig. 2 The electric double layer of a bubble in ultrapure water. a Simplified schematics of the gas–liquid interface of a bubble, depicting an unbalanced excess of OH⁻ ions. **b** Quantum-chemically computed redox potential for the HO•/OH⁻ couple as a function of the OH⁻ concentration, as calculated by considering electrostatic repulsions between OH⁻ (symbols), together with the tabled experimental[13] potential corresponding to standard conditions of 1 M (dashed line). Details on the calculations are in Supplementary Note 1. **c** Selected time-stamped timeframes obtained from bright-field microscopy imaging experiments (Supplementary Video 2), tracking the position of an oxygen bubble accelerating in ultrapure water toward the anode under an electric field of ca. 40 V cm⁻¹. Scale bars are 500 μm. **d** Photographs taken prior (left) and after (right) the formation of a fine gas–water emulsion obtained by generating a high quantity of nitrogen microbubbles (9.3×10^7 L⁻¹, average bubble diameter is 50 μm), see Supplementary Note 3. **e** Representative pH drop induced by the formation of a gas emulsion in water.

Supplementary Fig. 7) also reveal that the reach of the oxygen radicals away from the bubbles' surface is dramatically increased when peroxide is present, reflecting the million-fold increase in lifetime for $O_2^{\bullet-}$ over HO•[15,33]. The oxygen radical gradient around bubbles is schematized as a color map in Fig. 3c. Bubbles continuously grow as a result of oxygen-evolving upon the oxidation of HO_2^-, and they will occasionally collapse or detach (Fig. 3b and Supplementary Video 7).

The chemiluminescence emission is higher at the bubble interface than on the electrode surface, Fig. 3a, as expected from a higher concentration of HO• around bubbles (from OH⁻ oxidation) that react with HO_2^- to generate $O_2^{\bullet-}$. Luminol can be oxidized to its radical electrochemically (Supplementary Fig. 8), and/or by HO•, and $O_2^{\bullet-}$ forms when HO• oxidizes HO_2^-. The latter has to be present in order to observe chemiluminescence. Therefore, both luminol and HO_2^- might compete for HO•, which would make the emission intensity reach a maximum value at a specific HO_2^-/luminol ratio, and then decrease as this ratio further increases[15], as was effectively observed (Fig. 3d).

The polymerization reaction starts at the bubble interface from the free oxygen radical attack to luminol (Supplementary Note 6). XPS analysis indicates that multiple pathways are operative, with a film curiously consisting of 50% polyaminophthalate, and 50% of polyaminophthalazine and/or polyluminol (Supplementary Note 4). Theoretical calculations suggest that the polymerization mechanism is a stepwise radical process in which a "step" is first initiated via hydrogen transfer by the HO• radical from aniline functionality of the monomer (Fig. 3e and Supplementary Note 6). Two such resulting radicals couple to form an

intermediate that then undergoes a second hydrogen transfer followed by coupling with the radical of a further monomer unit to regenerate the active end group in its nonradical form. In total, three monomer units are joined per step, and four molecules of HO• are consumed. Calculations show that the pathway is feasible for all monomers and hence copolymerization is likely.

Figure 3f (solid line) shows the experimental amperometric curve (electrochemical current vs. time) for the polymerization reaction, with a characteristic shape of an electrodeposition process[34], confirming that the electrode acts as an electron sink rather than being a homogeneous redox reaction. The electrochemical current goes through a rapid initial increase due to the formation and growth of independent nuclei under hemispherical diffusion control. When these diffusion fronts overlap, as a result of a small separation between nuclei, the overall current reaches a maximum and then starts to decrease. The experimental amperometric curves show a good fitting for a diffusion-limited nucleation growth[34]. The initial exponential decay is due to the oxidation of the adsorbed polymer, and this process was accounted for in the fitting as an additional component over the diffusion-limited instantaneous nucleation, see Supplementary Note 7[35]. The peak maxima observed in Fig. 3f represent the point in time at which diffusion fronts theoretically overlap (t_{max}), and roughly coincide with the point in Fig. 3a when the polymer films growing between bubbles start overlapping ($t = 13$ s).

Our results demonstrate that at anodes operating in the water, surface static bubbles are not inert cavities but rather highly reactive redox sites. The electrochemical reactivity of an adherent bubble originates from its corona's ability to accumulate an
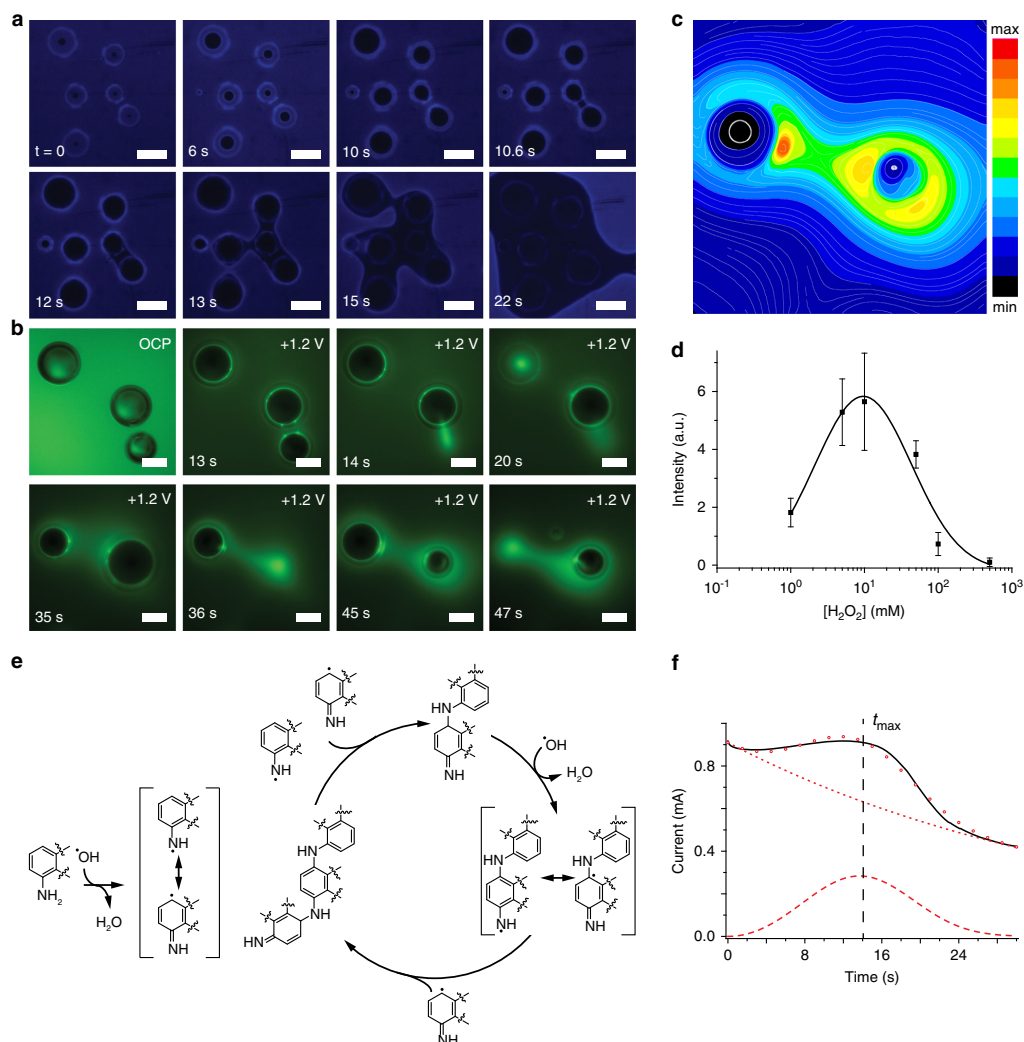
ARTICLE

Fig. 3 Step polymerization initiated at the corona of surface bubbles. a Selected chemiluminescence microscopy (10×, em 440 nm) timeframes (Supplementary Video 5) of the anisotropic polymerization reaction initiated at the gas–liquid interface of oxygen bubbles adhered on an ITO anode (+1.2 V vs. SHE) in an aqueous solution of sodium hydroxide (0.1 M), luminol (0.05 M), and hydrogen peroxide (0.3% v/v). Scale bars are 200 µm. **b** Selected epifluorescence microscopy timeframes (Supplementary Video 7) for the detection of reactive oxygen species around oxygen bubbles adhering on an ITO electrode (OCP and +1.2 V vs. SHE) in a solution containing DCFH$_2$-DA (100 µM), sodium hydroxide (0.1 M), and hydrogen peroxide (0.3% v/v). Scale bars are 200 µm. **c** Contour line color map representing the O$_2^{\bullet-}$ gradient around bubbles, as from the epifluorescence image in (**b**) ($t = 45$ s). **d** Competition of luminol and HO$_2^-$ for HO$^\bullet$ revealed by measurements of electrochemiluminescence intensity as a function of the hydrogen peroxide concentration (platinum gauze as working electrode, +1.2 V vs. SHE, 5.0×10^{-2} M luminol, 0.1 M sodium hydroxide). Mean values with a 90% confidence limit were calculated based on three independent measurements. The mean values were fitted with a Gaussian function (solid line). **e** Polymerization mechanism. **f** Amperometric curve recorded during the experiment in (**a**), solid line. Symbols are simulated curves, including contributions from a diffusion-limited instantaneous growth (long dashes) and from an electron transfer of an adsorbed electroactive species (short dashes). Details on fitting parameters and the model are in Supplementary Note 7.

unbalanced excess of hydroxide anions. In the proximity of the electrode surface, unbalanced anions are oxidized to highly reactive hydroxyl radicals at potentials as low as +1.2 V vs. SHE. The gradient of reactive oxygen species surrounding adherent bubbles can affect anisotropic oxidative redox chemistry. The results presented here are likely to be a general mechanism to initiate, enhance, or localize oxidative processes occurring in water electrolytes.

ARTICLE

Methods

Chemicals and materials. Unless specified otherwise, all chemicals were of analytical grade and used as received. Hydrogen peroxide (H_2O_2, MOS Puranal, 30%, Sigma Aldrich), luminol (97%, Sigma Aldrich), 2′,7′-dichlorodihydrofluorescein diacetate (DCFH$_2$-DA, ≥97%, Sigma Aldrich), 3′-(p-hydroxyphenyl) fluorescein (HPF, 5 mM solution in N,N-dimethylformamide, DMF, ThermoFisher), dimethyl sulfoxide (DMSO, 99%, Ajax Finichem), sodium hydroxide (NaOH, 95%, Ajax Finichem), hydrochloric acid (HCl, 37%, Sigma Aldrich), nitric acid (HNO$_3$, 70%, Ajax Finichem), sulfuric acid (H_2SO_4, 97%, Scharlau), monosodium phosphate (NaH$_2$PO$_4$, 99%, Sigma Aldrich), oxygen (O_2, 99.95%, Coregas), nitrogen (N_2, 99.9%, Coregas), and argon (Ar, 99.997%, Coregas) were used as received. Milli-Q¯ water (>18 MΩ cm) was used for surface cleaning procedures and for preparing all solutions. ITO-coated glass slides were purchased from Delta Technologies (8–12 Ω/sq in sheet resistance).

Measurements of the zeta potential of bubbles. To measure the zeta potential of suspended microscopic oxygen and nitrogen bubbles (50 μm in diameter), we used a method based on the procedure of Takahashi[9]. In brief, oxygen or nitrogen gas was bubbled for 1.5 h across an ultrapure water sample held inside a frit-free soda-lime glass H cell (see Supplementary Fig. 9). The cell consisted of two vertical arms of 10 cm in length connected by a horizontal arm 4-cm long. All arms had an internal diameter of 1 cm. A gas dispersion tube of 25–50-μm porosity (Z408743-1EA, Sigma) was used to pass the oxygen or nitrogen gas along with one of the vertical arms. The oxygen or nitrogen flow was stopped, and a bias of 200 V was applied using a Keysight source/measure unit (model B2902A) between two platinum wire electrodes (99.99 + %, 0.5-mm diameter, Goodfellow Cambridge Ltd) inserted in each of the two vertical compartments of the H cell. The bubbles' movement (speed) in the horizontal channel, and along a horizontal direction pointing from the cathode toward the anode, was used to estimate the bubble zeta potential. Specifically, videos to estimate the bubble position as a function of time were recorded at 25.13 frames per second, using a CCD camera (DCC1240C, Thorlabs) fitted with a 6.5× zoom (MVL6X123Z and MVL133A, Thorlabs). Video recordings were analyzed frame by frame using Fiji image processing package[36]. To minimize electroosmotic forces, possibly interfering with the bubble migration velocity in the field[37], the focus of the camera was aimed toward the center of the H-cell horizontal arm. This is to minimize surface-related artifacts on the zeta potential measurement. The 95% confidence interval of the zeta potential means is reported as $t_{n−1}$ $s/n^{0.5}$, where $t_{n−1}$ depends on the number of repeats, s is the standard deviation, and n is the number of independent measurements (which was 11 for the oxygen bubbles and 23 for the nitrogen bubbles)[38].

Determination of the OH$^−$ excess at the gas–water interface. In addition to quantitative data obtained by electrokinetic experiments (Fig. 2c), the excess of OH$^−$ at the interface of a gas bubble suspended in water was also estimated from bulk pH changes (Fig. 2e) recorded when forcing large fluxes of microscopic nitrogen (99.9%) bubbles in a water sample (Fig. 2d). These vigorously aerated samples have a large gas–water interface area (surface-to-volume ratio, determined by optical microscopy) and were obtained by flowing an aqueous solution (800 mL in a 1-L borosilicate glass beaker) of potassium chloride (0.1 M) of variable pH (adjusted by dropwise addition of a sodium hydroxide aqueous solution (0.1 M)) through a microbubble generator nozzle (CARMIN D2, Ylec, France). The solution was first deaerated for 30 min by flowing nitrogen gas through the solution using a gas dispersion tube of 25–50-μm porosity (Z408743-1EA, Sigma), while water was pumped (and continuously recirculated) by a diaphragm pump (Xylem Flojet AD49/0) at a liquid flow of 3 L/min. The gas dispersion tube was disconnected and the pH allowed to stabilize over a time frame >600 s ($dpH/dt < 0.002$ units min$^{−1}$, Fig. 2e and Supplementary Fig. 5). The nozzle was then connected to the pump circuit. The design of the aerator is that the flowing liquid causes concomitant suction of a gas, in this case, ultra-high-purity nitrogen gas (99.9%, Coregas), into the solution, through the nozzle. A low-conductivity pH probe (model HI1053, Hanna Instruments), connected to a pH meter (HI5221) with computer connectivity, was used to monitor the solution pH over time. All measurements were performed inside an acrylate glovebox kept under positive nitrogen pressure (99.9%, Coregas). Videos, used to estimate the total surface-to-volume ratio of the suspended bubbles, were recorded using a CCD camera (DCC1240C, Thorlabs) fitted with a 6.5× zoom. The experimental setup is shown in Supplementary Fig. 10.

Deposition of bubbles on the electrode. Oxygen, nitrogen, and argon bubbles were deposited on the ITO-coated glass electrode with the aid of a gas dispersion tube of 10–20-μm porosity (Z408727, Sigma Aldrich). In brief, the electrochemical cell holding the ITO electrode was initially filled with water, then the gas flow was forced across the liquid, and after being visually inspected the ITO slide to confirm the presence of adherent gas bubbles, a concentrated solution containing the chemical species of interest was added so to reach a specific final concentration.

Amperometry, epifluorescence, and electrochemiluminescence microscopy. A custom-made three-electrode single-compartment electrochemical cell (Supplementary Fig. 11) was used for all electrochemical and fluorescence experiments. An ITO-coated glass slide served as the working electrode (7.1 cm^2, geometric area), a

platinum foil as the counter electrode (25.8 cm^2, geometric area), and an Ag|AgCl| KCl (sat.) electrode as reference. The cell's ohmic resistance was 13 ohm, measured in a 0.1 M aqueous solution of sodium hydroxide. The counter- and reference electrodes are kept at a distance of 1 cm from the working electrode, and the cell was generally loaded with 20 mL of electrolyte/fluorophore solutions. The three electrodes were connected to an EmStat3 potentiostat (PalmSens BV). All potentials are reported against the standard hydrogen electrode (SHE). Luminol electrochemiluminescence and fluorescein fluorescence were detected using a Nikon Eclipse Ti2 inverted fluorescence microscope equipped with a 14-bit monochromatic camera (Nikon DS-Qi2), Plan Fluor 10×/0.30 Ph1 objective, and Semrock quad-band excitation/emission filter (LED-DA/FI/TR/Cy5). Images were captured at 1024 × 1024-pixel (px) resolution. For the detection of OH$^•$ and OH$^−$, 470-nm excitation and 515-nm emission were used. For the detection of luminol electrochemiluminescence, the sample was kept in the dark and no emission filter was used. For the wide-field videos (Supplementary Video 6), the luminol electrochemiluminescence was recorded using a CMOS camera (CS235CU, Thorlabs) equipped with a focusing lens (MVL50M23, Thorlabs, 50 mm, f/2.8). For the detection of reactive oxygen species by fluorescence, we used aqueous solutions containing either $1.0 × 10^{−4}$ M DCFH$_2$-DA or $1.0 × 10^{−5}$ M HPF. The $1.0 × 10^{−4}$ M DCFH$_2$-DA solution was prepared from a $1.0 × 10^{−3}$ M DCFH$_2$-DA stock solution in dimethyl sulfoxide so that the final concentration of dimethyl sulfoxide during the imaging experiments is 1% v/v. The $1.0 × 10^{−5}$ M HPF solution was prepared from a $5.0 × 10^{−3}$ M DCFH$_2$-DA stock solution in DMF, with a 0.4% v/v final concentration of DMF. For the electrochemiluminescence detection, an aqueous solution of 0.1 M sodium hydroxide, 0.05 M luminol, and 0.3% v/v hydrogen peroxide was used.

Confocal microscopy. 12-bit fluorescence and differential interference contrast microscopy images at 512 × 512-px resolution were captured using a Nikon A1R laser scanning confocal system attached to a Nikon Ti-E inverted microscope, using a Plan Apo λ 10×/0.45 objective with excitation set to 488 nm, emission to 525/50 nm, and with a DU4 detector. Images were captured at 1.00× zoom and a pinhole size of 17.9 μm. The electrochemical cell was the same as that used for the epifluorescence and chemiluminescence microscopy experiments.

Competition of H_2O_2 and luminol for HO$^•$. The competition of hydrogen peroxide and luminol for HO$^•$ as their oxidant was studied by electrochemiluminescence spectroscopy with a Cary Eclipse Fluorescence spectrophotometer, using a spectroelectrochemical cell from BASi (EF-1362) fitted with a platinum gauze as the working electrode, a platinum wire as the counter electrode, and an Ag/AgCl/KCl (sat.) as the reference electrode. All electrochemical measurements were performed using a potentiostat from PalmSens BV (EmStat3). All potentials are reported against the SHE. The electrochemiluminescence intensity was measured at the peak maxima (425 nm) at an applied potential of +1.2 V in a solution containing $5.0 × 10^{−2}$ M luminol, 0.1 M sodium hydroxide, and concentrations of hydrogen peroxide ranging from $1 × 10^{−3}$ to 0.5 M. The platinum electrodes were cleaned after each measurement by electrochemical cycling (20 cycles at a sweep rate of 0.1 V/s) in 0.5 M aqueous nitric acid and then rinsed with Milli-Q¯ water.

X-ray photoelectron spectroscopy. X-ray photoelectron spectroscopy was performed with an ESCALab 250 Xi spectrometer (ThermoFisher Scientific) fitted with a monochromated Al Kα source. The pressure in the analysis chamber during measurements was <10$^{−8}$ mbar. The pass energy and step size for narrow scans were 20 and 0.1 eV, respectively, and the take-off angle was normal to the sample surface. Spectral analysis was performed by using the Avantage 4.73 software and curve fittings were carried out with a mixture of Gaussian–Lorentzian functions. Emission peaks were calibrated by applying a rigid binding energy shift to bring the C1s emission of the C — C signal to 284.3 eV.

Theoretical procedures. Quantum-chemical calculations were undertaken to assess the possibility of electrostatically driven peroxide homolysis, to determine the effect of charge repulsion on hydroxide oxidation, and to ascertain the mechanism of luminol polymerization. A summary of the methods is given below, further details are provided in the relevant Supplementary Notes.

Calculations on peroxide homolysis and luminol polymerization were carried out with the Gaussian 16.C01[39] software package, at the M06-2X/6-31 + G(d,p) level of theory for both geometry optimizations and frequency calculations. Where relevant, conformational searching was also carried out at this level using the energy-directed tree search algorithm[40]. For peroxide homolysis, a thermocycle approach was used to obtain aqueous-phase Gibbs free energies from gas-phase Gibbs free energies and SMD[41] solvation energies. For the polymerization, geometries in the gas and aqueous phases were significantly different, and so the direct method[42] was used instead. In both cases, standard partition functions for an ideal gas under the harmonic oscillator-rigid rotor approximation were used. For peroxide homolysis, the electric field was applied using the field command in Gaussian with values of 2 and 10 atomic units, the former corresponding best to the estimated field at the bubble surface[6–8]. Multiple directions were screened and the most stabilizing directions applied in all cases.

ARTICLE

To assess the effects of charge repulsion on hydroxide oxidation, a 1 M solvent system comprising 1 hydroxide and 52 water molecules was extracted from the trajectory of 1 ns NVT simulation of a system containing 1 hydroxide and 100 water molecules in cubic boxes with a length of 14.46 angstrom based on the density of water. The initial cubic box was set up using the Packmol program[43], and the Travis program[44] was used to place a solute molecule (HO⁻ or HO•) in the center of each simulation box. For each cluster, the GFN2-xTB method[45] implemented in the xtb[46] code (version 6.2.3) is used to optimize the structure, and the most stable cluster is taken for further optimization using the B97-3c method[47] with the ORCA program[48]. Improved energies were calculated with RI-PWPB95-D3(BJ)[49,50]/def2-QZVPP[51] single-point energies and these were further corrected to the CCSD(T)/CBS[52,53] level via an ONIOM approximation[54] in which the core system was the isolated reagent. Oxidation potentials were computed using a value of 4.281V[55] for the reference electrode and Boltzmann statistics for the electron. The effect of electrostatic repulsion was assessed by repeating the calculations for simulation boxes in which 1 (2 M) or 2 (3 M) extra HO⁻ ions were included.

Data availability

References

1. Perron, A. L., Kiss, L. I. & Poncsák, S. Mathematical model to evaluate the ohmic resistance caused by the presence of a large number of bubbles in Hall-Héroult cells. *J. Appl. Electrochem.* **37**, 303–310 (2007).
2. Moussallem, I., Jörissen, J., Kunz, U., Pinnow, S. & Turek, T. Chlor-alkali electrolysis with oxygen depolarized cathodes: history, present status and future prospects. *J. Appl. Electrochem.* **38**, 1177–1194 (2008).
3. Sand H. J. III. On the concentration at the electrodes in a solution, with special reference to the liberation of hydrogen by electrolysis of a mixture of copper sulphate and sulphuric acid. *Philos. Mag.* **1**, 45–79 (1901).
4. Angulo, A., van der Linde, P., Gardeniers, H., Modestino, M. & Fernández Rivas, D. Influence of bubbles on the energy conversion efficiency of electrochemical reactors. *Joule* **4**, 555–579 (2020).
5. Chaplin, M. Theory vs experiment: what is the surface charge of water. *Water* **1**, 1–28 (2009).
6. Kathmann, S. M., Kuo, I. F. W. & Mundy, C. J. Electronic effects on the surface potential at the vapor–liquid interface of water. *J. Am. Chem. Soc.* **130**, 16556–16561 (2008).
7. Wick, C. D., Kuo, I. F. W., Mundy, C. J. & Dang, L. X. The effect of polarizability for understanding the molecular structure of aqueous interfaces. *J. Chem. Theory Comput.* **3**, 2002–2010 (2007).
8. Wick, C. D., Dang, L. X. & Jungwirth, P. Simulated surface potentials at the vapor-water interface for the KCl aqueous electrolyte solution. *J. Chem. Phys.* **125**, 024706 (2006).
9. Takahashi, M. ζ potential of microbubbles in aqueous solutions: electrical properties of the gas–water interface. *J. Phys. Chem. B* **109**, 21858–21864 (2005).
10. Creux, P., Lachaise, J., Graciaa, A., Beattie, J. K. & Djerdjev, A. M. Strong specific hydroxide ion binding at the pristine oil/water and air/water interfaces. *J. Phys. Chem. B* **113**, 14146–14150 (2009).
11. von Grotthuß, T. *Mémoire sur la décomposition de l'eau et des corps qu'elle tient en dissolution à l'aide de l'électricité galvanique* (1805).
12. Taqieddin, A., Nazari, R., Rajic, L. & Alshawabkeh, A. Review—physicochemical hydrodynamics of gas bubbles in two phase electrochemical systems. *J. Electrochem. Soc.* **164**, E448–E459 (2017).
13. Armstrong, D. A. et al. Standard electrode potentials involving radicals in aqueous solution: inorganic radicals (IUPAC Technical Report). *Pure Appl. Chem.* **87**, 1139–1150 (2015).
14. Reyhani, A., McKenzie, T. G., Fu, Q. & Qiao, G. G. Fenton-chemistry-mediated radical polymerization. *Macromol. Rapid Commun.* **40**, 1900220 (2019).
15. Merenyi, G. & Lind, J. S. Role of a peroxide intermediate in the chemiluminescence of luminol. A mechanistic study. *J. Am. Chem. Soc.* **102**, 5830–5835 (1980).
16. Pokhrel, N., Vabbina, P. K. & Pala, N. Sonochemistry: science and engineering. *Ultrason. Sonochem.* **29**, 104–128 (2016).
17. Suslick, K. S. Sonochemistry. *Science* **247**, 1439 (1990).
18. Fernandez Rivas, D. et al. Ultrasound artificially nucleated bubbles and their sonochemical radical production. *Ultrason. Sonochem.* **20**, 510–524 (2013).
19. Kempler, P. A., Coridan, R. H. & Lewis, N. S. Effects of bubbles on the electrochemical behavior of hydrogen-evolving Si microwire arrays oriented against gravity. *Energy Environ. Sci.* **13**, 1808–1817 (2020).
20. Peñas, P. et al. Decoupling gas evolution from water-splitting electrodes. *J. Electrochem. Soc.* **166**, H769–H776 (2019).
21. Molecular ProbesTM 36003. *Indicators for Highly Reactive Oxygen Species.* https://assets.thermofisher.com/TFS-Assets/LSG/manuals/mp36003.pdf (2005).
22. Dukovic, J. The influence of attached bubbles on potential drop and current distribution at gas-evolving electrodes. *J. Electrochem. Soc.* **134**, 331 (1987).
23. Kralchevsky, P. A., Danov, K. D. & Denkov, N. D. Chemical physics of colloid systems and interfaces. in *Handbook of Surface and Colloid Chemistry.* (CRC Press, 2008).
24. Smoluchowski, M. Elektrische Endosmose und Strömungsströme. *Handbuch der Elektrizität und des Magnetismus* (ed Graetz L) (1921).
25. A. L. Loeb J. T. G. O., P. H. Wiersema. *The Electrical Double Layer Around a Spherical Colloid Particle.* (The M.I.T. Press, 1961).
26. Beattie, J. K. & Djerdjev, A. M. The pristine oil/water interface: Surfactant-free hydroxide-charged emulsions. *Angew. Chem. Int. Ed.* **43**, 3568–3571 (2004).
27. Miao, W. Electrogenerated chemiluminescence and its biorelated applications. *Chem. Rev.* **108**, 2506–2553 (2008).
28. Vogel, Y. B., Darwish, N. & Ciampi, S. Spatiotemporal control of electrochemiluminescence guided by a visible light stimulus. *Cell Rep. Phys. Sci.* **1**, 100107 (2020).
29. Zhang, G.-F. & Chen, H.-Y. Studies of polyluminol modified electrode and its application in electrochemiluminescence analysis with flow system. *Anal. Chim. Acta* **419**, 25–31 (2000).
30. Focke, W. W., Wnek, G. E. & Wei, Y. Influence of oxidation state, pH, and counterion on the conductivity of polyaniline. *J. Phys. Chem.* **91**, 5813–5818 (1987).
31. Lind, J., Merenyi, G. & Eriksen, T. E. Chemiluminescence mechanism of cyclic hydrazides such as luminol in aqueous solutions. *J. Am. Chem. Soc.* **105**, 7655–7661 (1983).
32. Uri, N. Inorganic free radicals in solution and some aspects of autoxidation. *Free Radicals in Inorganic Chemistry.* (American Chemical Society, 1962).
33. Pryor, W. A. Oxy-radicals and related species: their formation, lifetimes, and reactions. *Annu. Rev. Physiol.* **48**, 657–667 (1986).
34. Scharifker, B. & Hills, G. Theoretical and experimental studies of multiple nucleation. *Electrochim. Acta* **28**, 879–889 (1983).
35. Vogel, Y. B., Darwish, N., Kashi, M. B., Gooding, J. J. & Ciampi, S. Hydrogen evolution during the electrodeposition of gold nanoparticles at Si(100) photoelectrodes impairs the analysis of current-time transients. *Electrochim. Acta* **247**, 200–206 (2017).
36. Schindelin, J. et al. Fiji: an open-source platform for biological-image analysis. *Nat. Methods* **9**, 676–682 (2012).
37. Graciaa, A., Morel, G., Saulner, P., Lachaise, J. & Schechter, R. S. The ζ-potential of gas bubbles. *J. Colloid Interface Sci.* **172**, 131–136 (1995).
38. Miller, J. & Miller, J. C. *Statistics and Chemometrics for Analytical Chemistry.* (Pearson Education, 2018).
39. Frisch M. J. et al. *Gaussian 16 Rev. C.01.* (2016).
40. Izgorodina, E. I., Yeh Lin, C. & Coote, M. L. Energy-directed tree search: an efficient systematic algorithm for finding the lowest energy conformation of molecules. *Phys. Chem. Chem. Phys.* **9**, 2507–2516 (2007).
41. Marenich, A. V., Cramer, C. J. & Truhlar, D. G. Universal solvation model based on solute electron density and on a continuum model of the solvent defined by the bulk dielectric constant and atomic surface tensions. *J. Phys. Chem. B* **113**, 6378–6396 (2009).
42. Ribeiro, R. F., Marenich, A. V., Cramer, C. J. & Truhlar, D. G. Use of solution-phase vibrational frequencies in continuum models for the free energy of solvation. *J. Phys. Chem. B* **115**, 14556–14562 (2011).
43. Martínez, L., Andrade, R., Birgin, E. G. & Martínez, J. M. PACKMOL: a package for building initial configurations for molecular dynamics simulations. *J. Comput. Chem.* **30**, 2157–2164 (2009).
44. Brehm, M. & Kirchner, B. TRAVIS - A free analyzer and visualizer for Monte Carlo and molecular dynamics trajectories. *J. Chem. Inf. Model.* **51**, 2007–2023 (2011).
45. Bannwarth, C., Ehlert, S. & Grimme, S. GFN2-xTB—an accurate and broadly parametrized self-consistent tight-binding quantum chemical method with multipole electrostatics and density-dependent dispersion contributions. *J. Chem. Theory Comput.* **15**, 1652–1671 (2019).
46. xtb. https://github.com/grimme-lab/xtb (2020).
47. Brandenburg, J. G., Bannwarth, C., Hansen, A. & Grimme, S. B97-3c: a revised low-cost variant of the B97-D density functional method. *J. Chem. Phys.* **148**, 064104 (2018).
48. Neese, F. The ORCA program system. *WIREs Comp. Mol. Sci.* **2**, 73–78 (2012).

ARTICLE

49. Eichkorn, K., Treutler, O., Öhm, H., Häser, M. & Ahlrichs, R. Auxiliary basis sets to approximate Coulomb potentials. *Chem. Phys. Lett.* **240**, 283–290 (1995).

50. Goerigk, L. & Grimme, S. Efficient and accurate double-hybrid-meta-GGA density functionals—evaluation with the extended GMTKN30 database for general main group thermochemistry, kinetics, and noncovalent interactions. *J. Chem. Theory Comput.* **7**, 291–309 (2011).

51. Weigend, F. & Ahlrichs, R. Balanced basis sets of split valence, triple zeta valence and quadruple zeta valence quality for H to Rn: design and assessment of accuracy. *Phys. Chem. Chem. Phys.* **7**, 3297–3305 (2005).

52. Purvis, G. D. & Bartlett, R. J. A full coupled-cluster singles and doubles model: the inclusion of disconnected triples. *J. Chem. Phys.* **76**, 1910–1918 (1982).

53. Dunning, T. H. Gaussian basis sets for use in correlated molecular calculations. I. The atoms boron through neon and hydrogen. *J. Chem. Phys.* **90**, 1007–1023 (1989).

54. Izgorodina, E. I. et al. Should contemporary density functional theory methods be used to study the thermodynamics of radical reactions? *J. Phys. Chem. A* **111**, 10754–10768 (2007).

55. Kelly, C. P., Cramer, C. J. & Truhlar, D. G. Single-ion solvation free energies and the normal hydrogen electrode potential in methanol, acetonitrile, and dimethyl sulfoxide. *J. Phys. Chem. B* **111**, 408–422 (2007).

Author contributions
Y.B.V. and S.C. conceived the study. Y.B.V. performed most of the experiments, carried out the analysis, and produced the figures. C.W.E. assisted with the microscopy experiments. M.B. performed the electrokinetic experiments. L.X. studied the effect of HO⁻ repulsion on oxidation. M.L.C., I.C.R., L.J.Y., and A.K.K.F. determined the polymerization mechanism. I.C.R. and N.S.H. evaluated peroxide homolysis as an alternative source of HO•. V.R.G. performed the XPS experiments. N.D., M.L.C., K.S.I., and S.C. supervised the project. Y.B.V. and S.C. wrote the paper with contributions from all authors.

Competing interests
The authors declare no competing interests.

Additional information
Supplementary information is available for this paper at https://doi.org/10.1038/s41467-020-20186-0.

Correspondence and requests for materials should be addressed to M.L.C., K.S.I. or S.C.

Peer review information *Nature Communications* thanks the anonymous reviewers for their contributions to the peer review of this work.

Reprints and permission information is available at http://www.nature.com/reprints

Publisher's note Springer Nature remains neutral with regard to jurisdictional claims in published maps and institutional affiliations.

5.3 Summary

In this chapter, the features of air-water interfaces were reviewed, and the air-water interface was proposed as a platform for electrostatic catalysis. We used the semi-empirical GFN-XTB method based MD simulation, accurate DFT calculations and ONIOM(CCSD (T)/CBS:DFT) multi-scale energy calculations to study the effects of the concentration of the OH anion and the associated electrostatic interactions at the bubble surface on the oxidation potential. Our computational results, which is confirmed by the experimental findings of the polymerization reaction, suggest that the bubble system can be used as an excellent platform for electrostatic catalysis.

Bibliography

[1] C. D Wick, L. X Dang, and P Jungwirth, "Simulated surface potentials at the vapor-water interface for the KCl aqueous electrolyte solution", *The Journal of Chemical Physics* **125**(2), pp. 024706 (2006).

[2] D. R MacFarlane, M Forsyth, P. C Howlett, J. M Pringle, J Sun, G Annat, W Neil, and E. I Izgorodina, "Ionic liquids in electrochemical devices and processes: managing interfacial electrochemistry", *Accounts of Chemical Research* **40**(11), pp. 1165–1173 (2007).

[3] W Schmickler and E Santos, *Interfacial electrochemistry*, Springer Science & Business Media (2010).

[4] A. L Barker, M Gonsalves, J. V Macpherson, C. J Slevin, and P. R Unwin, "Scanning electrochemical microscopy: beyond the solid/liquid interface", *Analytica Chimica Acta* **385**(1-3), pp. 223–240 (1999).

[5] A Angulo, P van der Linde, H Gardeniers, M Modestino, and D. F Rivas, "Influence of bubbles on the energy conversion efficiency of electrochemical reactors", *Joule* **4**(3), pp. 555–579 (2020).

[6] A Perron, L Kiss, and S Poncsák, "Mathematical model to evaluate the ohmic resistance caused by the presence of a large number of bubbles in hall-héroult cells", *Journal of Applied Electrochemistry* **37**(3), pp. 303–310 (2007).

[7] M. A Cooksey, M. P Taylor, and J. J Chen, "Resistance due to gas bubbles in aluminum reduction cells", *JOM* **60**(2), pp. 51–57 (2008).

[8] C. D Wick, I.-F. W Kuo, C. J Mundy, and L. X Dang, "The effect of polarizability for understanding the molecular structure of aqueous interfaces", *Journal of Chemical Theory and Computation* **3**(6), pp. 2002–2010 (2007).

[9] M Takahashi, "ζ potential of microbubbles in aqueous solutions: electrical properties of the gas-water interface", *The Journal of Physical Chemistry B* **109**(46), pp. 21858–21864 (2005).

[10] M Chaplin, "Theory vs experiment: what is the surface charge of water", *Water* **1**(1), pp. 1–28 (2009).

[11] M. C Monteiro, F Dattila, B Hagedoorn, R García-Muelas, N López, and M. T Koper, "Absence of CO_2 electroreduction on copper, gold and silver electrodes without metal cations in solution", *Nature Catalysis* , pp. 1–9 (2021).

[12] X Chen, X Shen, T.-Z Hou, R Zhang, H.-J Peng, and Q Zhang, "Ion-solvent chemistry-inspired cation-additive strategy to stabilize electrolytes for sodium-metal batteries", *Chem* **6**(9), pp. 2242–2256 (2020).

[13] R Kusaka, S Nihonyanagi, and T Tahara, "The photochemical reaction of phenol becomes ultrafast at the air–water interface", *Nature Chemistry* , pp. 1–6 (2021).

[14] S. M Kathmann, I.-F. W Kuo, and C. J Mundy, "Electronic effects on the surface potential at the vapor-liquid interface of water", *Journal of the American Chemical Society* **130**(49), pp. 16556–16561 (2008).

[15] M Brehm, "ORCA 5.0 molecular dynamics module", https://brehm-research.de/orcamd.php, Accessed: 2022-03-02.

[16] M Brehm, M Thomas, S Gehrke, and B Kirchner, "TRAVIS—a free analyzer for trajectories from molecular simulation", *The Journal of Chemical Physics* **152**(16), pp. 164105 (2020).

[17] K. P Gregory, G. B Webber, E. J Wanless, and A. J Page, "Lewis strength determines specific-ion effects in aqueous and nonaqueous solvents", *The Journal of Physical Chemistry A* **123**(30), pp. 6420–6429 (2019).

[18] P Bauduin, A Renoncourt, D Touraud, W Kunz, and B. W Ninham, "Hofmeister effect on enzymatic catalysis and colloidal structures", *Current Opinion in Colloid & Interface Science* **9**(1-2), pp. 43–47 (2004).

Chapter 6

Conclusions and Outlook

In this thesis, a range of chemical properties and reactions such as solvation free energy, pK_a, redox potential, electrostatic catalysis and ionic liquids under external electric fields were studied with multi-scale computational chemistry techniques including post-HF, DFT, semi-empirical methods, polarizable force field and wave function analysis methods. Main contributions of this thesis and outlook for future works are summarised herein.

6.1   Main Contributions

1. An extensive review of recent literature on the modelling of solvation free energies, solution-phase properties (e.g., pK_a, redox potential, photochemical properties), reaction mechanisms and catalysis was undertaken. Recommended database and parameters for solvation modelling were presented. We introduced a collection of key works published in the last five years employing computational methods at different scales to model solvent effects. The reported computational methods included quantum chemical methods (post-HF, DFT, tight-binding and semi-empirical QM, multiscale and fragmentation based QM methods), force field methods (polarizable, reactive and coarsed-grain force field methods), as well as the use of cheminformatics, machine learning methods and GPU. This literature review will guide the choice of computational methods and other important factors in the future studies related with computational solvation in different systems. For example, ESF values and theoretical level used for implicit solvent models, hydration free energy of proton for accurate pK_a predictions.

2. The theoretical background of implicit solvent models, the SCRF method, solute cavity, SMD and PCM solvent models were reviewed. We examined various methods to improve the accuracy of SMD solvation free energy calculations, including tuning theoretical levels, scaling solute cavities, and using explicit solvent molecules. These methods were compared using pK_a prediction of a wide range of solute types. pK_a calculations were conducted with thermodynamic cycle method where accurate CBS-QB3(SP)//M062X/6-31+G(d,p) method was used for gas-phase free energy calculations. Our study suggests incorporating explicit solvent molecules improves the accuracy of SMD solvation free energies and associated aqueous pK_a predictions of anions (e.g., carboxylic acids and thiols), but is not necessary for cations and neutral species, as confirmed by pK_a calculations of methyl-substituted nucleic acid bases and aliphatic amines. The mixed theoretical level

155

method we developed performs better than M052X/6-31G(d). Effects and limitations of cavity scaling were analysed in detail. Using mixed theoretical level for neutral species and cations without explicit solvent while employing M052X/cc-PVTZ with one explicit solvent molecule for anions (i.e., protocol 1 for cations and neutral species while protocol 3 for anions in *Publication 2*), outperforms two cavity scaling methods reported in the literature. Our method for SMD solvation free energy is more accurate, easy to use and versatile for CHNO small molecules. Additional pK_a tests on carbon acids, alcohols and anilines further confirmed above conclusions.

The advantages and shortcomings of UAHF and UAKS atomic radii were discussed in detail. An extensive optimization of ESF with the MNSol-v2012 data base was conducted. These benchmarking results, together with associated pK_a tests for amines, thiols, carbon acids, pyridines, alcohols, anilines, carboxylic acids and phenols in water and acetonitrile suggest that: (1) ESF = 1.2 should be used for hydration free energy calculations with PCM-UAHF and PCM-UAKS methods; (2) Different ESF values should be used for neutral species and ions; (3) With optimized ESF values, the accuracy of CPCM-UAHF is close to that of SMD and exceeds that of COSMO-RS for the test of 82 solute/solvent combinations, which suggests our optimized CPCM-UAHF model is an excellent alternative to these two popular implicit solvent models.

These contributions are expected to be useful in future predictions of pK_a and redox potential in solution phase.

3. The concept of electrostatic catalysis and previous works in this field were reviewed. Although we focused on analysing the effects of external electric field, influence of other external factors (e.g., solid-liquid interactions and temperature) on the ordering of solvent were briefly discussed. We highlighted the bottleneck for electrostatic catalysis in polar solvent and how ordered solvent could be a strategy to solve this bottleneck. A workflow was designed to study the effects of solvent ordering on the activation energy of the model hydrogen-transfer reaction. Used methods include polarizable force field, wave function analysis, post-HF method, DFT and semi-empirical methods, and ONIOM multi-scale energy calculations. The effects of snapshots number on the calculated activation energy were analysed. Different methods were used to investigate and characterize the ordered solvent structures. The phenomenon of "breaking ion cage" and its relationship with the decrease of RDF of ionic liquids under external electric field was examined. Further, the change of dipole moment of solvent environment and its relationship to reaction axis of the solute was analysed.

The structure and properties of ionic liquids under an external electric field were studied with experimental and computational techniques. The observed OCP plateau was proposed as a simple method to characterize the ordered structure of ionic liquids. Various computational results were discussed including RDF, angular distribution functions, the angle between dipole moment direction and electric field direction, ion dipole projection, and the diffusion coefficient of the cation and its volume. A good correlation was determined between the measured OCP and calculated quantities of [EMIM][PF$_6$], [HMIM][PF$_6$], [EMIM][EtSO$_4$] and [BMIM][NTf$_2$].

These contributions provide a deep understanding of electrostatic catalysis and are expected to be useful in the design of suitable catalysts, particularly in complex solvent environments and polar solvents. Further, these works will assist in the future study of ionic liquids under electric fields and associated electrochemical devices.

4. The accumulation of anions and associated local electric field at the bubble surface were introduced as another platform for electrostatic catalysis. We developed a workflow to calculate oxidation potential of the OH anion at different concentrations, using GFN-XTB based MD simulation, semi-empirical QM, DFT, CCSD(T)/CBS methods and ONIOM multi-scale energy calculations. Our results suggested that the high concentration of OH anions and the associated electrostatic interactions can dramatically promote the oxidation of OH anions at the interface. The generated OH radical by the oxidation of OH anions was proved to be useful for the polymerization of luminol.

This contribution is expected to aid the design of efficient catalysts acting at the water-air and other interfaces.

6.2   Outlook

This thesis has led to a number of additional research questions in computational solvent modelling and electrostatic catalysis. These are summarised below and identify where future efforts in the field can be focussed.

1. There is still a further room for improving the accuracy of implicit solvent models. Although more extensive benchmarking might be useful, existed works have already concluded that the error of solvation free energy of certain species, e.g., anions, are usually large.[1] Thus, the first step for future work could be including more tricky systems like anions into current training set (e.g., MNSOL-v2012) of solvation models. Current parameters of implicit solvent models can be updated based on the new training set using different methods. For example (1) ML could be a powerful tool for the systematic and multi-objective optimization of the parameters in the implicit solvent models.[2, 3] A correlation between optimized ESF values in *Publication 3* and descriptors of solute and solvent could be developed. The solute classification and solvent parameters in the MNSOL-v2012 data base[4] could be used as descriptors. ML techniques especially deep learning methods require a large and high quality data set, which is a potential difficulty for ML based solvation model and other chemistry applications. Especially, computed and experimental data are rare for solvation free energies in non-aqueous solvent. This problem might be able to solved using transfer learning technique[5] but the prediction accuracy needs to be further analysed; (2) ML can also be employed for direct prediction of solution-phase properties. Examples include pK_a[6–8], redox potential[9], photochemical properties[10], force field parameters (e.g., partial charge[11]) and reaction mechanisms[12] without explicitly calculating the solvation free energies; (3) Further, ML has also been employed for explicit solvent based hydration free energy calculations (e.g., the alchemical methods);[13] (4) Implicit solvent models should be developed for more complicated solvent environments (e.g., solvent mixtures, ionic liquids,[14] deep eutectic solvents, electrolyte solutions, temperature and pressure effects) without significantly increasing computational costs. This is very challenging while previous works of SM8T[15] and SMD-GIL[16] have proved the feasibility. Further works in this regard might need expansion of training set and more sophisticated techniques for global optimization of related parameters; (5) Finally, the mixed theoretical level method and the mixed ESF method proposed in this thesis should be extended to the calculations of other properties (e.g., partition coefficients in the SAMPL7 blind challenge).[17]

2. For some reactions, the prediction of activation energy using implicit solvent mod-

els is accompanied by significant uncertainty.[18] Recently, the importance of solvation dynamics in studying reaction mechanisms has been highlighted, as shown in some representative works.[19, 20] Thus, it is important that future method development can further improve the accuracy of implicit solvent models and efficiently include solvation dynamic effects for studying reaction mechanisms.

3. Because electrostatic and polarization interactions in electrostatic catalysis is related with bond breaking and forming steps, accuracy of quantum chemical methods in the evaluation of electrostatic interactions is critical. However, long-time MD simulations at QM level are not practical, so this thesis has investigated electrostatic catalysis using low-level (polarizable force field and semi-empirical QM methods) MD simulations and high-level (semi-empirical, DFT and post-HF methods) energy calculations. This protocol can be further improved by introducing additional considerations. For example: (1) Enhanced sampling methods[21] are usually more accurate than the end-point sampling. While it is sometimes challenging to design reasonable collective variables or intermediate states for a complicated chemical process, employing enhanced sampling methods could offer new insights in understanding more details of electrostatic catalysis in complex solvent environments; (2) Multi-scale energy calculations in this work were conducted with the ONIOM scheme, which can be improved by using more sophisticated quantum embedding methods (e.g., projector-based embedding[22]) with a more accurate description of the mutual polarization between two scales; (3) Machine learning potential techniques such as DPMD method are ground-breaking contributions in recent years which enable modelling complicated systems with high accuracy while affordable computational costs.[23] It has recently been employed in the study of chemical reactions in solution[24] and in the future could be employed to the modelling of electrostatic catalysis for large systems with accurate AIMD methods combined with enhanced sampling methods; (4) Investigating the effects of solvent ordering on other properties (e.g., excited-state properties[25]) and reaction selectivity; (5) Combining solute-solvent non-covalent interactions[26, 27] (e.g., hydrogen-bonding interactions) with CFG[28] in electrostatic catalysis and examining the interplay between non-covalent interactions and CFG; (6) Further studying chemical properties and reactions in other complex environments (e.g., molecular junction[29], nanoconfined space[30], solid-liquid interactions[31], micro-droplets[32–34]) and associated catalysis.

4. In light of our findings on the concentration of OH anions at the gas-liquid interface, the associated electric field and application to electrostatic catalysis, further investigation of the unique environment at this interface is warranted, and could offer distinct advantages compared to chemistry in the bulk solution. Several examples of future works are now summarized: (1) The computational protocol used in this work can be further improved by using a more accurate description of the gas-water interface and using additional configurations while keeping computational costs affordable. To model reactions at the air-water interface, effects of the size of the bubble, its curvature, and counterions should be included. For some reactions, inclusion of nuclear quantum effects[35–38] could also be important. Besides, bubble stability is also an important factor, which could be influenced by dissolved electrolytes and specific ion effects. The structures of electrodes and detailed chemical interactions could also be crucial. Thus, these factors can be harnessed to design efficient electrostatic catalysis systems; (2) The cluster size used in this work is very large for high-level DFT calculations, it is reasonable to ignore the hydrogen bond-

ing interactions between extracted clusters and exterior molecules. However, arriving at a rigorous conclusion might need further works trying larger clusters. This is not easy as we need to find a good balance between a proper size of cluster and an appropriate choice of QM method.(3) Further exploration of other properties at the gas-water interface, including non-equilibrium solvation, photochemical peroperties and superfast reactions. Some experimental works have been undertaken in this field recently,[39] and computational chemistry could offer further insight; (4) Besides the gas-water interface, other interface phenomena (e.g., "on water" reactions[40] and reactions at the water-mineral interface[41] or even the negatively charged bilayer phospholipid membrane surface[42]) can be investigated computationally for electrostatic catalysis; (5) Further exploration of the role of concentration of unbalanced charges in electrochemical applications besides redox potential[43, 44].

5. Extending upon the foundation in this thesis, further investigations of the structure and properties of ionic liquids under electric fields are warranted. For example, (1) the uniform external electric field employed in the MD simulations can be replaced with the more realistic constant potential method[45–48]; (2) The explicit interactions between charged electrodes and ionic liquids should also be included by performing AIMD simulations,[49] which can be further combined with the machine learning potential technique mentioned above for accelerating long-time simulations; (3) It is also worthwhile to study the direct connections between the calculated ion projector, measured OCP plateau and the performance of electrochemical devices, for example, batteries.

6. Developing methods for accurate and fast search of conformation and configuration of solvated molecules and clusters. With the increase of complexity, it is often challenging to arrive the global optimization, especially in solution phase, while it has been shown that the combination of QM calculations and data science could be a solution.[50]

7. The design of bespoke solvents using computational techniques and their translation to experimental chemistry is likely to provide benefit in the areas of CO_2 capture by ionic liquids[51], thermocells using ionic liquids[52] or deep eutectic solvents[53], and in energy storage as battery electrolytes.[54] There is great opportunity for solvent modelling to play a key role in these applications and the development of next generation devices.

Bibliography

[1] N Sadlej-Sosnowska, "Calculation of acidic dissociation constants in water: solvation free energy terms. their accuracy and impact", *Theoretical Chemistry Accounts* **118**(2), pp. 281–293 (2007).

[2] H Lim and Y Jung, "Delfos: deep learning model for prediction of solvation free energies in generic organic solvents", *Chemical Science* **10**(36), pp. 8306–8315 (2019).

[3] A Alibakhshi and B Hartke, "Improved prediction of solvation free energies by machine-learning polarizable continuum solvation model", *Nature Communications* **12**(1), pp. 1–7 (2021).

[4] A. V Marenich, C. P Kelly, J. D Thompson, G. D Hawkins, C. C Chambers, D. J Giesen, P Winget, C. J Cramer, and D. G Truhlar, "Minnesota solvation database", *Minnesota Solvation Database* **20** (2012).

[5] F. H Vermeire and W. H Green, "Transfer learning for solvation free energies: From quantum chemistry to experiments", *Chemical Engineering Journal* **418**, pp. 129307 (2021).

[6] Q Yang, Y Li, J.-D Yang, Y Liu, L Zhang, S Luo, and J.-P Cheng, "Holistic prediction of the pK_a in diverse solvents based on a machine-learning approach", *Angewandte Chemie* **132**(43), pp. 19444–19453 (2020).

[7] J Sandoval-Lira, G Mondragón-Solórzano, L. I Lugo-Fuentes, and J Barroso-Flores, "Accurate estimation of pK_b values for amino groups from surface electrostatic potential (vs, min) calculations: The isoelectric points of amino acids as a case study", *Journal of Chemical Information and Modeling* **60**(3), pp. 1445–1452 (2020).

[8] X Pan, H Wang, C Li, J. Z Zhang, and C Ji, "Molgpka: A web server for small molecule pK_a prediction using a graph-convolutional neural network", *Journal of Chemical Information and Modeling* **61**(7), pp. 3159–3165 (2021).

[9] Y Okamoto and Y Kubo, "Ab initio calculations of the redox potentials of additives for lithium-ion batteries and their prediction through machine learning", *ACS Omega* **3**(7), pp. 7868–7874 (2018).

[10] C.-W Ju, H Bai, B Li, and R Liu, "Machine learning enables highly accurate predictions of photophysical properties of organic fluorescent materials: emission wavelengths and quantum yields", *Journal of Chemical Information and Modeling* **61**(3), pp. 1053–1065 (2021).

[11] P Bleiziffer, K Schaller, and S Riniker, "Machine learning of partial charges derived from high-quality quantum-mechanical calculations", *Journal of Chemical Information and Modeling* **58**(3), pp. 579–590 (2018).

[12] C. W Coley, R Barzilay, T. S Jaakkola, W. H Green, and K. F Jensen, "Prediction of organic reaction outcomes using machine learning", *ACS Central Science* **3**(5), pp. 434–443 (2017).

[13] J Scheen, W Wu, A. S Mey, P Tosco, M Mackey, and J Michel, "Hybrid alchemical free energy/machine-learning methodology for the computation of hydration free energies", *Journal of Chemical Information and Modeling* **60**(11), pp. 5331–5339 (2020).

[14] K Low, R Kobayashi, and E. I Izgorodina, "The effect of descriptor choice in machine learning models for ionic liquid melting point prediction", *The Journal of Chemical Physics* **153**(10), pp. 104101 (2020).

[15] A. C Chamberlin, C. J Cramer, and D. G Truhlar, "Extension of a temperature-dependent aqueous solvation model to compounds containing nitrogen, fluorine, chlorine, bromine, and sulfur", *The Journal of Physical Chemistry B* **112**(10), pp. 3024–3039 (2008).

[16] V. S Bernales, A. V Marenich, R Contreras, C. J Cramer, and D. G Truhlar, "Quantum mechanical continuum solvation models for ionic liquids", *The Journal of Physical Chemistry B* **116**(30), pp. 9122–9129 (2012).

[17] A Viayna, S Pinheiro, C Curutchet, F. J Luque, and W. J Zamora, "Prediction of n-octanol/water partition coefficients and acidity constants (pKa) in the SAMPL7 blind challenge with the IEFPCM-MST model", *Journal of Computer-Aided Molecular Design* **35**, pp. 803–811 (2021).

[18] A. M Maldonado, S Hagiwara, T. H Choi, F Eckert, K Schwarz, R Sundararaman, M Otani, and J. A Keith, "Quantifying uncertainties in solvation procedures for modeling aqueous phase reaction mechanisms", *The Journal of Physical Chemistry A* **125**(1), pp. 154–164 (2021).

[19] V. A Roytman and D. A Singleton, "Solvation dynamics and the nature of reaction barriers and ion-pair intermediates in carbocation reactions", *Journal of the American Chemical Society* **142**(29), pp. 12865–12877 (2020).

[20] Z Chen, Y Nieves-Quinones, J. R Waas, and D. A Singleton, "Isotope effects, dynamic matching, and solvent dynamics in a Wittig reaction. Betaines as bypassed intermediates", *Journal of the American Chemical Society* **136**(38), pp. 13122–13125 (2014).

[21] Y. I Yang, Q Shao, J Zhang, L Yang, and Y. Q Gao, "Enhanced sampling in molecular dynamics", *The Journal of Chemical Physics* **151**(7), pp. 070902 (2019).

[22] S. J Bennie, B. F Curchod, F. R Manby, and D. R Glowacki, "Pushing the limits of EOM-CCSD with projector-based embedding for excitation energies", *The Journal of Physical Chemistry Letters* **8**(22), pp. 5559–5565 (2017).

[23] L Zhang, J Han, H Wang, R Car, and E Weinan, "Deep potential molecular dynamics: a scalable model with the accuracy of quantum mechanics", *Physical Review Letters* **120**(14), pp. 143001 (2018).

[24] M Yang, L Bonati, D Polino, and M Parrinello, "Using metadynamics to build neural network potentials for reactive events: the case of urea decomposition in water", *Catalysis Today* , pp. 143–149 (2021).

[25] M Rini, A.-K Holm, E. T Nibbering, and H Fidder, "Ultrafast UV-mid-IR investigation of the ring opening reaction of a photochromic spiropyran", *Journal of the American Chemical Society* **125**(10), pp. 3028–3034 (2003).

[26] L. R Pestana, H Hao, and T Head-Gordon, "Diels–Alder reactions in water are determined by microsolvation", *Nano Letters* **20**(1), pp. 606–611 (2019).

[27] Z Yang, C Doubleday, and K Houk, "QM/MM protocol for direct molecular dynamics of chemical reactions in solution: The water-accelerated Diels–Alder reaction", *Journal of Chemical Theory and Computation* **11**(12), pp. 5606–5612 (2015).

[28] H. M Aitken and M. L Coote, "Can electrostatic catalysis of Diels–Alder reactions be harnessed with pH-switchable charged functional groups?", *Physical Chemistry Chemical Physics* **20**(16), pp. 10671–10676 (2018).

[29] L Mejía, D Garay-Ruiz, and I Franco, "Diels–Alder reaction in a molecular junction", *The Journal of Physical Chemistry C* **125**(27), pp. 14599–14606 (2021).

[30] A. B Grommet, M Feller, and R Klajn, "Chemical reactivity under nanoconfinement", *Nature Nanotechnology* **15**(4), pp. 256–271 (2020).

[31] A. C Mendonça, P Malfreyt, and A. A Padua, "Interactions and ordering of ionic liquids at a metal surface", *Journal of Chemical Theory and Computation* **8**(9), pp. 3348–3355 (2012).

[32] X Yan, R. M Bain, and R. G Cooks, "Organic reactions in microdroplets: reaction acceleration revealed by mass spectrometry", *Angewandte Chemie International Edition* **55**(42), pp. 12960–12972 (2016).

[33] H Xiong, J. K Lee, R. N Zare, and W Min, "Strong electric field observed at the interface of aqueous microdroplets", *The Journal of Physical Chemistry Letters* **11**(17), pp. 7423–7428 (2020).

[34] C. F Chamberlayne and R. N Zare, "Simple model for the electric field and spatial distribution of ions in a microdroplet", *The Journal of Chemical Physics* **152**(18), pp. 184702 (2020).

[35] B. J Berne and D Thirumalai, "On the simulation of quantum systems: path integral methods", *Annual Review of Physical Chemistry* **37**(1), pp. 401–424 (1986).

[36] J Kessler, H Elgabarty, T Spura, K Karhan, P Partovi-Azar, A. A Hassanali, and T. D Kuhne, "Structure and dynamics of the instantaneous water/vapor interface revisited by path-integral and ab initio molecular dynamics simulations", *The Journal of Physical Chemistry B* **119**(31), pp. 10079–10086 (2015).

[37] A. R Menzeleev, N Ananth, and T. F Miller III, "Direct simulation of electron transfer using ring polymer molecular dynamics: Comparison with semiclassical instanton theory and exact quantum methods", *The Journal of Chemical Physics* **135**(7), pp. 074106 (2011).

[38] J. A Morrone and R Car, "Nuclear quantum effects in water", *Physical Review Letters* **101**(1), pp. 017801 (2008).

[39] R Kusaka, S Nihonyanagi, and T Tahara, "The photochemical reaction of phenol becomes ultrafast at the air–water interface", *Nature Chemistry* , pp. 1–6 (2021).

[40] Y Jung and R Marcus, "On the theory of organic catalysis "on water"", *Journal of the American Chemical Society* **129**(17), pp. 5492–5502 (2007).

[41] S Laporte, F Pietrucci, F Guyot, and A. M Saitta, "Formic acid synthesis in a water–mineral system: Major role of the interface", *The Journal of Physical Chemistry C* **124**(9), pp. 5125–5131 (2020).

[42] S Cukierman, W. C Zinkand, R. J French, and B. K Krueger, "Effects of membrane surface charge and calcium on the gating of rat brain sodium channels in planar bilayers.", *Journal of General Physiology* **92**(4), pp. 431–447 (1988).

[43] F Yang, Y.-S Liu, X Feng, K Qian, L. C Kao, Y Ha, N. T Hahn, T. J Seguin, M Tsige, and W Yang, "Probing calcium solvation by XAS, MD and DFT calculations", *RSC Advances* **10**(46), pp. 27315–27321 (2020).

[44] J Huang, P Li, and S Chen, "Quantitative understanding of the sluggish kinetics of hydrogen reactions in alkaline media based on a microscopic hamiltonian model for the Volmer step", *The Journal of Physical Chemistry C* **123**(28), pp. 17325–17334 (2019).

[45] Z Wang, Y Yang, D. L Olmsted, M Asta, and B. B Laird, "Evaluation of the constant potential method in simulating electric double-layer capacitors", *The Journal of Chemical Physics* **141**(18), pp. 184102 (2014).

[46] T Dufils, G Jeanmairet, B Rotenberg, M Sprik, and M Salanne, "Simulating electrochemical systems by combining the finite field method with a constant potential electrode", *Physical Review Letters* **123**(19), pp. 195501 (2019).

[47] S Li, Z Zhao, and X Liu, "Electric double layer structure and capacitance of imidazolium-based ionic liquids with FSI- and Tf- anions at graphite electrode by molecular dynamic simulations", *Journal of Electroanalytical Chemistry* **851**, pp. 113452 (2019).

[48] Z Gong and A. A Padua, "Effect of side chain modifications in imidazolium ionic liquids on the properties of the electrical double layer at a molybdenum disulfide electrode", *The Journal of Chemical Physics* **154**(8), pp. 084504 (2021).

[49] E Paek, A. J Pak, and G. S Hwang, "On the influence of polarization effects in predicting the interfacial structure and capacitance of graphene-like electrodes in ionic liquids", *The Journal of Chemical Physics* **142**(2), pp. 024701 (2015).

[50] L Fang, E Makkonen, M Todorovic, P Rinke, and X Chen, "Efficient amino acid conformer search with bayesian optimization", *Journal of Chemical Theory and Computation* **17**(3), pp. 1955–1966 (2021).

[51] I. O Furtado, T. C dos Santos, L. F Vasconcelos, L. T Costa, R. G Fiorot, C. M Ronconi, and J. W. d. M Carneiro, "Combined theoretical and experimental studies on CO_2 capture by amine-activated glycerol", *Chemical Engineering Journal* **408**, pp. 128002 (2021).

[52] M Russo, H Warren, G. M Spinks, D. R MacFarlane, and J. M Pringle, "Hydrogels containing the Ferri/Ferrocyanide redox couple and ionic liquids for thermocells", *Australian Journal of Chemistry* **72**(2), pp. 112–121 (2018).

[53] N. F Antariksa, T Yamada, and N Kimizuka, "High seebeck coefficient in middle-temperature thermocell with deep eutectic solvent", *Scientific Reports* **11**(1), pp. 1–7 (2021).

[54] X Chen, X Shen, T.-Z Hou, R Zhang, H.-J Peng, and Q Zhang, "Ion-solvent chemistry-inspired cation-additive strategy to stabilize electrolytes for sodium-metal batteries", *Chem* **6**(9), pp. 2242–2256 (2020).

Appendix

The documents for the statement of contribution of all publications are provided here.

Statement of Contribution

This thesis is submitted as a Thesis by Compilation in accordance with https://policies.anu.edu.au/ppl/document/ANUP_003405

I declare that the research presented in this Thesis represents original work that I carried out during my candidature at the Australian National University, except for contributions to multi-author papers incorporated in the Thesis where my contributions are specified in this Statement of Contribution.

Title: Recent Advances of Solvation Modelling in Studying Chemical Properties, Reaction Mechanisms and Catalysis

Authors: Longkun Xu, Michelle L. Coote

Publication outlet: Annual Reports in Computational Chemistry

Current status of paper: Submitted

Contribution to paper: I reviewed the literature and wrote the draft manuscripts

Senior author or collaborating authors endorsement: Michelle Coote

Longkun Xu		30/07/2021
Candidate – Print Name	Signature	Date

Endorsed

Michelle Coote		13/8/2021
Primary Supervisor – Print Name	Signature	Date
Luke Connal		18/8/2021
Delegated Authority – Print Name	Signature	Date

Statement of Contribution

This thesis is submitted as a Thesis by Compilation in accordance with https://policies.anu.edu.au/ppl/document/ANUP_003405

I declare that the research presented in this Thesis represents original work that I carried out during my candidature at the Australian National University, except for contributions to multi-author papers incorporated in the Thesis where my contributions are specified in this Statement of Contribution.

Title: Methods To Improve the Calculations of Solvation Model Density Solvation Free Energies and Associated Aqueous pKa Values: Comparison between Choosing an Optimal Theoretical Level, Solute Cavity Scaling, and Using Explicit Solvent Molecules

Authors: Longkun Xu, Michelle L. Coote

Publication outlet: The Journal of Physical Chemistry A

Current status of paper: Published

Contribution to paper: I am the first author of this paper. All computational results and subsequent discussion are my own work under the supervision of Prof. Michelle Coote, who edited the paper.

Senior author or collaborating authors endorsement: Michelle Coote

Longkun Xu		30/07/2021
Candidate – Print Name	Signature	Date

Endorsed

Michelle Coote		13/8/2021
Primary Supervisor – Print Name	Signature	Date
Luke Connal		18/08/2021
Delegated Authority – Print Name	Signature	Date

Statement of Contribution

This thesis is submitted as a Thesis by Compilation in accordance with https://policies.anu.edu.au/ppl/document/ANUP_003405

I declare that the research presented in this Thesis represents original work that I carried out during my candidature at the Australian National University, except for contributions to multi-author papers incorporated in the Thesis where my contributions are specified in this Statement of Contribution.

Title: Improving the Accuracy of PCM-UAHF and PCM-UAKS Calculations Using Optimized Electrostatic Scaling Factors

Authors: Longkun Xu, Michelle L. Coote

Publication outlet: Journal of Chemical Theory and Computation

Current status of paper: Published

Contribution to paper: I am the first author of this paper. All computational results and subsequent discussion are my own work under the supervision of Prof. Michelle Coote, who edited the paper.

Senior author or collaborating authors endorsement: Michelle Coote

Longkun Xu		30/07/2021
Candidate – Print Name	Signature	Date

Endorsed

Michelle Coote		13/8/2021
Primary Supervisor – Print Name	Signature	Date
Luke Connal		18/08/2021
Delegated Authority – Print Name	Signature	Date

168

Statement of Contribution

This thesis is submitted as a Thesis by Compilation in accordance with https://policies.anu.edu.au/ppl/document/ANUP_003405

I declare that the research presented in this Thesis represents original work that I carried out during my candidature at the Australian National University, except for contributions to multi-author papers incorporated in the Thesis where my contributions are specified in this Statement of Contribution.

Title: Ordered Solvents and Ionic Liquids Can Be Harnessed for Electrostatic Catalysis

Authors: Longkun Xu, Ekaterina I. Izgorodina, Michelle L. Coote

Publication outlet: Journal of the American Chemical Society

Current status of paper: Published

Contribution to paper: I am the first author of this paper. All computational results and subsequent discussion are my own work under the supervision of Prof. Ekaterina I. Izgorodina and Prof. Michelle Coote, co-edited the paper.

Senior author or collaborating authors endorsement: Michelle Coote

Longkun Xu		30/07/2021
Candidate – Print Name	Signature	Date

Endorsed

Michelle Coote		13/8/2021
Primary Supervisor – Print Name	Signature	Date
Luke Connal		18/8/2021
Delegated Authority – Print Name	Signature	Date

169

Australian National University

Statement of Contribution

This thesis is submitted as a Thesis by Compilation in accordance with https://policies.anu.edu.au/ppl/document/ANUP_003405

I declare that the research presented in this Thesis represents original work that I carried out during my candidature at the Australian National University, except for contributions to multi-author papers incorporated in the Thesis where my contributions are specified in this Statement of Contribution.

Title: Experimental Evidence of Long-Lived Electric Fields of Ionic Liquid Bi-layers

Authors: Mattia Belotti, Xin Lyu, Longkun Xu, Peter Halat, Nadim Darwish, Debbie S. Silvester, Ching Goh, Ekaterina I. Izgorodina, Michelle L. Coote, Simone Ciampi

Publication outlet: Journal of the American Chemical Society

Current status of paper: Published

Contribution to paper: I am the first computational chemistry author of this work. I performed all preliminary calculations and wrote the initial discussion. These formed the basis for improved calculations that were performed by Peter Halat, whose results are the final ones included in the manuscript. Prof. Michelle L. Coote and Prof. Ekaterina I. Izgorodina supervised and co-wrote up the computational work, and the rest of the authors contributed to the experimental part of this work.

Senior author or collaborating authors endorsement: Michelle Coote

Longkun Xu		30/07/2021
Candidate – Print Name	Signature	Date

Endorsed

Michelle Coote		13/8/2021
Primary Supervisor – Print Name	Signature	Date
Luke Connal		18/8/2021
Delegated Authority – Print Name	Signature	Date

Statement of Contribution

This thesis is submitted as a Thesis by Compilation in accordance with https://policies.anu.edu.au/ppl/document/ANUP_003405

I declare that the research presented in this Thesis represents original work that I carried out during my candidature at the Australian National University, except for contributions to multi-author papers incorporated in the Thesis where my contributions are specified in this Statement of Contribution.

Title: The corona of a surface bubble promotes electrochemical reactions

Authors: Yan B. Vogel, Cameron W. Evans, Mattia Belotti, Longkun Xu, Isabella C. Russell, Li-Juan Yu, Alfred K. K. Fung, Nicholas S. Hill, Nadim Darwish, Vinicius R. Gonçales, Michelle L. Coote, K. Swaminathan Iyer, Simone Ciampi

Publication outlet: Nature Communications

Current status of paper: Published

Contribution to paper: I am the first computational chemistry author in this paper. All semi-empirical MD simulation and quantum chemistry computational results and subsequent discussion about the effect of OH anion repulsion on oxidation are my own work under the supervision of Prof. Michelle Coote. This constitutes Supplementary Note 1 of the supporting information which I wrote, the conclusion of which explained the central finding of the paper. All experimental sections and all other computational sections (e.g. the field effects on peroxide splitting and the polymerization mechanism) are the work of others, as is the writing of the manuscript.

Senior author or collaborating authors endorsement: Michelle Coote

Longkun Xu		30/07/2021
Candidate – Print Name	Signature	Date

Endorsed

Michelle Coote		13/8/2021
Primary Supervisor – Print Name	Signature	Date
Luke Connal		18/8/2021
Delegated Authority – Print Name	Signature	Date

171